CATALYTIC HYDRODEMETALLATION OF NICKEL PORPHYRINS: REACTIVITY AND CATALYST SURFACE STUDIES

by

Ian Alexander Webster

B.Sc., University of Strathclyde (U.K.)
(1976)

M.S., Cornell University
(1979)

Submitted to the Department of
Chemical Engineering
in Partial Fulfillment of the
Requirements for the
Degree of

DOCTOR OF SCIENCE

at the

MASSACHUSETTS INSTITUTE OF TECHNOLOGY
February 1984

Signature of Author _____
Department of Chemical Engineering
January 13, 1984

Certified by _____
James Wei
Thesis Supervisor

Accepted by _____
Robert C. Reid
Chairman, Departmental Committee
on Graduate Students

CATALYTIC HYDRODEMETALLATION OF NICKEL PORPHYRINS: REACTIVITY AND CATALYST SURFACE STUDIES

by

IAN ALEXANDER WEBSTER

Submitted to the Department of Chemical Engineering on January 13, 1984 in partial fulfillment of the reuirements for the Degree of Doctor of Science in Chemical Engineering

ABSTRACT

The kinetics and mechanism of hydrodemetallation (HDM) of nickel etioporphyrin (NI-EP) and nickel tetra(3-methylphenyl) porphyrin (Ni-T3MPP) have been studied using alumina supported Group VIII metals, Co-Mo, and Ni-Mo as catalysts, and a white oil as a solvent. The metalloporphyrin solution simulates a metals containing residua, and was demetallized at 1000 psig H_2 and temperatures in the range 300 to 375°C. Over all catalysts, both porphyrins react via a sequential mechanism, involving initial hydrogenation to activate the porphyrin, followed by terminal hydrogenolysis which cleaves the ring, and deposits nickel onto the catalyst surface. While the global HDM mechanism is the same for both porphyrins, the intricacies of the HDM scheme are intimately linked to the structural differences on the periphery of the tetra-pyrrolic ring. With the Group VIII metals/γ-Al_2O_3 the selectivity of the HDM mechanism (terminal hydrogenolysis rate constant/initial hydrogenation rate constant) has been varied over two orders of magnitude. Group $VIII_1$ metals favor hydrogenolysis, while the Group $VIII_3$ metals have a high selectivity for hydrogenation. The HDM activity of the Group VIII metals is comparable to that of Co-Mo.

Ni-EP was reacted over a series of Ru-Cu/Al_2O_3 catalysts. The addition of Cu to the Ru system suppresses the rate of the hydrogenolysis reaction, while having little effect on the hydrogenation reaction. Based on XPS measurements these observations were rationalized by geometrical effects. XPS also indicated that the chemical state of nickel deposited on a catalyst via HDM differs from its state and degree of interaction with the support in a Ni-Mo/Al_2O_3 catalyst.

Oil soluble cobalt and molybdenum napthenates were also dissolved in the white oil, and demetallized over bare γ-Al_2O_3 support at temperatures of 290°C and 360°C, and pressures of 500 and 1000 psig H_2. These in situ synthesized Co-Mo catalysts were subsequently used in Ni-T3MPP HDM. The catalysts which were generated at 360°C, 1000 psig H_2 had a higher Ni-T3MPP HDM activity than the commercially manufactured Co-Mo/Al_2O_3. SEM/EDX and

AES measurements indicate that a thick carbonaceous overlayer envelopes the Al_2O_3 particles during napthenate demetallation. However this overlayer remains porous enough to permit all metals to ultimately deposit on the alumina.

Model, non-porous polycrystalline alumina supported Co-Mo catalysts were made with surface compositions in the range $0 \leq [Co/(Co+Mo)] \leq 1$ and used for Ni-T3MPP HDM. The catalysts were aged in HDM experiments in a spinning basket reactor at 360°C and 1000 psig H_2. The aged catalysts were scrutinized by a variety of surface spectroscopic techniques (XPS, AES, SIMS, ISS and SEM/EDX). HDM activity was a maximum in the range $0.5 < [Co/(Co+Mo)] \leq 0.7$. The initially oxidic catalysts were reduced during HDM (Mo^{6+} to Mo^{4+}, and Co^{2+} to Co^{0}). Both metallic Ni and NiO were observed on the aged catalysts, however, the latter entity is most probably a result of air contamination, and it is not present in the working HDM environment. ISS results were consistent with the existence of a Co-Mo double layer, in both the real γ-Al_2O_3 supported catalysts and the model catalysts, with a Mo rich layer residing atop a Co rich layer. The basic elements Na and K are strongly surface segregated and in intimate contact with the Mo, thereby moderating its acidity. The aged catalyst is covered with a carbonaceous overlayer possessing holes, through which bare Mo patches are exposed. These islands are speculated to remain coke and metals free as the catalyst operates. A conceptual model for the working hydrotreating catalyst surface is proposed which integrates all surface spectroscopic findings. The model emphasizes the hydrogen storage and exchange capabilities of the carbonaceous overlayer which must be viewed as an integral feature of the working catalyst surface.

Thesis Supervisor: Dr. James Wei
Department Head and Warren K. Lewis
Professor of Chemical Engineering

This thesis is dedicated

to my mother and father

Charles and Helen Webster

whose encouragement and understanding

through my long education has been

a source of inspiration.

ACKNOWLEDGEMENTS

Many people have contributed to the final state of this thesis. I wish to thank:

* my thesis supervisor Professor James Wei, and thesis committee of Professors Charles N. Satterfield, Michael P. Manning, Adel F. Sarofim, Robert C. Reid, Herbert H. Sawin, Sylvia T. Ceyer and Dr. Frederick A. Putnam;

* The Department of Chemical Engineering and the National Science Foundation for financial support;

* for analytical assistance, John R. Martin, MIT, (XPS,AES); Leonard I. Sudenfield, MIT, (SEM/EDX); Dr. Chi-Wen Hung, Chevron Research Co., (Hydrogen chemisorption); Dr. Alan Miller, Alcoa Research, (ISS, SIMS); Dr. Elizabeth Myers, American Cyanamid Research, (Co-Mo catalyst supplies and their characterization);

* my future employer, Union Oil Company of California, especially Dr. J. Wayne Miller, for understanding the delays I experienced during this last year of my thesis work;

* my friends (in no particular order, of course), Bob Ware, Shan Hsi Yang, Morris Smith, Chris (have a beer) Schwier, Mark Manton, Kent Goklen, George Corbin, Norm Margolus and Deb Dickinson. The nights we conducted fluid mechanics research from Harvard Square to Downtown to Route 2 to Chelsea to East Boston to the Big Dipper are indelibly etched in the scars on my body; "It doesn't get any better than this."

* Sharon Gray for typing this thesis.

CONTENTS

PREFACE

Each chapter in this thesis is self-contained. They each have their own summary, literature review, experimental, discussion, and reference sections. For the sake of brevity, the thesis contains no raw data directly from the many hundreds of batch experiments which were run. Copies of these numbers are held by the author at Union Oil Research Center, Brea, California, and by Professor James Wei, MIT.

CHAPTER I

The Hydrodemetallation of Nickel Porphyrins Catalyzed by Group VIII metals/ γ-Al_2O_3: Mechanism, Reactivity and Selectivity

I. A. Summary of Chapter

The kinetics and mechanism of hydrodemetallation (HDM) of nickel etioporthyrin (Ni-EP) and nickel tetra (3-methylphenyl) porphyrin (Ni-T3MPP) have been studied using alumina supported Group VIII metals as catalysts, and a white oil as a solvent. The metallo-porphyrin solution simulates a metals containing residua, and was demetallized at 1000 psig H_2 and temperatures in the range 315-375°C. Both porphyrins react in a sequential mechanism, involving initial hydrogenation to activate the porphyrin, and deposits nickel onto the catalyst surface. While the global HDM mechanism is the same for both prophyrins, the intricacies of the HDM scheme are intimately linked to the structural differences on the periphery of the tetra-pyrrolic ring. By using Group VIII metal /γ-Al_2O_3 catalysts we have been able to vary the selectivity of the HDM mechanism (hydrogenolysis rate constant/hydrogenation rate constant) over two orders of magnitude, at best. This behavior correlates with the percentage d-character of the Group VIII metal. The HDM activity of the Group VIII metals is comparable to that for Co-Mo/Al_2O_3, to which we compare our data. Ni-EP has also been reacted over a series of Ru-Cu/Al_2O_3 catalysts, where

the copper is perceived as an inert "spacer" element which divides up ensembles of ruthenium atoms required for the porphyrin hydrogenolysis reaction. Addition of copper to the ruthenium catalyst suppresses hydrogenolysis while having little effect on the hydrogenation reaction. These observations have been interpreted in terms of geometrical effects. XPS measurements on the aged Group VIII metal catalysts suggests that the catalytically deposited nickel does not interact strongly with the support.

I. B. Introduction

One of the major refining technological challenges of the 1980's is the conversion of heavy residual oils into lighter fuel oils. During the hydrotreating operation the heavy oils' heteroatoms, sulfur, nitrogen, oxygen and trace metals (chiefly, Ni, V, and Fe) are catalytically cleared from the oil. S, N and O leave via the gas phase as H_2S, NH_3, and H_2O while the metals irreversibly deposit on the hydrotreating catalyst. This catalyst is usually Co-Mo/Al_2O_3.

The metals are particularly troublesome, and can be present in concentrations as high as 1300 ppm by weight Ni and V (1). During hydrotreating these metals deposit on the catalyst causing fouling of active sites, which leads to rapid catalyst deactivation. At longer operating times the metals cause pore mouth plugging, thereby occluding the less severely poisoned interior volumes of the catalyst.

The nickel and vanadium compounds in heavy oils are present as oil soluble organic species, and can be classified into two groups namely, the metallo-porphyrins and the non-porphyrinic metals. Since in real crudes, metal in the porphyrin form can account for up to 50% of the oil's total metal content (2), metallo-porphyrin spiked oils represent an ideal model

crude, with which to investigate the hydrodemetallation (HDM) kinetics of real oils.

The approach of our research group has been to investigate the catalytic HDM of a model crude synthesised by dissolving Ni-porphyrins in a clean, sulfur and nitrogen free white oil. The kinetics and mechanism of HDM have been investigated. There is a definite need for such model compound studies in order to clarify the conflicting and incomplete studies of previous investigators.

For example, Riley (3) observed apparent first order removal kinetics for both nickel and vanadium. Higher order demetallation kinetics were reported by Van Dongen et al (4), such as 1.5 order for vanadium. Oleck and Sherry (5) reported second order HDM kinetics for both Ni and V. With real crudes the presence of more than one class of metal compound, reacting with different rates make it impossible to determine the true kinetic orders, rate parameters and mechanism of the HDM reactions.

Model compound HDM studies were pioneered by Hung and Wei (6,7) who demetallized both nickel and vanadyl porphyrins over an oxide Co-Mo/Al_2O_3 catalyst. Total metal removal rates were found to follow fractional order kinetics. This observation was subsequently interpreted by Agrawal and Wei (8) to be the result of a sequential HDM mechanism, with the final metal deposition step occurring via an hydrogenated intermediate not originally present in the oil. More recently Ware and Wei (9), Rankel (10,11) and Kameyama and Amano (12) have investigated the HDM kinetics and reaction pathways of nickel and vanadyl porphyrins with model compounds. All their work confirms the sequential nature of the HDM mechanism.

The "work horse" hydrotreating catalyst employed in all the

aforementioned studies was Co-Mo/Al_2O_3 (13). Co and Ni-promoted Mo and W catalysts are also popular (14). However, as petroleum feedstocks dwindle, there is an ever increasing need to formulate, experimentally investigate, and develop a new generation of highly selective hydroprocessing catalysts.

The objectives of this work have been to experimentally investigate the kinetics of model oil HDM reactions over alumina supported Group VIII metal catalysts, and a Group VIII-IB bimetallic catalyst, namely Ru-Cu/Al_2O_3. The rationale for why this merits investigation is developed in the following literature review section. We believe this to be one of the first studies investigating catalytic HDM over supported Group VIII metals.

I. B. 1. Literature Review and Research Rationale

Recent work from our laboratory has shown how during catalytic HDM the porphyrins react via a sequential mechanism, first involving hydrogenation of peripheral double bonds, followed by a final hydrogenolysis step which fragments the ring, and removes the metal. Agrawal and Wei (8) demetallized Ni-etioporphyrin (Ni-EP) (for structure see Fig. 1) at realistic hydrotreating process conditions (290-345°C, 600-1400 psig hydrogen) over Co-Mo/Al_2O_3 catalyst. Only one hydrogenated intermediate called Ni-EP chlorin (Ni-EPH_2) was observed. The Ni-EPH_2 then reacted via a hydrogenolysis step which cracked the ring and deposited the metal on the catalyst surface.

Subsequently Ware and Wei (9) experimented with the HDM of Ni-tetra (3-methylphenyl) porphyrin (Ni-T3MPP) (Fig. 1). This investigation permitted a comparison with the Ni-EP HDM kinetics and mechanism. Both porphyrins have similar four pyrrole ring macro structures and conjugation,

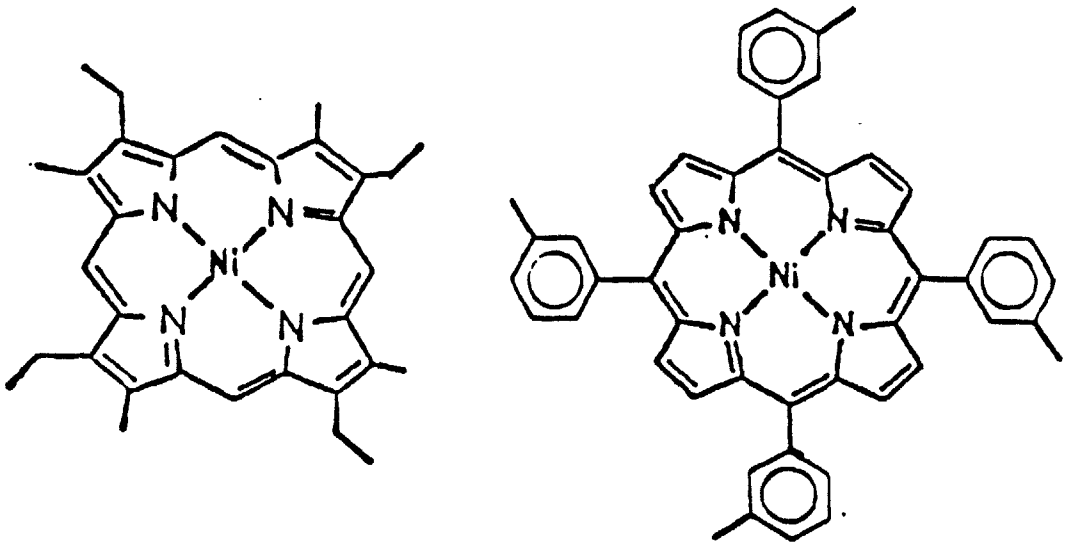

Ni-Etioporphyrin (Ni-EP)

Ni-tetra(3-methylphenyl)porphyrin (Ni-T3MPP)

Figure 1: Structure of model nickel compounds

but have structural differences around the periphery of the macrocycle. Ni-EP has methyl, and ethyl groups on the β-pyrrolic positions and open methine bridges, whereas, Ni-T3MPP has open β-pyrrolic positions and tolyl substitutents at the methine bridges.

Ware and Wei's study (9) revealed that while the general scheme of porphyrin hydrogenation followed by porphyrin hydrogenolysis and metal deposition was maintained, the reaction pathways for the two porphyrins were different. Ni-T3MPP reacted through two hydrogenated porphyrin intermediates (Ni-T3MPP chlorin [Ni-T3MPPH_2] and Ni-T3MPP isobacteriochlorin [Ni-T3MPPH_4]) and a non-porphyrinic, contracted ring structure. Moreover, the Ni-T3MPP HDM pathway has shown to possess two routes for metal deposition: one from Ni-T3MPPH_4 and the other from the contracted ring structure, which Ware (15) has speculated to be an hydrogenated nickel-corrin (16).

Because of the bifunctional nature of the HDM mechanism (initial hydrogenation followed by terminal hydrogenolysis) we sought catalysts that would permit us to vary the selectivity or, hydrogenolysis to hydrogenation rate constant ratio, in the HDM pathway. The benefits of being able to realize this are obvious. A catalyst that can hydrogenate the porphyrin, but is relatively poor for its hydrogenolysis, can be used to conduct the mandatory hydrogenation step(s), but ultimately have little nickel deposited on it, because of its relatively low cracking activity. The process implications are that the hydrogenation reactions could be carried out in upstream catalyst bed. The hydrogenated metallo-prophyrinic intermediates would then be passed over another catalyst, in a downstream bed, which possessed a high hydrogenolysis activity. Nickel would be

deposited in this bed. The pore size distribution of this latter catalyst would be engineered so that it could acummulate a heavy nickel loading without encountering problems of pore mouth plugging (17, 18).

Supported Group VIII metals and supported Group VIII-IB bimetallic catalysts have been shown to have widely varying activities for conducting hydrogenation and hydrogenolysis reactions.

Pioneering work on the relative activities of the Group VIII metals for hydrogenation and hydrogenolysis was conducted by Sinfelt and coworkers (19-25). Two relevant pieces of information from their investigations, which we exploit in this study, are depicted in Figs. 2 and 3. Sinfelt et al used ethane and cyclopropane as the test molecules for measuring hydrogenolysis and hydrogenation rates respectively. Figure 2 shows the catalytic activities of the Group VIII metals for ethane hydrogenolysis as a function of their periodic position. Within each transition series hydrogenolysis activity varies dramatically (ca. six orders of magnitude in the second and third transition series), and can be broadly correlated with the percentage d character of the metallic bond. This quantity is introduced in Pauling's valence bond theory of metals to represent the extent of participation of d orbitals in the bonding between atoms in a metal lattice (26). This parameter has no clear physical significance (27), and has come under considerable general criticism (28, 29). Nevertheless, the hydrogenolysis capabilities of the Group VIII are remarkably well correlated with percentage d character. For example, Boudart and Ptak (30) measured the rates of hydrogenolysis of neopentane on supported Group VIII metal catalysts, and successfully correlated the catalysts' activity over ten orders of magnitude, with percentage d-bond

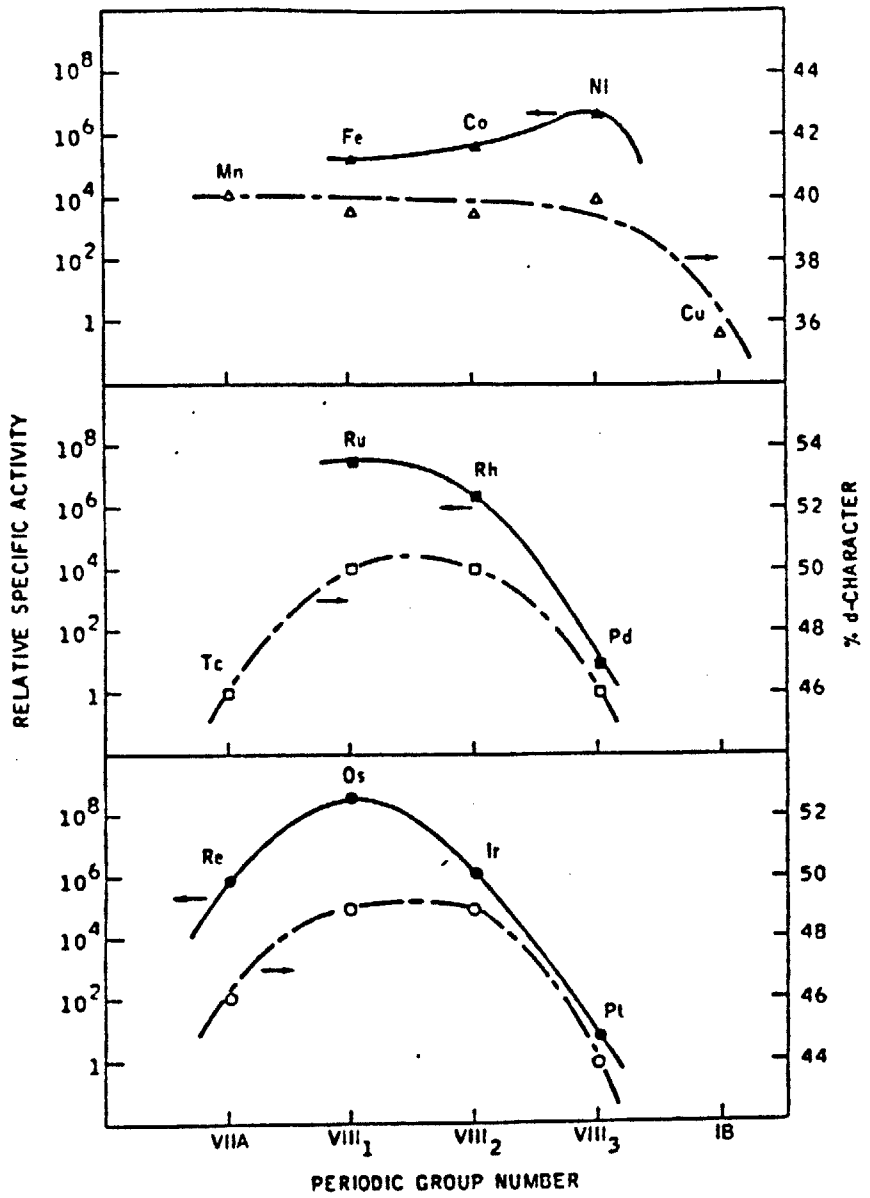

Figure 2: Catalytic activities of metals for ethane hydrogenolysis in relation to the percentage d-character of the metallic bond. From Ref. 20.

character.

Figure 3, taken from the work of Dalla Betta et al (25) compares the activity patterns of the 3rd transition series of the Group VIII metals for cyclopropane hydrogenation and ethane hydrogenolysis. Platinium has high activity for hydrogenation, however is relatively poor for hydrogenolysis. Moving in the direction of decreasing atomic number across the third transition series triad from platinium to iridium to osmium, the metals' hydrogenation capability decreases while its hydrogenolysis activity increases.

It is evident that by using these Group VIII metals in an HDM pathway, incorporating both hydrogenation and hydrogenolysis steps, it may be possible to manipulate a priori the selectivity of the mechanism, based on which particular catalytic metal is chosen. This is the first goal of the research reported here.

In one of the most exciting catalytic developments of the past decade, catalytic chemists have also shown how the selectivity of high dispersed supported Group VIII-IB bimetallic catalysts depends on the atomic ratio of the Group IB element to the Group VIII element. The first significant work in this area was also accomplished by Sinfelt and coworkers (31).

Working with unsupported nickel-copper alloys as catalysts, Sinfelt et al (32) investigated the hydrogenation of cyclohexane to benzene, and the hydrogenolysis of ethane to methane. Their results are shown in Fig. 4. The hydrogenolysis activity is seen to decrease by approximately five orders of magnitude, as the atom % copper is increased from 0 to 74%, while the rate of cyclohexane dehydrogenation remains "fairly insensitive" to alloy composition.

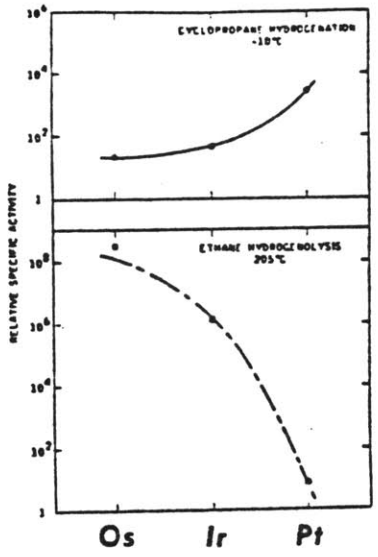

Figure 3: Comparison of activity patterns of the Group VIII noble metals for cyclopropane hydrogenation and ethane hydrogenolysis. From Ref. 25.

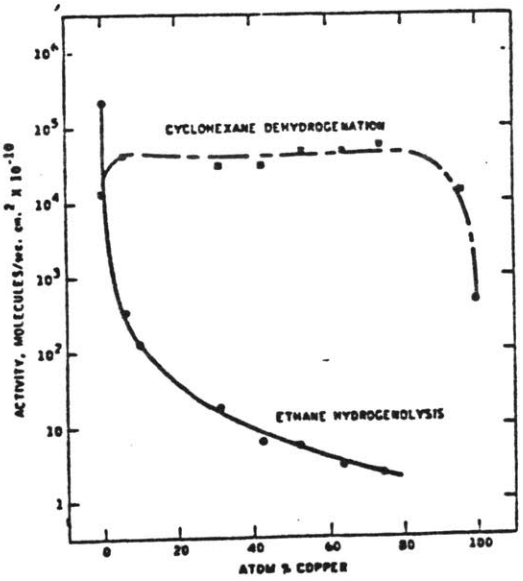

Figure 4: Activities of copper-nickel alloy catalysts for the hydrogenolysis of ethane to methane, and the dehydrogenation of cyclohexane to benzene. From Ref. 32.

These observations can be explained by each of the two theories currently in vogue to rationalize the catalytic capabilities of bimetallic catalysts; namely the geometrical theory and the electronic theory (33-36).

The geometrical theory assumes that "multiplets" (37) or "ensembles" (38,39) of the catalytically active metal atoms (Group VIII) are required to form an active catalytic site (40), where the reactant molecule chemisorbs in a particular configuration before undergoing rearrangement. The role of the inactive Group IB metal is therefore perceived to be solely that of a diluent, which due to its ability to surface segregate (lower heat of sublimation (40-42)) destroys active metal ensembles. Due to this phenomenon the rates of reactions which require the presence of surface multiplets are therefore dramatically reduced by alloying inert spacer atoms, compared to reactions which simply proceed through chemisorption on a single active atom.

It is also reasonable to expect that the electronic energy level of an active metal atom will be affected by the contiguous presence of an inactive metal atom (43,44). Such ideas are the basis of the "ligand" or electronic theory of catalysis by bimetallics. The spacer atom (Group IB) will affect the reactants' chemisorption bond strength, since its heat of adsorption on either of the two metals will differ. Since the strength of the bond(s) of the reactant to the active catalytic metal can be correlated to catalytic activity (45), it is evident how alloying can alter the reactant turnover at a particular site.

Sinfelt et al (32) expained the rapid decline in hydrogenolysis activity and the insensitivity of hydrogenation activity to catalyst composition by invoking both the geometrical theory (Ni duplets are

required for chemisorption of hydrogen deficient dicarbon surface residues and their number is reduced by alloying) and the electronic theory (the electronic effect of Cu on Ni is to reduce its percentage d character, whose magnitude, as already discussed has been proposed as being directly proportional to the hydrogenolysis activity of the Group VIII metal (19,22,24,30,46)).

Reactions that proceed through chemisorbed intermediates that are bound to many adjacent catalytically active atoms, are inhibited more strongly by alloying than reactions which only require small ensembles. The former reactions are structure sensitive, while the latter tend to be structure insensitive (47). Ponec (34) has noted that structure insensitive reactions such as hydro-dehydrogenation are little affected by the introduction of inert Group IB metal atoms on the catalyst's surface, while structure sensitive reactions involving C-C bond dissociation are affected.

It is highly probable that some of the reactions involved in the catalytic HDM of nickel porphyrins are structure sensitive, since the large porphyrinic tetra-pyrrole plate will most likely form multiple bonds at the catalytically active site. We can envision the hydrogenated form of the porphyrin molecule forming a multiply bonded intermediate prior to the ring opening step which releases the nickel atom onto the catalyst surface, and leaves cracked fragments of the porphyrin ring bonded to adjacent active sites.

Our previous research (8,15) also substantiated by work in this paper, has elucidated the HDM mechanism. Nickel porphyrin hydrogenation is followed by a terminal hydrogenolysis step. The first reaction may be

structure insensitive, while the latter is structure sensitive. The second goal of our research is now evident. We will show how it is possible to control the selectivity of the HDM mechanism by exploiting the ability of bimetallic catalysts to suppress the rates of hydrogenolysis reactions, while having little affect on the rate of the simultaneously occurring hydrogenation reaction. XPS measurements on low surface area polycrystalline alumina (PCA) supported bimetallic catalysts, indicate that the effect of the Group IB metal is mainly geometrical.

I. C. Experimental

I. C. 1. Experimental Apparatus

The kinetics of HDM was studied with batch autoclave experiments. The reaction vessel is a standard one liter batch autoclave (Autoclave Engineers, Erie, PA, Model AFP 1005). The entire system is exactly as described elsewhere (6), except that an additional discharge line with a 0.5μ filter was positioned at the bottom of the reactor. This permitted the reactor's contents to be quickly discharged, while retaining the catalyst in the reactor for a subsequent demetallation experiment.

I. C. 2. Materials

(a) Catalysts

The chemical properties of the catalysts, and alumina used to make some of the catalysts are detailed in Table 1. For the catalysts actually employed in HDM experiments the support material was always γ-Al_2O_3. The Co-Mo and Ni-Mo hydrotreating catalysts (HDS-16A and HDS-9A) were supplied by American Cyanamid (Bound Brook, NJ) as 1/16" diameter extrudates. Prior to use the extrudates were crushed and sieved to the size range 75-90μ.

All the supported Group VIII metal catalysts were loaded to 5 wt %

Table 1: Summary of Catalysts Investigated in HDM study

Catalyst System*	Composition (wt %)	Supplier or Self Made	Cu/Ru atomic ratio in Group VIII-IB bimetallics
Co-Mo(HDS-16A)	CoO 5.7		
	MoO_3 12.1	American	
	Na_2O 0.03	Cyanamid	
	Fe 0.04		
Ni-Mo(HDS-9A)	NiO 3.2		
	MoO_3 17.5		
	Na_2O 0.03	American	
	Fe 0.03	Cyanamid	
	SO_4 0.4		
	SiO_2 0.5		
Co	5	Strem	
Ni	5	Harshaw	
Ru	5	Strem	
Rh	5	Strem	
Pd	5	Strem	
Re	5	Strem	
Os	5	Self made	
Ir	5	Self made	
Pt	5	Strem	
Ru-Cu	Ru 5, Cu 0	Self made	0
	Ru 5, Cu 1.57	Self made	0.5
	Ru 5, Cu 3.14	Self made	1.0

*All catalysts supported on γ-Al_2O_3 (>99.85 wt %; Na_2O<0.015; SiO_2<0.09; Fe_2O_3<0.06 wt %)

metal, and were purchased from Strem Chemicals (Newburyport, MA) with the exception of the iridium and osmium catalysts. These catalysts were prepared by individually impregnating γ-Al_2O_3 (Norton Co., Akron, OH) with solutions of $IrCl_3 . 3H_2O$ and $OsCl_3$ (Aldrich Chemical Co., Milwaukee, WI). During impregnation approximately 1 ml of the aqueous impregnating solution of appropriate concentration was employed per gram of alumina (48).

The alumina supported Ru-Cu bimetallic catalysts of the compositions listed in Table 1 were prepared by a simple co-impregnation procedure, using aqueous salts on acids of the two metals in question. The compounds used were $RuCl_3$ (Aldrich Chemical Co.) and $Cu(NO_3)_2 . 3H_2O$ (Aldrich). Solutions of the first of these compounds were prepared by dissolving the salt in 38% hydrochloric acid solution (Ashland Chemical Co.) to prevent hydrolysis of the salt, and the precipitation of the metal hydroxide.

After impregnation, all the self made γ-Al_2O_3 supported catalysts were then essentially treated similarly. They were all dried overnight at ca. 100°C in air, with the exception of the osmium catalyst which was dried in a vacuum oven at ca. 70°C. Each resulting catalyst cake was reground and sized to 75-90μ prior to being placed in a fused silica boat, which was then positioned in a tube furnace. The catalyst was reduced in flowing hydrogen at 500°C for approximately three hours prior to the HDM experiment. The catalysts were also prereduced before catalyst characterization by hydrogen chemisorption. A few runs were also made with the oxide forms of the Group VIII metal catalysts (i.e. no pre-reduction).

A series of polycrystalline alumina (PCA) supported Ru-Cu bimetallic catalysts were also prepared, purely for use in XPS measurements. We have shown elsewhere (49) that these low surface area catalysts realistically

mimic the catalytic behavior of their high surface area γ-Al_2O_3 counterparts, and are more amenable for study in the ultra high vacuum environment of XPS. The preparation procedure has alreay been outlined in detail (49). Briefly, 1 cm^2 slabs of non-porous PCA (99.9% Al_2O_3, Grade AD-999, Coors Porcelain Company) were meticulously cleaned by alternate soakings in chromic acid-sulfuric acid cleaning solution (Fisher Scientific Company) and distilled water. The PCA squares were calcined at 600°C in ultra high purity air (Matheson, Zero Gas), and subsequently co-impregnated with a carefully monitored volume of 38% HCl solution containing the desired amounts of the aforementioned salts of Ru and Cu. Trial-and-error experimentation showed that 30µl of liquid was an optimum volume to deposit on the PCA square from a syringe. This liquid puddle was swirled on the PCA square with the syringe needle tip in an attempt to produce a uniform coating of the impregnate on the alumina surface. A uniform surface coating was difficult to attain, and this point will be further amplified later. Each PCA catalyst was then treated identically to the self made γ-Al_2O_3 supported catalysts, i.e. dried at 100°C overnight in air, then reduced at 500°C for three hours in flowing hydrogen. Immediately prior to XPS analysis the model catalysts were again reduced, and carefully transferred to the ultra high vacuum environment of the spectrometer in a glove bag, under an Argon atmosphere. Every attempt was made to avoid air contamination of the catalysts. The compositions of the PCA supported catalysts that were prepared are listed in Table 2. The 30µl solution volumes that were spread over each PCA square contained enough of the Group VIII metal such that if it was to uniformly coat the surface, 30 monolayers of the metal would exist. With catalysts which contained copper, the

Table 2: Summary of Group VIII-IB model polycrystalline alumina (PCA) supported catalysts prepared for investigation by XPS

Catalyst Number	Metals	Composition
1	Ru	30 monolayers
2	Cu	30 monolayers
3	Ru-Cu	Cu/Ru atomic ratio = 1 30 monolayers Ru

ruthenium metal loading was the same, with sufficient copper being added to make the [Cu/Ru] atomic ratio equal to unity. While these model PCA catalysts are far more heavily surface loaded than the γ-Al_2O_3 supported catalysts detailed in Table 1, we nevertheless believe they represent good idealizations of the real catalyst surface, and are especially amenable to scrutiny by XPS.

The pore size distributions (PSDs) of all Group VIII metal catalysts were measured by nitrogen adsorption (Digisorb 2500). Some typical distributions are depicted in Fig. 5. All catalysts possessed similar physical properties. The PSDs of of the American Cyanamid supplied Co-Mo/Al_2O_3 catalyst, and the Norton γ-Al_2O_3, each measured by mercury penetration, are reported in Fig. 6.

(b) Model metal compound and oil

Model nickel containing heavy oils were synthesized by dissolving Ni-Etioporphyrin (Ni-EP) and Ni-tetra (3-methylphenyl) porphyrin (Ni-T3MPP) individually in a clean mineral oil. The porphyrins were purchased from Midcentury Chemicals (Posen, IL) and the mineral oil, marketed under the name Nujol, from Plough Inc. (Memphis, TN). The molecular structures of the porphyrins are shown in Fig. 1. The metallo etioporphyrins are found in petroleum (50), whereas the metallo tetra-phenyl porphyrins are not. However, they are probably more representative of condensed porphyrins of higher aromaticity which have been speculated as comprising the asphaltene component of residua (51).

The composition of the mineral oil has been described by Fiero (52), and although it is a mixture of several hydrocarbons, it consists only of napthenes, paraffins, and isoparaffins, with napthenes dominating.

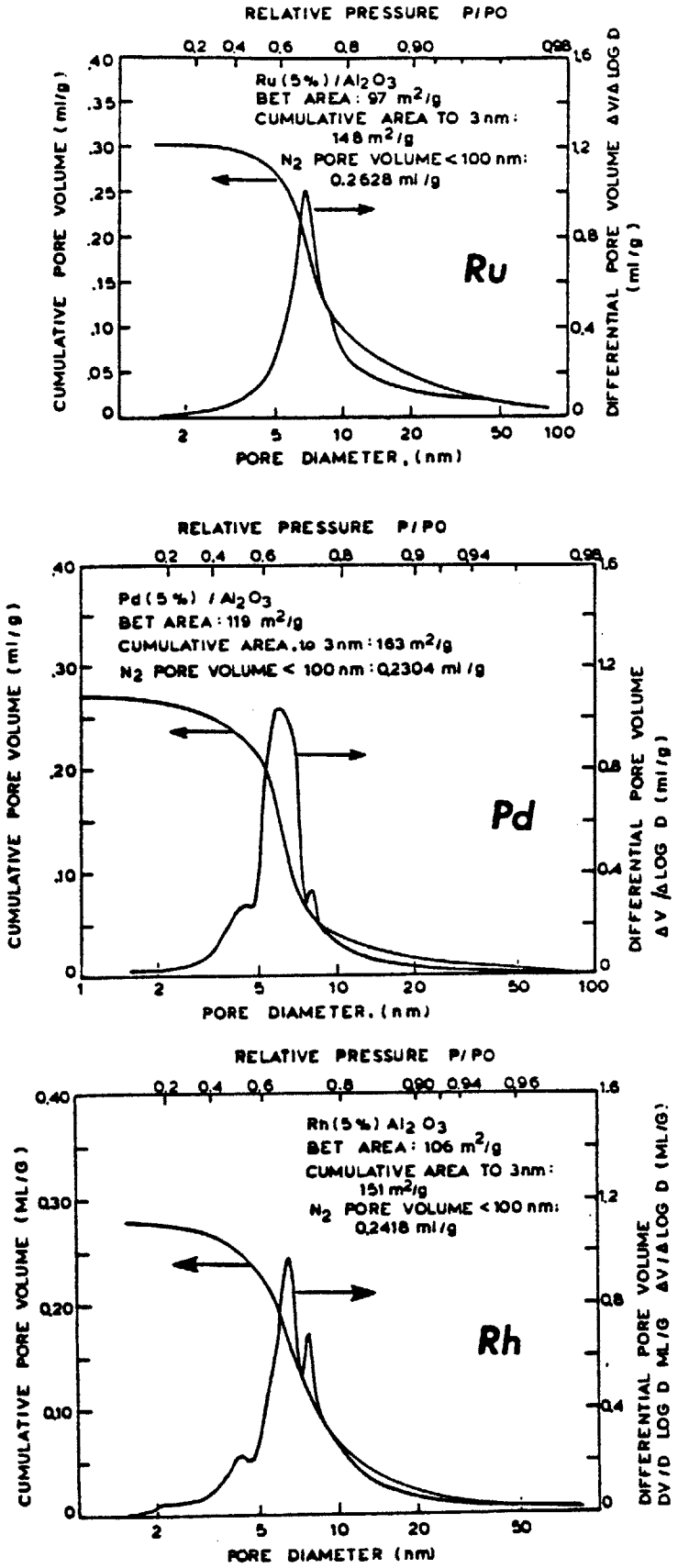

Figure 5: Pore size distributions for Group VIII metal catalysts Ru, Pd and Rh on γ-Al_2O_3.

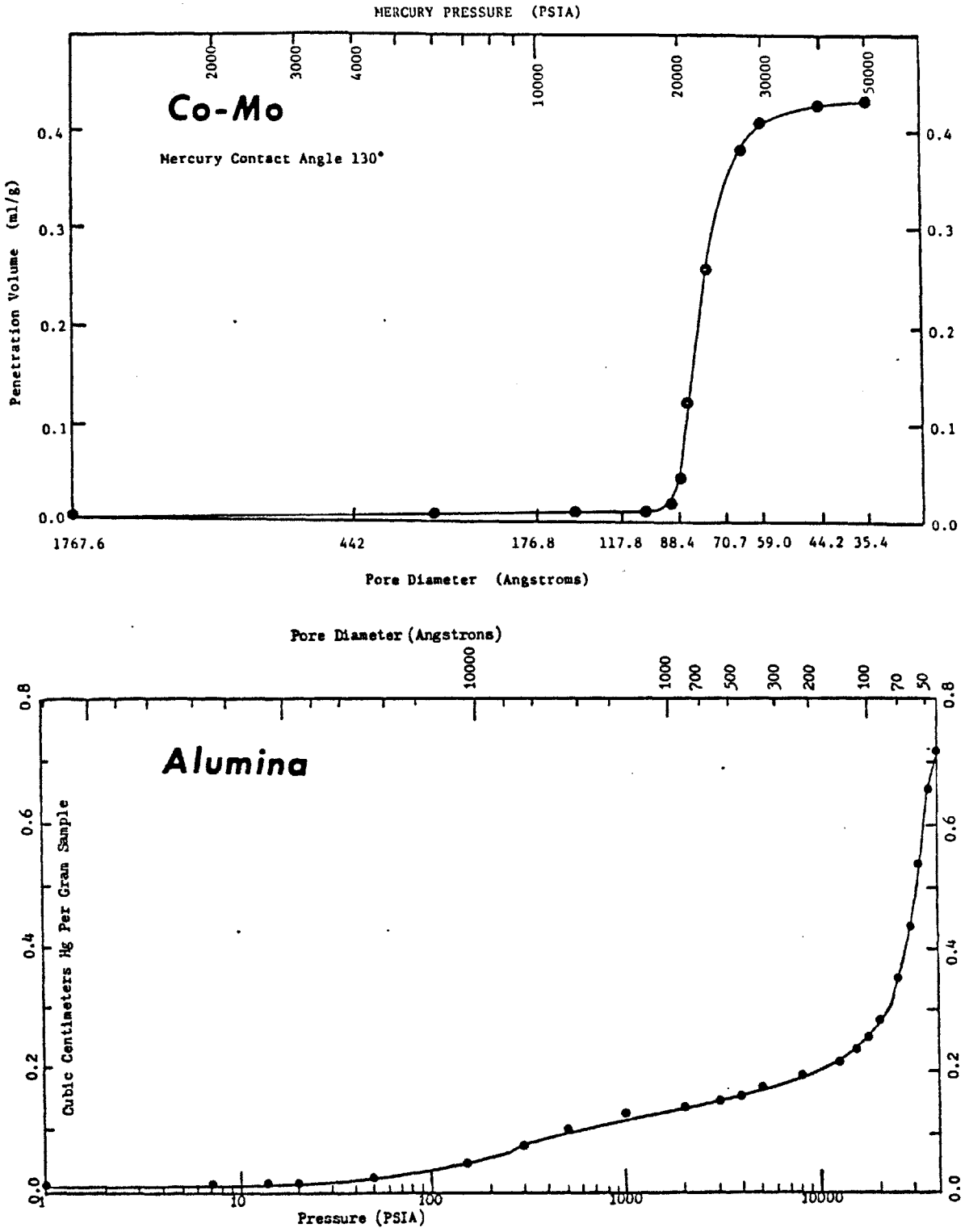

Figure 6: Pore size distributions for Co-Mo/-γAl_2O_3 (HDS-16A) and γ-Al_2O_3 catalyst support.

The procedure for dissolving the porphyrins in the Nujol has been fully documented elsewhere (6,15,53,54). The process essentially consists of de-aerating the Nujol by filtering it through a 5μ filter (Millipore Corp., Bedford, MA) and then stirring the Nujol-metalloporphyrin mixture together at ca. 300°C for ca. six hours, under a helium atmosphere. The resulting solution is finally filtered through a 0.5μ filter to remove any undissolved porphyrin.

Ni-EP, and Ni-T3MPP were always dissolved to achieve model oil nickel concentrations of ca. 30 and 60 ppm, respectively.

(c) Gases

All gases used were of high purity and purchased from Matheson Gas Products (Gloucester, MA). Hydrogen was at least 99.95% pure, helium 99.995% pure, and Argon 99.999% pure. Moreover, hydrogen being passed to the reactor system flowed through a packed bed of 1/8" Pt (0.5 wt%)/Al_2O_3 catalyst pellets (Engelhard Industries, Newark, NJ) for oxygen removal. The oxygen removal catalyst in the helium line comprised a mixture of CuO(10 wt%)/Al_2O_3 (1/8" pellets, Harshaw Chemical Co., Cleveland, OH) and ZnO (100%) (3/16" pellets, Harshaw). Both gas streams subsequently passed over Linde 3A molecular sieve (Union Carbide Corp., South Plainfield, NJ) for water removal.

I.C.3. Hydrodemetallation experiment-procedure

All catalysts, with the exception of Co-Mo/Al_2O_3, were prereduced at 440°C for 12 hours under flowing hydrogen in a tube furnace (Lindberg Type 55035, Watertown, WI), immediately prior to a run. The Co-Mo catalyst was used in the oxide state, and was simply preheated under helium at 440°C for

12 hours to remove water. Generally, a 10% wt loss occurred.

Typical operating conditions are given in Table 3. 400g of oil was initially charged to the batch autoclave which had been thoroughly cleaned with xylene and acetone following the previous run. With the reactor header in place, and the system pressure tested to twice its anticipated operating pressure, the reactor's contents were brought to run temperature under a helium atmosphere. The catalyst batch was rapidly removed from the tube furnace, and quickly slurried with ca. 20g of model oil. The slurry was placed in the catalyst loader. The atmosphere in the autoclave was switched from helium to hydrogen to permit the oil to become saturated with hydrogen. Ware (15) has demonstrated that an equilibrium condition, where there is 100 times as much hydrogen in the oil than porphyrin, on a molar basis, is rapidly established. A run is commenced by rapidly releasing the pressure in the autoclave (typically from 1000 to 300 psig H_2), and injecting the contents of the loader into the reactor at 1000 psig H_2 back pressure. To ensure that all catalyst was injected, the injection procedure was repeated at least three times. The run proceeded by carefully monitoring the autoclave's temperature and pressure, and collecting oil samples from the liquid sampling line. In each run 100% demetallation of the oil batch was achieved. If the same catalyst batch was to be used for the next HDM run (as was generally the case with the Group VIII metals), the oil was discharged from the reactor, through the 0.5μ filter in the liquid sampling line, thereby retaining the catalyst batch within the reactor. The reactor was immediately refilled with a fresh batch of porphyrin containing oil, and brought to the desired temperature under helium, for the next run. This run was considered

Table 3: Typical Batch Autoclave Reactor Operating Conditions

Oil	:	420g (ca. 400g is initially charged to the reactor at the beginning of any demetallation sequence; 20g is injected via the catalyst loader. In successive runs, when the same catalyst batch is retained within the reactor, 420g of oil is directly charged through the catalyst loader port.)
Catalyst	:	ca. 0.9g - HDS-16A, Co-Mo/Al_2O_3 predried under helium, 440°C, 12 hours; injected in oxide state. Group VIII and Group VIII-IB metals on alumina, prereduced under hydrogen, 440°C, 12 hours; injected reduced. All catalysts sized 74-88 μ (170-200 mesh).
Hydrogen Pressure	:	1000 psig (typically)
Temperature	:	with Co-Mo/Al_2O_3, 300-370°C
	:	with Group VIII metal/Al_2O_3, the temperature sequence for demetallizing six oil batches with the one catalyst batch is 353, 353, 336, 315, 374, and 353°C
	:	with Group VIII-IB/Al_2O_3, 337°C
Impeller Speed	:	ca. 500 rpm

initiated, when the helium was vented and replaced with hydrogen. The temperature sequence that was followed in a series of demetallation experiments, over the one catalyst batch, is detailed in Table 3.

I.C.4. Analytical

(a) Oil

The 1 ml oil samples withdrawn from the reactor were diluted with xylene (X-16, Fisher Scientific Co., Fair Lawn, NJ) so that their total nickel concentration was in the range 0-5 ppm. Atomic Absorption spectrophotometry (Perkin Elmer model 360, Norwalk, CT) was used to analyze for total nickel, and UV-Visible spectrophotometry (Bausch and Lomb, model Spectronic 2000) analyzed for nickel in its porphyrinic forms.

Ni-EP and Ni-EPH_2 absorb at 552 and 616 nm respectively. The calibration factors for these elements, at these wavelengths are, respectively, 0.478 and 0.72 absorbance units/ppm Ni.

Ni-T3MPP, Ni-$T3MPPH_2$ and Ni-$T3MPPH_4$ absorb at 526, 616 and 593 nm, respectively. The calibration factors for these porphyrins, at these wavelengths are respectively, 0.272, 0.498 and 0.77 absorbance units/ppm Ni. Further procedural details are given in Refs. 15, 53, and 54.

(b) Catalysts

The catalysts were examined, both in their fresh and aged states, by a variety of characterization techniques including, X-ray diffraction, hydrogen chemisorption, nitrogen adsorption, X-ray photoelectron spectroscopy (XPS), and scanning electron microscopy in conjunction with energy dispersive X-ray analysis (SEM/EDX). Details are briefly outlined below.

(i) X-ray diffraction

X-ray diffraction was performed on the fresh γ-Al_2O_3 supported Ru-Cu bimetallic catalysts. A Phillips diffractometer employing CuKα radiation was used. Prior to X-ray diffraction measurements the catalysts were prereduced at 450°C for three hours under flowing hydrogen.

(ii) Hydrogen chemisorption

Hydrogen adsorption isotherms, collected at room temperature, were measured on all the γ-Al_2O_3 supported Group VIII and Group VIII-IB catalyst in their unaged state. The apparatus (Digisorb 2500) is a conventional high vacuum system, where the amount of hydrogen adsorbed is determined volumetrically.

(iii) Nitrogen adsorption

Nitrogen adsorption and desorption isotherms were measured on all γ-Al_2O_3 supported Group VIII metal catalysts, at 77°K. Catalyst pretreatment involved heating the sample at 350°C for two hours under vacuum. The Digisorb 2500 apparatus (Micromeritics Instrument Corp., Norcross, GA) calculated pore size distributions, catalyst surface areas, and pore volumes from the desorption isotherm.

(iv) XPS

XPS measurements were made on two Group VIII metal catalysts (Rh/Al_2O_3, Pt/Al_2O_3) which had been aged in an HDM experiment. Measurements were also made on all the PCA supported Group VIII-IB model catalysts already described under "Catalysts."

Details of the spectrometer system and its use in analyzing model PCA catalysts have been given elsewhere (49). Briefly, the

spectrometer is a Perkin-Elmer Physical Electronics Model 548 which has been digitally interfaced to a PHI Multiple-technique Analytical Computer System (MACS) supplied by PHI (Eden Prairie, MN). MgKα radiation was the excitation source operated at 10kV and 40mA. The system pressure was 10^{-8} torr or lower. Ion sputter profiling was performed with a differentially pumped argon ion gun at 5keV. All binding energie were referenced to Au ($4f_{7/2}$) at 83.8eV.

Catalyst samples for XPS analysis were prepared as follows. The aged γ-Al_2O_3 supported catalysts were recovered from the last run oil batch by filtering the demetallized oil through a 5μ filter. The catalysts were washed in xylene in a Soxhlet extractor (Fisher Scientific, Medford, MA) and subsequently dried overnight in an oven at 80°C. Thin circular catalyst disks were fabricated by compressing ca. 0.5g of the powder at 5000 psig in a 13mm diameter homemade die. The disks were decorated with a 3mm diameter Au dot, by evaporating Au (Edwards Model 306A evaporative coater) through a hole in an aluminum foil mask placed over the entire disk. For a 48 hours period immediately prior to analysis the disks were dried in a heated (60°C) vacuum dessicator. If this drying procedure was not followed severe outgassing of the sample would prohibit operation of the spectrophotometer.

No outgassing results with the non porous model PCA catalysts. This major attribute makes them very suitable for XPS analyses. Every attempt was made to not expose these catalysts to the atmosphere as they were prepared for XPS measurements. Initially the catalysts were gold dotted, and then reduced at 500°C for four

hours in a fused silica boat, in a tube furnace under flowing hydrogen. The catalysts were cooled to room temperature under flowing hydrogen, and then carefully removed from the furnace with tweezers under an inert Argon atmosphere. The argon atmosphere was maintained by a glove bag, into which the furnace had been placed. The PCA catalysts were transported to the XPS apparatus in the glove bag and placed on the spectrometer mounts, all under argon.

(v) SEM/EDX

Scanning electron microscopy (SEM)--Energy Dispersive X-ray analysis (EDX) on an AMR Model 1000A SEM, equipped with a Tracor Northern TN2000 X-ray analyzer was used to examine the catalysts' surface morphology and intrapellet metal profiles. Catalysts which had been aged in the HDM environment were cleaned with xylene in a Soxhlet extractor (see XPS section). The procedure used to mount and section the cleaned catalyst particles is the same as before (15, 54, 55). For X-ray analysis the beam energy was 20keV, and X-ray counts were accumulated for 60 seconds.

I. D. Results

We have investigated the intrinsic kinetics of hydrodemetallation (HDM) of Ni-EP and Ni-T3MPP over an industrial Co-Mo/Al_2O_3 catalyst, and Group VIII metals/Al_2O_3 catalysts. Both porphyrins (Fig. 1) possess similar central aromatic cores but have different substitution patterns around their periphery. As will be seen these slight structural differences dramatically modify the reaction pathway.

I. D. 1. Ni-Etio porphyrin HDM over Group VIII metals

Ni-EP HDM kinetics were initially reported by Agrawal (54), who worked exclusively with the oxide form of Co-Mo/Al_2O_3 (HDS-16A). His major

finding was that the Ni-EP molecule demetallized through an hydrogenated intermediate (Ni-EPH_2) not originally present in the oil. Agrawal's (54) mechanism is shown in Fig. 7. The first reaction step involves reversible hydrogenation of a peripheral double bond in one of the four pyrrole rings making up the macrocycle, to form Ni-Etio chlorin (Ni-EPH_2). Ni-EPH_2 then undergoes hydrogenolysis to deposit nickel on the catalytic surface.

In this work Ni-EP was demetallized over all the Group VIII metal on γ-Al_2O_3 catalysts listed in Table 1. In each case the HDM mechanism of Fig. 1 was followed. This was verified by our ability to sum the porphyrinic species nickel concentrations, as measured by UV-Vis spectrophotometry, to obtain the oils total nickel concentration, which was independently measured by atomic absorption spectrophotometry. Also, visible spectra of the oil, withdrawn from the reactor at all levels of Ni-EP conversion, showed only absorption peaks due to Ni-EP (517, 553 nm) and Ni-EPH_2 (626 nm) (56) (see Fig. 8).

Some typical plots of total nickel, Ni-EP and Ni-EPH_2 concentration versus reaction time are shown in Figs. 9 to 11. Fig. 9 is for catalyst HDS-16A, the commercial Co-Mo/Al_2O_3 hydrotreating catalyst; Fig. 10 is for Pd and Ru on alumina, Group VIII metals, second transition series; Fig. 11 is for Re, Os and Pt on alumina, Group VIII metals, third transition series. All the data were collected at 374°C, 1000 psig hydrogen pressure, similar oil to catalyst mass ratios, and total nickel starting concentration (ca. 30 ppm Ni).

The solid lines in Figs. 9 to 11 represent model calculations based on the kinetic scheme of Fig. 7. Each reaction step is assumed to be first order in porphyrinic species concentration. The rate coefficients (k's)

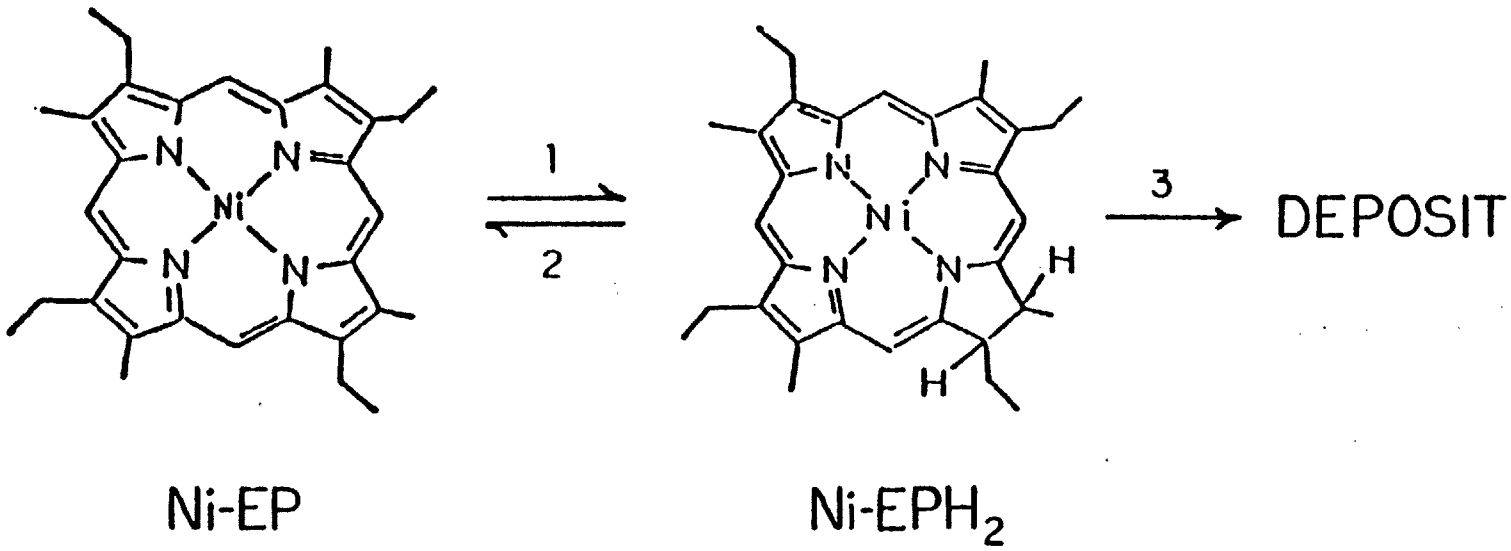

Figure 7: Reaction sequence for Ni-etioporphyrin hydrodemetallation.

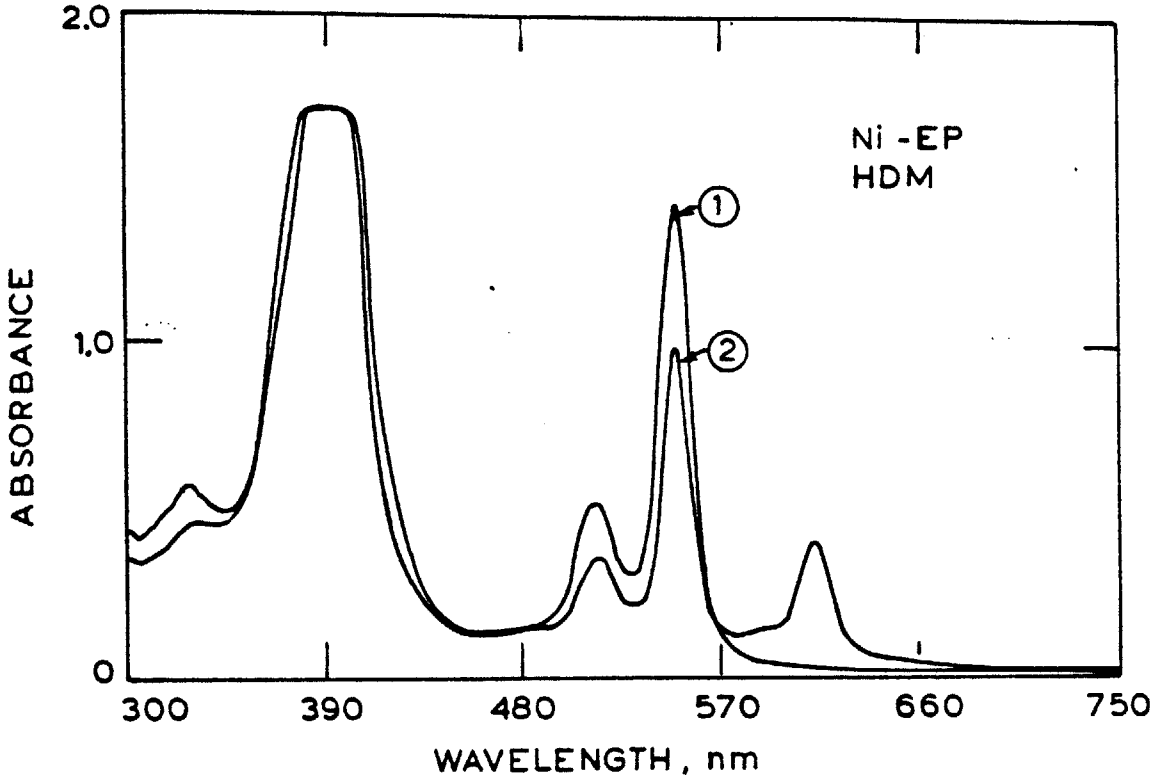

Figure 8: Absorption spectra of oil samples taken during demetallation of Ni-EP over Pd/Al_2O_3 at 353°C, 1000 psig H_2. Background is xylene. Spectrum 1 is Ni-EP only (peaks at 517 and 553 nm) and was taken before catalyst was injected into the reactor. Spectrum 2, taken after 0.25 h reaction time, contains an extra peak at 616 nm due to $Ni\text{-}EPH_2$.

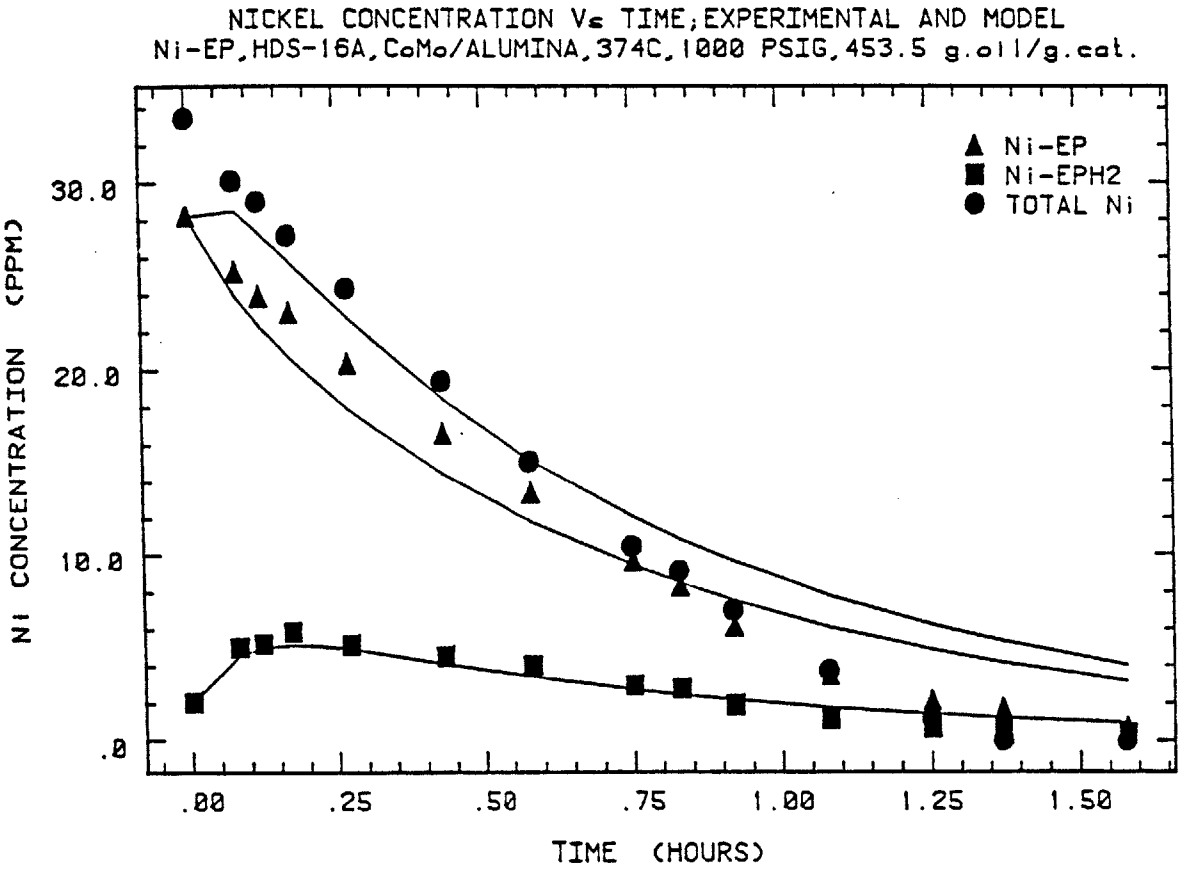

Figure 9: Concentration versus time results for Ni-EP demetallation over Co-Mo/Al_2O_3 catalyst at 374°C, 1000 psig H_2, 453.5 g. oil/g. cat. Solid lines are model calculations.

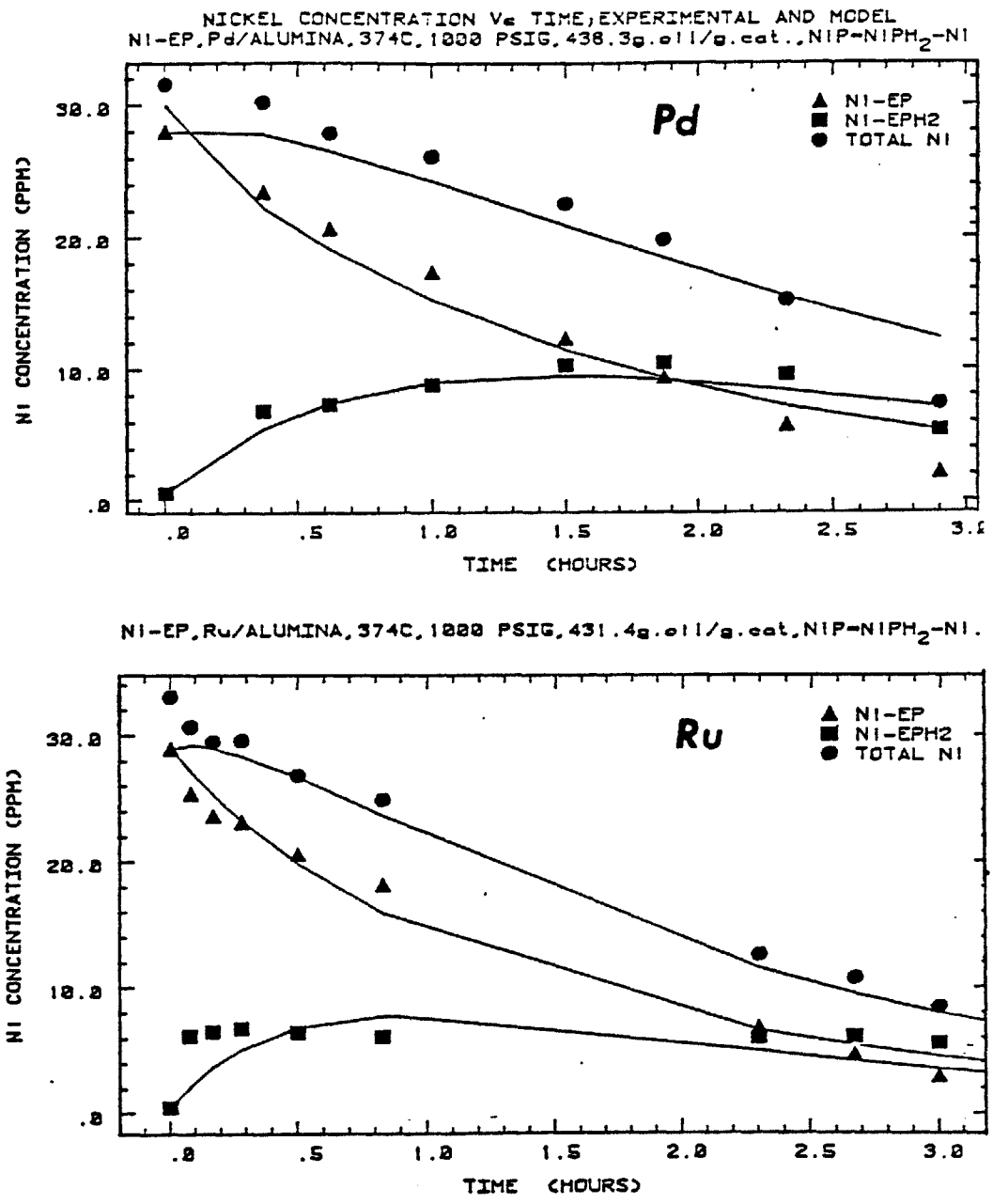

Figure 10: Concentration versus time results for Ni-EP demetallation over Pd (top) and Ru (bottom) on alumina, at 374°C, 1000 psig H_2 and ca. 435 g. oil/g. cat. Solid line are model calculations.[2]

a

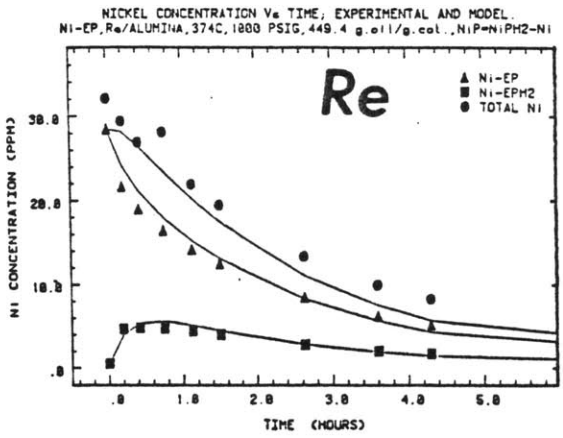

b

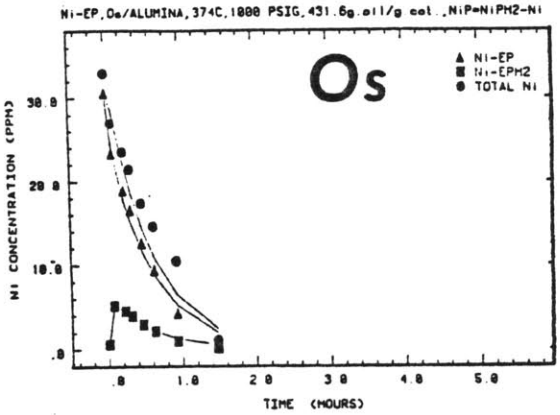

c

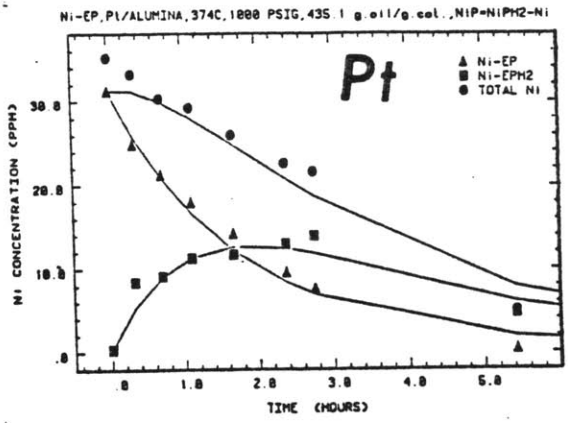

Figure 11: Concentration versus time results for Ni-EP demetallation over (a) Re, (b) Os, and (c) Pt on alumina at 374°C, 1000 psig H_2 and ca. 435 g. oil/g. cat. Solid lines are model calculations.

were evaluated by the Himmelblau-Jones-Bischoff technique (57) and the theoretical concentration v's time solutions are then evaluated, with these k's, using the Wei-Prater (58) solution to the coupled set of rate equations. The computer programs are listed in the theses of Agrawal (54) and Ware (15). Representative rate constants for Ni-EP HDM over the Group VIII metal catalysts at 353°C and 1000 psig H_2 calculated by this procedure are given in Table 3A.

The general pattern in Ni-EP HDM is that there is a rapid build-up of the intermediate Ni-EPH_2 at short times. The discrepancy between total Ni and Ni-EP readings can always be accounted for by the Ni in Ni-EPH_2. The gradual decline of Ni-EP, and the maximum exhibited by Ni-EPH_2 are characteristic of a sequential type mechanism. Catalysts which Sinfelt (19) has noted possess a strong hydrogenation capability (Fig. 3) such as Pt and Pd generate a larger pool of the Ni-EPH_2 hydrogenated intermediate, than do metals of the first and second columns of Group VIII (compare Figs 11a and 11b). The model fit, in all cases, is excellent.

Total Ni and Ni-EP removal data over second and third transition series Group VIII metal catalysts, is plotted in first order kinetic plots in Fig. 12. In both Figs. 12(a) and (b) the process conditions are 336°C, 1000 psig H_2, ca. 440 g. oil/g. cat. and deposited nickel loadings are in the range of 2.8-5.0 wt % (i.e. the catalyst is not fresh). The straight line data fit is adequate and first order rate constants calculated from the slopes of the lines, are listed in Table 4. They provide a quick method of comparing the activity and hydrogenation selectivity of the catalysts in each Group VIII transition series.

For a given catalyst the porphyrin removal rate constant always

Table 3A: Representative rate constants in Ni-EP HDM. Fresh catalysts, prereduced; 353°C, 1000 psig H_2, 30 ppm Ni starting concentration. Units: g.oil/g.cat.h.

	Co-Mo(HDS-16A)	Co	Ni
k_1	787	467	298
k_2	422	981	690
k_3	1990	5749	127

	Ru	Rh	Pd
k_1	760	420	278
k_2	1813	798	472
k_3	1104	761	203

	Re	Os	Ir	Pt
k_1	154	411	452	332
k_2	288	703	827	647
k_3	11	16797	18256	4649
Periodic Position	VIIB	$VIII_1$	$VIII_2$	$VIII_3$

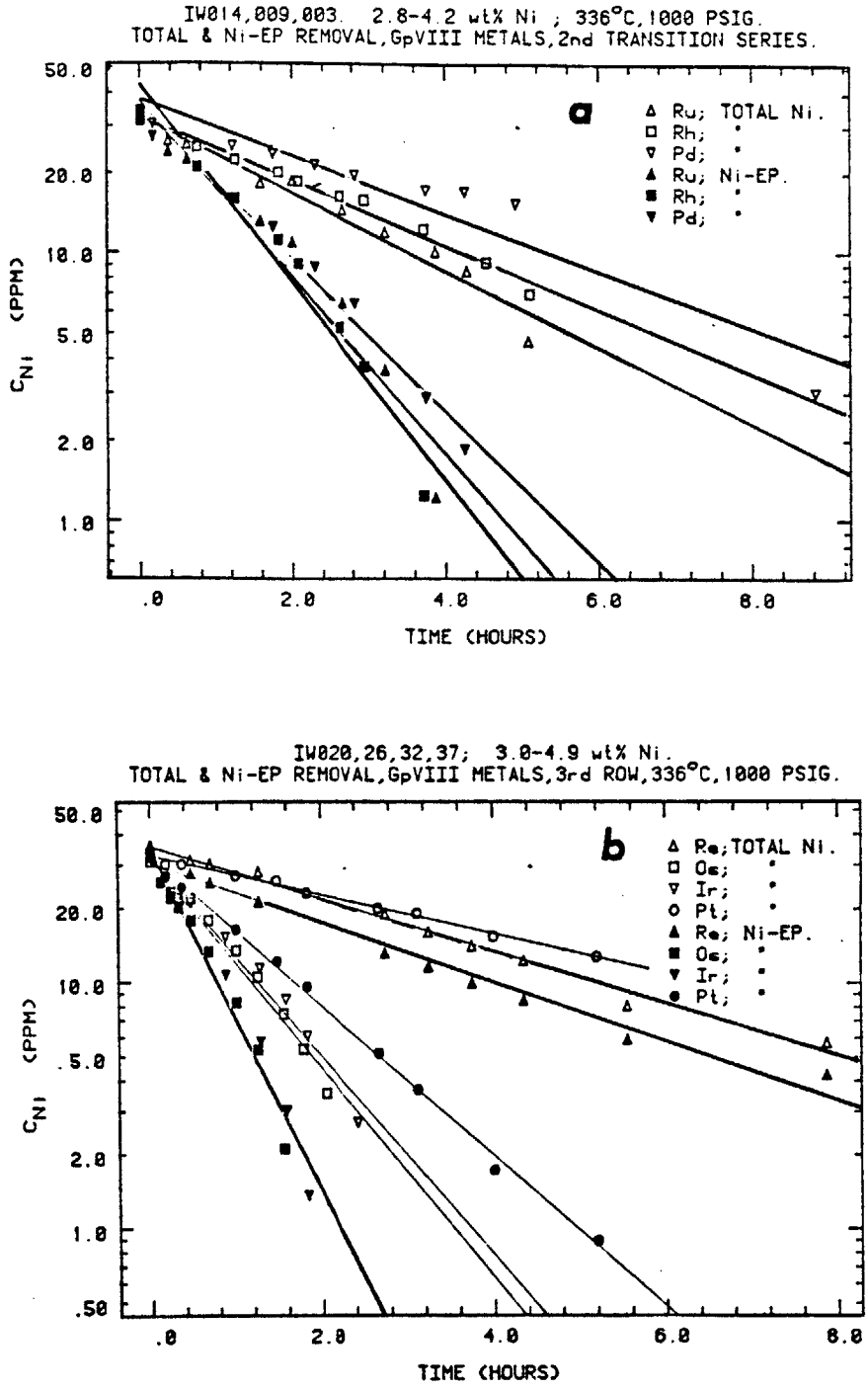

Figure 12: (a) First order kinetic plot of Ni-EP demetallation over second transition series, Group VIII metals. Data are for total Ni and Ni-EP removal. Conditions: 336°C, 1000 psig H_2 and 435 g. oil/g. cat.

(b) Same plot as (a) for third transition series, Group VIII metals in Ni-EP demetallation. Conditions: 336°C, 1000 psig H_2 and 430 g. oil/g. cat.

Table 4:

Representative values of 1st order rate constants (total nickel and nickel porphyrin removal) in Ni-EP HDM. Process conditions: 336°C, 1000 psig H_2, nickel deposits on catalyst are in weight range 2.8-4.9 wt % Ni, and oil to catalyst ratio is 440 g.oil/g.cat. Each catalyst is loaded with 5 wt % of the catalytically active metal, supported on γ-Al_2O_3

Run No.	Catalytically active metals (5 wt % loading Al_2O_3)	First order rate constants (g.oil/g.cat. hr.) Ni-EP ($k_{1,NiP}$)	Total Ni ($k_{1,Ni}$)	$\frac{k_{1,Nip}}{k_{1,Ni}}$
IW014	Ru	168.2	62.0	2.7
IW009	Rh	175.3	53.8	3.3
IW003	Pd	130.7	29.4	4.4
IW020	Re	54.2	47.4	1.1
IW026	Os	389.9	185.9	2.1
IW032	Ir	344.1	221.0	1.6
I0037	Pt	133.5	34.63	3.9
IW149	Co	160.9	125.3	1.3
IW145	Ni	12.0	7.9	1.5
IW106	Co-Mo (HDS-16A)	130.6	125.5	1.0
IW070	Al_2O_3	17.7	11.4	1.6

exceeds the total nickel removal rate constant. This is because of Ni-EPH_2 production. The Group $VIII_3$ meals Pd and Pt, previously noted by Sinfelt (19,25) as possessing good hydrogenation activity and poor hydrogenolysis activity relative to their counterparts in the same long period of the Periodic Table (see Fig. 3), exhibit the highest value of the rate constant ratio $k_{1,NiP}/k_{1,Ni}$. With Pd the ratio is 4.4, and with Pt it is 3.9. In contrast the value is ca. 1 for the commercially available Co-Mo/Al_2O_3. This is indicative of the ability Pt and Pd have to accelerate the hydrogenation step in the mechanism displayed in Fig. 7, while suppressing the terminal hydrogenolysis step. The order of activities for total metal removal follow the patterns:

First Transition Series	Co>>Ni
Second Transition Series	Ru~Rh~Pd
Third Transition Series	Ir~Os>>Re~Pt

The variation of the first order kinetic rate constants with periodic position, at different reaction temperatures is shown in Fig. 13, for the second and third transition series elements.

A major problem in the collection of data in HDM studies is being certain that the catalyst has attained a steady state condition. In reality, a true steady state catalyst surface condition can never be achieved since carbon and metals are continually being deposited, thereby altering the integrity of the catalytic surface. Carbon deposits rapidly build up to a steady state equilibrium loading (49), whereas the nickel deposits irreversibly, its loading continually increasing with time. The concensus in the literature is that coking always causes deactivation (59-61) whereas metal deposition may either increase or decrease the

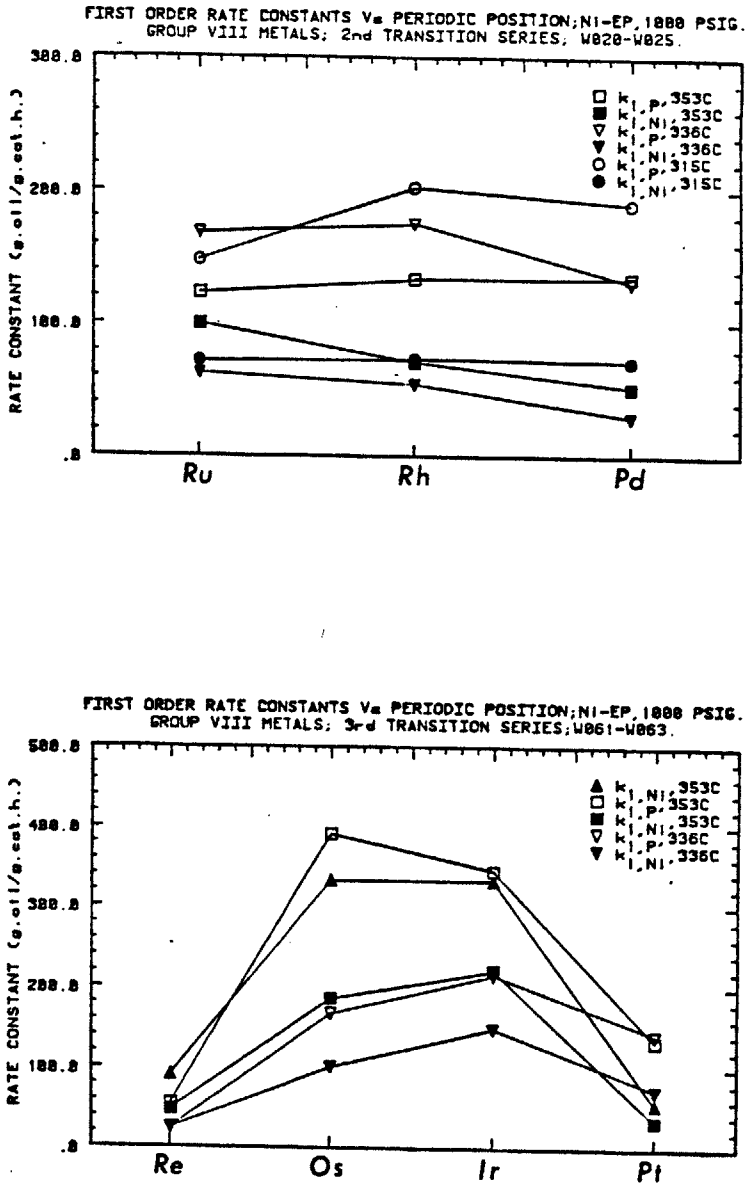

Figure 13: Variation of first order Ni-EP demetallation rate constants (total Ni and Ni-EP removal) as a function of periodic position; top--second transition series; bottom--third transition series. Data are for various temperatures (315-353°C) and 1000 psig H_2.

catalyst's activity. Tamm et al's (17) explanation for the initial deactivation of hydroprocessing catalysts is that the Ni and V cover active sites and exhibit a level of activity less than that of the original metals (Co and Mo). In contrast, Sie (62) has demonstrated the autocatalytic nature of metal removal reactions by using bare alumina, which gradually exhibited metals removal activity when exposed to a residuum under hydroprocessing conditions. We have also demonstrated (63) that autocatalysis is present in our model HDM studies. Ni-T3MPP HDM rates over both Mo and Co-Mo/Al_2O_3 catalysts increased with Ni laydown.

In this study, however, we believe our kinetic data have been collected under conditions of practically steady state catalytic activity. The temperature sequence we always obeyed when demetallizing six successive oil batches is given in Table 3. To ensure that the catalytic activity had not appreciably changed when running at different temperatures we always ran our sixth experiment at the same temperature as runs one and two. A representative plot of how the first order rate constants for total Ni and Ni-EP removal changed with the weight % Ni loading on the catalyst (estimated by mass balance) is shown in Fig. 14. Catalyst activity does decrease significantly over the first run, where about 2 wt % Ni is deposited. Thereafter the activity appears to stabilize; that is, the catalytic activities of our supported Group VIII metals is uniform as their nickel loadings increased from ca. 2 to 8 wt. %. It is within this nickel loading range, that the temperature of our batch run experiments was varied in order to generate Arrhenius plots.

Representative Arrhenius plots, for rate constants of the Ni-EP reaction pathway of Fig. 7, over the Group VIII metal catalysts and

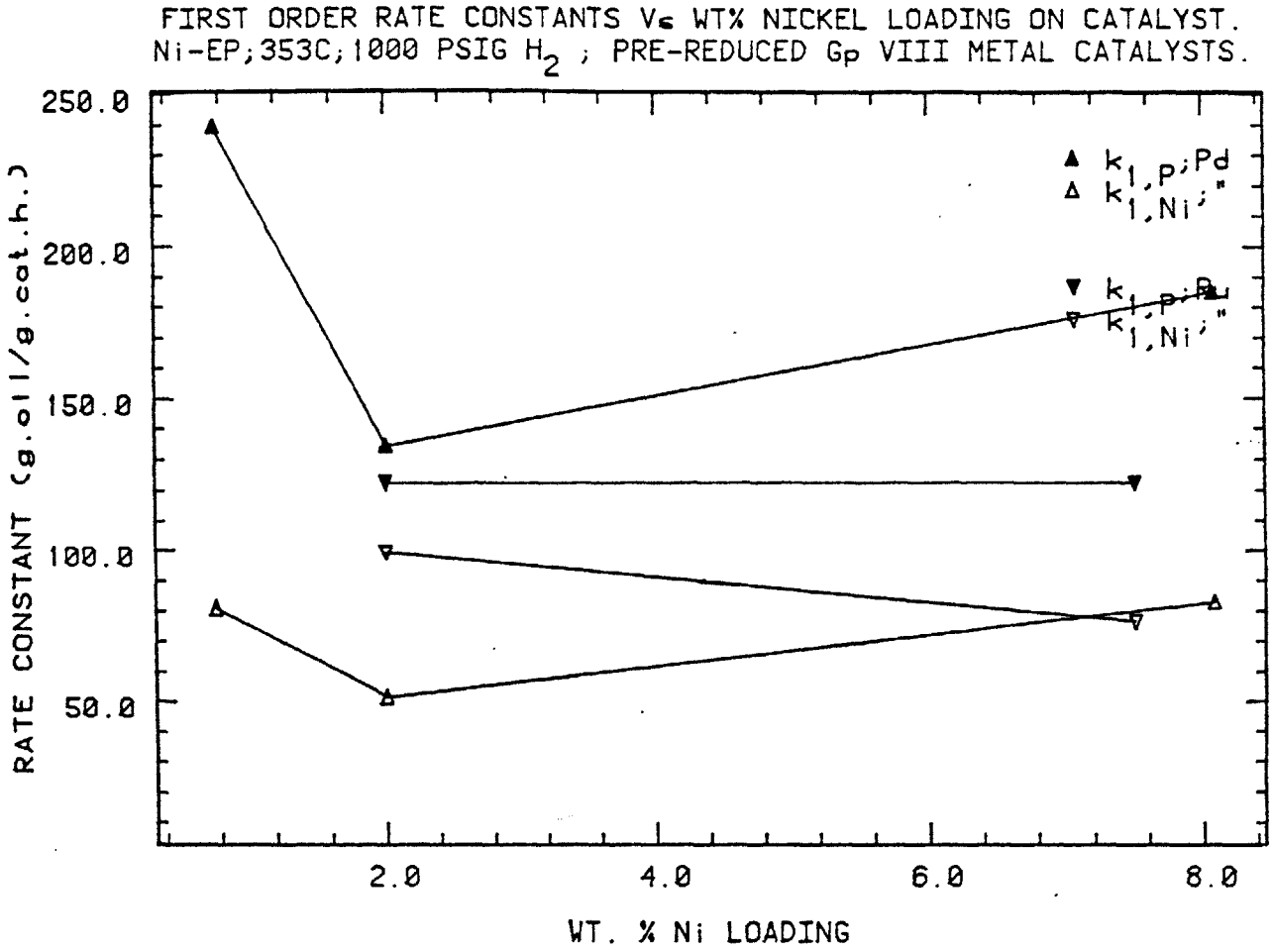

Figure 14: Effect of Group VIII metal catalysts' nickel loading on activity. Kinetic data are shown for Ru and Pd catalysts involved in Ni-EP demetallation at 353°C, and 1000 psig H_2.

Co-Mo/Al_2O_3 (HDS-16A) are shown in Figs. 15 to 17. The total Ni and Ni-EP first order removal rate constants are also graphed. Activation energies are given in Table 5. Activation energies for the Ni and Rh catalysts are not reported. We found these values to be unrealistically high (i.e. ca. 40 kcal/mole) and attribute this to the extremely high oil to catalyst mass ratio used in these two runs (ca. 8500 g oil/g. cat.). At these low catalyst loadings, the rate of the homogeneous reaction (which will have a high activation energy) may be faster than the heterogeneous reaction.

With reference to Table 5, we note that all the HDM reaction steps over all Group VIII metals have lower activation energies than when the catalyst is the commercial Co-Mo/Al_2O_3. The E_A values obtained over the Group $VIII_3$ metals Pd and Pt are the smallest. Metals which Sinfelt (19) has found possess good catalytic activity for hydrogenolysis and in contrast are relatively poor for hydrogenation (namely, Ru, Rh, Re, Os, Ir) all have activation energies for the hydrogenolysis step (k_3) of Fig. 7, much less than the E_A values for the initial Ni-EP hydrogenation step. In contrast, Pd which should exhibit good hydrogenation activity, according to Sinfelt (19), has the relative magnitude of its activation energies for hydrogenolysis reversed. This is expected if hydrogenation is facile over Pd.

The relative magnitudes of the rate constants k_1 (hydrogenation) and k_3 (hydrogenolysis) in Ni-EP HDM can also be gleaned from the Arrhenius plots, Figs. 15 to 17. The rate limiting step in the overall HDM scheme is Ni-EP hydrogenation, <u>except</u> with the Group $VIII_3$ metals as catalysts. Their strong hydrogenation activity causes the hydrogenolysis step (k_3) to be rate limiting. Research from this laboratory to-date (8,54), using the

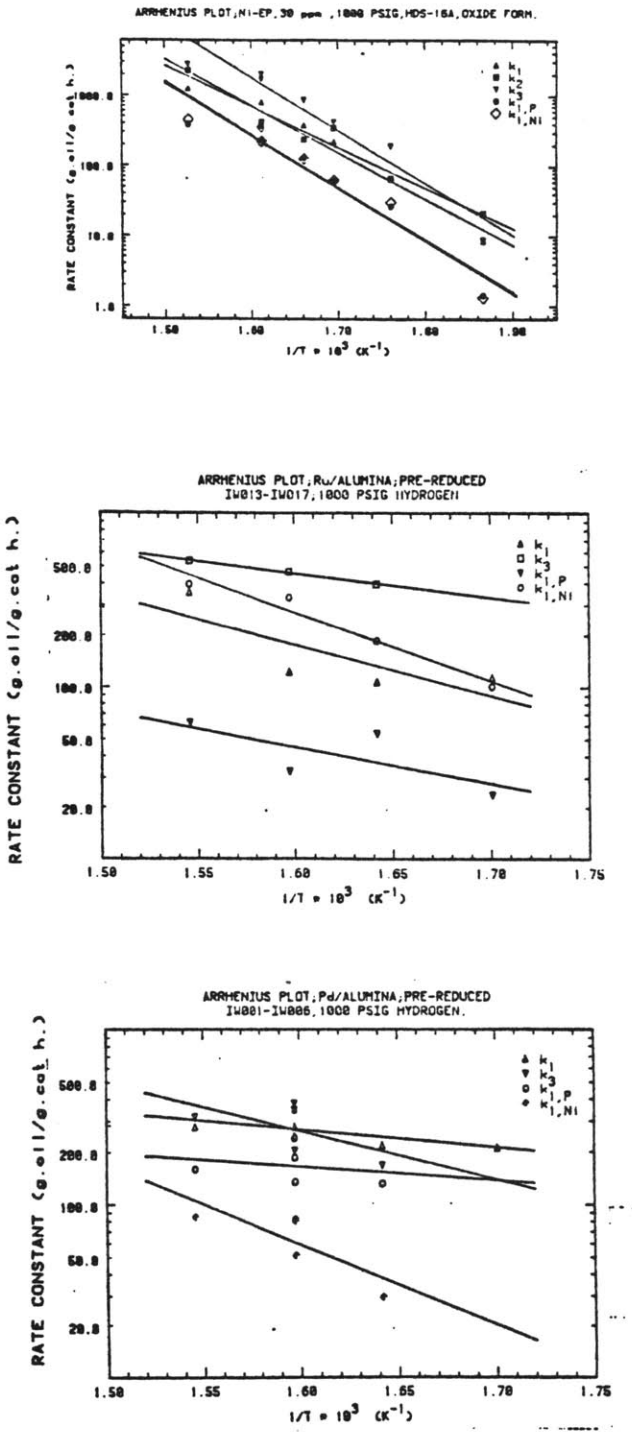

Figure 15: Arrhenius plots for the first order rate parameters for Ni-EP demetallation at 1000 psig H_2. Top: Co-Mo/Al_2O_3; Middle: Ru/Al_2O_3; Bottom: Pd/Al_2O_3.

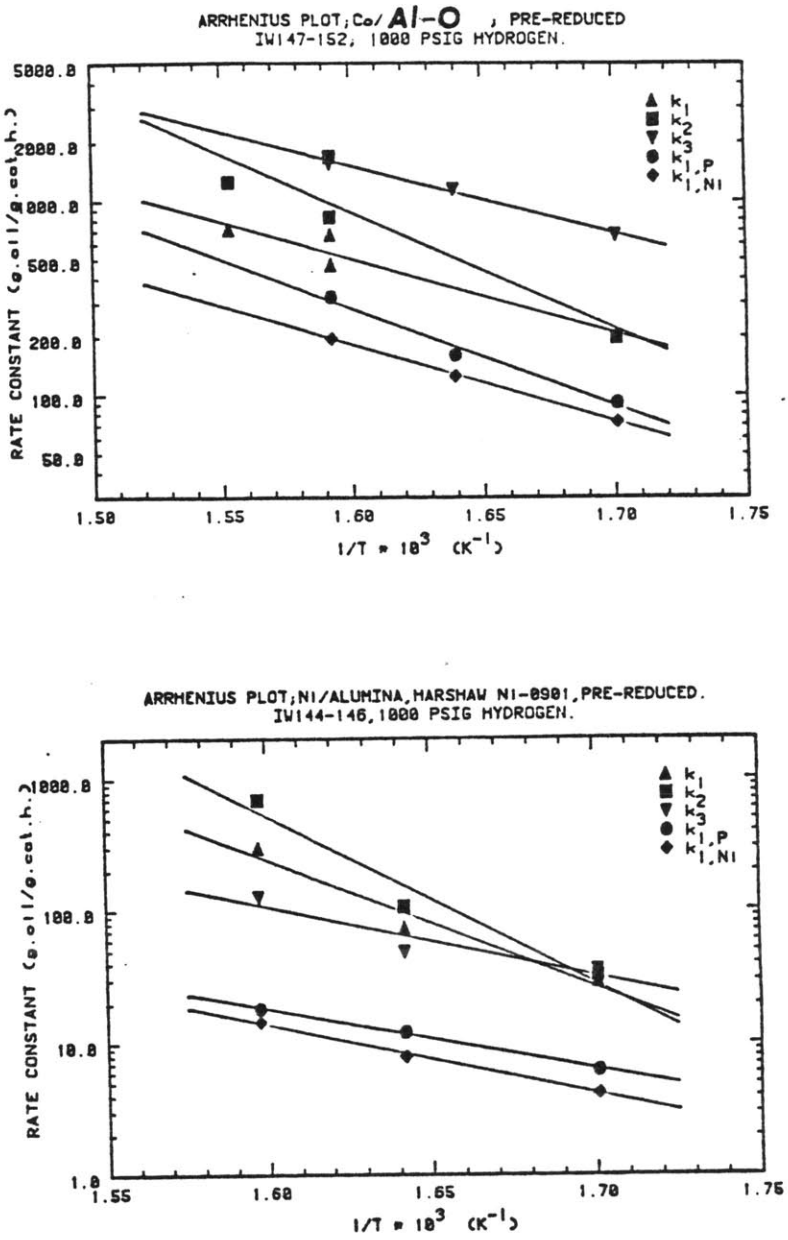

Figure 16: Arrhenius plots for the first order rate parameters for Ni-EP demetallation at 1000 psig H_2. Top: Co/Al_2O_3; Bottom: Ni/Al_2O_3.

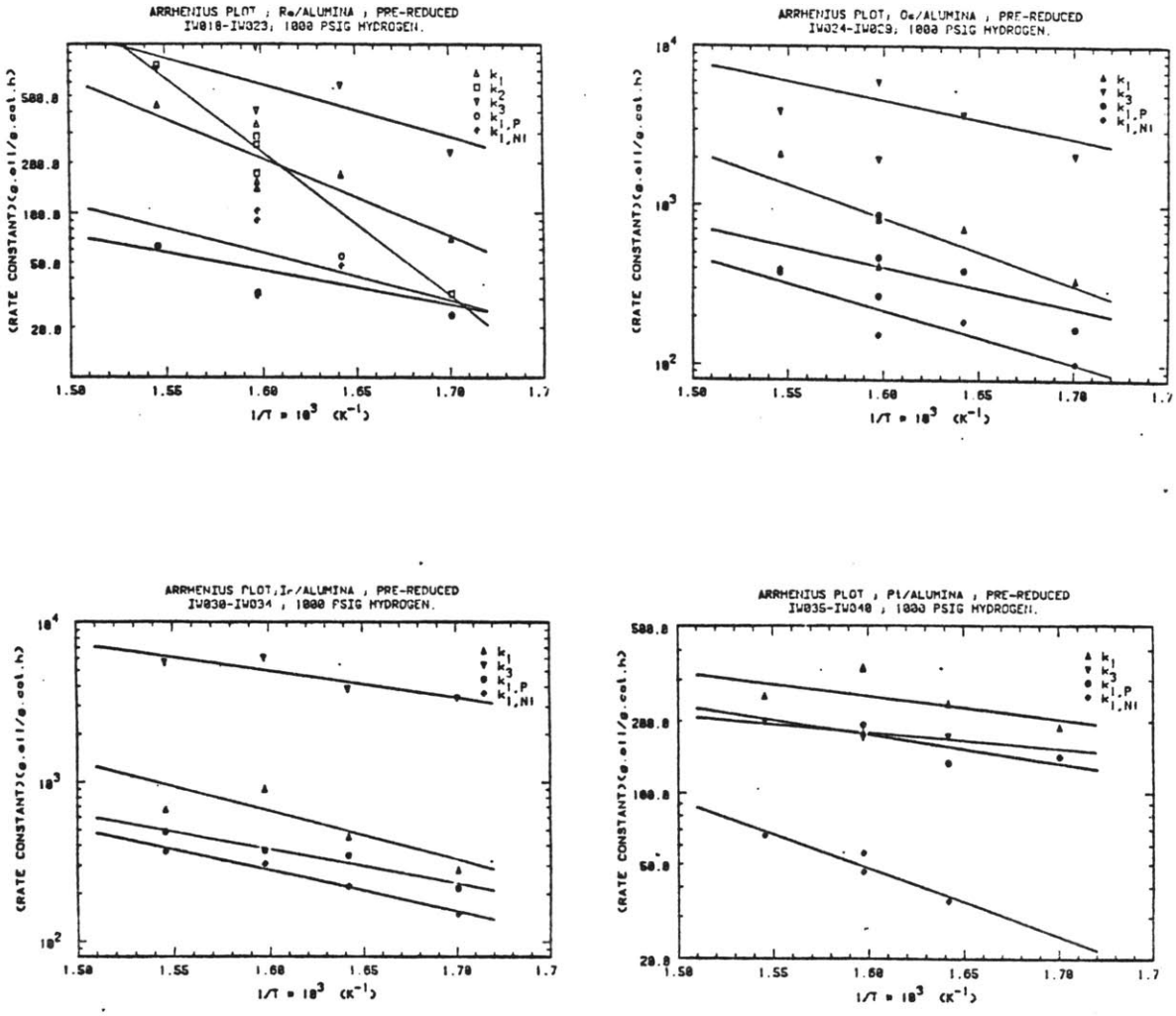

Figure 17: Arrhenius plots for the first order rate parameters for Ni-EP demetallation at 1000 psig H_2. Top: Re/Al_2O_3 (L), Os/Al_2O_3 (R); Bottom: Ir/Al_2O_3 (L), Pt/Al_2O_3 (R).

Table 5: Activation Energies (E_A) for Rate Constants; k_1, k_3, $k_{1,NiP}$, $k_{1,Ni}$; Ni-EP; 1000 psig H_2, ca. 30 ppm Ni starting concentration. Units: kcal/mole

	Co-Mo(HDS-16A)	Co	Ni
k_1	30.4	17.4	
k_3	34.6	15.8	
$k_{1,NiP}$	34.1	23.0	
$k_{1,Ni}$	34.7	18.2	

	Ru	Rh	Pd
k_1	13.6		4.8
k_3	6.4		12.7
$k_{1,NiP}$	9.8		3.7
$k_{1,Ni}$	18.2		21.1

	Re	Os	Ir	Pt
k_1	21.5	19.3	14.1	4.6
k_3	14.2	11.0	7.7	3.2
$k_{1,NiP}$	9.8	11.7	9.9	5.6
$K_{1,Ni}$	13.4	15.4	11.7	13.1
Periodic Position	VIIB	$VIII_1$	$VIII_2$	$VIII_3$

traditional Co-Mo catalyst has always resulted in the finding that Ni-EP hydrogenation is rate limiting. This is the first occasion we have succeeded in forcing the [hydrogenolysis (k_3)/hydrogenation (k_1)] rate constant ratio less than one, during Ni-EP HDM, thereby making the hydrogenolysis step rate limiting.

The hydrogenolysis selectivity (k_3/k_1) for the Group VIII metal catalysts in Ni-EP HDM is plotted as a function of periodic position in Figs. 18 and 19. These figures show the selectivity ratio at various reaction temperatures (315-374°C), weight percent nickel loadings and initial catalyst conditions (Figs. 18 and 19a are for prereduced catalyst; Fig. 19b is for oxide catalyst). Selectivities are also listed in Table 5A for fresh forms of the catalyst, while Fig. Table 5A shows the change in the selectivity ratio (k_3/k_1) as nickel accumulates on the catalyst. Accompanying the data for each transition series is a graph of how the % d character varies with periodic position. The general trends are obvious and show that Sinfelt's findings (Figs. 2 and 3) relating the % d character of the transition elements' metallic bond to its hydrogenolysis activity are also applicable when assessing the selectivity of these same elements in catalyzing the HDM reaction.

Elements such as Ru and Rh selectively enhance hydrogenolysis relative to hydrogenation, whereas Pd, with its good hydrogenation activity has a lower k_3/k_1 ratio (Fig 18a). Our kinetic data is most complete over the elements of the third transition series (see Fig. 18b). Re and Ir, which have the maximum values of % d character generate values of the k_3/k_1 ratio as high as 40. For example, from Fig. 18b, we note that with the fresh catalysts, conducting Ni-EP HDM at 353°C, and only accumulating an

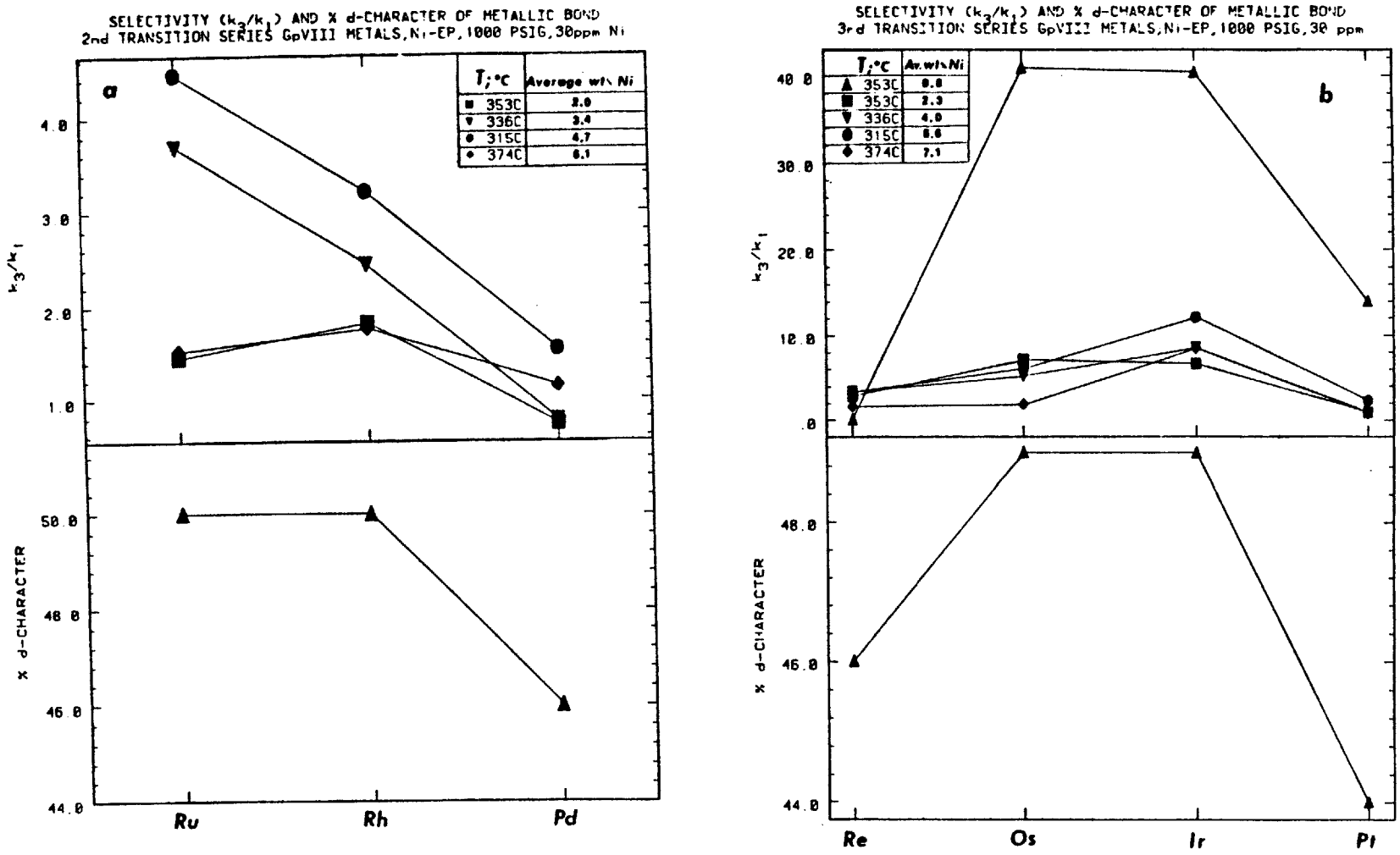

Figure 18: Selectivity of Group VIII metals for Ni-EP hydrogenolysis in relation to periodic position and percentage d-character of the metallic bond. (a) Second transition series, (b) Third transition series. Data are at 1000 psig H_2 and various temperatures over prereduced catalysts.

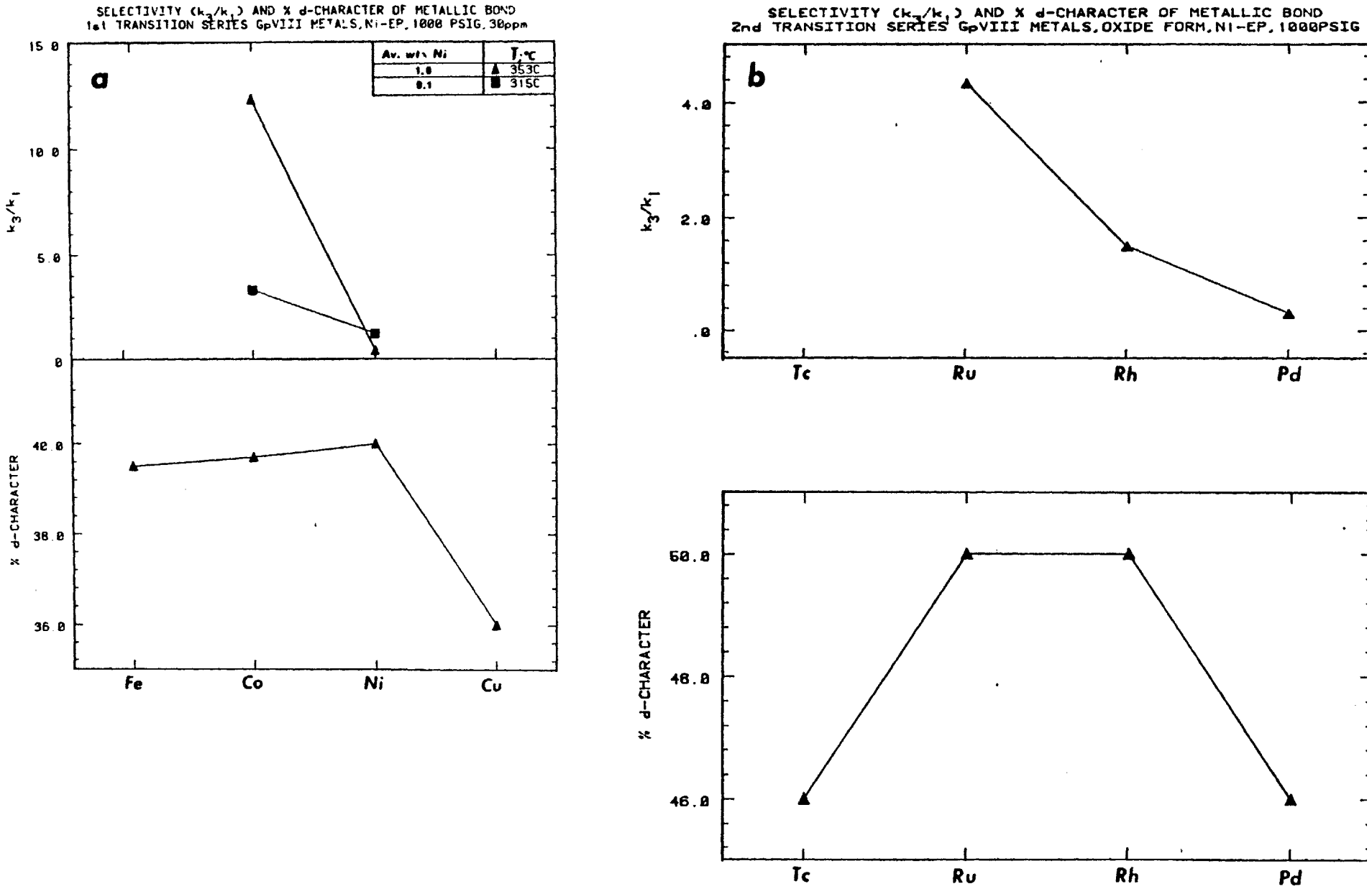

Figure 19: Selectivity of Group VIII metals for Ni-EP hydrogenolysis in relation to periodic position and percentage d-character of the metallic bond. (a) First transition seies, prereduced catalyst, (b) Second transition series, oxide catalyst. Data are for 1000 psig H_2 and various temperatures.

Table 5A

Selectivity ratio (k_3/k_1) as a function of the periodic position of the catalytic metal. Selectivities are for Ni-EP HDM at 353°C, 1000 psig H_2, and 30 ppm Ni starting concentration. All catalysts were fresh and prereduced, and accumulated ca. 2 wt % Ni during experiment.

VIIB	$VIII_1$	$VIII_2$	$VIII_3$
		Co 12.31	Ni 0.43
	Ru 4.45	Rh 3.21	Pd 1.54
Re 0.07	Os 40.87	Ir 40.39	Pt 14.01

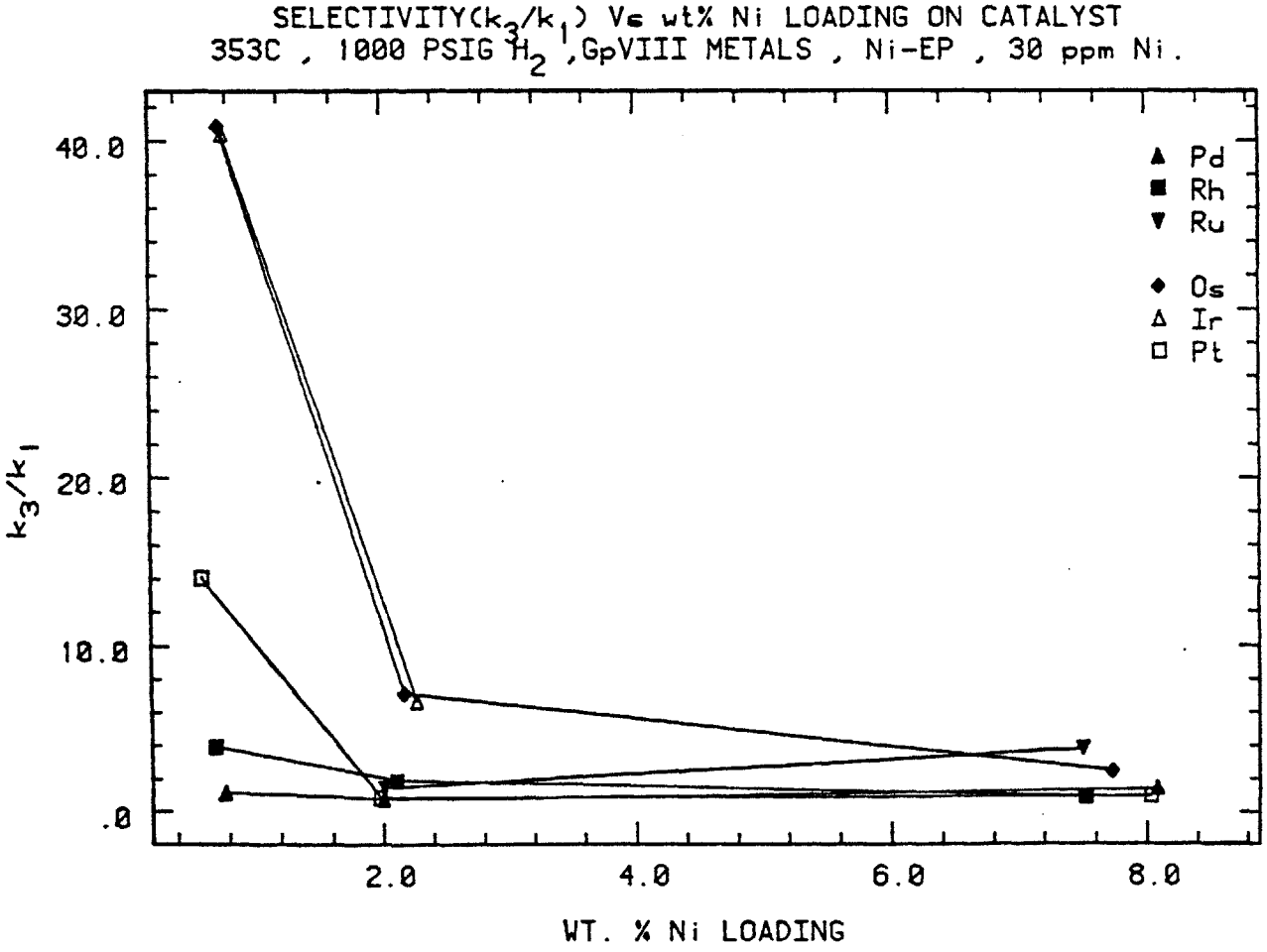

Figure Table 5A: The effect of nickel deposit loading on Group VIII metal catalysts selectivity ratio , k_3/k_1. The data is for Ni-EP HDM at 353°C, and 1000 psig H_2.

average nickel loading of 0.74 wt % during the batch run, the change in the selectivity, k_3/k_1, between Re and Os is a factor of 584. (0.07 to 40.87).

I. D. 2. Ni-tetra(3-methylphenyl) porphyrin HDM over Group VIII metals

A less extensive investigation of Ni-T3MPP demetallation over the Group VIII metal catalysts was performed. Ware (15) has made a comprehensive study of the HDM mechanism of Ni-T3MPP over Co-Mo/Al_2O_3 catalyst. While the global HDM scheme of porphyrin hydrogenation followed by hydrogenolysis and metal deposition still persists, the actual mechanism is more complex than for Ni-EP, and involves more intermediates, and a branched pathway. The reaction mechanism is depicted in Fig. 20. Ni-T3MPP is hydrogenated to Ni-chlorin (Ni-PH_2) and Ni-isobacteriochlorin (Ni-PH_4). As noted in the Analytical section each of these species absorb at distinctly different wavelengths, thereby making their identification and measurement straightforward (56). UV-Visible spectra of oil samples in the progress of reaction are shown in Fig. 21. Absorption peaks for Ni-T3MPP (526nm), Ni-T3MPPH_2 (626nm) and Ni-T3MPPH_4 (593nm) are evident. Scheer (64) has noted that central metals favor the hydrogenation of adjacent pyrrole groups, when forming tetrahydroporphyrins.

Typical concentration versus time plots for Ni-T3MPP demetallation at 336°C, and 1000 psig H_2 over three of the supported Group VIII metal catalysts, namely Re, Rh and Pd, are shown in Fig. 22. The points represent experimental measurements, whereas the solid lines are model calculations.

An important feature of Fig. 22 is that not all the dissolved Ni within the oil (diamond symbol) is accounted for by summing the nickel

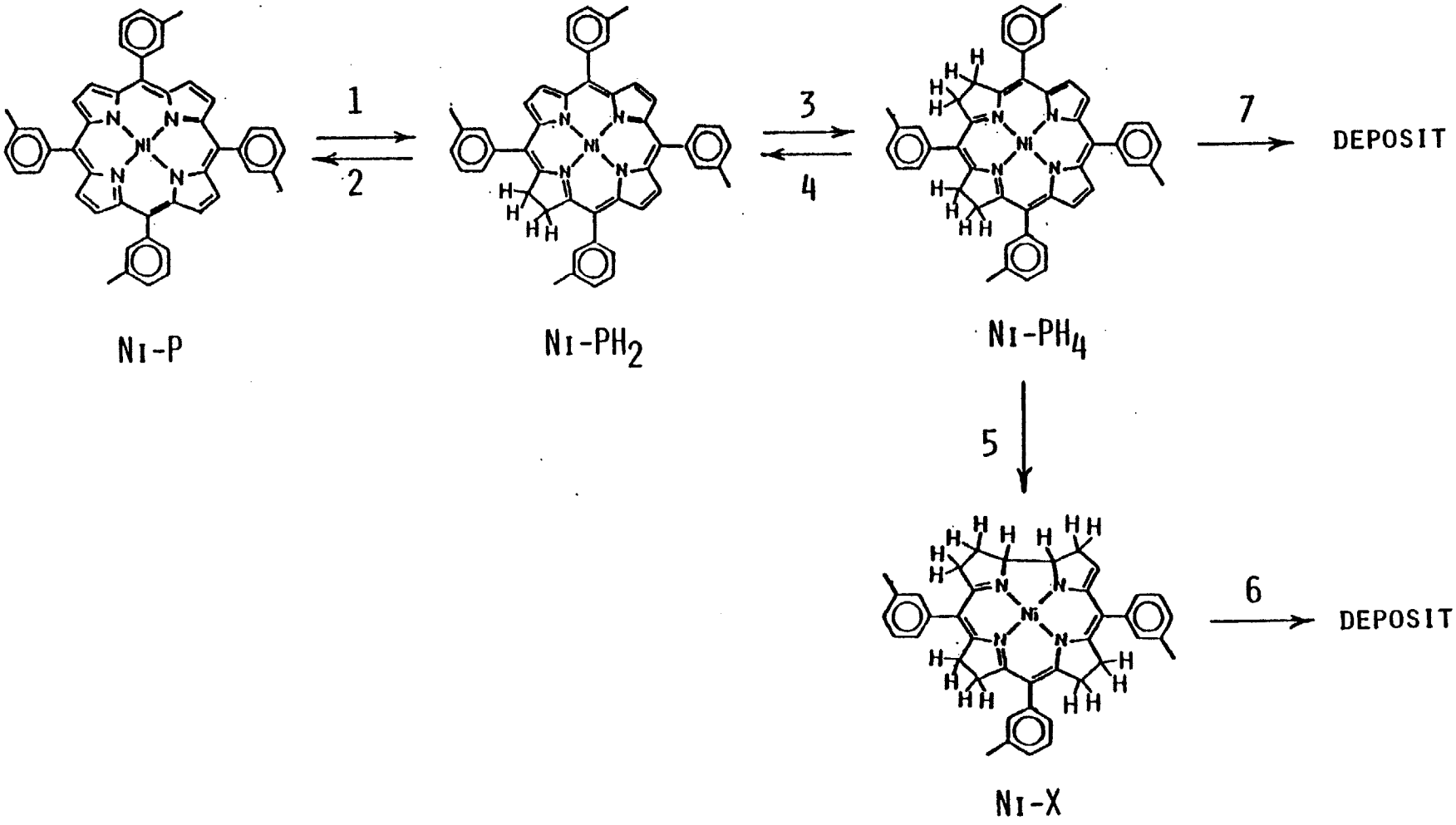

Figure 20: Reaction sequence for Ni-tetra (3-methylphenyl) porphyrin.

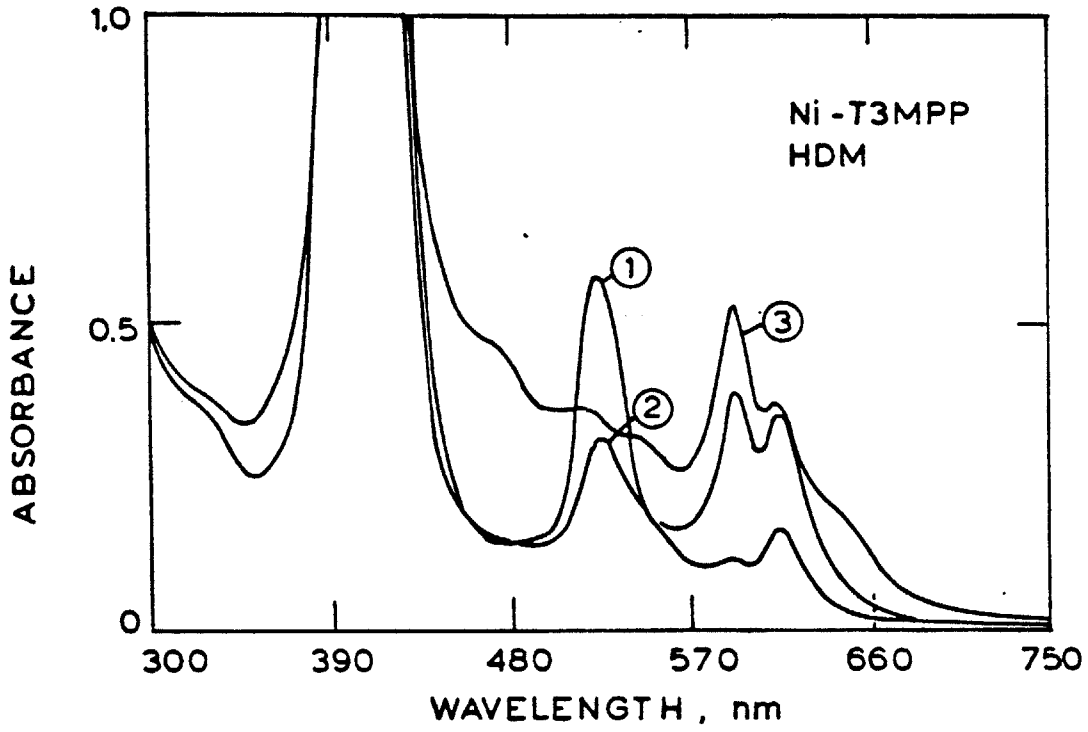

Figure 21: Absorption spectra of oil samples taken during demetallation of Ni-T3MPP over Rh/Al_2O_3 at 336°C, 1000 psig H_2. Background is xylene. Spectrum 1 is primarily Ni-T3MPP (peak at 526 nm) and was taken immediately after catalyst injection. Spectra 2 and 3, taken at run times of 0.5 h and 6.25 h, respectively, have extra peaks at 593 nm and 616 nm due to Ni-T3MPP isobacteriochlorin and Ni-T3MPP chlorin, respectively.

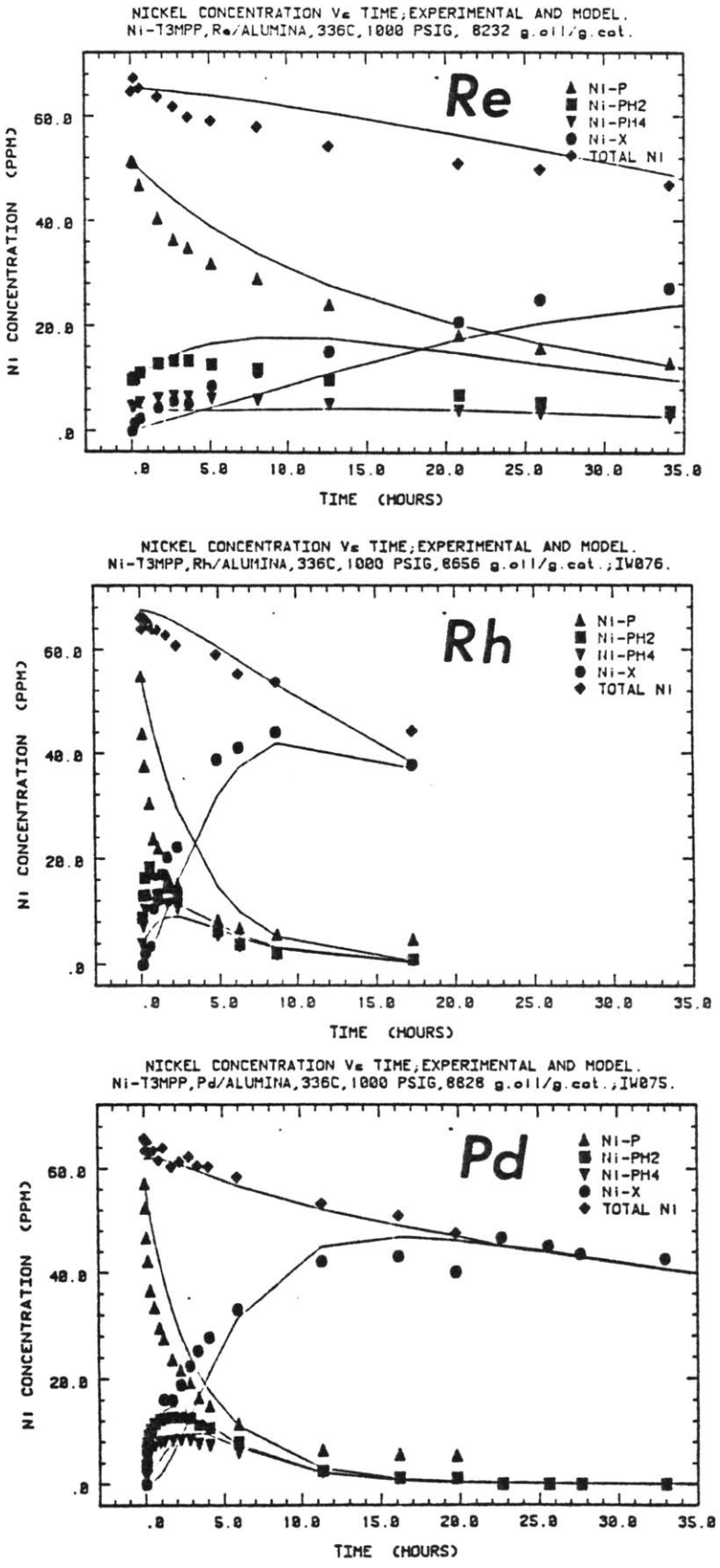

Figure 22: Concentration versus time results for Ni-T3MPP demetallation over Re (top), Rh (middle) and Pd (bottom) on alumina, at 336°C, 1000 psig H_2 and ca. 8500 g. oil/g. cat. (average). Solid lines are model calculations.

porphyrinic species (Ni-T3MPP, Ni-PH_2 and Ni-PH_4). Using HPLC, MS, and IR analysis, Ware (15) has proposed that this non-porphyrinic pool of nickel is present as an hydrogenated nickel-corrin type species (Ni-X). A molecular structure for the non-porphyrinic nickel carrier, Ni-X, consistent with analytical observations (no porphyrinic absorption peaks ca. 400 nm and a molecular weight of 632 by MS) is shown in Fig. 20. Reaction step 5 involves contraction of the macrocyclic ring at a bridge position adjacent to one of the hydrogenated pyrrole rings in Ni-PH_4, and elimination of the methine bridge carbon as a xylyl group. Grigg (65) points out that the central nickel atom will aid in this transformation by ensuring that α-pyrrolic carbon atoms which join to form Ni-X, are favorably positioned relative to each other.

Ni-T3MPP HDM kinetics have been modelled with a sequence of first order reaction steps in the mechanism of Fig. 20. The seven rate constants were evaluated from the set of four coupled differential equations by application of the Himmelblau-Jones-Bischoff technique (57). The computer programs are listed elsewhere (15).

As for the Ni-EP runs, the kinetic data for total nickel removal and Ni-T3MPP removal have been plotted in a first order kinetic plot in Fig. 23. While a straight line fit of the data is not excellent, the apparent first order rate constants evaluated from the slopes of the lines serve as a useful measure of the intrinsic activity of the catalysts. First order rate constants at 336°C, 1000 psig H_2 and ca. 65 ppm Ni starting concentration, are given in Table 6. These rate parameters should be compared with the Ni-EP HDM first order rate constants in Table 4. We note that Ni-T3MPP HDM is generally faster over all the Group VIII metal

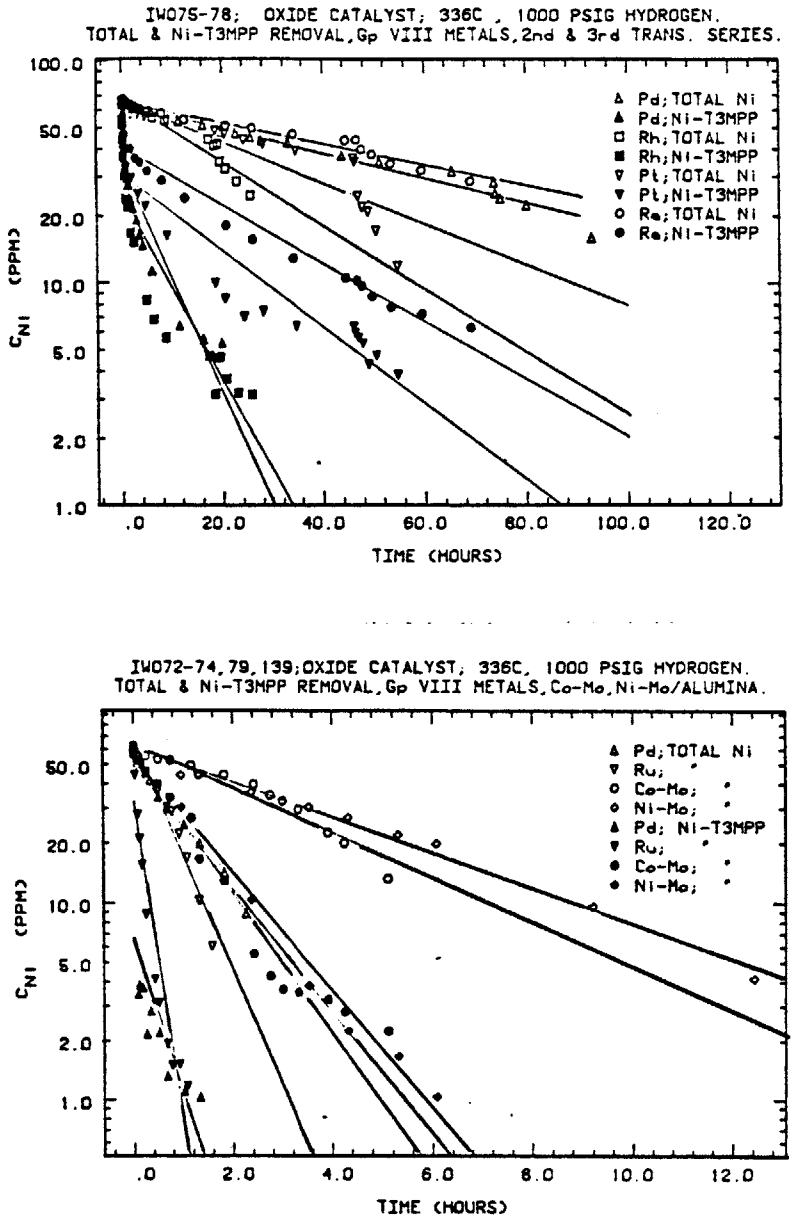

Figure 23: First order kinetic plots for Ni-T3MPP demetallation at 336°C, 1000 psig H_2. Data are for total nickel removal and Ni-T3MPP removal. Top: Demetallation over Group VIII metals Pd, Pt, Rh, Re all supported on alumina, non-prereduced catalysts, with oil/catalyst ratio at ca. 8500 g. oil/g. cat. (average). Bottom: Demetallation activity of Group VIII metals Pd and Ru, and commercially manufactured Co-Mo and Ni-Mo/Al_2O_3. Catalysts not prereduced with 435 g. oil/g. cat. (average).

Table 6:

Representative values of 1st order rate constants (total nickel and nickel porphyrin removal) in Ni-T3MPP HDM. Process conditions: 336°C, 1000 psig H_2, ca. 65 ppm Ni starting concentration.

Run No.	Catalytically active metals	First order rate constants (g.oil/g.cat. h.)		$\frac{k_{1,Ni\text{-}T3MPP}}{k_{1,Ni}}$
		Ni-T3MPP ($k_{1,Ni\text{-}T3MPP}$)	Total Ni ($k_{1,Ni}$)	
IW074	Ru	689.2	250.8	2.7
IW076	Rh	360.3	122.5	2.9
IW075	Pd	449.4	49.0	9.2
IW078	Re	107.0	38.2	2.8
IW077	Pt	138.8	73.7	1.9
IW073	Co-Mo (HDS-16A)	146.4	52.6	2.8
IW139	Ni-Mo (HDS-9A)	133.2	40.0	3.3

catalysts. With Co-Mo/Al_2O_3 catalyst, the first order rate constants for porphyrin removal are almost equal for Ni-EP and Ni-T3MPP, however, total nickel removal from Ni-EP is ca. 2.4 times faster than it is from Ni-T3MPP.

The trend in Group VIII metal catalyst hydrogenation selectivity increasing as one moves across the Group VIII metals from left to right (i.e. from Ru→Rh→Pd), is also exhibited in Ni-T3MPP HDM. For example, the first order rate constant ratio [$k_{1,Ni\text{-}T3MPP}/k_{1,Ni}$] increases from 2.7 for Ru, to 9.2 for Pd for the data of Table 6. [$k_{1,Ni\text{-}T3MPP}/k_{1,Ni}$] is 2.8 for Co-Mo catalyst whereas it is 3.3 for Ni-Mo. Co-Mo is typically used is hydrosulfurization (HDS) operations, whereas Ni-Mo is used for hydrodenitrogenation (HDN) where a stronger hydrogenation function is required (66), and hydrogen consumption is higher (67). The larger value of the selectivity ratio for Ni-Mo catalyst indicates that its greater hydrogenation activity, relative to Co-Mo, is also expressed in porphyrin HDM.

Ni-T3MPP HDM runs were only conducted at a range of temperatures with the Co-Mo and Ni-M./Al_2O_3 catalysts. Rate constants calculated from the model calculations are plotted in Arrhenius plots in Fig. 24. In contrast to Ni-EP, where the rate limiting step in the mechanism of Fig. 7, is generally the initial porphyrin hydrogenation ($k_1<k_3$), hydrogenation of Ni-T3MPP (k_1) is rapid relative to the hydrogenolysis step k_6, which deposits the majority of the metal onto the catalyst surface from the intermediate, Ni-X. The other hydrogenolysis step, k_7, which deposits nickel directly from Ni-PH_4 is faster than the initial hydrogenation step, making the relative ranking of the initial hydrogenation and terminal hydrogenolysis steps: $k_7>k_1>k_6$. Activation energies calculated from Fig.

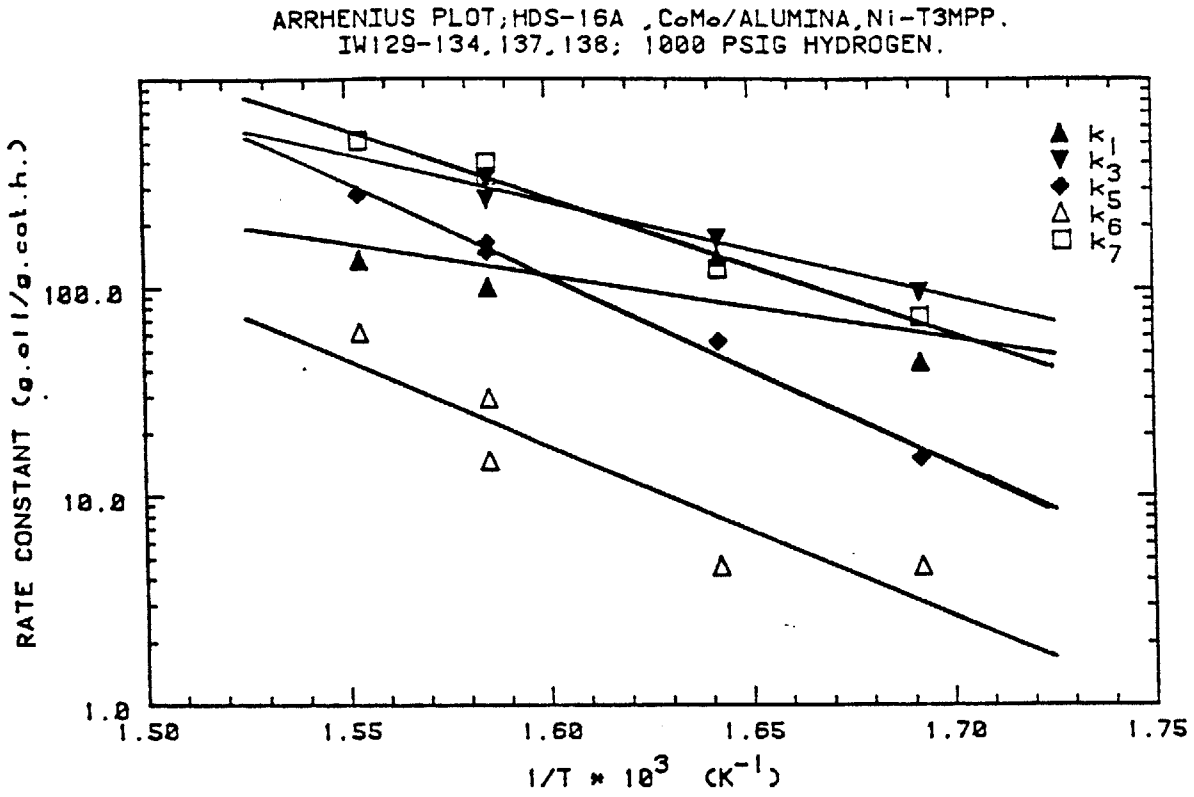

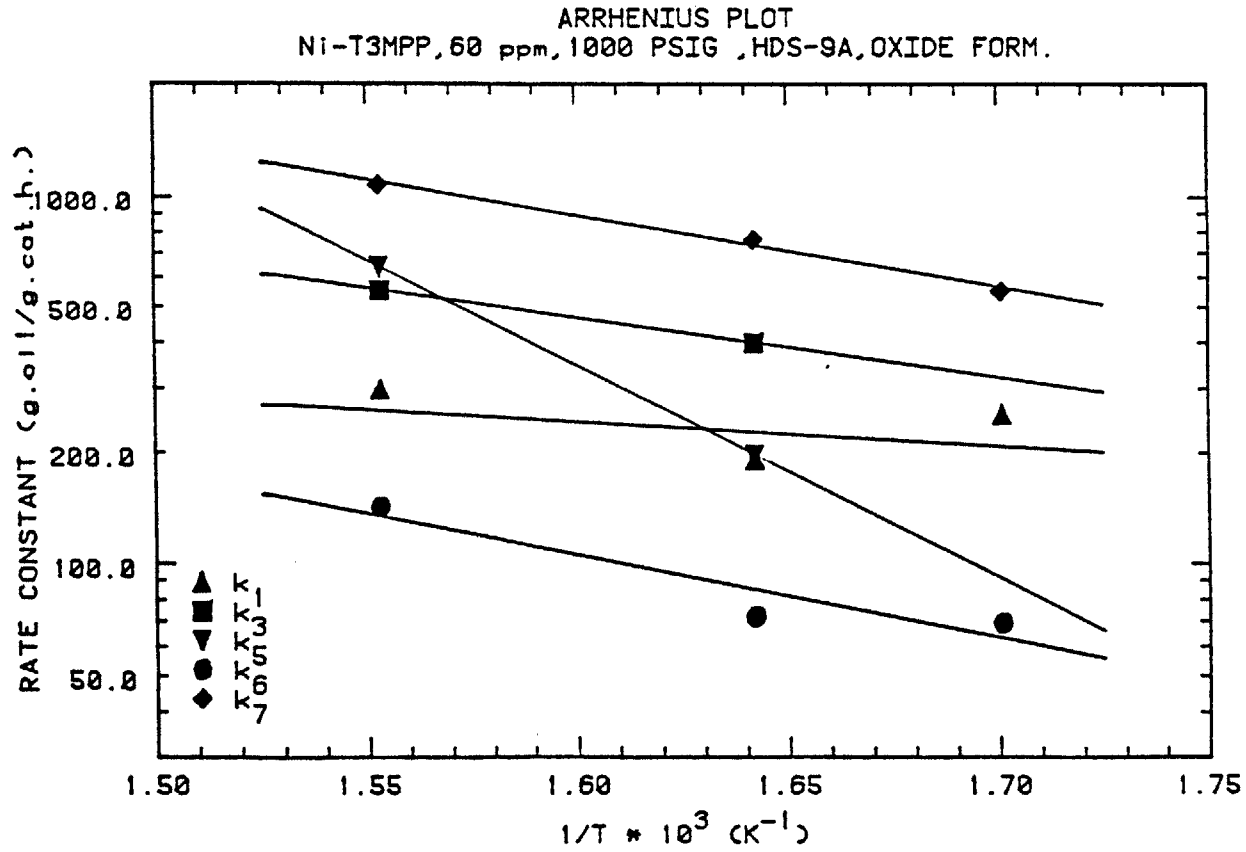

Figure 24: Arrhenius plots for first order rate parameters for Ni-T3MPP demetallation at 1000 psig H_2. Top: Co-Mo/Al_2O_3 (HDS-16A); Bottom: Ni-Mo/Al_2O_3 (HDS-9A).

24 are listed in Table 7. With Co-Mo the hydrogenation rate constants have smaller E_A values with Ni-T3MPP HDM, than with Ni-EP HDM. This is intuitively correct since Ni-T3MPP HDM is more facile than Ni-EP HDM. The hydrogenolysis rate constants in both porphyrin demetallation mechanisms have similar activation energies. With Ni-Mo, Ni-T3MPP hydrogenation activation energies are low. This is consistent with the aforementioned fact that Ni-Mo has a strong hydrogenation activity (due to the Ni) relative to Co-Mo.

A few Ni-T3MPP HDM runs were performed over the Group VIII metals of the second transition series; namely Ru, Rh and Pd. The catalysts were not prereduced, but simply dried under helium at 440°C, overnight, before being injected into the autoclave. The HDM runs were performed at 336°C and 1000 psig H_2. Typical concentration versus time plots are shown in Fig. 22. Representative rate constants in the Ni-T3MPP demetallation mechanism of Fig. 20, when the catalysts are from the 2nd transition series of the Group VIII metals, are listed in Table 8.

Once again, our objective was to attempt to manipulate the ratio of the terminal hydrogenolysis rate constants (k_6, k_7), to the initial hydrogenation rate constant (k_1), and observe any correlation in these ratios, with the % d-character of the catalytically active meetal.

Our results are depicted in Fig. 25. Both hydrogenolysis rate constants (k_6, and k_7) are divided by k_1, and plotted as a function of periodic position in the upper panel. Percent d-character as a function of periodic position is displayed in the lower panel. As with Ni-Etio, our results with Ni-T3MPP are qualitatively consistent with the findings of Sinfelt (19) (Fig. 2) that hydrogenolysis activity decreases in the

Table 7:

Activation energies (in kcal/mol.) for the forward rate constants in the Ni-T3MPP HDM reaction scheme displayed in Fig. 20; 1000 psig H_2 and ca. 60 ppm Ni starting concentration in batch experiments.

	E_A (kcal/mol)	
Catalyst / Rate Constant	$Co\text{-}Mo/Al_2O_3$ (HDS-16Å)[3]	$Ni\text{-}Mo/Al_2O_3$ (HDS-9Å)[3]
k_1	13.7	3.0
k_3	20.7	7.4
k_5	40.8	26.3
k_6	37.3	10.1
k_7	29.6	8.9

Table 8: Representative rate constants in Ni-T3MPP HDM. Catalysts initially in oxide state; 336°C, 1000 psig H_2, 65 ppm Ni starting concentration.

Rate constant (g.oil/g.cat.h)	Catalyst		
	Ru	Rh	Pd
k_1	2300	2850	3225
k_2	1561	1499	1511
k_3	6270	5600	5899
k_4	1861	1232	672
k_5	3390	7857	6413
k_6	279	421	97
k_7	1297	1015	891

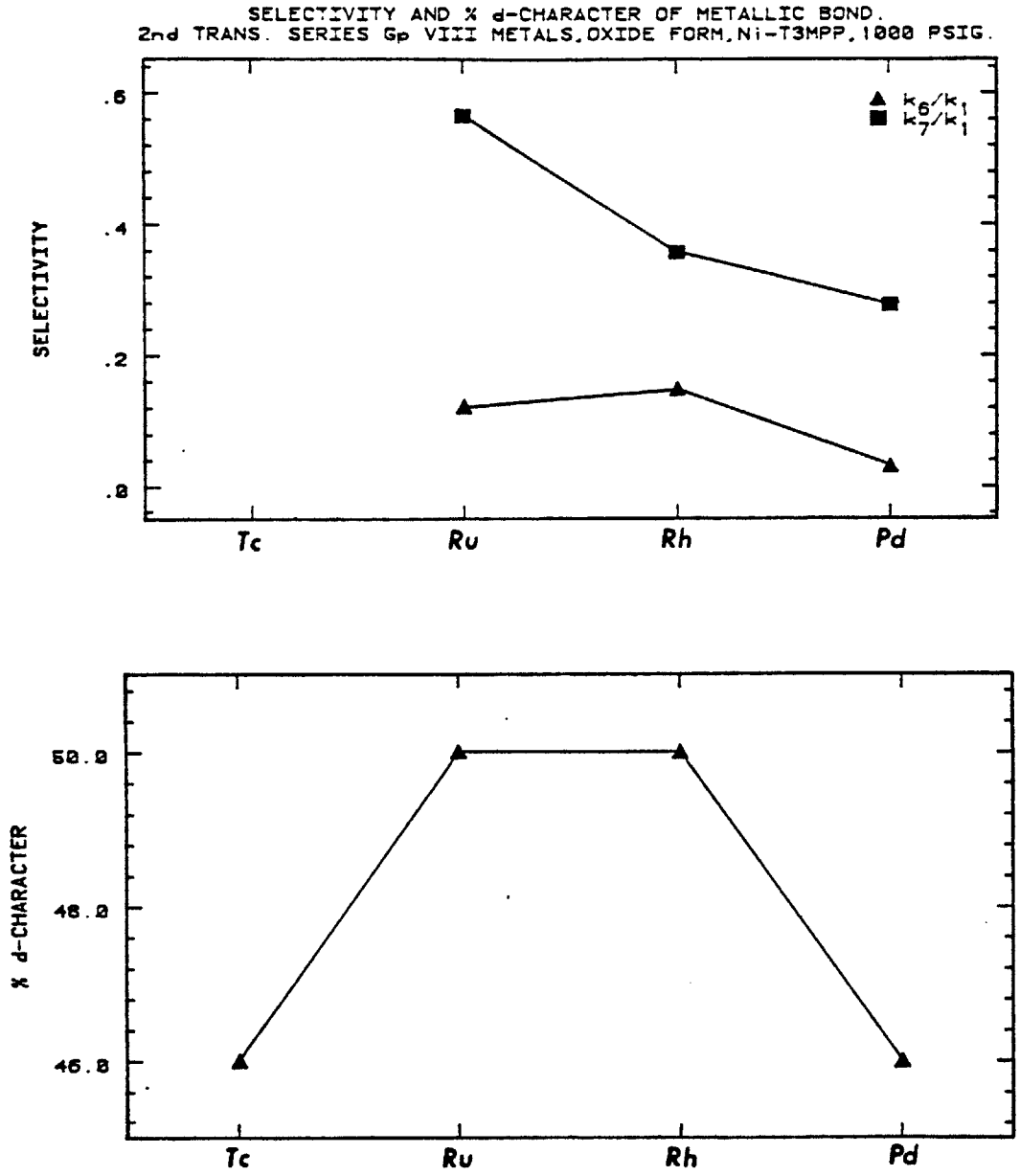

Figure 25: Selectivity of third transition series of Group VIII metals for Ni-T3MPP hydrogenolysis in relation to periodic position, and percentage d-character of the metallic bond. Data are at 336°C, and 1000 psig H_2.

direction Ru→Rh→Pd, whereas hydrogenation activity increases in the same direction. The hydrogenolysis activity or (hydrogenolysis/hydrogenation) selectivity can be broadly correlated with % d-character.

I. D. 3 Post HDM experiment catalyst characterization

Aged catalysts were scrutinized by SEM/EDX and XPS. XPS is an extremely surface sensitive analytical technique, which probes the catalyst surface to a depth of about 30Å (68). EDX samples to depth of ca. 1 micron, making this technique much more of a bulk measurement. Further details on the applications of these and other spectroscopic techniques to aged HDM catalysts have been given by Webster and Wei (49).

Figure 26 is an electron micrograph of a sectioned Pd (5%)/Al_2O_3 catalyst particle which was used in the demetallation of Ni-T3MPP at 360°C, 1700 psig H_2 and 60 ppm Ni starting concentration. The catalyt particle has been exposed along its mid-section, and an X-ray line scan for Ni has been superimposed on the micrograph. The uniformity of this profile substantiates our claim that the kinetic data we collected was intrinsic and not diffusionally masked. Thiele modulus calculations also theoretically preduct that diffusion is not limiting with these 100μ sized catalyst particles (53).

The upper panel of Fig. 27 is an EDX spectrum on a Rh (5%)/Al_2O_3 catalyst particle used in Ni-T3MPP HDM. This particular particle was not sectioned, and indicates that the fate of the porphyrinic nickel is actually on the catalyst surface. A more surface sensitive appreciation of the aged catalyst's surface condition is achieved through XPS. The lower panel of Fig. 27 shows an XPS survey scan on the Pt (5%)/Al_2O_3 catalyst used to obtain the kinetic data in Fig. 17 (lower right) on Ni-EP HDM. The

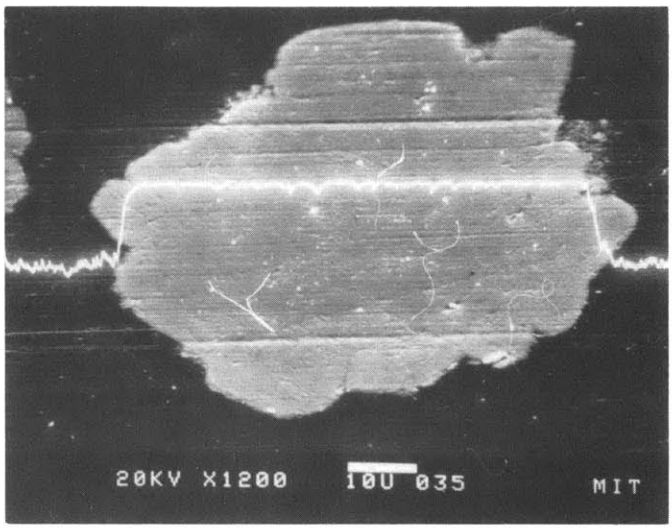

Figure 26: Intra-catalyt particle nickel profile. Measurement is by SEM/EDX on sectioned Pd (5%)/Al_2O_3 particle used in the demetallation of Ni-T3MPP at 360°C, 1000 psig H_2 and 65 ppm Ni starting concentration. No intra-particle nickel gradient exists. Marker bar is 10 microns.

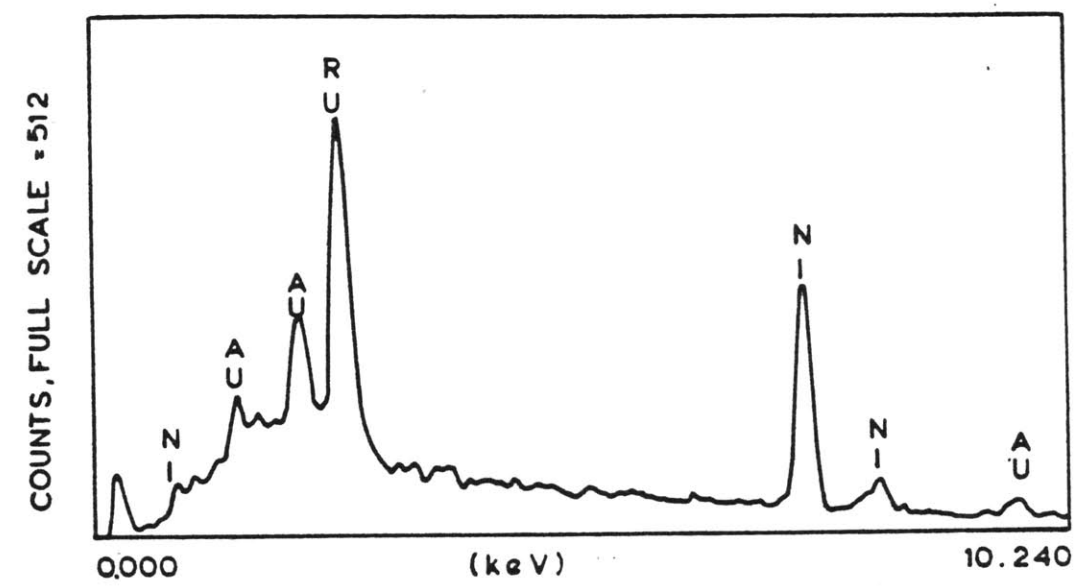

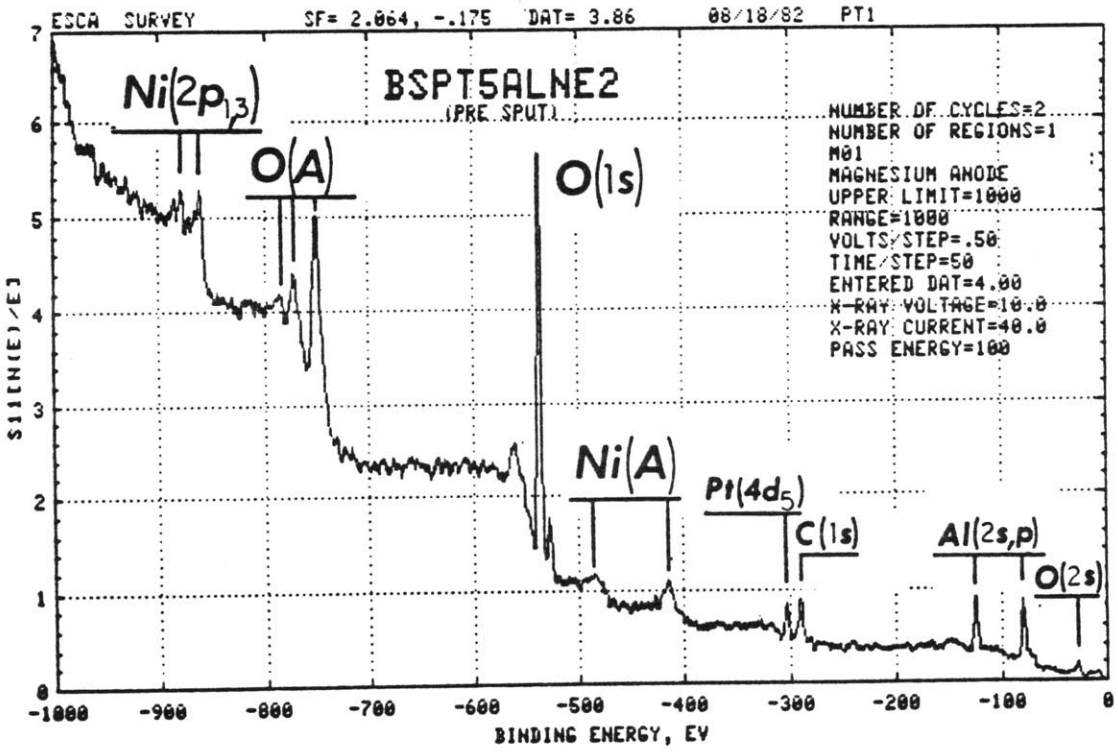

Figure 27: (Top) Energy dispersion X-ray spectrum from aged Ru (5%)/Al_2O_3 catalyst used in Ni-EP HDM. Based on a mass balance the average nickel loading is ca. 8 wt. %.
(Bottom) XPS survey scan on aged Pt (5%)/Al_2O_3 catalyst used in Ni-EP HDM. (A) signifies Auger peak. The average nickel loading on this catalyst was ca. 8 wt. %.

catalyst surface is covered with a layer of carbon and nickel. From a mass balance, based on the quantity of Ni actually removed from oil, the nickel loading on the aged Pt catalyst is ca. 8.8 wt %. Despite this relatively high Ni loading, a strong Pt signal ($4d_{5/2}$ at 316eV) persists. This observation is consistent with our findings on aged model Co-Mo catalysts (49), where bare patches of Mo continued to exist on the catalyst surface, despite the deposition of much coke and metals. Also, Davis et al (69) have recently proposed a model for the working Pt/Al_2O_3 reforming catalyst, based on their work in reforming hydrocarbons over unsupported single Pt crystals. A prominant feature of their model is that a small concentration of uncovered Pt surface sites (ca. 2-25%) always persists in the presence of carbon deposits. We may tentatively conclude, based on Fig. 27 (lower panel) that a similar situation exists on the surface of the Group VIII metal catalysts when used in HDM.

Figure 28 shows XPS survey scans on an aged Rh (5%)/Al_2O_3 catalyst. This catalyst was used in Ni-EP HDM at 1000 psig H_2, at a range of temperatures (315-353°C). Based on a mass balance its nickel loading is ca. 8.3 wt %, which is substantially less than that required for uniform monolayer coverage (14 wt %). The spectra in Fig. 28 were collected on the untreated aged catalyst surface, and also after it had been sputtered for numerous time intervals, up to a maximum of 5.5 minutes. With sputtering, the Ni (2p) peak decays, especially during the initial 1/2 minute. The Rh (3d) and C(1s) signals increase with sputtering time, and then stablize (compare spectra after 3.5 and 5.5 minutes sputtering). Wukasch and Rase (70) have estimated that argon sputtering at the intensity used in our experiments (5keV) would erode a noncharging surface at a rate

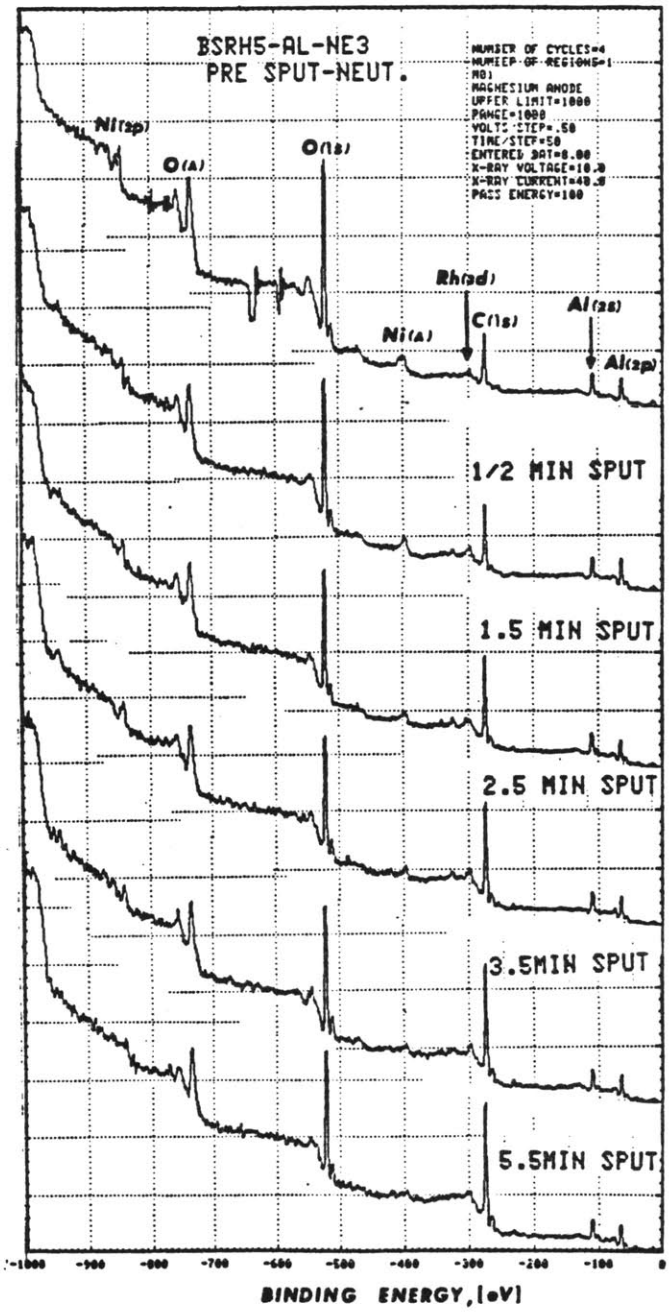

Figure 28: A series of XPS survey scans taken on Rh (5%)/Al_2O_3 used in Ni-EP HDM after sputtering for up to 5.5 minutes. The average nickel loading is ca. 8 wt. %. (A) signifies Auger peak. Sputtering was performed by argon at 5keV.

between 5 and 300 Å/min. Based on work with standards we have reported elsewhere (49), we believe the latter figure to be most accurate.

XPS spectra of the Ni $2p_{3/2}$ and $2p_{1/2}$ peaks for fresh, untreated Ni-Mo/Al_2O_3 (HDS-9A), and Pt and Rh/Al_2O_3 catalysts which have been used for the HDM of Ni-EP, are displayed in Fig. 29. The spectrum collected on Ni-Mo/Al_2O_3 (top panel) serves as a useful reference to which we can compare the state of the nickel which was catalytically deposited on the Pt and Rh catalysts. It is unwise to infer information on the chemical state of nickel on the surface of the Pt and Rh catalysts in the working environment, from the spectra of Fig. 29. This is because the catalysts were exposed to air when they were filtered from the oil, post-run. However, what can be learned from the Ni spectra is the degree of interaction that the metal has with the support.

Wu and Hercules (71) conducted an XPS study of Ni/Al_2O_3 catalysts. Nickel was shown to strongly interact with the alumina support. Three types of nickel were shown to exist. At low nickel content (<17 wt %), two forms co-exist, namely nickel ions in tetrahedral and octahedral sites of the γ-alumina. Their existence has also been proven by other techniques such as magnetic measurements and reflection spectroscopy (72,73). At higher nickel contents (>17 wt %) a third nickel species (present as NiO in Wu and Hercules' (71) oxide catalysts) forms a separate phase on top of the nickel monolayer which saturates the surface sites of γ-alumina.

It is reasonable to postulate that because of the low nickel loading on the American Cyanamid Ni-Mo/Al_2O_3 (HDS-9A) catalyst (3.2 wt % NiO) and its relatively high calcination temperature (ca. 600°C (74)) that most of the nickel exists in tetrahedra sites (Ni-t). The Ni($2p_{3/2}$) peak position

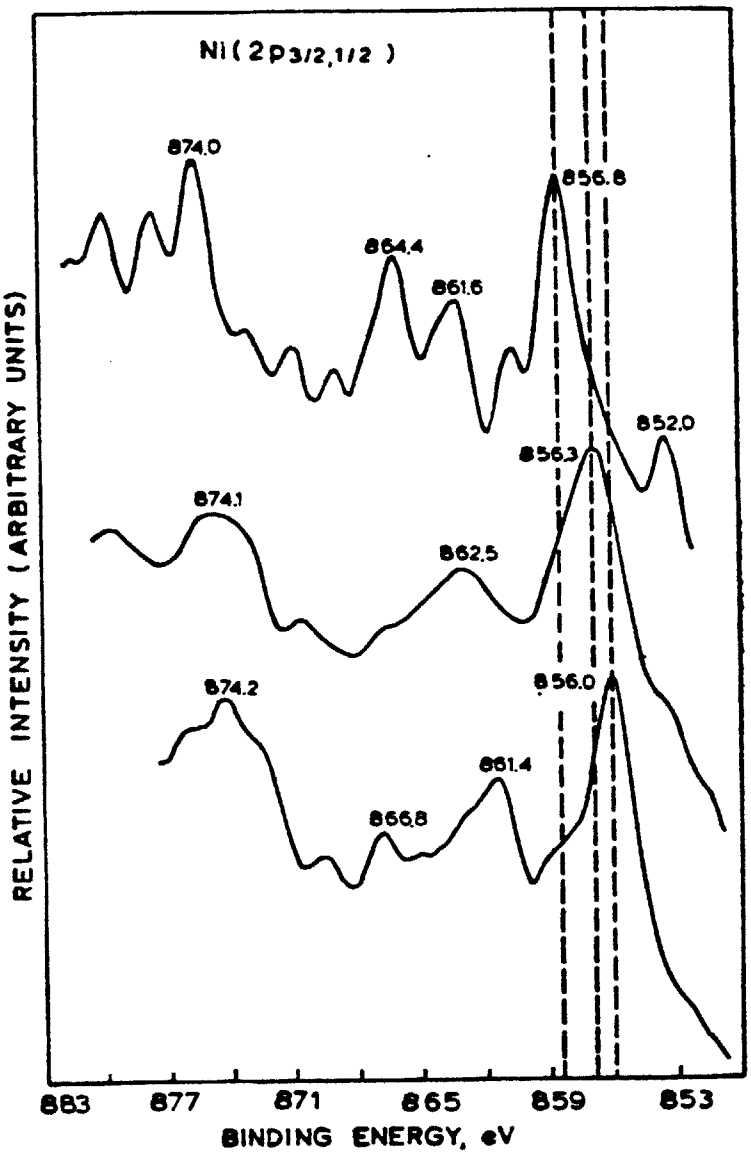

Figure 29: XPS spectrum of Ni ($2p_{3/2,1/2}$) core levels in fresh Ni-Mo/Al_2O_3 (HDS-9A) (top), Pt/Al_2O_3 used for Ni-EP HDM (middle) and Rh/Al_2O_3 used for Ni-EP HDM (bottom).

in Ni-Mo/Al_2O_3 catalyst is at 856.8eV (Fig. 29, top panel), while it is shifted to lower binding energies (BE's) at 856.3 and 856.0 eV, on the aged Pt and Rh/Al_2O_3 catalysts, respectively. This shift of the Ni($2p_{3/2}$) peak to lower BE, for the nickel that was catalytically deposited onto these catalysts via the HDM reaction, suggests that the ultimate fate of this Ni is in the octahedral site of γ-alumina.

All spectra in Fig. 29 indicate the presence of small quantities of metallic nickel (BE of Ni($2p_{3/2}$) at 852.3ev). The Ni-Mo catalyst exhibits a distinct peak at 852eV, whereas on the Pt (middle panel) and Rh (bottom panel) catalysts, metallic nickel only generates shoulders on the low BE side of the Ni($2p_{3/2}$) peak.

All the spectra in Fig. 29 are complex, however, the spectra for the catalytically deposited nickel contain fewer peaks than the spectra for nickel in the Ni-Mo/Al_2O_3 catalyst. Ni in Ni-Mo/Al_2O_3 has two shake-up satellites at BE's of 861.6 and 864.4 eV, whereas the catalytically deposited Ni on the Pt and Rh catalysts only have one satellite each, at 862.5 and 861.4 eV, respectively. This is indicative of the fact that the catalytically deposited nickel interacts less strongly with the support, than it does when it is deposited initially as a salt and then calcined, as occurs in the catalyst manufacturing procedure (71). This fact is of importance when assessing the catalytic activity of the Ni deposited during the HDM reaction. Elsewhere, we have shown (63) that the deposited Ni does possess catalytic activity for the HDM reaction. Also, Tayer et al (75) have shown that the specific activity of nickel varies with the support, suggesting that the nickel's activity is strongly dependent on how strongly it interacts with the support. Since we have shown that Ni deposited via

the HDM reaction interacts less strongly that Ni added in the preparation of a catalyst, we believe it is incorrect to equate the catalytic activities of these two types of nickel.

I. D. 4. Ni-Etio porphyrin HDM over Group VIII-IB metals

We have already shown how the relative rates of the hydrogenolysis and hydrogenation steps in the overall HDM mechanism can be varied depending on which supported Group VIII metal is used to catalyze the reaction. This approach can be viewed as one of altering the HDM reactions selectivity by exploiting the intrinsic catalytic activity of an individual metal to catalyze mechanistically different reactions to different degress.

Another method may exist whereby the HDM reactions selectivity can be altered at will. Fundamental research on gas phase reactions catalyzed by supported Group VIII-IB bimetallic catalysts has revealed that the rates of hydrogenolysis reactions are much more strongly inhibited by the addition of the Group IB metal than are hydrogenation reactions (34). The effect of the Group IB metal is thought to be mainly structural. In a highly dispersed system the Group IB metal is envisioned as an inert spacer atom which divides up ensembles of the Group VIII metal atoms. Hydrogenolysis reactions are postulated a proceeding through chemisorbed intermediates bound to larger ensembles than required for hydrogenation reactions (32).

Since the HDM mechanism we have shown for Ni-EP (Figure 7) contains an initial hydrogenation step followed by a terminal hydrogenolysis step we have attempted to alter its selectivity by catalyzing the reaction over alumina supported Ru-Cu bimetallic catalysts. The loading of the Group VIII metal on the catalyst was always held constant (at 5 wt %), while the atom percent copper was varied from zero to one. Copper only weakly

chemisorbs hydrogen and is essentially inactive in Ni-EP HDM. It can be envisioned as the inert spacer atom.

The compositions of the Ru-Cu/Al_2O_3 catalysts used for Ni-EP HDM are listed in Table 1. The specifications of their model PCA supported counterparts, are detailed in Materials under Experimental. These PCA catalysts were used solely in XPS analysis in an attempt to ascertain whether "structural" or "electronic" effects dictated the catalysts selectivity.

The γ-Al_2O_3 supported catalysts were also subjected to SEM/EDX and X-ray diffraction analysis. None of the reduced caalysts, with or without copper, gave X-ray diffraction lines of any metallic phase. This was our wish, and suggests that the metals are highly dispersed with crystallite sizes less than 50Å (76). Some results of the SEM/EDX analysis are shown in Fig. 30. This figure shows a sectioned Ru (5%)-Cu(3.4%)/Al_2O_3 catalyst particle (top) with an accompanying Ru map (bottom) of the area in the top micrograph. The Ru composition is uniform through the particle. Similar uniformity of composition was found for Ru and Cu in all the different catalysts. Small quantities of chlorine were detected in some EDX spectra, persumably remaining from the catalyst impregnation step when $RuCl_3$ was used. However, we do not believe the presence of chlorine has substantially affected our kinetic studies, since we have shown elsewhere (77), that oxidic and pre-chlorided Al_2O_3 exhibit similar catalytic activities for HDM. Hydrogen chemisorption studies on both the Ru and Ru-Cu/Al_2O_3 catalysts indicated that the Ru dispersion was high, and at all times exceeded 85%. Copper only weakly chemisorbs hydrogen (76). Ruthenium and copper are also immissible in the bulk state (78).

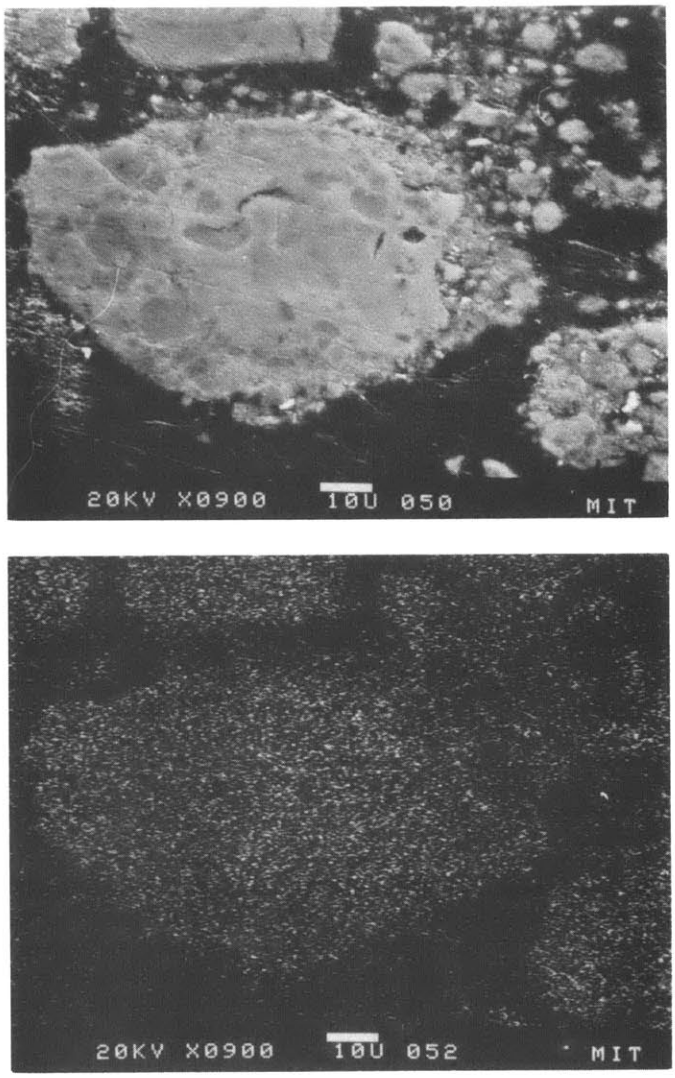

Figure 30: SEM/EDX for intra-catalyst particle metal distributions on Ru(5%)-Cu(3.14%)/Al_2O_3 bimetallic catalyst. Top: SEM of sectioned catalyst particle. Bottom: Ru map for region shown in SEM. Marker bar is 10 microns.

We have demetallized Ni-EP at 30 ppm starting nickel concentration, over each of the Ru-Cu/Al_2O_3 catalysts listed in Table 1, at 336°C and 1000 psig H_2. Ni-EP demetallized according to the mechanism of Fig. 7, and the rate constants were evaluated as before. The pertinent results are presented in Fig. 31. The upper figure shows the variation of the hydrogenation (k_1), hydrogenolysis (k_3), and total nickel ($k_{1,Ni}$) and porphyrin ($k_{1,p}$) removal rate constants with catalyst composition. As is common in Ni-EP HDM, hydrogenation is rate limiting at all catalyst compositions.

The most striking feature of Fig. 31(a) is that the hydrogenolysis rate constant, k_3, is far more strongly affected by the addition of copper to the catalyst surface, than is the Ni-EP hydrogenation rate constant, k_1. For example, as the atomic ratio of Cu to Ru is increased from zero to one, (0 to 50 atom % Cu), k_3 decreases by a factor of 2.3, whereas k_1 remains insensitive to catalyst composition. The data have been replotted as the selectivity ratio k_3/k_1 (hydrogenolysis/hydrogenation) against Ru-Cu catalyst composition in Fig. 31(b). This figure clearly shows that the addition of copper to a highly dispersed Ru/Al_2O_3 catalyst system, can alter the selectivity of that catalyst when it is used for Ni-EP HDM. Moreover, while the <u>selectivity</u> decreases with copper addition, the overall catalysts <u>activity</u> is little affected by the catalyst's composition, as exemplified by the invariance of k_1,Ni with catalyst composition (Fig. 31a). This occurs because the rate limiting step of Ni-EP hydrogenation (k_1), is little affected by the addition of Cu to Ru/Al_2O_3.

As already mentioned, our highly dispersed bimetallic catalyst system comprises two immiscible elements. Nevertheless, our HDM catalytic studies

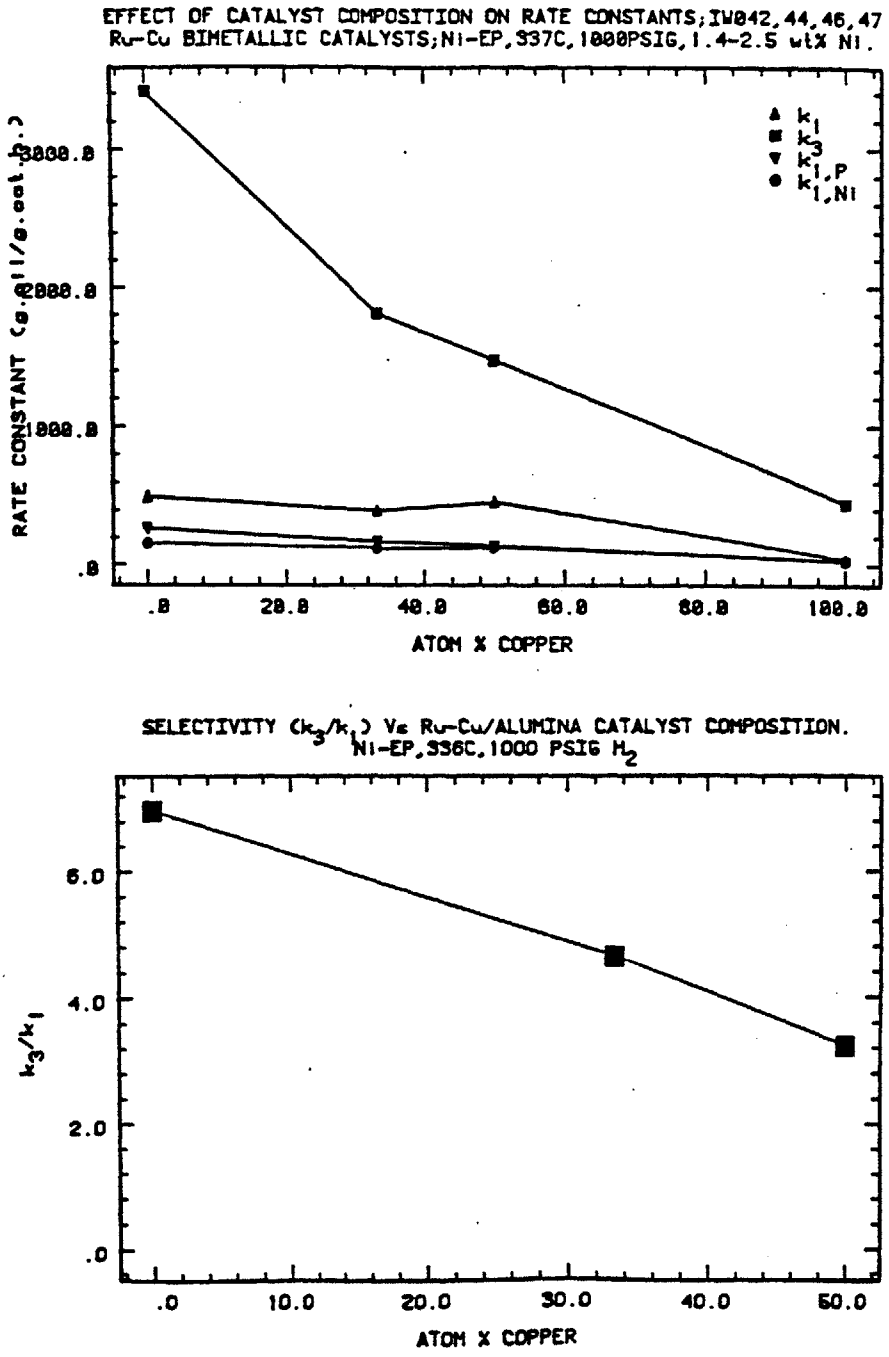

Figure 31: The effect of copper concentration on the hydrogenation (k_1) and hydrogenolysis (k_3) rate constants for Ni-EP HDM over Ru-Cu/Al_2O_3 catalysts at 336°C, and 1000 psig H_2. Top: Absolute change in rate constants as a function of catalyst composition. Bottom: Selectivity (k_3/k_1) as a function of catalyst composition.

suggest that the two metals do interact, since the hydrogenolysis rate constant (k_3) is suppressed by copper addition. If copper and ruthenium existed as separate entities on the carrier, we should not expect the hydrogenolysis activity of the bimetallic catalyst to be significantly different from that of the supported ruthenium alone.

As already noted these experimental observations can be rationalized by either the geometrical or electronic theories of catalysis by bimetallics. We believe the geometrical (structural) effects to be of prime importance is our catalytic system. This conclusion is drawm from the XPS spectra for Ru, and Cu collected on the model PCA supported catalysts.

Relevant spectra are shown in Fig. 32. Column A is the Cu ($2p_{3/2}$) spectra for the monometallic Cu/PCA, and bimetallic Ru-Cu/PCA. Column B is the Ru ($3d_{5/2}$) spectra for the same catalysts. Some of spectra have been obtained after ion sputtering. All spectra are referenced with respect to Au ($4f_{7/2}$) at 84.0 eV.

With copper there is no change in the $2p_{3/2}$ peak position (932.8 eV) when Cu exists on the support by itself, or in intimate contact with Ru. Collection of the Ru ($3d_{5/2}$, $3d_{3/2}$) spectra were hampered by the presence of a C (1s) signal at 284.6eV. This convolutes with the Ru ($3d_{3/2}$) signal at 284.1 eV. The carbon was presumably deposited on the model catalysts' surface as it was being prereduced in the tube furnace, prior to introduction to the spectrometer. For this reason the spectra in Fig. 32-B show only the Ru ($3d_{5/2}$) spectra. Once again, as for Cu, the change in peak position for Ru ($3d_{5/2}$) (ca. 280.6 eV before sputtering, and decreasing to ca. 280.0 eV after sputtering) whether it exists in the

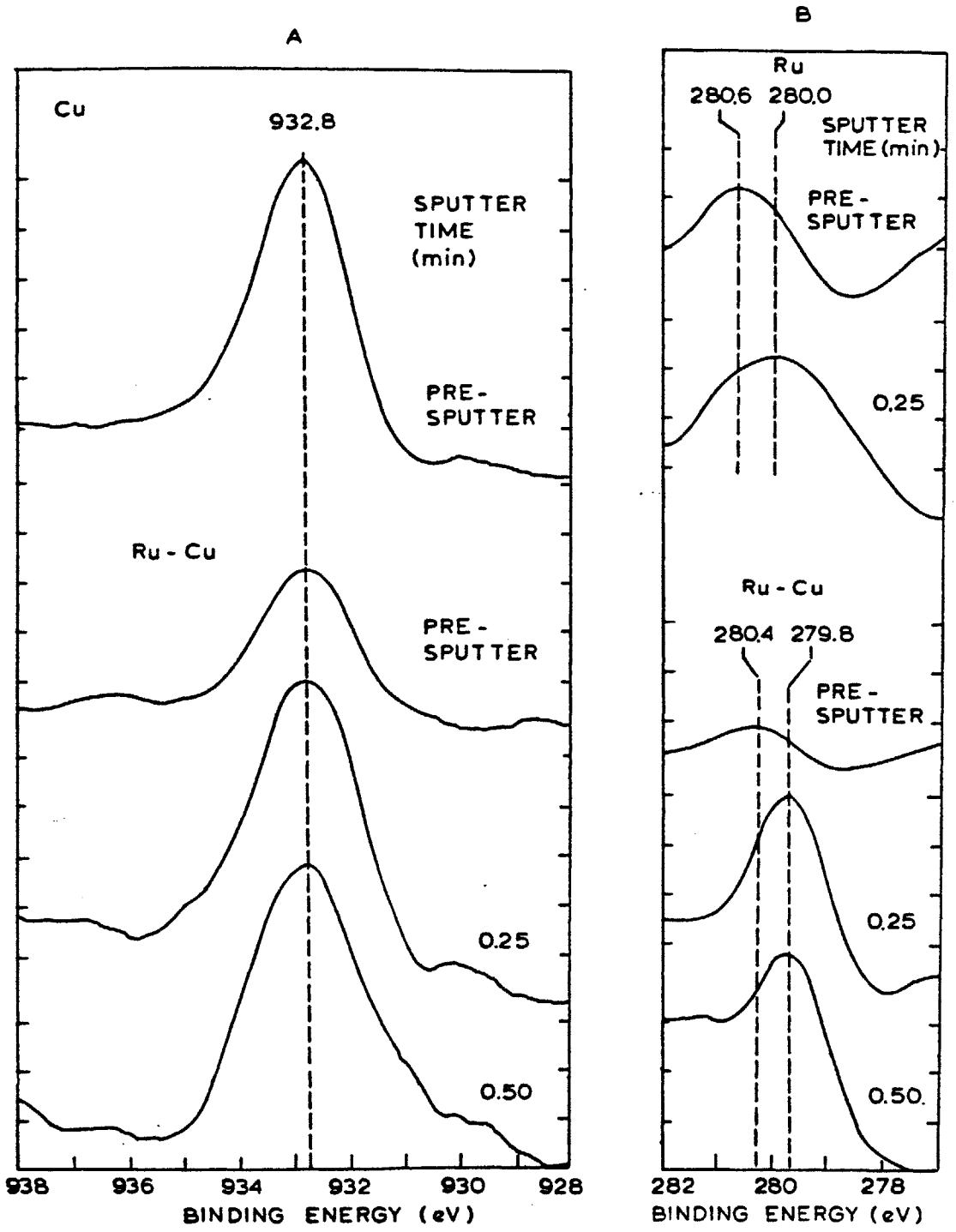

Figure 32: XPS spectra of Cu($2p_{3/2}$) (A) and Ru ($3d_{5/2}$) (B) core levels in Ru-Cu/PCA, Ru/PCA and Cu/PCA model catalysts. Some spectra are shown before and after argon sputtering at 5keV.

monometallic environment, or in the bimetallic environment. The downward shift in Ru ($3d_{5/2}$) peak position with sputtering can be attributed to the removal of an oxide layer, which must have formed during the catalyst transfer operation from furnace to spectrometer, despite our efforts to avoid exposure to air. The oxide layer is probably RuO_2 (79) which is sputter removed to exposure Ru.

The constancy of Ru and Cu peak positions signifies that the copper atoms have little influence electronically on their ruthenium neighbors, and that there is little sharing of electrons between Cu and Ru.

Thus, while it is unlikely that a geometric effect can be completely divorced from an electronic effect, we believe that geometrical effects are of overriding importance in our highly dispersed Ru-Cu catalyst system. Sinfelt (76) has speculated that both effects are importanct in the Ru-Cu system, however, since his work there is increasing evidence, albeit on other bimetallic systems, that geometrical effects do dominate. Ponec (34) has reviewed the situation and favored the purely structural effects caused by a Group IB diluent. Toolenaar et al (80) and Sachtler and Somorjai (81) having worked with an alumina supported Cu-Pt system, and a single crystal Au-Pt (111) system, believe that geomtrical effects predominate.

I. E. Discussion

We have investigated the catalytic HDM of Ni-EP and Ni-T3MPP over γ-Al_2O_3 supported Group VIII metal catalysts. The kinetics and mechanism of each reaction have been reported. The HDM mechanism for each porphyrin is sequential first involving hydrogenation to activate the molecule, followed by terminal hydrogenolysis steps which fragment the tetrapyrrolic ring and deposit nickel on the catalyst surface.

While the global reaction scheme is the same for Ni-EP and Ni-T3MPP the details of each mechanism differ significantly (compare Figs. 7 and 20). Ni-EP demetallates through a single stable hydrogenated intermediate, whereas Ni-T3MPP reacts through two hydrogenated porphyrin intermediates, and a non-porphyrinic contracted ring structure. These mechanisms are the same as reported by Agrawal (54) and Ware (15) who extensively investigated Ni-EP and Ni-T3MPP demetallation, respectively, over Co-Mo/Al_2O_3 catalyst.

Our results indicate that the Ni-porphyrin HDM schemes remain unaltered when Group VIII metal catalysts are used for HDM. The same porphyrins react via the same intermediates.

For over sixty years catalysts such as Co-Mo/Al_2O_3 have been used in the hydroprocessing of petroleum fractions (82). There is a need to develop more active and selective catalysts. It is with this in mind that we have demetallized our model Ni containing residua over the Group VIII metals, and particularly focussed on what hydrogenolysis/hydrogenation selectivity ratios can be achieved within the aforementioned porphyrin HDM mechanisms.

The reasons why Ni-EP demetallates via a short reaction sequence, and Ni-T3MPP through a long reaction sequence have been fully described by Ware (15). Briefly, the steric hindrance associated with the methyl and ethyl groups on the β-pyrrolic positions in Ni-EP inhibit its hydrogenation, whereas in Ni-T3MPP these positions are open (see Fig. 1). Also when the porphyrin is hydrogenated there results an enhancement of the reactivity of the methine bridge adjacent to the pyrroline ring (82). In the HDM sequence it is likely that cleavage of the macrocyclic ring occurs at this position. In Ni-EP the methine bridge position is exposed. This results

in rapid fragmentation of Ni-EPH$_2$ and metal deposition, with no further generation of more reduced intermediates. In contrast, when Ni-T3MPP is hydrogenated the tolyl groups at the methine bridges sterically hinder interaction of the activated methine bridge sites with the catalyst surface. This prevents initial fragmentation of the macrocycle after a single hydrogenation, thereby generating Ni-PH$_4$ species.

Agrawal (54) showed that in Ni-EP HDM over Co-Mo hydrogenation was always rate limiting ($k_1<k_3$ in Fig. 7). In contrast, Ware (15) showed that with Ni-T3MPP HDM over the same catalyst, the hydrogenolysis steps were always rate limiting ($k_1>k_6$ and k_7 in Fig. 20).

This work has shown that it is possible to vary the selectivity for hydrogenolysis (k_3/k_1 for Ni-EP, and k_7/k_1 or k_6/k_1 for Ni-T3MPP) in a predictable manner when Group VIII metal catalysts are used. In general, through, we were unable to change either of the porphyrins' rate limiting steps, except in the case where Ni-EP was demetallized over Pd (Fig. 18a). In some cases the strong hydrogenation functionality of this catalyst so accelerated the rate of Ni-EP hydrogenation, that Ni-EPH$_2$ hydrogenolysis became rate limiting.

With Group VIII elements of the first transition series we varied the Ni-EP mechanism selectivity ratio (k_3/k_1) by a factor of 28.6 in moving from Co to Ni (Fig. 19a). In the second transition series, k_3/k_1 was varied by a factor of 4.8 in crossing from Ru to Pd (Fig 18a). With the catalysts of the third transition series we realized our most dramatic variation in k_3/k_1. The selectivity ratio was at best, varied by a factor of 584 in moving from Re to Os (Fig. 18b). This was only achieved with the fresh catalyst in the first batch runs.

The trends in the selectivity ratio as a function of periodic position (Figs. 18, 19, and 25) are the same as the pattern of variation of percentage d-character. Many authors have proposed that percentage d-character can be correlated with a Group VIII metal's hydrogenolysis activity (30,31). Moreover, our work on a liquid phase catalytic reaction involving both hydrogenation and hydrogenolysis reactions in series, has verified Sinfelt's observations (19) on the prowess of the Group VIII metals for selectively performing these reactions. Sinfelt noted that the Group $VIII_3$ elements possessed good hydrogenation activity, and relatively poor hydrogenolysis activity. The Group $VIII_1$ elements were good for hydrogenolysis but relatively poor at hydrogenation. These same trends were observed when the Group VIII metals were employed for HDM; for example the Pd catalyst's (k_3/k_1) ratio in Ni-EP was always less than the same ratio for the Ru catalyst. A quick assessment of the hydrogenation activity of a particular catalyst can be made by looking at the concentrations of intermediates it generates. For example, in the Ni-EP HDM data plotted in Figs. 9 and 10 the concentration of Ni-EPH_2 generated by Pd (ca. 10 ppm Ni) is about twice that produced by either Co-Mo or Ru.

The HDM <u>activities</u> of the supported Group VIII metals are comparable to those of Co-Mo and Ni-Mo (see Tables 4 and 6 for details), however, their <u>stability</u> is poor. Deposition of small quantities of nickel (ca. 2 wt %) appear to cause a rapid decline in catalytic activity (Fig. 24). The activity the stabilizes and remains essentially constant in the nickel loading range of 2-8 wt %. It is in this nickel loading range that we collected our kinetic data, and claim it to be steady state. This, of course, cannot be strictly correct since the integrity of the catalytic

surface will always be changing at a microscopic level during HDM (49). The activity decline at low nickel loadings with the Group VIII metals is in contrast to result we have obtained over Mo/Al_2O_3 catalyst employed in Ni-T3MPP HDM (63). There, the deposited Ni was found to exert an autocatalytic effect, and the HDM rate actually increased as more nickel was deposited. Other investigators, such as Sie (6), have noted a similar effect when their starting catalyst was bare alumina.

A limited amount of aged catalyst characterization has been performed, primarily by SEM/EDX and XPS. All intrapellet nickel profiles are uniform, indicating that our kinetic data is not diffusionally masked. Our XPS measurements presented in Figs. 27 to 29 indicate that the aged catalyst surface is heavily covered with nickel and carbon. However, the catalytically active Group VIII metal still persistently gives an XPS signal in the presence of these poisons. This may indicate that some high activity (turnover) sites remain uncovered. Elsewhere (49) we have proposed a conceptual model for the working hydrotreating catalyst surface, which includes, as one of its salient features, the continued presence of active sites uncovered by carbon and metals. There is independent preliminary evidence that such sites are maintained through the catalyst's lifetime, when deposited nickel loadings may be as high as 50 wt % (83).

By comparing the XPS spectra of nickel in an unaged commercially supplied $Ni-Mo/Al_2O_3$ catalyst, with the same spectra for the nickel deposited on HDM-aged Pt and Rh/Al_2O_3 catalysts, we have concluded that the catalytically deposited nickel interacts less strongly with the support, than if it had been added during the catalyst preparation procedure. Intuitively, this indicates that nickel (in itself, a good hydrogenation

catalyst) will exhibit different catalytic activities depending on how it is added to the support surface. This implies that at nickel loadings sufficiently low to avoid pore plugging, the activity of the catalyst will not depend so much on how nickel has been deposited, but rather on its oxidation state, and ability to remain highly dispersed on the support.

It has been speculated (84) that some hydrotreating reactions may be, in the classification of Boudart (47), structure sensitive. The large heteroatom containing molecules require to chemisorb in the correct orientation on the Co-Mo active sites (85). When this information is combined with the facts (86) that hydrogenation reactions are often structure insensitive, while hydrogenolysis reactions are structure sensitive, it is evident that the selectivity of the HDM reaction (which incorporates hydrogenation and hydrogenolysis in series) may be manipulable if an inert element which disrupts catalytic sites is added to the catalyst's surface. Research with Group VIII-IB bimetallic catalysts has shown (32,36,76) that hydrogenolysis reactions, which are postulated to occur on multi-Group VIII metal atom ensembles, are much more strongly affected by the addition of the Group IB metal than hydrogenation reactions. Hydrogenation reactions are little affected by the addition of the Group IB elements, implying they occur on single atom sites.

Our investigations involved Ni-EP HDM over a series of highly dispersed Ru-Cu/Al_2O_3 catalysts. Both these supported elements are insoluble, and we recall that Ni-EP demetallates via a simple two step mechanism; hydrogenation followed by hydrogenolysis. As the catalyst's copper content was increased, at a fixed ruthenium content the hydrogenolysis rate constant decreased significantly, while the

hydrogenation rate constant remained insensitive to catalyst composition (Fig. 31a).

These findings imply that in Ni-EP HDM, hydrogenation is structure insensitive occurring on sites comprised of a small number of Ru atoms. These sites are not destroyed by the addition of copper to the catalyst surface. In contrast, the hydrogenolysis reaction involving cleavage of the porphyrin ring is structure sensitive and occurs on much larger ruthenium multiplets. The number of these large multiplets is rapidly reduced by the addition of copper to the ruthenium catalyst system. Copper acts as an inert spacer atom which divides up ruthenium multiplets. These multiplets probably consist of between five and ten ruthenium atoms (87). Since the diameter of a ruthenium atom is 2.64 Å (88), while Ni-EP's diameter is ca. 14 Å (54), it is easy to visualize how a Ni-EPH_2 molecule can be multiply bonded to a 10 atom Ru ensemble. Multiple point bonding would then facilitate cleavage of the porphyrin ring, and subsequent nickel deposition.

Our XPS measurements on a series of model PCA supported catalysts indicate that the effect of copper on the catalytic activity of ruthenium is geometrical. That is, there is little sharing of electrons between copper and ruthenium. However, while the elements are immiscible they remain in intimate contact on the catalyst support.

Such results open up intriguing possibilities since it now appears feasible to control the relative rates of hydrogenation and hydrogenolysis within a hydroprocessing reaction network by controlling the structural arrangement of the catalytic centers on the support. An important system for further study is Cu-Mo. Both these elements are insoluble (78), and Mo

is known to comprise the active site in industrial hydroprocessing catalysts.

I. F. Conclusions

The main conclusions of this study on Ni-EP and Ni-T3MPP HDM are:

(i) The demetallation mechanism is sequential, involving initial hydrogenation step(s) to activate the metallo-porphyrin followed by terminal hydrogenolysis steps which fragment the porphyrin ring, and deposit nickel on the catalyst's surface.

(ii) The intrinsic HDM kinetics over highly dispersed γ-Al_2O_3 supported Group VIII metals have been measured. The HDM mechanism's selectivity ratio, defined as the terminal hydrogenolysis step rate constant divided by the initial hydrogenation step rate constant, can be varied at will by as much as two orders of magnitude depending on the catalyst used. Group $VIII_1$ metals enhance the hydrogenolysis step, while Group $VIII_3$ metals enhance the hydrogenation step. The selectivity ratio can be correlated with the Group VIII metals percentage d-character.

(iii) The selectivity of the HDM mechanism can be varied in predictable manner by employing a highly dispersed bimetallic Group VIII-IB catalyst system. We used Ru-Cu/Al_2O_3. The addition of copper to the ruthenium catalyst decreased the rate constant for hydrogenolysis by a factor of 2.3, while little affecting the hydrogenation rate constant. These observations were rationalized on the basis of the "geometrical theory", with the hydrogenolysis step being structure sensitive, and the hydrogenation step structure insensitive.

I. G. REFERENCES

1. Yen, T.F., in "The Role of Trace Metals in Petroleum," T.F. Yen, Ed., Ann Arbor Publishers, Inc., Michigan, 1975, Chap. 10.

2. Yen, T.F., Boucher, L.J., Dickie, J.P., Tynan, E.C. and Vaughan, G.B., Amer. Chem. Soc., Div. Pet. Chem. Preprints 13 (1), 59 (1968).

3. Riley, K.L., Amer. Chem. Soc., Div. Pet. Chem. Preprints 23, 1104 (1978).

4. Van Dongen, R.H., Bode, D., Van der Eijk, H., and Van Klinken, J., Ind. Eng. Chem. Proc. Des. Dev. 19, 630 (1980).

5. Oleck, S.M. and Sherry, H.S., Ind. Eng. Chem. Proc. Des. Dev. 16, 525 (1977).

6. Hung, C.-W. and Wei, J., Ind. Eng. Chem. Proc. Des. Dev. 19, 250 (1980).

7. Hung, C.-W. and Wei, J., Ind. Eng. Chem. Proc. Des. Dev. 19, 257 (1980).

8. Agrawal, R. and Wei, J., paper submitted.

9. Ware, R.A. and Wei, J., Paper No. 61a presented at AIChE Annual Meeting, Los Angeles, California, Nov. 14-19, 1982.

10. Rankel, L.A., Amer. Chem. Soc., Div. Pet. Chem. Preprints 26(3), 689 (1981).

11. Rankel, L.A. and Rollmann, L.D., Fuel 62, 44 (1983).

12. Kameyama, H. and Amano, A., J. Japan Petrol. Inst. 25, 118 (1982).

13. Grange, P., Catal. Rev. - Sci. Eng. 21, 135 (1980).

14. Katzer, J.R. and Sivasubramanian, R. Cat. Rev.-Sci. Eng. 20, 155 (1979).

15. Ware, R.A., "Reactivity of Nickel Porphyrins in Catalytic Hydrodemetallation," Sc.D. Thesis, M.I.T., (September, 1983).

16. Rasetti, V., "Synthesis of Nickel (II)-$\Delta^{18,19}$-dehydrocorrinates and isobacteriochlorins," Ph.D. Thesis, ETH-Zurich (1979), p.77.

17. Tamm, P.W., Harnsberger, H.F., and Bridge, A.G. Ind. Eng. Chem. Proc. Des. Dev. 20, 262 (1981).

18. Newson, E., Ind. Eng. Chem. Proc Des. Dev. 14, 27 (1975).

19. Sinfelt, J.H., Advan. Catal. 23, 91 (1973).

20. Sinfelt, J.H., Catal. Rev.-Sci. Eng. 3, 175 (1969).

21. Sinfelt, J.H., Taylor, W.F., and Yates, D.J.C. J. Phys. Chem. 69, 95 (1965).

22. Sinfelt, J.H., and Yates, D.J.C., J. Catal. 8, 82 (1967).

23. Sinfelt, J.H., and Yates, D.J.C., J. Catal. 10, 362 (1968).

24. Yates, D.J.C., and Sinfelt, J.H., J. Catal. 14, 182 (1969).

25. Dalla Betta, R.A., Cusumano, J.A., and Sinfelt, J.H. J. Catal. 19, 343 (1970).

26. Pauling, L., Proc. Roy. Soc. (London), A196, 343 (1949).

27. Johnson, O., J. Catal.-, 503 (1973).

28. Thomas, J.M. and Thomas, W.J., "Introduction to the Principles of Heterogeneous Catalysis," Academic Press, London, 1967.

29. Hayward, D.O., in "Chemisorption and Reactions of Metallic Films," J.R. Anderson, Ed., Academic Press, New York, 1971, Chap.4.

30. Boudart, M. and Ptak, L.D., J. Catal. 16, 90 (1970).

31. Sinfelt, J.H., Catal. Rev.-Sci. Eng. 9, 147 (1974).

32. Sinfelt, J.H., Carter, J.L. and Yates, D.J.C., J. Catal. 24, 283 (1972).

33. Clarke, J.K.A., Chem. Rev. 75, 291 (1975).

34. Ponec, V., Surf. Sci. 80, 352 (1979).

35. Ponec, V., Catal. Rev.-Sci. Eng. 11, 41 (1975).

36. Sinfelt, J.H., Acc. Chem. Res. 10, 15 (1977).

37. Balandin, A.A., Adv. Catal. 10, 96 (1958).

38. Ponec, V. and Sachtler, W.M.H., J. Catal. 24, 250 (1972).

39. Dowden, D.A. in Proc. 5th Int. Congr. Catal., J.W. Hightower, Ed., North-Holland, Amsterdam, 1973, p.621.

40. Sachtler, W.M.H. and Dorgelo, G.J.H., J. Catal. 4, 654 (1965).

41. Bouwman, R. and Sachtler, W.M.H., J. Catal. 19, 127 (1970).

42. Williams, F.L. and Boudart, M. J. Catal. 30, 438 (1973).

43. Soma-Noto, Y. and Sachtler, W.M.H. J. Catal. 32, 315 (1974).

45. Gates, B.C., Katzer, J.R., and Schmit, G.C.A., "Chemistry of Catalytic Processes," McGraw-Hill, New York, 1979, pp.206-213.

46. Boudart, M., J. Am. Chem. Soc. 72, 1040 (1950).

47. Boudart, M. Adv. Catal. 20, 153 (1969).

48. Anderson, J.R. "Structure of Metallic Catalysts," Academic, New York, 1975, Chap.4.

49. Webster, I.A. and Wei, J. This thesis, Chap. 3.

50. Yen, T.F. in "The Role of Trace Metals in Petroleum," T.F. Yen, Ed., Ann Arbor Science, 1975, Chap.1.

51. Vaughan, G.B., Tynan, E.C. and Yen, T.F., Chem. Geol. 6, 203 (1970).

52. Fiero, G.W., Annals of Allergy 23, 226 (1965).

53. Hung, C.-W., "The Kinetics of Hydrodemetallation of Metalloporphyrins," Ph.D. Thesis, M.I.T., August, 1979.

54. Agrawal, R., "Kinetics and Diffusion in Hydrodemetallation of Nickel and Vanadium Porphyrins," Sc.D. Thesis, M.I.T., August, 1980.

55. Webster, I.A. and Wei, J., this thesis, Chap.2.

56. Smith, K.M. ed. "Porphyrins and Metalloporphyrins" Elsevier (1975).

57. Himmelblau, D.M., Jones, C.R. and Bischoff, K.B. Ind. Eng. Chem. Fundam. 6, 539 (1967).

58. Wei, J. and Prater, C.D. Adv. Catal. 13, 203 (1962).

59. Beuther, H. and Schmid, B.K., Proc. 6th World Petrol. Congr., Section III, paper 20 (1963).

60. Beuther, H., Larson, O.A., and Perrotta, A.J. in, "Catalyst Deactivation: Studies in Surface Science and Catalysis, Vol. 6," B. Delmon and G.F. Froment, Eds., Elsevier, 1980, p.271.

61. Galiasso, R. and Morales, A., Appl Catal. 7, 57 (1982).

62. Sie, S.T. in, "Catalyst Deactivation: Studies in Surface Science and Catalysis, Vol. 6," B. Delmon and G.F. Froment, Eds., Elsevier, 1980, p.545.

63. Webster, I.A. and Wei, J., to be published.

64. Scheer, H. in "The Porphyrins," D. Dolphin, Ed., Academic, New York,

1978, Vol.2, Chap.1.

65. Grigg, H. in "The Porphyrins," D. Dolphin, Ed., Academic, New York, 1978, Vol.2, Chap.10.

66. Ahuja, S.P., Derrien, M.L. and LePage, J.F., Ind. Eng. Chem. Prod. Res. Dev. 9, 272 (1970).

67. Katzer, J.R. and Sivasubramanian, R., Catal. Rev.-Sci. Eng. 20, 155 (1979).

68. Swingle, R.S. and Riggs, W.M. in, "Critical Reviews in Analytical Chemistry, Vol.5," CRC Press, 1975, p.267.

69. Davis, S.M., Zaera, F. and Somorjai, G.A., J. Catal. 77, 439 (1982).

70. Wukasch, J.E., and Rase, H.F., Ind. Eng. Chem. Prod. Res. Dev. 21, 558 (1982).

71. Wu, M. and Hercules, D.M., J. Phys. Chem. 83, 2003 (1979).

72. Lo Jacono, M., Schiavello, M. and Cimino, A., J. Phys. Chem. 75, 1044 (1971).

73. Cimino, A., Lo Jacono, M. and Schiavello, M., J. Phys. Chem. 79, 243 (1975).

74. Myers, E., personal communication, Stamford Research Center, American Cyanamid Co., 1982.

75. Tayer, W.F., Yates, D.J.C. and Sinfelt, J.H., J. Phys. Chem. 68, 2962 (1964).

76. Sinfelt, J.H. J. Catal. 29, 308 (1973).

77. Webster, I.A. and Wei, J., this thesis, Chap.2.

78. Hansen, M., "Constitution of Binary Alloys," McGraw-Hill, New York, 1958, pp.600 and 620.

79. Kim, K.S. and Winograd, N., J. Catal. 35, 66 (1974).

80. Toolenaar, F.J.C.M., Stoop, F., and Ponec, V. J. Catal. 82, 1 (1983).

81. Sachtler, J.W.A. and Somorjai, G.A. J. Catal. 81, 77 (1983).

82. Fuhrhop, J.H., in "The Porphyrins," D. Dolphin, Ed., Academic, New York, 1978, Vol.II, Chap.5.

83. Miller, J.W., personal communication, Union Oil Co. of California, 1983.

84. Broderick, D.H. and Gates, B.C. AIChE. J. 27, 663 (1981).

85. Voorhoeve, R.J.H. and Stuiver, J.C.M. J. Catal. 23, 243 (1971).

86. Somorjai, G.A., "Chemistry in Two Dimensions: Surfaces," Cornell University Press, Ithaca, New York, 1981, p.401.

87. Burch, R., Acc. Chem. Res. 15, 24 (1982).

88. Hume-Rothery, W. and Raynor, G.V., "The Structure of Metals and Alloys," 4th ed., The Institute of Metals, London, 1962, p.95.

CHAPTER II

The Synthesis of Co-Mo/Al_2O_3 Catalysts for Hydrodemetallation (HDM) of Heavy Oils by Metal Napthenate Demetallation over γ-Al_2O_3. Their activity measurements and characterization (SEM/EDX, AES) in the HDM of nickel tetra (3-methylphenyl) porphyrin.

II. A. Summary of Chapter

Oil soluble cobalt and molybdenum napthenates have been dissolved in a clean white oil, and demetallized over γ-Al_2O_3 catalyst supports in batch autoclave experiments at temperatures of 290°C and 360°C, and hydrogen pressures of 500 and 1000 psig H_2. These *in situ* synthesized Co-Mo/Al_2O_3 catalysts were subsequently used for the catalytic hydrodemetallation (HDM) of a model metal containing residua consisting of Ni-tetra (3-methylphenyl) porphyrin dissolved in a clean white oil at 60 ppm Ni. This test HDM reaction at 360°C, 1000 psig H_2 was used as a measure of the activity of the synthetic catalysts. An *in situ* synthesized Mo/Al_2O_3 catalyst prepared by depositing the Mo at 360°C, 1000 psig H_2, exhibited a higher HDM catalytic activity than traditional commercially manufactured Co-Mo/Al_2O_3 and Ni-Mo/Al_2O_3 catalysts. SEM/EDX and AES measurements on the catalyst

showed that metal napthenate demetallation coats the Al_2O_3 particles in a carbonaceous sludge, which however, remains porous enough to permit metals to primarily deposit on the Al_2O_3. It is suggested that the methodology of using metal napthenates to synthesize and regenerate hydrotreating catalysts may be best accomplished in a slurry reactor.

II. B. Introduction

During the catalytic upgrading of heavy oils, the catalysts, which are typically either Co-Mo or Ni-Mo/γ-Al_2O_3 (1), require to function efficiently in the presence of catalyst poisons. These deposits are primarily the metals Ni, V, and Fe, and carbonaceous deposits, commonly referred to as coke. Catalyst coking occurs relatively quickly during the lifetime of the catalyst. For example, Beuther and Schmid (2) found that one half of the carbon deposited in 16 days of operation was deposited during the first 2 hours. After the initial rapid rise in carbon loading, the value tends to stabilize in the range 10-20 wt % carbon (2,3), once some form of dynamic equilibrium between coke formation and destruction, is established. In work reported elsewhere (4) we have explained how the carbonaceous overlayer should be viewed as an integral feature of the working hydrotreating catalyst. It is capable of hydrogen exchange reactions with reactant oil molecules, and facilitates the desorption of molecules which may be strongly bound at the catalyst's active site.

In contrast, deposition of the metal contaminants Ni, V and Fe is irreversible. In the short term these deposits poison active sites, and eventually dictate the catalysts's lifetime when they plug its pores (5-7). The metals loading tolerance of hydrotreating catalysts has reported to be within the range 50 to 65 wt % metals (8,9).

As with hydrodesulfurization (10) and hydrodenitrogenation (11), model compound studies in catalytic hydrodemetallation (HDM) have been useful in delineating the heteroatom removal reaction network, and kinetics. Since in real crudes, metal in the porphyrinic form can account for up to 50% of the oil's total metal content (12), we (13-15) and others (16,17) have used nickel and vanadyl porphyrins as model metal bearing compounds in catalytic HDM studies.

Hung and Wei (13,14) investigated the HDM of nickel etioporphyrin (I), (Ni-Etio), nickel tetraphenylporphine (Ni-TPP), and vanadyl etioporphyrin (VO-Etio) when dissolved in a white oil as a solvent. More recently, Ware and Wei (15) have reported on the HDM of nickel tetra(3-methylphenyl) porphyrin (Ni-T3MPP). Each of these compounds is similar in that the tetra-pyrrolic ring structure within which the metal atom is coordinated remains the same, however, different substituents are present either at the methine bridge carbons which link the pyrrole molecules, or at the pyrrolic hydrogens. Porphyrin and metalloporphyrin structures are fully described by Smith (18).

All of the aforementioned experiments were conducted on the oxidic form of a Co-Mo/Al_2O_3 catalyst. Hung and Wei's (13,14) experiments were conducted with a batch autoclave reactor, and for each run a fresh batch of catalyst was used. Their data are therefore representative of events occurring over fresh, unaged catalyst, which is not the condition at which the catalyst efficiently functions for the majority of its working life (2,7). Similarly Ware and Wei (15) performed their experiments so that metals loading never exceeded ca. 1 wt %. These conditions are also representative of a fresh catalyst.

Hydroprocessing catalysts deactivate in a very characteristic fashion as recently described by Tamm et al (7). A deactivation curve from their work is reproduced in Fig. 1, where the average catalyst temperature required to meet a particular product specification is plotted as a function of run time. Out with the time periods of the initial and ultimate declines in catalyst activity, attributed to rapid coking and pore mouth plugging by metals, respectively, it would seem desirable to explore method whereby the intrinsic catalytic activity of the catalyst could be regenerated in situ as the reactor operates. Since the decline in catalytic activity during stage 2 of Fig. 1 is most likely a result of poisoning of the Co-Mo/Al_2O_3 active sites by contaminant metals (4), a method whereby a new catalytically active overlayer of Co and Mo can be deposited on the aged substratrum is therefore worthy of attention.

In this paper we describe how we have approached this problem by depositing Co and Mo from oil soluble metal napthenates. Starting a batch HDM run with the γ-Al_2O_3 support as the only catalytic material in a well mixed autoclave, we show how we can generate catalysts in situ in the reaction environment, which are then subsequently active for HDM. The location of the metals deposits has been determined by SEM/EDX and AES. It is observed that metal napthenate demetallation leaves the alumina particles buried in a thick carbonaceous deposit, which is apparently permeable to the model oil's metalloporphyrins. Nickel from Ni-T3MPP was found to deposit only on the Al_2O_3 core of such particles.

Because of the coke build-up which accompanies metal napthenate demetallation it is unlikely that such compounds can be used for Group VIII-VIB metal deposition in the regeneration of aged hydroprocessing

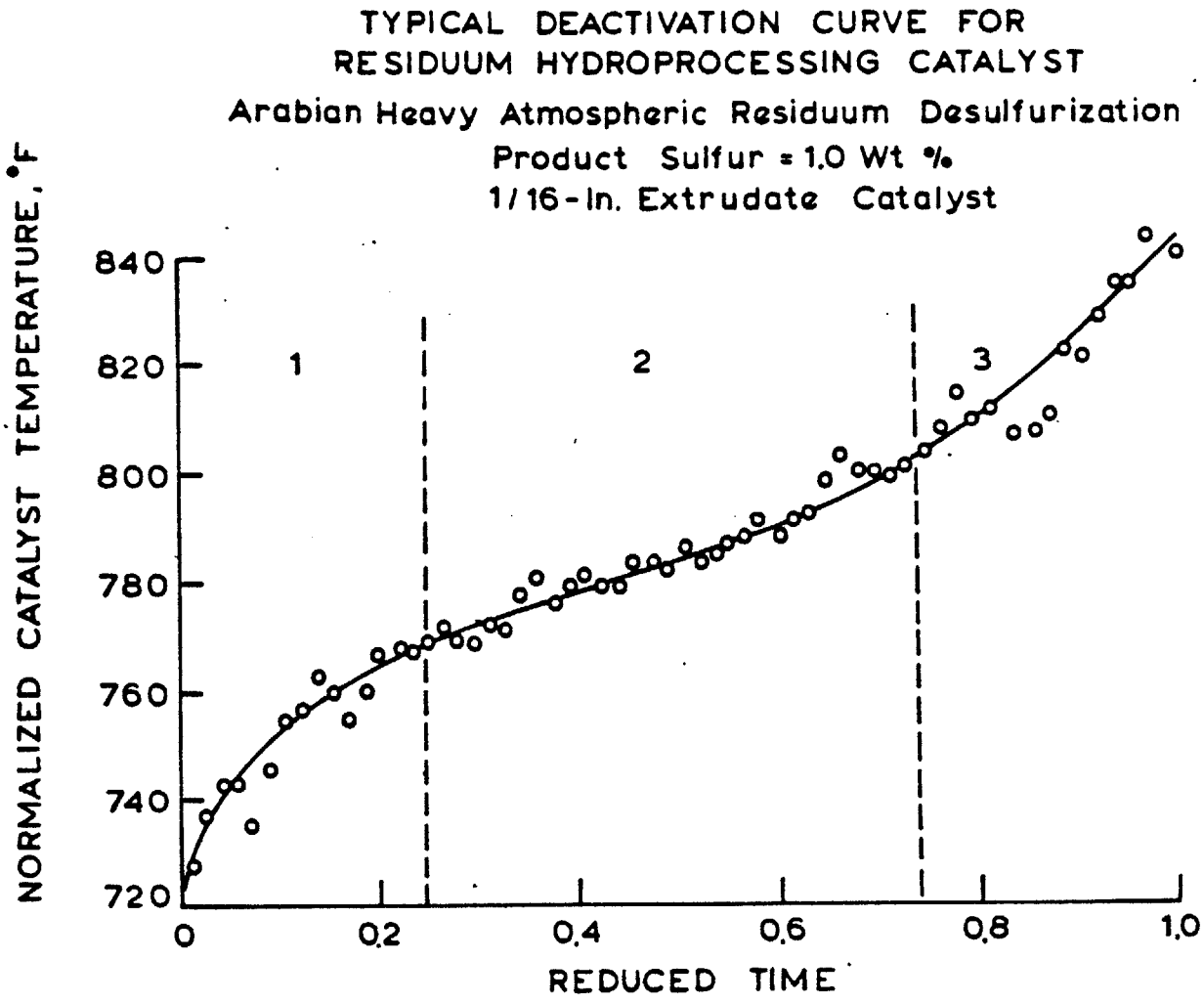

Figure 1: A typical deactivation curve for a residuum hydroprocessing catalyst, from Tamm et al (7). Three distinct regions of deactivation exist. The accelerated activity decay in Region 1 and 3 is attributed to the build-up of a carbonaceous overlayer (4), and pore mouth plugging by deposited metals, respectively.

catalysts within fixed bed hydrotreaters. In such a reactor the pressure drop during napthenate demetallation for in situ catalyst regeneration, would soon become unacceptably high, because of bed plugging. However, these problems do not arise when HDM is conducted within a slurry bed reactor, where the small catalyst particles (100μ size) are kept suspended an oil/hydrogen gas/catalyst broth. Increased emphasis is being put on these reactors for resid upgrading (19).

II. C. Experimental

The catalytic HDM experiments were performed within a well-mixed 1 liter batch autoclave reactor (Autoclave Engineers, Erie, PA, Model AFP 1005). The system is exactly a described previously (13) except that an extra discharge line with a 0.5μ filter inlet was positioned at the bottom of the reactor so that its contents could be quickly discharged, while retaining the catalyst in the reactor for a subsequent demetallation experiment. With this mode of operation successive HDM experiments could be performed over the one charge of catalyst, which would become heavily contaminated by the metal and carbon deposits collected during an HDM run. The initial injection of the Al_2O_3 support was achieved by using a special catalyst loader system, also previously discussed (13).

The starting catalyst for each experiment was a commerically available γ-Al_2O_3 catalyst support (SA-6273, Norton Company, Akron, OH), whose chemical and physical properties are given in Table 1. The catalyst was received a 1/16" diameter spheres, and then crushed and sized to 65-80 mesh (175-208 microns diameter). Prior to an experiment, the required amount of catalyst was heated for 12 hours at 440°C under flowing helium, in a tube furnace (Lindberg) to drive off water.

Table 1: Properties of γAl_2O_3 support (Norton Co. SA-6273, Lot Number 62731)

(i) Chemical Composition

Al_2O_3	>	99.85 wt %
Na_2O	<	0.015 wt %
SiO_2	<	0.09 wt %
Fe_2O_3	<	0.06 wt %

(ii) Physical Properties

Crystal phase (by X-ray diffraction): γAl_2O_3

Pore volume, (H_2O): 0.67 cm^3/g.

Average pore diameter: 68Å

Surface Area: 218.7 m^2/g.

A model residua was made by dissolving nickel tetra(3-methylphenyl) porphyrin (Ni-T3MPP) (Midcentury Chemicals, Posen, IL) in a clean white oil (Nujol, Plough, Inc., Memphis, TN) to a concentration of ca. 60 ppm Ni. The molecular structure of Ni-T3MPP is depicted in Fig. 2. While Ni-T3MPP has not been definitively found in real crudes (21), it may be representative of condensed porphyrins of higher aromaticity which have been speculated as comprising asphaltenes (22). Nujol is a complex mixture of napthenates, paraffins and isoparaffins, (20) and is sulfur and nitrogen free, so our HDM experiments were not complicated by the simultaneous occurrence of HDN and HDS reactions. The porphyrin dissolution method has been fully detailed previously (13). The key points in this process are that dissolved air is removed from the Nujol, and the Ni-T3MPP/Nujol mixture is heated under an inert atmosphere of helium.

To deposit the metals cobalt, molybdenum, nickel and vanadium onto the Al_2O_3 particles demetallation experiments with cobalt (Mooney Chemicals, Inc., Cleveland, OH), molybdenum and vanadyl (Shepherd Chemical Co., Cincinnati, OH) and nickel (Pfaltz and Bauer, Inc., Stamford, CT) napthenates dissolved in Nujol were performed. Experiments were ran with solutions of both one and more than one metal. The procedure for dissolving the metal napthenates in Nujol was the same as that for porphyrins (13) except that no heat was applied. The concentrations of the catalytically active metals (Co, Mo) in the napthenate/Nujol oil mixtures are given in Table 2. The concentrations are such that when 420g of the Co and Mo oil mixtures are completely demetallatized over 1g of alumina, the resulting catalyst has the same Co and Mo loadings as American Cyanamid's commercially manufactured HDS-16A Co-Mo/Al_2O_3 hydrotreating catalyst. The

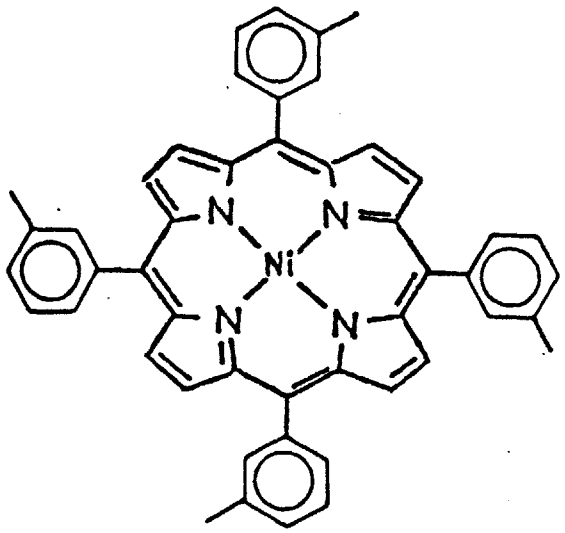

Figure 2: Molecular structure of Ni (II)-tetra (3-methylphenyl) porphyrin (Ni-T3MPP). This compound was used as the model metal bearing molecule in the synthetic crude used for the HDM experiments.

Table 2: Metal conentrations of metal-napthenate/Nujol oil mixtures. The metal napthenates were supplied as containing 6 weight percent metal.

Metal	Concentration of metal in metal napthenate/Nujol oil mixture (ppm)
Co	320
Mo	580
Ni	452
V	454

composition of American Cyanamid's HDS-16A and HDS-9A hydrotreating catalysts is given in Table 3. Some Ni-T3MPP demetallation experiments were also performed over these catalysts, to compare their activity with the in situ generated catalysts formed by metal napthenate demetallation over γ-Al_2O_3. The commercial catalysts were received a 1/16" diameter extrudates, and crushed and sieved into the size range 170-200 mesh (74-88μ) for use. We have independently verified that catalysts of this size are not limited by diffusion. Like the Al_2O_3, the only pretreatment of the HDS-16A and HDS-9A catalysts was a heat treatment at 440°C for 12 hours in a tube furnace under flowing helium to drive off water. The catalysts were initially injected into the reactor in the oxide state.

One HDM experiment was performed over γ-Al_2O_3 that was pre-chlorided prior to injection into the reactor. The chloriding apparatus is depicted in Fig. 3. The alumina was placed in a fused silica boat and contacted with a flowing stream of hydrogen, saturated with chloroform (MCB Reagents, Gibbstown, NJ) for 12 hours at 440°C. After cooling the catalyst under flowing hydrogen, the desired amount of chlorided alumina was immediately injected into the reactor to perform HDM.

The hydrogen gas used in all experiments was ultrahigh purity at 99.999% H_2 with less than 3 ppm O_2. Helium was at 99.995% purity. Both gases were purchased from Matheson Gas Products, Gloucester, MA.

The most commonly employed experimental conditions are listed in Table 4. The model residua (Ni-T3MPP dissolved in Nujol at ca. 60 ppm Ni) was generally demetallatized at 358°C, and 1000 psig H2. The mass of alumina injected into the reactor to initiate a series of runs was approximately 0.95g, while the oil mass averaged 420g. The demetallation conditions for

Table 3: Properties of American Cyanamid's HDS-16A and HDS-9A hydrotreating catalysts.

A. Chemical Composition (wt. percent)

	HDS-16A	HDS-9A
CoO	5.7	-
NiO	-	3.2
MoO_3	12.2	17.5
Na_2O	0.03	0.03
Fe	0.04	0.03
SO_4	-	0.4
SiO_2	-	0.5
Al_2O_3	balance	balance

B. Physical properties

pore volume (cm^3/g)	0.50	0.52
pore diameter (Å)	80.4	88
surface area (m^2/g)	176	170

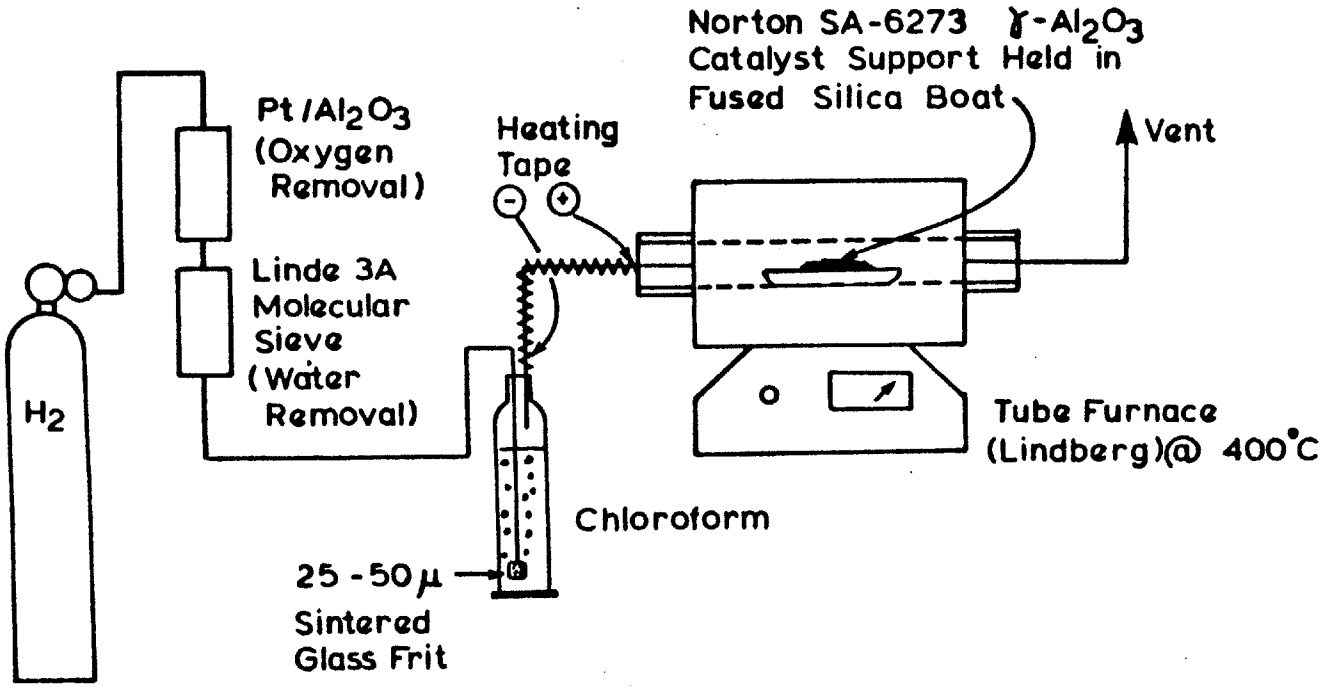

Construction Materials : 316 - Stainless Steel Tubing, and Fittings, Ground Glass Fittings

Figure 3: Schematic of apparatus used to chloride γ-Al_2O_3. Hydrogen gas was saturated with chloroform and then blown over the γ-Al_2O_3 for ca. 12 hours at 400°C. Catalyst was cooled under flowing hydrogen and immediately injected into autoclave.

Table 4: Typical Operating Conditions

Oil	:	420g (400g is initially charged to the reactor at the beginning of any particular demetallation sequence; 20g is injected via the catalyst loader. In successive runs within the one demetallation sequence, when the catalyst is already contained within the autoclave, 420g of Ni-T3MPP/Nujol or metal napthenate/Nujol mixture is directly charged to the reactor)
Catalyst	:	ca. 0.95g SA-6273 γ-Al_2O_3, or HDS-16A, or HDS-9A. Catalyst is predried under helium atmosphere. Sized either 74-88μ (HDS-16A, HDS-9A) or 175-208μ (SA-6273)
Hydrogen Pressure	:	1000 psig for Ni-T3MPP demetallation; 500 or 1000 psig for metal napthenate demetallation
Temperature	:	290-360°C
Impeller Speed	:	ca. 500 rpm

the napthenate-Nujol solutions for rapidly depositing the catalytically active metals Co and Mo, ranged from mild at 290°C, 500 psig H_2 to severe at 358°C, 1000 psig.

A series of seven demetallation sequences were performed with alumina as the starting catalyst. Within each sequence, and between Ni-T3MPP HDM experiments, which were used to assess the catalyst's activity, the alumina was treated in different ways by contacting it with the napthenate-Nujol solutions at process conditions.

Oil samples were withdrawn from the reactor during an HDM experiment and diluted with xylene (X-16, Fisher Scientific Co., Fairlawn, NJ) such that their total nickel concentration was in the range 0-5 ppm. They were then analyzed for both total nickel and Ni-T3MPP concentrations by atomic absorption spectrophotometry (Perkin-Elmer Model 360), and UV-Visible spectrophotometry (Bausch and Lomb Spectronic 2000), respectively. Ni-T3MPP absorbs strongly in the visible range at 526 nm. This peak was used for analysis. Using Beer's law we estimated a conversion factor of 0.272 Absorbance Units/ppm Ni in Ni-T3MPP. More detailed analytical procedures have been furnished elsewhere (23).

At the termination of a run sequence the oil-catalyst slurry was pipetted from the reactor and the catalyst recovered by filtering the slurry through a 5μ filter (Millipore Corporation, Bedford, MA). The catalyst was then cleaned overnight with xylene in a Soxhlet extractor (Fisher Scientific Co.) and subsequently dried in a furnace (Blue-M, Blue Island, IL) at 100°C for six hours. This cleaned catalyst was examined by SEM-EDX and AES. Since it was desired to examine the morphology and distribution of metals through sectioned catalyst particles the catalysts

were mounted in an epoxy mixture (Epon hardener and resin) in a 1/4-inch diameter hole drilled in a 1-inch diameter phenolic resin disk (Miller Stephenson Chemical Co., Inc., Danbury, CT). The disk was then ground down successively on 400 and 600 grit sand papers, washed with copious quantities of distilled water, and finally polished on an 8-inch diameter Met-X polishing cloth with alumina powders of 1 and 0.3 microns (Mark V Laboratory Inc., East Granby, CT). The polished surface, with some of the catlyst particles now exposed through their mid-section, was washed clean with distilled water, dried, and then coated with a thin film of gold to a depth of ca. 200Å in an evaporative coater (Edwards, Model 306A). For SEM/EDX the entire surface containing the sectioned catalyst particles was coated to make the surface conductive. Gold coating does not mask the intensity of the X-ray signals since they emanate from a depth of ca. 1 micron (24).

With AES some attempt must also be made to increase the surface conductivity of the mounted catalysts to eliminate charging problems. Completely evaporatively coating the milled surface region containing the sectioned catalysts with gold is prohibited, since AES is an extremely surface sensitive analytical technique which probes depths on the order of 10-30Å (25,26). We solved this problem by masking half of the milled region with aluminum foil and evaporating gold onto the uncovered region. AES was then performed on sectioned catalyst particles that were located close to the interface of gold free-gold covered regions. Charge build up in this region was not a problem because of its intimacy with the conducting gold layer.

AES spectra were collected with a Perkin-Elmer Physical Electronics

590 scanning Auger microprobe (Eden Prairie, MN) which was digitally interfaced to a PHI Multiple-technique Analytical Computer System (MACS). The primary electron beam was operated at 3keV, 0.073 A, and a modulation voltage of 6V peak-to-peak. The analyzer was of the cylindrical mirror type (PHI Model 25-110).

Scanning Electron Microscopy (SEM)/Energy Dispersive X-ray analysis (EDX) was performed on an AMR Model 1000A SEM, equipped with a Tracor Northern TN2000 X-ray analyzer. The beam energy was set at 20keV, and during X-ray analysis the counting time was either 25 or 60 seconds. Both line scans and elemental maps were collected.

II. D. Results

II. D. 1. Kinetic Measurements

Details of each of the experimental run sequences are presented in Tables 5 and 6. Seven runs are shown, within which the same alumina batch catalyzed various demetallation experiments (A,B,etc.). In Table 5, the molecule that was demetallized, the temperature and pressure at which the demetallatization was performed, and the range of weight percent nickel on the alumina from the beginning to the end of the experiment, are listed. Table 6 lists the first order rate constants for total nickel removal and Ni-T3MPP removal, along with the figure number where the rate data are plotted.

Figures 4a and b show, in a first order plot form, the data for Ni-T3MPP and total nickel removal, respectively, from Table 6's Run number 1. In each figure two sets of data points for Ni-T3MPP demetallation over the commercially manufactured HDS-16A and HDS-9A catalysts (Table 3) are also included. Run 1 can be viewed as an initial exploratory experiment to

Table 5: Details of the Demetallation Run Sequences*

Run #	1	2	3	4	5	6	7
Starting Mass of Al_2O_3(g)	0.9369	0.9561	0.9613	0.9565	0.9503	0.9487	1.0005
Demetallation							
A	Ni-T3MPP 358,1000, 0-0.67	Co,Mo-nap 290,500 45.5	Co,Mo-nap 358,1000 18.0	Mo-nap 354,1000 34.30	Co-nap 360,1000 20.4	Ni-nap 360,1000 71.87	Al_2O_3 was prechlorided (see Fig. 3)
B	Ni-T3MPP 358,1000, 0.67-0.97	Ni-T3MPP 358,1000 0-1.66	Ni-T3MPP 360,1000 0-2.21	Ni-T3MPP 360,1000 0-2.34	Ni-T3MPP 360,1000 0-1.34	Ni-T3MPP 360,1000	Ni-T3MPP 360,1000 0-1.28
C	Mo-nap 290,500, 45.5	Co,Mo-nap 360,500 18.7	Ni-T3MPP 337,1000 2.21-4.48				
D	Ni-T3MPP 358,1000 0.97-2.94	Ni-T3MPP 358,1000 1.66-3.93	Ni-T3MPP 315,1000 4.48-6.91				
E	Mo-nap 290,500, 45.5	Ni-nap 358,500 35.3	V-nap 350,500 40.5				
F	Ni-T3MPP 358,1000 2.94-5.01	Ni-T3MPP 358,1000 3.93-6.28	Ni-T3MPP 315,1000 6.91-9.00				
G	Co-nap 290,500 68.17						
H	Ni-T3MPP 358,1000 5.01-5.81						

*Each entry gives the molecule being demetallized, the run temp (°C), the run pressure (psig H_2), and the range of weight % nickel on the alumina, respectively. In the metal napthenate demetallation experiments, (e.g. Run 1-C), the last number is the run time in hours. Each experiment went to 100% demetallation.

Table 6: First order rate constants for total nickel and Ni-T3MPP removal*

Run #	1	2	3	4	5	6	7
Demetallation							
A	0.46 1.80 (4)	-	-	-	-	-	-
B	0.09 1.33 (4)	4.91 9.57 (5)	56.41 127.03 (7)	164.87 243.20 (10)	3.05 9.01 (10)	1.91 5.73 (10)	1.32 3.07 (10)
C	-	-	36.44 79.00 (7)				
D	5.67 8.65 (4)	61.26 156.82 (5)	12.40 24.61 (7)				
E	-	-	-				
F	11.83 19.25 (4)	56.37 113.56 (5)	17.95 29.92 (9)				
G	-						
H	12.86 15.19 (4)						

American Cyanamid Catalysts

358°C, 1000 psig H_2

Catalyst	1st order rate constant (g.oil/g.cat.hr.)		Fig. No.
	Ni-T3MPP Removal	Total Ni Removal	
HDS-16A Co-Mo/Al_2O_3	235.2	126.1	4
HDS-9A Ni-Mo/Al_2O_3	83.8	34.0	4

*top number : 1st order rate constant, total Ni removal; g.oil/g.cat.hr.
middle number : 1st order rate constant, Ni-T3MPP removal; g.oil/g.cat.hr.
bottom number : Figure number in which the data are displayed.
(in parenthesis)

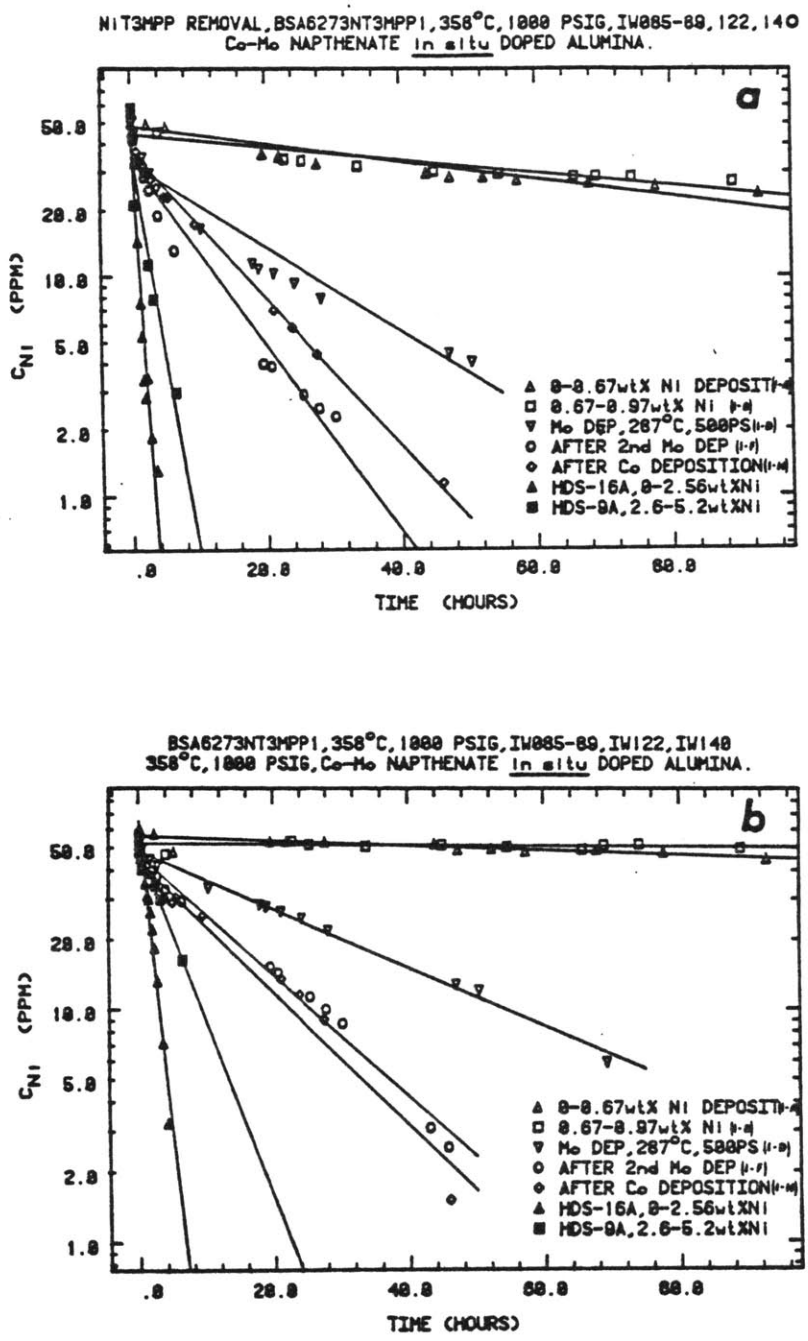

Figure 4: (a) First order rate plot of Ni-T3MPP removal during Run 1 of Table 6.
(b) Similar plot for total nickel removal during Run 1. Demetallation data over American Cyanamid's HDS-16A and HDS-9A catalysts are also shown. The temperature and pressure of each run was 358°C, and 1000 psig H_2, respectively.

see if Co and Mo deposition onto the alumina from the metal-napthenates, actually does increase the demetallation rate over the alumina. During Runs 1-A and -B the Ni-T3MPP was demetallatized over untreated Al_2O_3. Little demetallation activity was evident. In Run 1-A, by a mass balance, ca. 0.67 wt % Ni was deposited on the Al_2O_3. When this Ni impregnated Al_2O_3 was used as the starting catalyst, for demetallizing a second batch of Ni-T3MPP in Run 1-B, no significant change in HDM activity occurred (see rate constants in Table 6). Intuitively we had expected that the Ni impregnated Al_2O_3 of Run 1-B might show more activity than the fresh Al_2O_3 of Run 1-A, and in a sense be autocatalytic. The data of Runs 1-A and 1-B do not substantiate those ideas.

During Run 1-C, a Mo-napthenate/Nujol solution, at 580 ppm Mo (Table 2) was demetallized at 290°C, 500 psig for 45.5 hours over the same Al_2O_3 batch. At this time the Mo concentration, in the oil samples removed from the reactor and analyzed by atomic absorption, was zero, however we are uncertain as to whether all this Mo actually deposited onto the alumina substrate. This question will be more fully addressed later. However, if all the Mo in the Mo-napthenate/Nujol oil solution did deposit on the Al_2O_3, it would have formed a catalyst of composition Mo (26 wt %)/Al_2O_3. Since we did not perform an elemental analysis of the in situ formed catalysts, we cannot independently verify this figure. Nevertheless, we believe it to be unrealistically high.

Referring to the results of Ni-T3MPP demetallation run number 1-B, presented in Figs. 4a and b, respectively, it is evident that the in situ deposition of Mo has created a Mo/Al_2O_3 catalyst which exhibits HDM activity far superior to that of untreated Al_2O_3. The first order rate

constants are listed in Table 6; the rate of Ni-T3MPP removal over the *in situ* formed Mo/Al_2O_3 (Run 1-C) has increased 4.8 times over that of fresh Al_2O_3 (Run 1-A), while the rate of total nickel removal has increased by a factor of 12.3.

During Run 1-E, more Mo was deposited from a napthenate solution at the same process conditions as Run 1-C (290°C, 500 psig H_2). Again, according to oil samples withdrawn from the reactor during the run, complete Mo demetallation occurred. Further increases in Ni-T3MPP HDM activity were observed during Run 1-F over this more highly loaded Mo catalyst (Table 6). The rate of Ni-T3MPP removal has now been boosted to 10.6 times the rate over fresh Al_2O_3, and the rate of total nickel removal has been increased 25.71 times.

Run 1-G was subsequently performed which demetallized cobalt from a cobalt napthenate/Nujol solution at the same process conditions previously employed to demetallate the Mo-napthenate solutions. The only difference in run conditions between Runs 1-C, E and 1-G was that the latter experiment continued for 68.17 hours (versus 45.5 hours) to ensure complete cobalt demetallation as ascertained by oil sample analysis. Again, however, we are uncertain as to the exact fate of the cobalt. If all the cobalt had deposited on the initially injected alumina then its loading would be 14.3 wt % Co. As is discussed later, we believe this value to be high.

The deposition of cobalt in Run 1-G affected the rates of Ni-T3MPP removal, and total nickel removal in Run 1-H (relative to the rates in Run 1-F) in different ways:

(a) The rate of total nickel removal was slightly enhanced by cobalt

deposition. The first order rate constant increased by 8.7% from 11.83 to 12.86 g. oil/g. cat. hr..

(b) In contrast the first order rate constant for Ni-T3MPP removal decreased by 21.1% from 19.25 to 15.19 g. oil/g. cat. hr..

Thus in Run 1 the most active catalyst for total nickel removal was obtained after the demetallation of two Mo batches and one Co batch. The rate constant for total nickel removal was increased from 0.46 to 12.86 g. oil/g. cat. hr. by in situ deposition of the catalytically active metals onto the fresh Al_2O_3. The maximum demetallation rate achieved, however, was still far less than that obtained over the commercially manufactured HDS-16A (Co-Mo) and HDS-9A (Ni-Mo) catalysts. The demetallation behavior of Ni-T3MPP over fresh forms of these catalysts at the same process conditions as the Ni-T3MPP HDM experiments of Run 1 are shown in Figs. 4a and b. The first order rate constants are given in the inset in Table 6. For example, the first order rate constant for total nickel removal achieved a maximum value of 12.86 g. oil/g. cat. hr., while the same rate constant over the more efficient HDS-16A, and HDS-9A catalysts was 126.1, and 34.0 g. oil/g. cat. hr., respectively. Clearly the activity of the in situ synthesized catalyst has to be improved. This was the objective of Runs 2 to 5.

The variables at our disposal to realize an activity increase are the napthenate demetallation process conditions (temperature, and hydrogen pressure) and the sequence in which the catalytically active metals are deposited; either separately or simultaneously. We elected to keep the variable, of metal napthenate concentration, constant at the values in Table 2.

In Run 2 we examined the catalytic activity of Co-Mo doped alumina synthesized by the simultaneous demetallation of the Co and Mo napthenates. The metal-napthenate demetallation pressure was always held constant at 500 psig H_2, whereas the temperature was increased from 290°C (Run 2-A) to 360°C (Run 2-C). This latter temperature is more realistic of the temperature at which heavy oils are industrially hydrotreated (27). The relevant data from Run 2 are displayed in Fig. 5, where we show in first-order plot form the demetallation data from Runs 2-B, 2-D and 2-F. For comparison, HDM data over fresh, untreated Al_2O_3 (Run 1-A), and fresh HDS-16A are also graphed.

The first simultaneous deposition of Co and Mo occurred in Run 2-A. The subsequent HDM of Ni-T3MPP over the in situ generated catalyst occurred in Run 2-B (Fig. 5). During this run the first order rate constants for total Ni and Ni-T3MPP removal were 4.91 and 9.57 g. oil/g. cat. hr., respectively. This represents no significant change in the same rate constants which were found when Mo-napthenate was solely demetallized, and then the HDM kinetics measured in Run 1-D; there the rate constants were 5.67 and 8.65 g. oil/g. cat. hr. With this same catalyst batch held within the reactor, another mixed batch of Co and Mo napthenates were simultaneously completely demetallized, however in this run (2-C), the temperature was increased to 360°C (the same temperature as had been employed for Ni-T3MPP demetallation), while the pressure was still maintained at 500 psig H_2.

The subsequent Ni-T3MPP demetallation experiment of Run 2-D showed considerably enhanced rates, with the rate constants for total nickel and Ni-T3MPP removal being 61.26 and 156.82 g. oil/g. cat. hr., respectively.

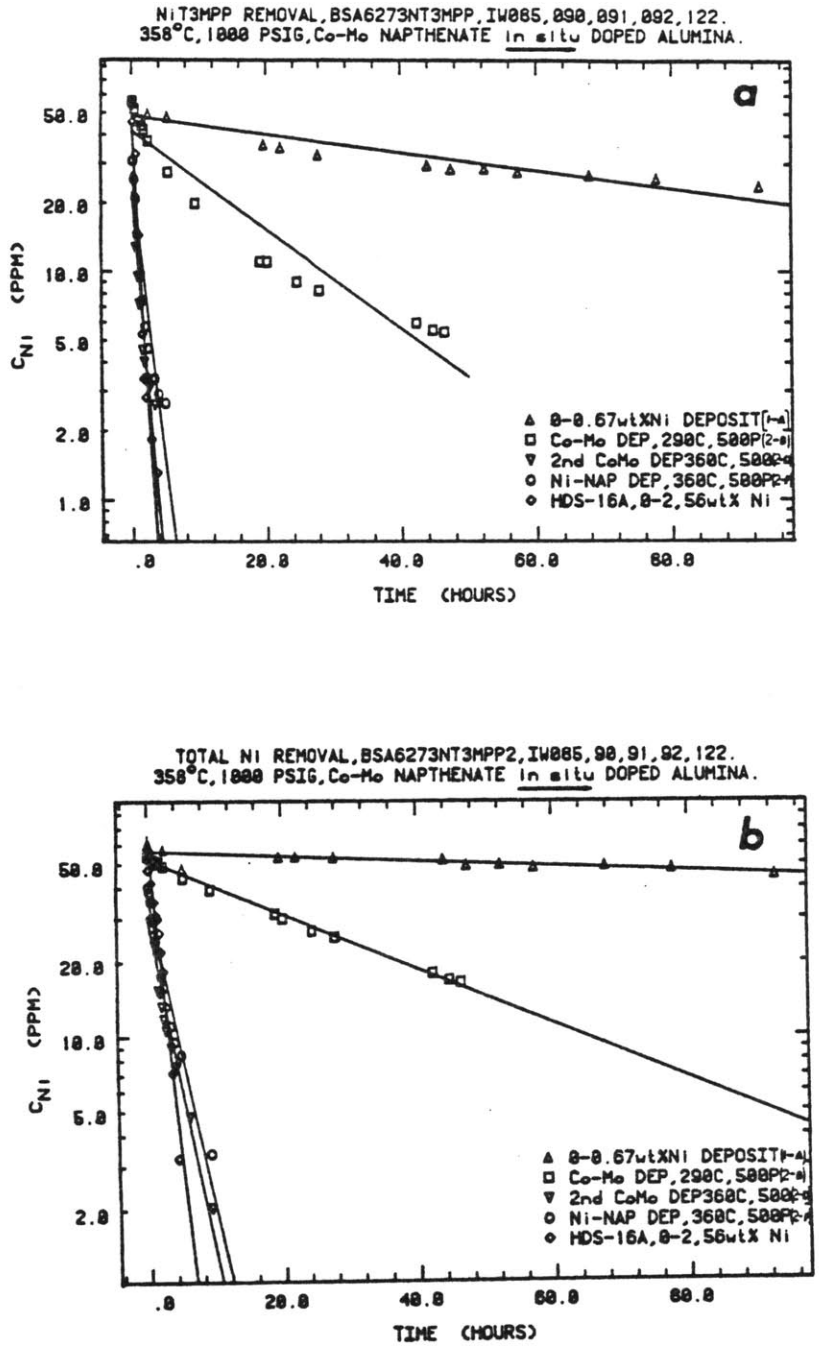

Figure 5: (a) First order rate plot of Ni-T3MPP removal during Run 2 of Table 6.
(b) Similar plot for total nickel removal during Run 2. Demetallation data over fresh American Cyanamid HDS-16A catalyst is also plotted for comparison. The temperature and pressure of each Ni-T3MPP run was 358°C and 1000 psig H_2. Metal napthenate demetallation, to deposit the metals Co, Mo, and Ni, on the alumina was performed at 290°C or 358°C, and at 500 psig H_2 (see Table 5).

As can be seen from Figs. 5a, 5b and the insert in Table 6, this last high temperature metal napthenate demetallation (Run 2-C), has generated a catalyst, from the initially untreated Al_2O_3, that has an HDM activity which exceeds that of American Cyanamid's HDS-9A catalyst, and is only slightly less than the activity of Co-Mo/Al_2O_3 (HDS-16A). It is also worth noting that the HDM kinetics on the commercial catalysts, probably represent a best case scenario since the kinetics over each of these catalysts, were measured with the fresh catalyst. Coke accumulation on the industrial catalysts can therefore be expected to be less than on the treated Al_2O_3 catalysts. Elsewhere (4), we have explained, with a conceptualized model of the working hydrotreating catalyst surface, how coke (or the carbonaceous overlayer) causes a decline in HDM activity. This model also explains how nickel, deposited onto the catalyst surface during demetallation, kills activity. In the last experiments of Run 2, (E and F), our objective was to see if we could reverse the trend of HDM activity enhancements we had effected through the deposition of Co and Mo from their oil soluble napthenates, by depositing Ni from a napthenate-Nujol solution, onto the now quite active <u>in situ</u> generated catalyst.

In Run 2-E, 420 g. of a Ni-napthenate/Nujol solution at 452 ppm Ni was completely demetallatized over the synthetic catalyst, retained in the reactor from Run 2-D. Even though the oil was completely demetallized, like the Co and Mo napthenate demetallations, we are uncertain as to whether the ultimate fate of all the nickel was on the initially injected Al_2O_3. This point will be amplified later. Nevertheless, from a simple mass balance, if all the nickel did deposit on the Al_2O_3, then its loading

based on the initial amount of support charged, would be 19.9 wt. per cent.

The Ni-T3MPP HDM kinetics of this nickel loaded catalyst were measured in Run 2-F. The rate constants and data are displayed in Table 6, and Fig. 5, respectively. Artificially loading the catalyst with nickel caused the first order rate constant for total Ni removal to decrease by 8.0%, while the same rate constant for Ni-porphyrin removal decreased by 27.6%.

With the realization that the in situ synthesized catalysts HDM activity appeared to be greater, the more severe were the Co or Mo napthenate demetallation conditions, all subsequent napthenate demetallations in Runs 3 to 6 were performed at ca. 358°C and 1000 psig H_2; the same conditions as typically employed for the Ni-T3MPP HDM experiments.

In Runs 3 to 5 we have examined the Ni-T3MPP HDM activity which results over the doped alumina, when 420g. batches of the Co and Mo napthenates, at the concentrations listed in Table 2, are demetallized either separately or together. In Runs 3-A, 4-A and 5-A, the napthenate/Nujol charge comprised of both Co and Mo, Mo alone, and Co alone, respectively. Each of these experiments was run to complete demetallation as monitored by oil sample analysis. The results of the HDM experiments which followed in Runs 3-B, 4-B and 5-B are displayed in Fig. 6. For comparison the Ni-T3MPP demetallation data obtained over the fresh untreated alumina support, and HDS-16A catalysts, are also shown.

The catalyst with the highest activity was made when Mo-napthenate was demetallized by itself (Run 4). Both its total Ni and Ni-T3MPP removal rates exceeded that of fresh HDS-16A (see rate constants in Table 6). The total Ni removal first order rate constant over the in situ synthesized Mo/Al_2O_3 catalyst was 1.31 times that for HDS-16A, while the rate constants

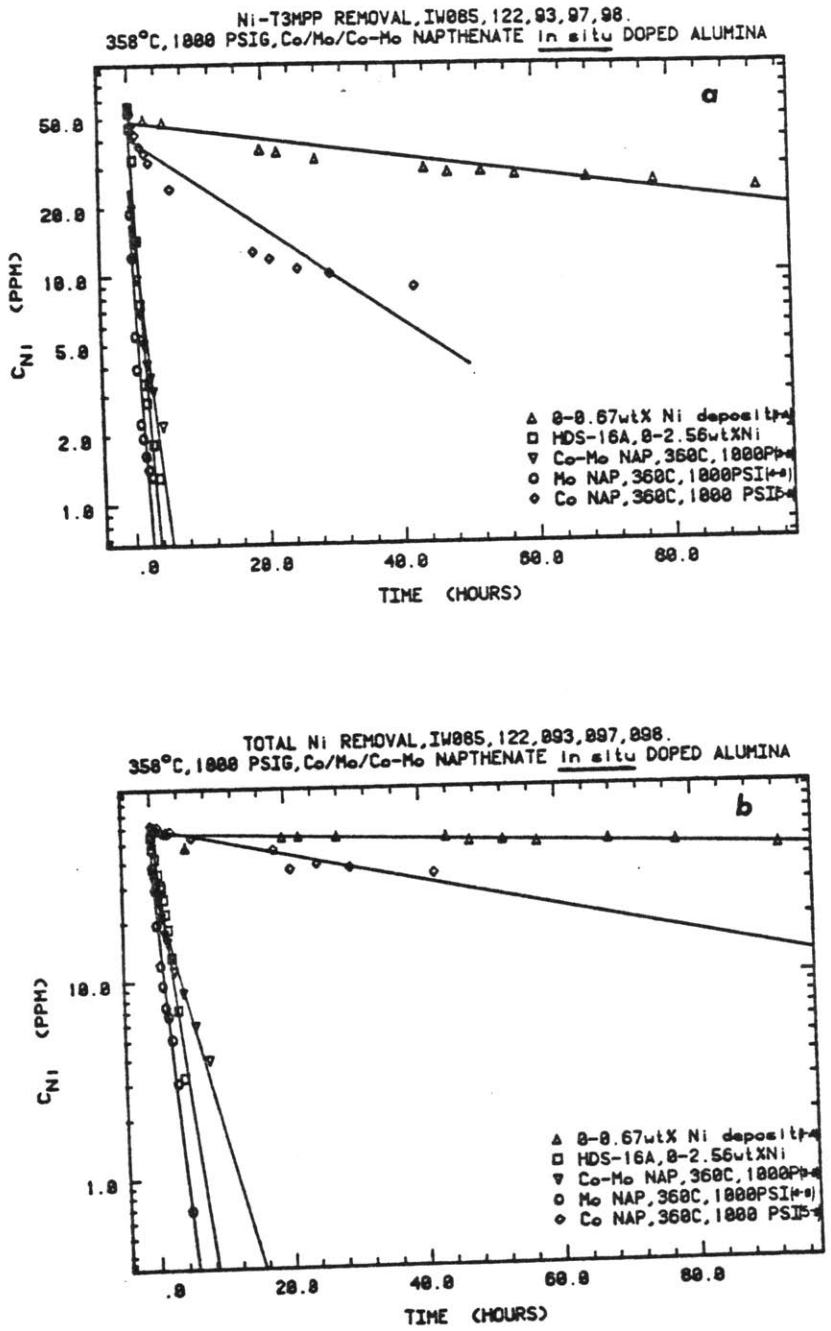

Figure 6: (a) First order plot for Ni-T3MPP removal during Runs 3-B, 4-B, and 5-B.
(b) Similar plot for total Ni removal. Demetallation data over fresh HDS-16A, and fresh Al_2O_3 are also shown for comparison. Each experiment was conducted at 360°C, 1000 psig H_2, including the experiments to deposit the catalytically active metals from the metal-napthenate/Nujol solutions.

for Ni-T3MPP removal were very similar (243.2 v's 235.2 g. oil/g. cat. hr.).

Both catalysts generated from the Co-Mo, and Co alone, napthenate solutions exhibited much reduced activity when compared to the Mo alone, and HDS-16A catalysts. The relative values of the first order rate constants for both total Ni and Ni-T3MPP over the various catalysts are given in Table 7. Also shown in Table 7 is the ratio of the first order rate constant for Ni-T3MPP removal to the rate constant for total nickel removal. This value is seen to progressively decrease as the activity of the catalyst increases.

Once the Co-Mo/Al_2O_3 catalyst had been formed during Run 3-A, the subsequent Ni-T3MPP demetallation Runs 3-B, C and D were run at temperatures between 315°C and 360°C, at 1000 psig H_2, in order to estimate activation energies for the rate constants. The relevant data are shown in Fig. 7. Also shown for comparison is Ni-T3MPP HDM data over HDS-16A, both in a fresh (0-2.56 wt % Ni) and an aged (6-11 wt % Ni) condition. The collection of HDM data on the aged HDS-16A catalyst has been reported elsewhere (28). The <u>in situ</u> generated Co-Mo/Al_2O_3 catalyst is seen to be more active than the aged HDS-16A catalysts at all temperatures.

The first order rate constants from Fig. 7, listed in Table 6, are replotted in Arrhenius plots in Fig. 8. In each plot three sets of data are depicted for fresh and aged HDS-16A catalyst, and the napthenate synthesized Co-Mo catalyst. The data shows considerable scatter, nevertheless, activation energies have been calculated, and are presented in Table 8 along with the correlation coefficients for the best fit straight lines in Fig. 8.

Table 7: Relative values of 1st order rate constants for total nickel and Ni-T3MPP removal over various catalysts at ca. 360°C, 1000 psig H_2. Exact details for each run are given in Tables 5 and 6.

Catalyst		Fresh Untreated Al_2O_3	Co-nap/ Al_2O_3	HDS-9A Ni-Mo/ Al_2O_3	Co-Mo-nap/ Al_2O_3	HDS-16A Co-Mo/ Al_2O_3	Mo-nap/ Al_2O_3
Relative Values of 1st Order Rate Constants (k_1)	Total Nickel Removal	1.0	6.6	73.9	122.6	274.1	358.4
	Ni-T3MPP Removal	1.0	5.0	46.6	70.6	130.7	135.1
$\frac{k_{1,Ni\text{-}T3MPP}}{k_{1,total\ Ni}}$		3.9	3.0	2.5	2.3	1.9	1.5

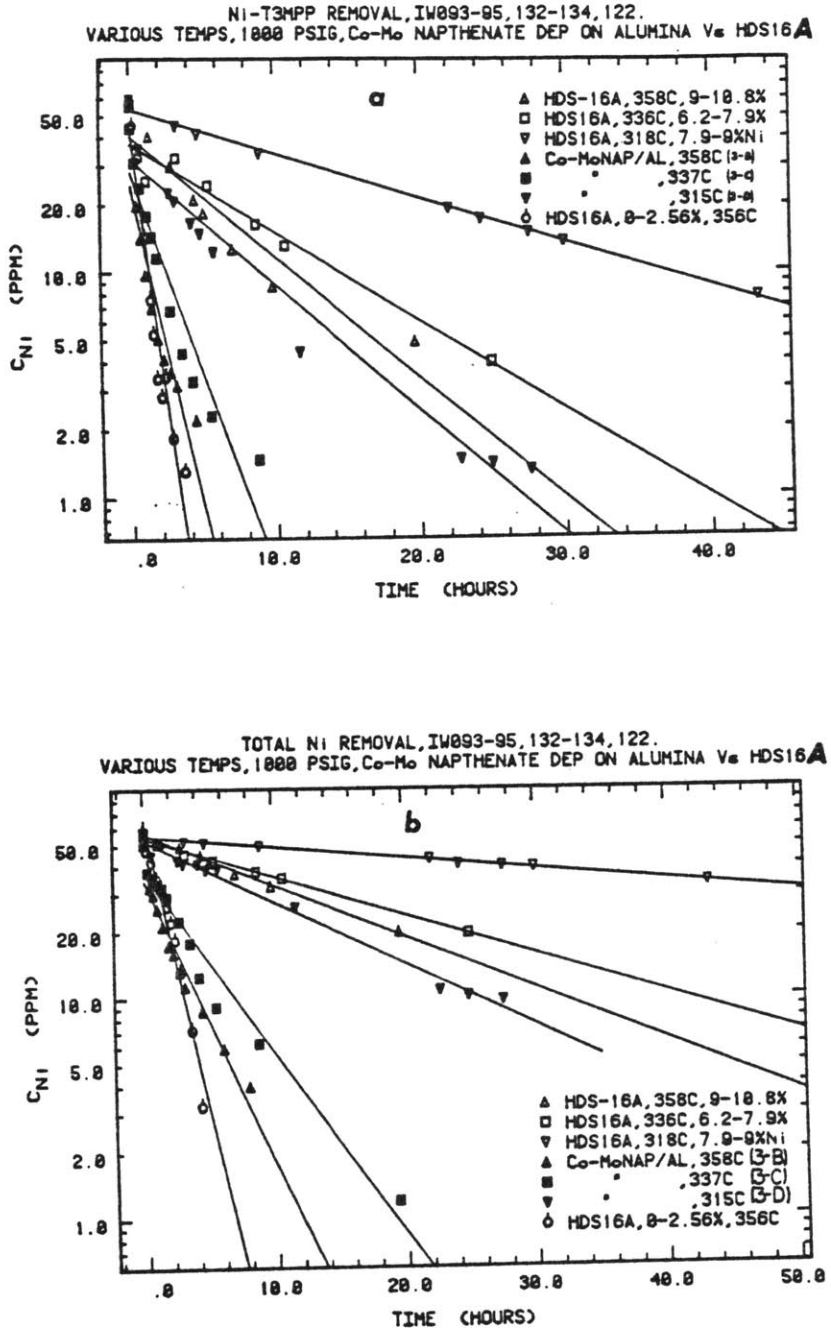

Figure 7: (a) Comparison of first order plots for Ni-T3MPP removal over in situ generated Co-Mo-nap/Al_2O_3 (Runs 3-B, 3-C and 3-D), aged HDS-16A, and fresh HDS-16A. The aged HDS-16A catalysts have a nickel loading in the range 6-11 wt %. Experiments were performed at temperatures in the range 315 to 360°C, and at 1000 psig H_2.
(b) Similar plot as (a) for total nickel removal.

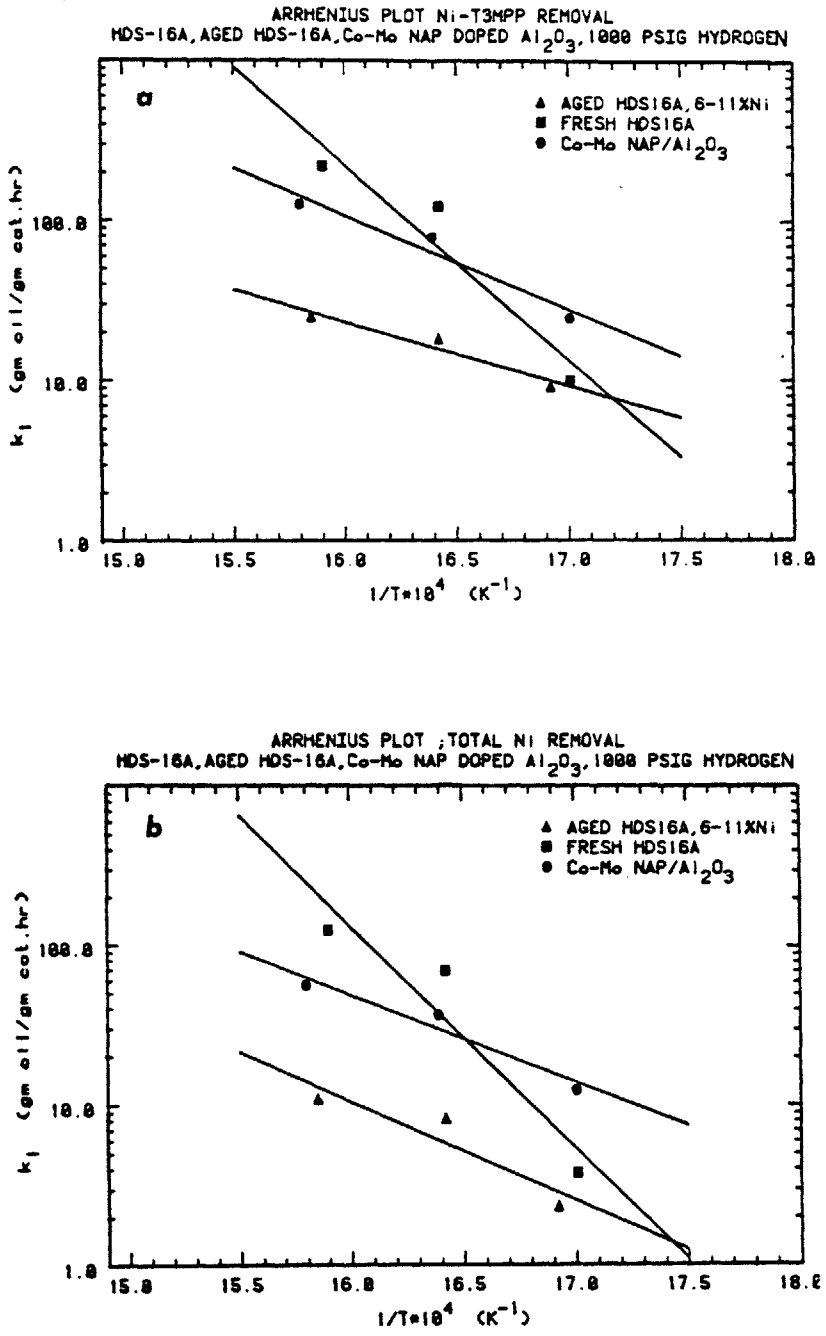

Figure 8: (a) Arrhenius plot for first order rate constants for Ni-T3MPP removal over fresh and aged (loaded with 6-11 wt % Ni) HDS-16A catalysts, and Co-Mo napthenate synthesized on Al_2O_3 catalysts.
(b) Similar plot as (a) for total nickel removal.

Table 8: Activation energies (in kcal/g.mol) for the first order rate constants for total nickel removal, and Ni-T3MPP removal, over napthenate synthesized Co-Mo/Al_2O_3, and fresh and aged (6-11 wt % Ni) HDS-16A catalysts. The number in parenthesis following the activation energy is the correlation coefficient of the best fit straight line in Fig. 8.

	Catalyst		
	Fresh HDS-16A	Aged HDS-16A	Metal Napthenate Synthesized Co-Mo-nap/Al_2O_3
Ni-T3MPP Removal	24.3 (0.9512)	8.0 (0.9687)	11.7 (0.9737)
Total Ni Removal	27.6 (0.9459)	12.3 (0.9273)	10.8 (0.9735)

Run 3 was concluded by examining the effect that napthenate deposited vanadium had on the activity of the in situ synthesized catalyst when performing Ni-T3MPP demetallation. Both Runs 3-D and F measured Ni-T3MPP HDM kinetics at 315°C, 1000 psig H_2, however, prior to Run 3-F, in Run 3-E, a solution of vanadyl napthenate in Nujol was demetallized at 350°C, 500 psig H_2. As listed in Table 2, the vanadium concentration was ca. 454 ppm. If all this vanadium deposited onto the catalyst, its loading would be 19.8 wt % based on the fresh weight of Al_2O_3 initially injected. However, as before, with previous napthenate demetallations, we are uncertain as to whether all the metal from the napthenate ultimately ended up on the catalyst. This point will be discussed later.

The kinetic data collected during Runs 3-D and F are displayed in a first order plot in Fig. 9. The deposition of vanadium is seen to actually increase the HDM activity of the in situ synthesized Co-Mo catalyst. This is in contrast to the behavior caused by the other principle contaminant of heavy oils, namely nickel, which in Runs 2-D, E and F (and Fig. 5) was shown to slightly poison the HDM activity of the napthenate synthesized Co-Mo/Al_2O_3 catalyst.

Since nickel hydrodemetallation kinetics has been the main thrust of our studies, and since nickel is a metal bound up in a heavy oil which possesses catalytic capabilities for a wide spectrum of hydrocarbon transformation reactions (29), we decided, in Run 6, to investigate the HDM activity of nickel napthenate doped alumina. In Run 7, a batch of alumina was prechlorided in the apparatus schematized in Fig. 3, as per the procedure outlined in the experimental section of this paper. This chlorided alumina batch was then used for Ni-T3MPP HDM in Run 7-B. The

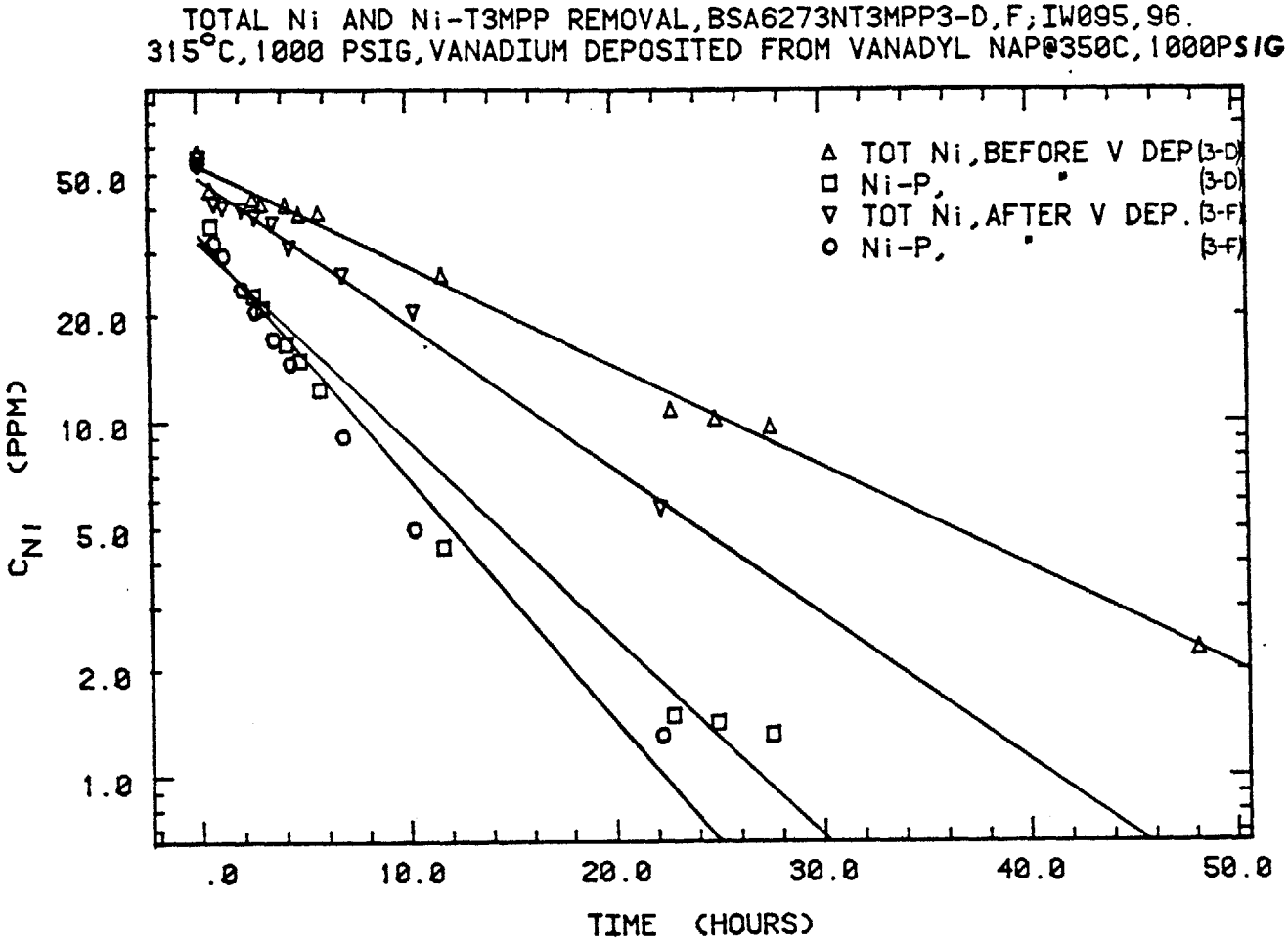

Figure 9: First order kinetic plot for total Ni and Ni-T3MPP removal before and after catalyst was used for the demetallation of vanadyl-napthenate/Nujol batch. Data are from Runs 3-D and F, at 315°C, 1000 psig H_2. Vanadium deposition enhances the demetallation rates.

data from Runs 6-B and 7-B are shown in Fig. 10, together with the kinetic data for HDM over fresh Al_2O_3, and the in situ synthesized Co and Mo on Al_2O_3 catalysts. In Run 6-A the Ni-napthenate/Nujol solution initially at a nickel concentration of ca. 450 ppm was completely demetallized, according to oil samples withdrawn from the reactor. Had all this nickel deposited on the alumina, its loading would have been 20 wt %, however, once again, discussion on this matter will be deferred till later.

Figure 10 shows that prechloriding the alumina was the least efficient way of treating the Al_2O_3 to enhance its HDM activity. With napthenate metal deposition, the doped alumina catalysts, exhibited HDM activity in the order Mo>Co>Ni. The molybdenum doped alumina was, by far, the most active catalyst. The rate constants calculated from Fig. 10 are given in Table 6, and their relative values are listed in Table 9.

II. D. 2. Catalyst Characterization

(i) SEM/EDX

Catalysts from Runs 2 and 7 were examined under a scanning electron microscope (SEM) equipped with an energy dispersive X-ray analyzer (EDX), which permitted a qualitative description of the spatial distribution of various elements to be made. The catalysts were cleaned, mounted and sectioned for this work, as already outlined in the experimental section.

During the metal napthenate-nickel demetallation runs the 0.5 micron filter in the oil sampling line, whose purpose is to keep the crushed catalyst in the reactor, was prone to plugging. This never occurred when we demetallatized Ni-T3MPP/Nujol solutions. Moreover, there was a pronounced increase in the mass of solid (catalyst + deposits) contained in the reactor after a run which involved metal napthenate demetallation. For

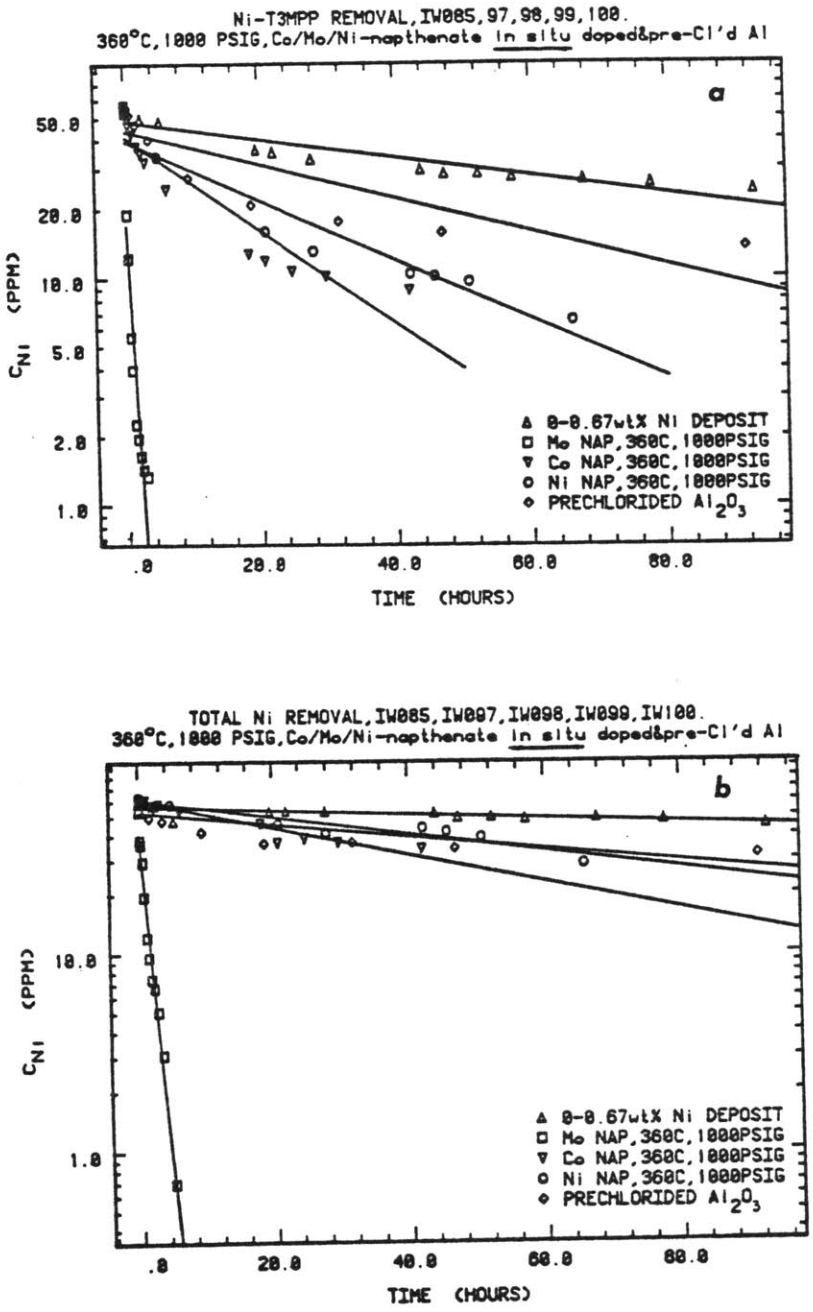

Figure 10: (a) A comparison of the Ni-T3MPP removal kinetic data from Runs 1-A, 4-B, 5-B, 6-B, and 7-B at 360°C, 1000 psig H_2.
(b) Same as (a), except for total nickel removal.

Table 9: Relative values of 1st order rate constants for total nickel and Ni-T3MPP removal over metal napthenate doped alumina catalysts. HDM runs are at 360°C, 1000 psig H_2.

Catalyst		Fresh Untreated Al_2O_3	Pre-Chlorided Al_2O_3	Napthenate Synthesized Catalysts Ni/Al_2O_3	Co/Al_2O_3	Mo/Al_2O_3
Relative Values of 1st Order Rate Constants (k_1)	Total Nickel Removal	1	2.9	4.2	6.6	358.4
	Ni-T3MPP Removal	1	1.7	3.2	5.0	135.1
$\frac{k_{1,Ni\text{-}T3MPP}}{k_{1,total\ Ni}}$		3.9	2.3	3.0	3.0	1.5

example, in Run 2, 0.9561 g. of alumina was initially injected into the reactor, whereas ca. 1.61 g. of in situ synthesized catalyst was recovered from the reactor at run's end. This latter number is also conservative since not all the catalyst was recovered. These observations prompted us to carefully scrutinize the aged catalyst.

Figure 11 is an SEM micrograph of a sectioned catalyst particle from Run 2. It shows an Al_2O_3 particle on the right (Region 1), attached to what we believe is a highly carbonaceous region (Region 2), created during metal napthenate demetallation. The catalyst particle in Fig. 11 has part of the Al_2O_3 exposed, on the right hand side of the particle. Presumably this condition also existed within the demetallation environment in the reactor, and allowed the Al_2O_3 to contact the oil. EDX spectra were taken for 60 seconds on 1μ diameter spots in the region of points 1 and 2, identified in Fig. 11. These spectra are shown in Figs. 12a and b for points 1 and 2, respectively. At point 1 on the Al_2O_3 particle, the Al signal is dominant (we have listed the exact energies of the X-ray emission lines of relevance in this study elsewhere (4); they are also available in Ref. 30). Other elements are present in smaller quantities, namely Au (evaporated onto the surface for SEM), Mo (which skews the Au peak at ca. 2.29 keV), and Co and Ni. In contrast, the spectrum from point 2, shown in Fig. 12b, reveals that the matrix which envelopes the Al_2O_3, and is deposited during reaction, is relatively low in the elements Al, Mo, Co and Ni. This is readily apparent once it is recognized that the intensities of the Au peaks in each of Figs. 12a and b, is the same. The aluminum signal dropped from 58,354 counts in 60 seconds at point 1, to 754 counts in 60 seconds at point 2.

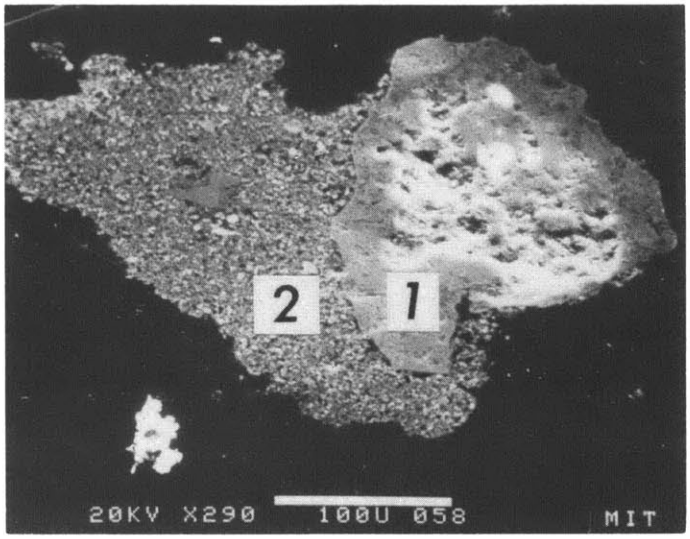

Figure 11: Scanning electron micrograph of sectioned catalyst particle from Run 2. Region 1 is an alumina particle. Region 2 is the carbonaceous matrix found associated with all particles, and is deposited during napthenate demetallation. Marker bar is 100 microns.

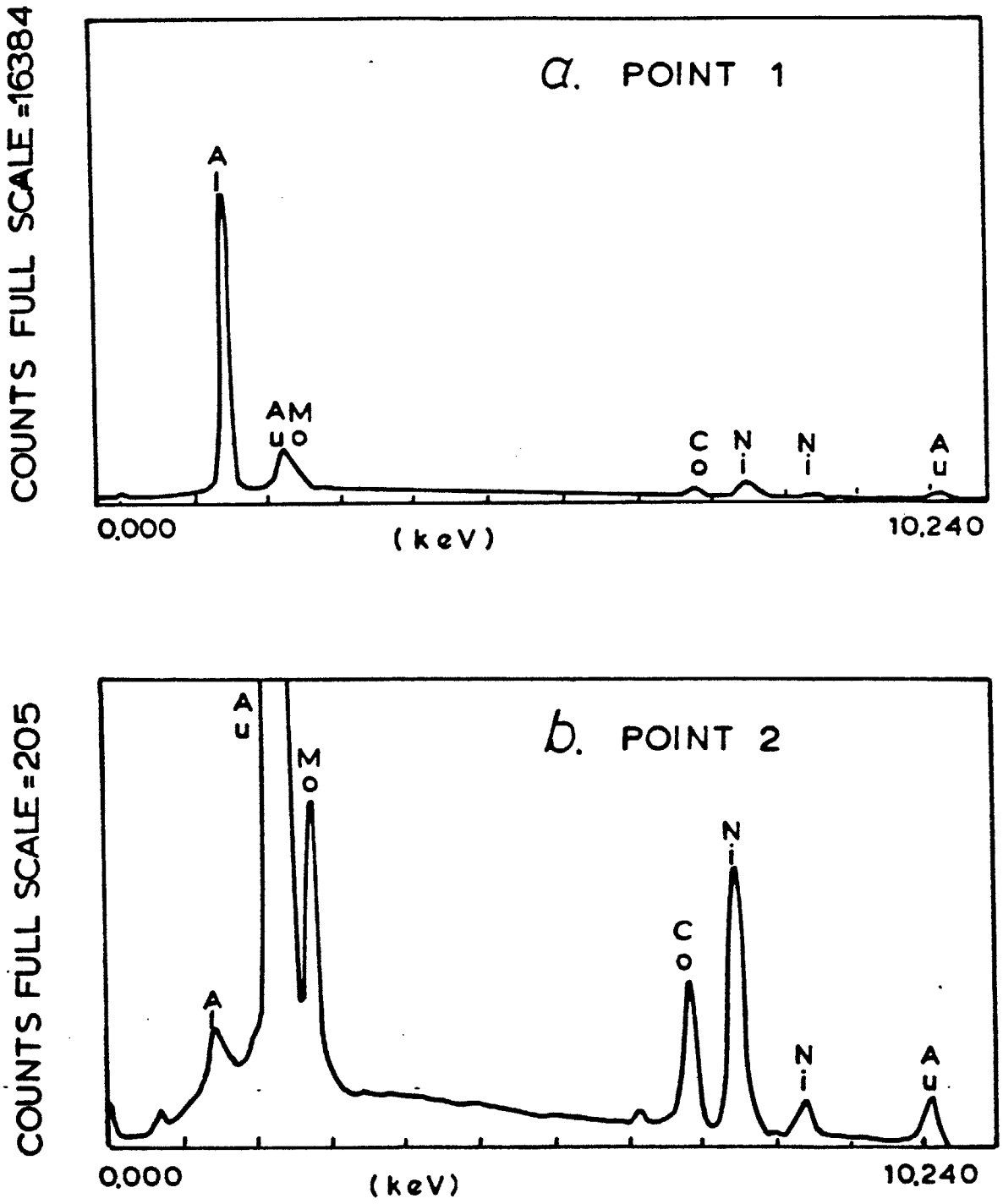

Figure 12: (a) EDX spectrum on point 1 in Fig. 11. Electron beam was focused to ca. 1 μm^2. The vertical full scale is 16,384 counts. Count time = 60s.
(b) EDX spectrum on point 2 in Fig. 11. The vertical full scale is 205 counts. Count time = 60s.

Unfortunately EDX cannot detect carbon, because of its low atomic number, so we cannot unequivocally say that region 2 has a high carbon content. Some work with Auger Electron Spectroscopy (AES), however, tends to confirm this hypothesis. The AES work is reported in the following section.

Larger lumps of the carbonaceous material were also discovered, which held more than one Al_2O_3 particle. One such particle is shown sectioned in Fig. 13a. It holds four alumina particles of about 100μ size. Two of these particles, located close to the crater in the epoxy binder, are the focus of micrograph Fig. 13b. Also shown across this micrograph is a line scan for aluminum, which confirms that the embedded particles are the Al_2O_3 support, which was initially injected into the reactor at the beginning of the run. Elemental maps were also taken of the region depicted in Fig. 13b. The maps for Al, Co, Mo and Ni are shown are in Figs. 13c to f, respectively. It is evident that the majority of the deposited metals, either from metal napthenate demetallation for synthesizing the catalyst, or from Ni-T3MPP HDM in assessing the catalysts activity, end up on the Al_2O_3 "core particles" which are enveloped in a carbonaceous skin. This implies that the carbonaceous skin is porous enough to permit rapid diffusion of the metal carrying molecules to the catalytically active sites, which reside on the alumina.

SEM/EDX was also performed on the chlorided alumina catalyst in Run 7, both pre and post Ni-T3MPP demetallation. A chlorine line scan is shown through a chlorided sectioned alumina particle in Fig. 14. This particle had not been aged in the HDM reaction of Run 7-B. The chlorine profile is uniform, indicating that the chloriding process was not diffusion limited.

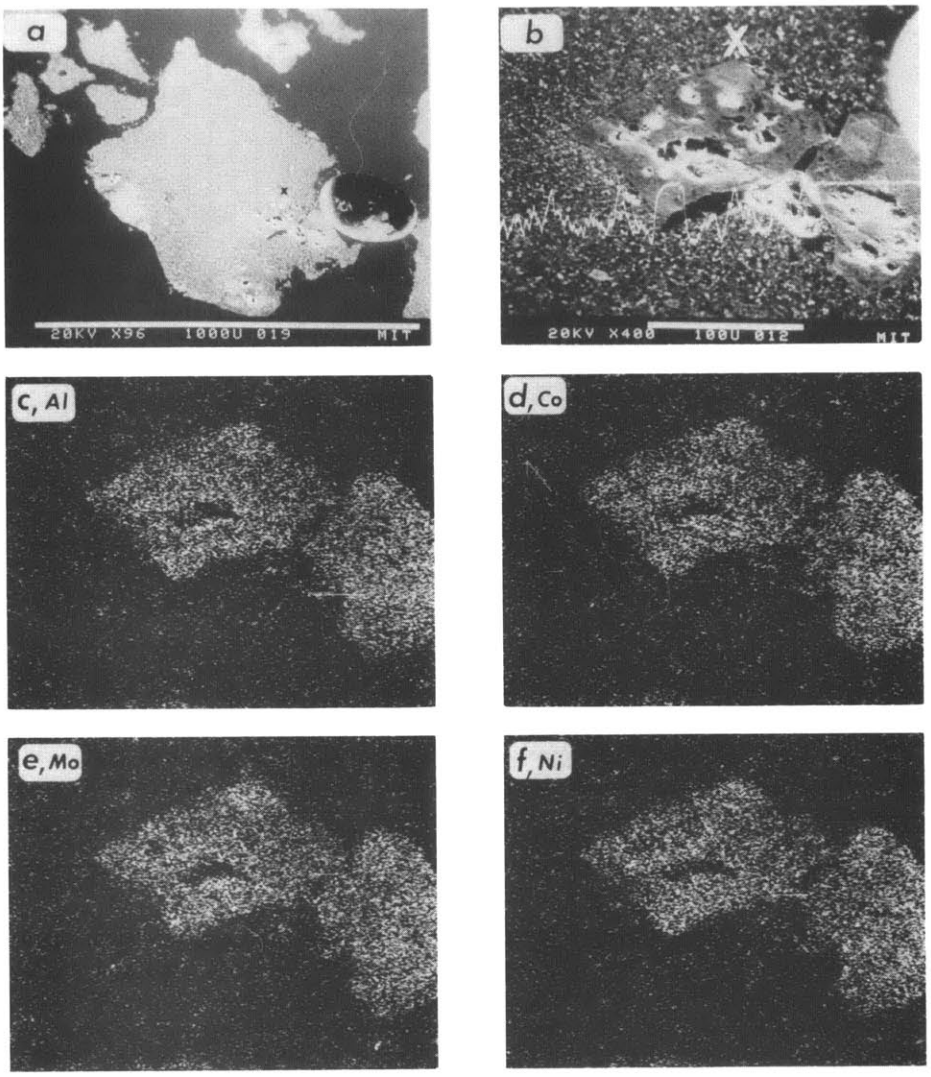

Figure 13: (a) Scanning electron micrograph of sectioned carbonaceous particle containing four alumina particle from Run 2. Marker bar is 1000 microns.
(b) Close up view of the two alumina particles located next to the crater in (a). X-ray line scan is for Al. Marker bar is 100 microns.
(c) X-ray map for Al over SEM in (b).
(d) X-ray map for Co over SEM in (b).
(e) X-ray map for Mo over SEM in (b).
(f) X-ray map for Ni over SEM in (b).

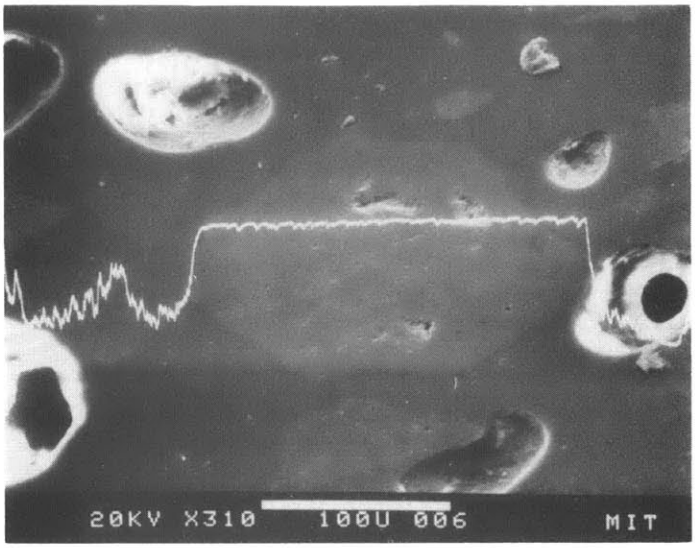

Figure 14: Scanning electron micrograph, with X-ray line scan for chlorine, through sectioned chlorided Al_2O_3 particle, that was used as the catalyst in Run 7. Marker bar is 100 microns.

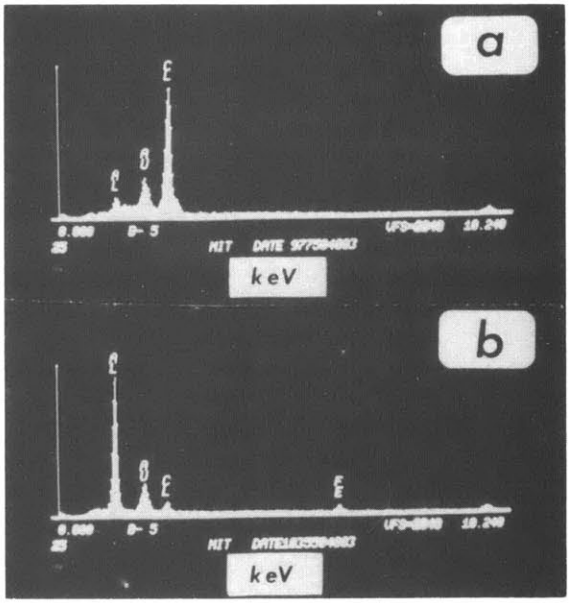

Figure 15: X-ray spectra by EDX of chlorided alumina catalyst (a) before and (b) after it was used for Ni-T3MPP HDM in Run 7. Vertical full scale is 2048 counts. Count time was 25 seconds.

Fig. 15 shows the EDX spectra taken on samples of the chlorided alumina both before (Fig. 15a) and after (Fig. 15b) the catalyst was used for demetallizing Ni-T3MPP in Run 7-B. Great chlorine loss occurs. The ratio of the areas under the Cl peak to the Al peak is 4.5 before HDM, and 0.06 after.

(ii) Auger Electron Spectroscopy (AES)

AES was performed on a catalyst sample from Run 2. Survey scans at a point within a sectioned Al_2O_3 particle, and at a point in the carbonaceous matrix which enveloped it, are depicted in Fig. 16 and 17, respectively. Fig. 16 shows strong Al, and O signals as expected. All the metals that were deposited during the demetallation experiments, namely, Co, Mo, and Ni, also give signals. The alumina particle also gives a carbon signal, however, this is to be expected since our earlier spectroscopic investigations (4) on model polycrystalline alumina catalysts revealed that these catalytic surfaces become heavily coked (ca. 80 atom % carbon in the surface layers) during Ni-T3MPP HDM. In contrast, the AES spectra (Fig. 17) on the matrix which envelopes the alumina particles is dominated by the carbon signal. There is also an indication that some nitrogen is present. To the best of our knowledge there is no nitrogen in the metal-napthenate solutions, so its source must be from Ni-T3MPP. This observation is not entirely unexpected since the molar ratio of nitrogen to nickel in Ni-T3MPP is 4 (Fig. 2). However, we never did see nitrogen in our more extensive XPS investigations (4) on model polycrystalline alumina catalysts which were aged in the HDM environment.

II. E. Discussion

Catalyst deactivation is a major problem in hydroprocessing. A

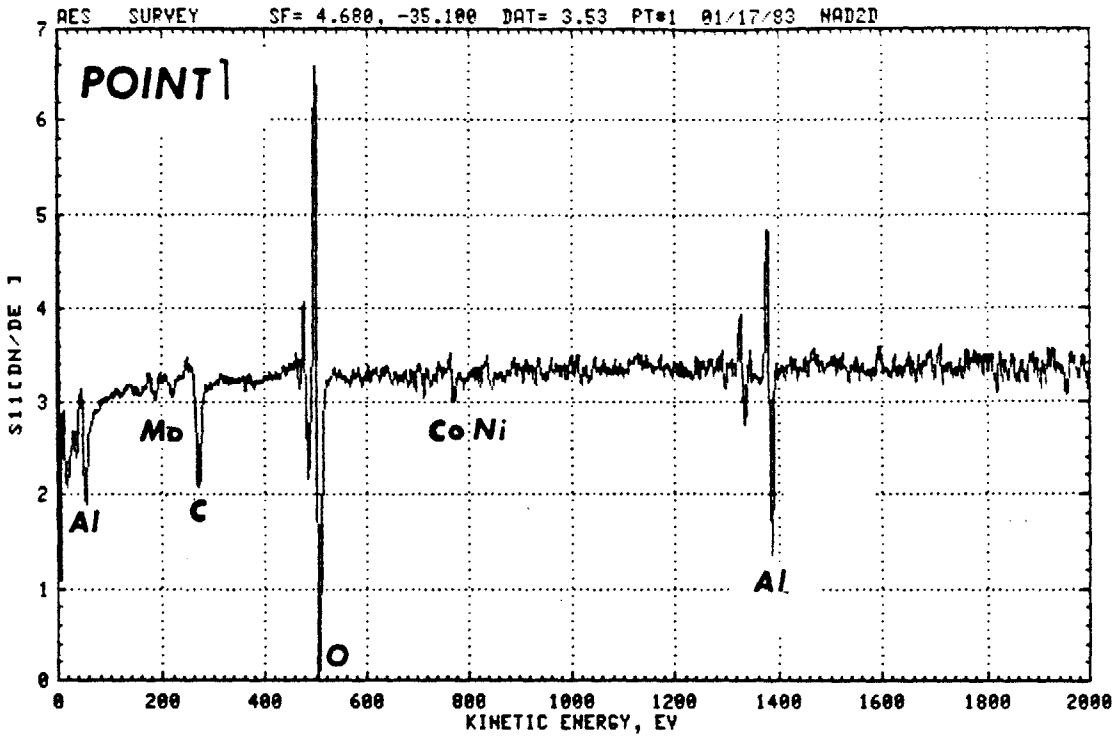

Figure 16: AES spectrum at point 1 in Fig. 11.

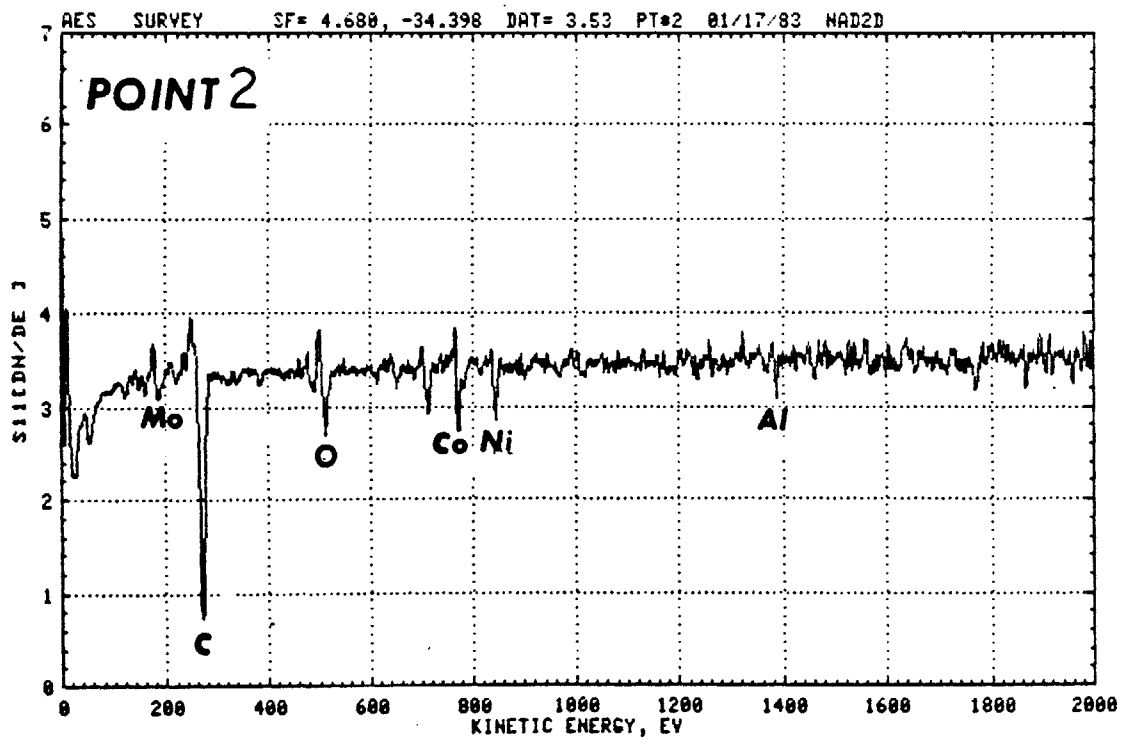

Figure 17: AES spectrum at point 2 in Fig. 11.

typical catalyst lifetime is about one year (27). On reactor start-up a virgin catalyst rapidly accumulates coke, that reaches a steady state carbon loading in the range 10-20 wt % (3). This causes the initial rapid deactivation of the catalyst as observed in Region 1 of Fig. 1. The coke overlayer henceforth exists in a state of dynamic equilibrium with coke being simultaneously formed on some sites, and cracked and hydrogenated off the surface at other sites (4). We have emphasized (4) that not all coke formation is deletrious, since a coke covered site can still function as an hydrodemetallation site, even though its hydrogenolysis capabilities are much reduced. Nickel and vanadium deposition via the HDM reaction, is, however, irreversible and is what ultimately dictates the catalyst lifetime (Region 3 of Fig. 1) (7). Because the original packed bed of catalyst, which typically operates as a trickle bed (31), is coated with coke and metals, bed plugging can be a problem (32). This ultimately necessitates that the entire catalyst bed be replaced, resulting in lost processing capacity because of reactor down-time.

It is because of these reasons that several processes based on slurry reactors are gaining in popularity (33-36,19). These reactors are not plagued by plugging problems, and moreover, catalyst can be readily removed and added to the reactor, in the oil phase, without disrupting operation. It is in this reactor system that the results we have found in this study may be most readily applied.

Our basic finding is that once fresh alumina is fed to a well mixed reactor system, its HDM catalytic activity can be raised from essentially zero to levels that exceed those of the commerically available Co-Mo/Al_2O_3 catalysts, by the <u>in situ</u> deposition of Co and Mo from metal napthenates.

The catalyst is actually synthesized in the HDM reactor, at the same process conditions (ca. 360°C, 1000 psig H_2) employed for HDM. The concept has potential for regenerating a deactivated catalyst in situ, by depositing a fresh layer of Co and Mo, from the oil soluble napthenates, over the deactivating layers of carbon, nickel and vanadium which were accumulated during HDM. This idea was not directly experimentally addressed in this paper, but is the subject of ongoing work (37). Untreated alumina was found to possess negligible HDM activity (Fig. 4), even once it had accumulated trace quantities of Ni via the HDM reaction.

Of all the metals deposited onto the Al_2O_3 from a napthenate/Nujol solution (Mo, Co, V and Ni), Mo was by far the best at increasing the alumina's HDM activity. These results are summarized in Table 9. While nickel can negligibly improve the activity of fresh alumina (Run 6), it was found to have the opposite effect on the activity of a napthenate synthesized Co-Mo/Al_2O_3 catalyst. The deposition of Ni-napthenate during Run 2-E on an in situ synthesized Co-Mo/Al_2O_3 catalyst decreased its subsequent HDM activity in Run 2-F (see Table 6).

The other principle metallic poison in heavy oils, namely vanadium, was found to enhance the HDM activity of the Co-Mo/Al_2O_3. This was explored in Runs 3-D to F (Tables 5 and 6), and the results are graphically displayed in Fig. 9.

Our initial experiments (Run 1) to deposit the catalytically active metals Co and Mo from the napthenates onto the alumina, were conducted at relatively mild process conditions, namely 290°C, and 500 psig H_2. This is because we wanted to eliminate any homogeneous demetallation reaction which may occur. For example, West et al (38), in one of the few

hydrodemetallation studies which have employed vanadyl napthenate as the model metal bearing molecule, rationalized their intra-catalyst pellet vanadium profiles by proposing that a homogeneous demetallation reaction ran in parallel with the heterogeneous one. The homogeneous effect was smallest at the lowest temperature at which they ran their experiments, namely, 325°C.

Later catalyst synthesis experiments (Runs 3-6) were run at HDM process conditions (360°C, 1000 psig H_2), with the result that the catalysts generated at the more severe conditions, were more catalytically active in HDM; compare rate constants in Table 6 for Runs 1-D and 4-B, of Table 5.

In Run 1-G, which immediately followed Run 1-F investigating HDM over a Mo-nap/Al_2O_3 catalyst, cobalt was demetallized over the in situ sythesized catalyst. In Run 1-H the HDM activity of this, now Co-Mo-nap/Al_2O_3 catalyst was measured, with the finding that its overall nickel removal rate constant had marginally increased (by 8.7%). This enhancement could be due to two factors: (i) the demetallation catalytic activity of Co-nap/Al_2O_3 in its own right (see Run 5 and its data displayed in Fig. 6, and Table 9), or (ii) the promotional aspect that Co has on the already deposited Mo. We have already shown (4) through XPS and AES studies on model supported Co-Mo catalysts that Co does promote the HDM catalytic activity of Mo within certain composition ranges. It also well established (39,40) that Co promotes Mo in HDN and HDS.

In previous work from this research group, Wei and co-workers (15,23,41) established that nickel metalloporphyrins demetallate via a sequential reaction mechanism. The mechanism is conceptually similar to

that for HDN (42). The metalloporphyrin (Fig. 2) is hydrogenated at peripheral double bonds within the pyrrole group, resulting in the formation of metallo-chlorins (one hydrogenation) and isobacteriochlorins (two hydrogenations, at adjacent pyrrole groups) (18). These hydro-porphyrins are subsequently cleaved open at one of the methine bridge positions, releasing the nickel atom from the porphyrin macrocycle. It also appears that if the metalloporphyrin possesses a bulky aromatic group at the methine bridge, non-porphyrin metal bearing fragments may be generated, which do not immediately deposit their metal on the catalyst surface (15,23).

This is the reason why in this study the rate of Ni-T3MPP removal always exceeded the total rate of nickel removal from the oil. In this study the concentrations of these intermediates was not monitored, since our primary goal was measurement and comparison of the in situ synthesized catalyst's activity. Nevertheless, an estimate of the artificially synthesized catalyst's capability to remove nickel from the porphyrinic structure, without prior hydrogenation (a desirable situation since it reduces hydrogen consumption) can be estimated by ratioing the first order rate constants for Ni-T3MPP removal, and total nickel removal. What we look for in a catalyst is a high activity, and the selectivity ratio being close to unity.

The relative catalyst activities and selectivity ratios are listed in Tables 7 and 9. From Table 7 we see that the most active catalysts, also have the most favorable selectivity ratios. In fact, the selectivity ratio continually declines to a best value of 1.5 with the most active Mo-napthenate synthesized catalyst. It is noteworthy that our artificially

made Mo-nap/Al_2O_3 catalyst outperforms both the fresh commercially made HDS-16A and HDS-9A catalysts for HDM, both in terms of activity and selctivity.

In Table 9, a poor activity, but relatively good selectivity ratio was achieved by the chlorided-alumina. The low activity is disappointing, however, the good selectivity ratio is not unexpected. Chlorine is purposely added to bifunctional reforming catalysts in an attempt to increase the acidity of the OH present on the alumina surface; chlorine helps withdraw electrons from the OH bond (43). In the HDM mechanism it can be envisioned that high acid strength would facilitate cleavage of the porphyrin macrocycle. Metal removal can then occur in the absence of prior hydrogenation, thereby reducing the selectivity ratio.

In Table 8, the activation energies for the first order rate constants are listed. The activation energies for HDM over the fresh HDS-16A catalyst are approximately twice those measured over a more aged form of the same catalyst (it had accumulated 6-11 wt % Ni), and over the in situ synthesized Co-Mo-nap/Al_2O_3 catalyst.

The scanning electron micrographs in Figs. 11 and 13 indicate that whenever metal napthenate demetallation occurs the Al_2O_3 particles become encased in a carbonaceous residue. That the residue has an extremely high carbon content (>70 atom % C) was determined by AES (Fig. 17). The carbonaceous residue was never observed with Ni-T3MPP demetallation alone (e.g. Fig. 14). The X-ray maps in Figs. 13c to f reveal, however, that the residue must be extremely porous and have little catalytic activity, since all the deposited metals appear to primarily end up on the Al_2O_3 particles embedded in the matrix. The bulk of the carbonaceous residue would cause

problems if metal napthenate demetallation was attempted as a means to recover lost catalytic activity in a fixed bed reactor. There, the interstices between the catalyst pellets would fill with the residue, leading to bed plugging. It is for this reason that we have suggested that metal napthenate catalyst synthesis can best be conducted *in situ* in a slurry reactor. West *et al* (38) also noted, what they called a "sludge," which adhered to their Co-Mo/Al_2O_3 catalyst and reactor walls, during the HDM of vanadyl napthenates dissolved in an oil base. "Sludge" formation was greater at higher temperatures indicating that sludge formation may be precipitated via a homogeneous reaction.

In summary, then, this paper has demonstrated the feasibility of generating Co-Mo/Al_2O_3 hydrotreating catalysts, by depositing the catalytically active metals onto the Al_2O_3 support, at the process conditions used for HDM. The most active catalysts formulated in this way, performed better in the HDM of a model heavy oil, than fresh unaged commercially manufactured Co-Mo/Al_2O_3. Cobalt and molybdenum napthenate demetallation is accomplished by the simultaneous deposition of a carbonaceous residue, which can completely envelope the Al_2O_3 particles. The Al_2O_3 particles do, however, seem to accumulate the majority of the deposited metals whether they be from napthenate or porphyrin demetallation.

II. F. References

1. Ahuja, S.P., Derrien, M.L. and Le Page, J.F., Ind. Eng. Chem. Prod. Res. Dev. 9, 272 (1970).

2. Beuther, H., and Schmid, B.K. in "Proceedings 6th World Petroleum Congress" Sec III, Paper 20, p.297 (1963).

3. Inoguchi, M., Kagaya, H., Daigo, K., Sakurada, S., Satomi, Y., Inaba, K., Tate, K., Nishiyama, R., Onishi, S., and Nagai, T., Bull. Jap. Pet. Inst. 13, 153 (1971).

4. This thesis, Chapter III.

5. Newson, E.J., Ind. Eng. Chem. Proc. Des. Dev. 14, 27 (1975).

6. Rajagopolan, K., and Luss, D., Ind. Eng. Chem. Proc. Des. Dev. 18, 459 (1979).

7. Tamm, P.W., Harnsberger, H.F., and Bridge, A.G., Ind. Eng. Chem. Proc. Des. Dev. 20, 262 (1981).

8. Ebel, R.H., Amer. Chem. Soc., Div. Pet. Chem. Preprints 17 (3) C46 (1972).

9. Ohtsuka, T. Catal. Rev. - Sci. Eng. 16, 291 (1977).

10. Houalla, M., Nag, N.K., Sapre, A.V., Broderick, D.H., and Gates, B.C. AIChE J. 24, 1015 (1978).

11. Shih, S.S., Katzer, J.R., Kwart, H. and Stiles, A.B., Amer. Chem. Soc., Div. Pet. Chem., Preprints 22, 919 (1977).

12. Yen, T.F., Boucher, L.J., Dickie, J.P., Tynan, E.C. and Vaughan, G.B., Amer. Chem. Soc., Div. Pet. Chem. Preprints 13(1), 59 (1968).

13. Hung, C.-W., and Wei, J., Ind. Eng. Chem. Proc. Des. Dev. 19, 250 (1980).

14. Hung, C.-W., and Wei, J., Ind. Eng. Chem. Proc. Des. Dev. 19, 257 (1980).

15. Ware, R.A. and Wei, J., Paper No. 61a presented at AIChE Annual Meeting, Los Angeles, California, Nov. 14-19, 1982.

16. Rankel, L.A., Amer. Chem. Soc., Div. Pet. Chem. Preprints 26, 689 (1981).

17. Kameyama, H., Sugishima, M., Yamada, M., Amano, A., J. Japan. Pet. Inst. 24, 317 (1981).

18. Smith, K.M., Ed., Porphyrins and Metalloporphyrins, Elsevier, 1975.

19. Miller, J.W., Union Science and Technology Division, personal communication.

20. Fiero, G.W., Ann. Allergy 23, 226 (1965).

21. Yen, T.F., in "The Role of Trace Metals in Petroleum" (T.F. Yen, Ed.) Chap 1, Ann Arbor Science, Michigan, 1975.

22. Vaughan, G.B., Tynan, E.C. and Yen, T.F., Chem. Geol. 6, 203 (1970).

23. This thesis, Chapter I.

24. Goldstein, J.I., Newbury, D.E., Echlin, P., Joy, D.C., Fiori, C., and Lifshin, E., Scanning Electron Microscopy and X-ray Microanalysis, Plenum, New York, 1981.

25. Somorjai, G.A., Chemistry in Two Dimensions: Surfaces, Cornell University Press, Ithaca, New York, 1981, p.40,72.

26. Swingle, II, R.S. and Riggs, W.M., Crit. Rev. Anal. Chem. 5 (3), 267 (1975).

27. Laine, J. and Trimm, D.L., J. Chem. Tech. Biotechnol. 32, 813 (1982).

28. Webster, I.A., unpublished results.

29. Satterfield, C.N., Heterogeneous Catalysis in Practice, McGraw-Hill, New York, 1980, pp.5-7.

30. Bearden, J.A., X-ray Wavelengths and X-ray Atomic Energy Levels, NSRDS-NBS14, National Bureau of Standards, Washington, D.C., 1967.

31. Satterfield, C.N., A.I.Ch.E. J. 21, 209 (1975).

32. Satterfield, C.N., Heterogeneous Catalysis in Practice, McGraw-Hill, New York, 1980, pp.123-126.

33. Gates, B.C, Chemtech 9, 97 (1979).

34. Gordon, K.C. J. Inst. Fuel 20, 42 (1946).

35. Weisser, P. and Landa, S., Sulfide Catalysts, their Properties and Applications, Pergamon, New York, 1970.

36. Symp. on Coal Liquefaction Fundamentals, Amer. Chem. Soc. Div. Fuel Chem. 24, 2 (1979).

37. Wei, J., Proposal on Catalytic Hydrodemetallation to NSF, 1983.

38. West, M., Smith, M.C., Petersen, E.E., Levy, A.V. and Heinemann, H., Paper No. 32e presented at AIChE Annual Meeting, Los Angeles, California, Nov. 14-19, 1982.

39. Grange, P., Catal Rev. - Sci. Eng. 21, 135 (1980).

40. Ratnasamy, P., and Sivasanker, S., Catal. Rev. - Sci. Eng. 22, 401 (1980).

41. Agrawal, R., and Wei, J., Ind. Eng. Chem. Proc. Des. Dev., paper submitted.

42. Satterfield, C.N., and Yang, S.H., Ind. Eng. Chem. Proc. Des. Dev., in press.

43. Gates, B.C., Katzer, J.R., and Schuit, G.C.A., Chemistry of Catalytic Processes, McGraw-Hill, 1979, pp. 258-260.

CHAPTER III

The Catalytic Hydrodemetallation (HDM) of a Model Heavy Oil over Polycrystalline Alumina Supported Co-Mo Catalysts. A Surface Study by AES, XPS, ISS, SIMS and SEM/EDX, and a Conceptual Model for the Working Hydrotreating Catalyst.

III. A. Summary of Chapter

Model polycrystalline alumina supported Co-Mo catalysts were made with a range of surface compositions and used for the catalytic hydrodemetallation of a model residual oil. The model oil was made by dissolving nickel tetra(3-methylphenyl) porphyrin in a mineral oil. The catalysts were aged in HDM experiments in a spinning basket type reactor at ca. 350°C and 1000 psig H_2. The aged catalysts were then examined by a variety of surface spectroscopic techniques (XPS, AES, SIMS, ISS, and SEM/EDX). Like the hydrotreating processes of desulfurization and denitrogenation, HDM activity was found to display a maximum within a narrow range of promoter loadings (Co/(Co+Mo) atomic composition ratio in the range 0.5 to 0.7). The model catalysts were initially placed in the reactor in the oxidic state, but were reduced during the HDM reaction. By XPS chemical shift measurements molybdenum was found to exist primarily as Mo^{4+}, while cobalt is reduced completely to the metal. The deposited nickel was found both as Ni and NiO, however, the latter entity may be due

to surface contamination by air exposure. ISS and SIMS data revealed the existence of a Co-Mo double layer, in both real γ-Al_2O_3 supported catalysts and the model catalysts. The molybdenum layer sits on top of a cobalt layer. The basic elements sodium and potassium were found to be strongly surface segregated and in intimate contact with the molybdenum monolayer. SEM/EDX work on the model catalyst surfaces indicated that nickel is non-uniformly deposited on the surface, with the majority of it residing in regions with a high cobalt-molybdate content. Comparatively little nickel deposited on regions of the support that have low concentrations of impregnated metals. The aged catalyst surface is covered with a carbonaceous overlayer which has holes through which bare molybdenum islands are exposed. A conceptual model for the working hydrotreating catalyst surface is presented which emphasizes such features as (i) the hydrogen storage and hydrogen exchange capabilities of the carbonaceous overlayer, (ii) the presence of bare molybdenum patches on the catalyst surface which remain coke-free and catalyze both hydrogenation and hydrogenolysis reactions, and (iii) the ability of the deposited Ni to hydrogenate surface absorbed coke precursors, and thereby protect acidic sites by keeping them coke-free.

III. B. Introduction

Since the world reserves of high sulfur, nitrogen and metals (principally nickel and vanadium) containing crude oils far exceeds those of extremely low sulfur content, it is reasonable to assume that the hydrotreating of residua will long be of importance to the oil industry. During the upgrading process, sulfur and nitrogen condensed heterocyclic compounds undergo a complex series of hydrogenation and hydrogenolysis

reactions, before the heteroatoms are ultimately released as H_2S and NH_3. Evidence for this is primarily based on fundamental studies with model crude oils, formed by dissolving, for example, dibenzothiophene (1) or quinoline (2) in a white oil.

While it is important to investigate the kinetics of hydrodesulfurization and hydrodenitrogenation for both processing and environmental reasons, knowledge of the kinetics of metal removal (hydrodemetallation (HDM)) is more important from the standpoint of catalyst lifetime. This is because the deposition of metals (Ni, V, Fe) on the catalyst is the principle cause of reduced activity, with 50 to 65 wt % metals deposits on a new catalyst being reported to be the tolerance (3,4). Catalyst deactivation occurs by direct poisoning of active sites, and at higher metals loadings, by physical blockage of the supports' pores. With a known metals tolerance, and metals deposition rate, catalyst lifetimes can be estimated (5,6).

However, despite the importance of catalytic HDM few fundamental studies have been conducted to examine the mechanism of metal removal from either real or model crudes. In real crudes nickel and vanadium are bound up in structures as porphyrins and asphaltenes (7). Metal in porphyrins can account for up to 50% of the total metal in the oil (8).

Using this information we have initiated a research program to investigate the catalytic HDM of nickel and vanadyl porphyrins dissolved in a white oil. Our work thus complements the fundamental HDS, and HDN studies already alluded to (1,2). Via this approach it is hoped, that by combining the results of all the fundamental studies on HDS, HDN and HDM, a realistic picture of how a real oil reacts under hydroprocessing conditions

will emerge.

Our reactivity studies to date have reported on the HDM of Nickel and Vanadyl-porphyrins over a commercially available $CoO-MoO_3/\gamma-Al_2O_3$ hydrodeulfurization catalyst (9-12). HDM was shown to be conceptually similar to HDS and HDN, with the metallo-porphyrin molecule progressing through a series of hydrogenation steps, before a terminal hydrogenolysis reaction cleaved the macrocyclic ring, and released the metal onto the catalyst surface. In all of these studies we only monitored total metal and metal-porphyrin concentrations within the oil phase. The condition of the oil phase at any particular set of conditions is obviously dictated by the chemical and physical condition of the catalyst, whose surface condition should ideally be continually monitored throughout the duration of an experiment. This is especially true in HDM where the deposition of carbon and metals must continually change the chemical composition of the catalyst surface, which is exposed to the oil.

Moreover, our previous work only employed one type of catalyst, whose chemical composition was fixed at a Co/(Co+Mo) atomic ratio of 0.47. With HDS catalysts it is well known that catalytic activity can be dramatically varied by changing the amount of cobalt promoter atoms in the active $Co-Mo/Al_2O_3$ catalyst. For example Wivel et al (13) could change the conversion of thiophene across a fixed bed reactor by an order of magnitude by changing the Co/(Co+Mo) ratio on an alumina supported catalyst from 0 to 0.43.

To the best of our knowledge similar studies on the HDM activity of a supported Co-Mo catalyst as a function of composition, as measured by the Co/(Co+Mo) ratio do not exist. The aim of the present work is to rectify

this situation. However, activity measurements computed by meauring bulk oil phase concentrations as a function of bulk catalyst composition have questionable utility chiefly because the catalytic activity of a catalyst is dictated by its surface composition. Surface compositions will differ from the bulk phase composition, as has been shown to exist in the Co-Mo/γ-Al_2O_3 working catalyst (14). The reliability of the activity data is also questionable unless great care has been exercised in manufacturing the catalysts of varying composition. For a catalyst at a given Co/(Co+Mo) ratio, its final activity is also dictated by the order of impregnation, the temperature of calcination, and the total amount of active phase present (15).

In order to circumvent the above problems encountered in working with real γ-Al_2O_3 supported catalysts, we elected to synthesize carefully prepared model supported Co-Mo catalysts, by co-impregnating $1cm^2$ slabs of high purity polycrystalline alumina (PCA) with metal salts. These model catalysts were simultaneously reacted in the oxide state with a model metal containing crude, comprised of a nickel porphyrin dissolved in Nujol, at realistic process conditions. The catalysts were then analyzed by the ultra-high vacuum surface spectroscopic techniques of X-ray photo-electron spectroscopy (XPS), Auger electron spectroscopy (AES), ion scattering spectrometry (ISS), secondary ion mass spectrometry (SIMS), and examined under a scanning electron microscope (SEM) equipped with an energy-dispersive X-ray analyzer (EDX). Using AES we were able to ascertain an optimum model catalyst composition for HDM. By using ISS, the highly dispersed form of the model catalyst (see later) was shown to exhibit a surface Co-Mo double layer. This phenomenon has recently been

shown to exist with a real, high surface area, γ-Al_2O_3 supported Co-Mo catalyst (14,16). ISS and SIMS revealed that the PCA catalysts contained small quantities of the basic elements Na, K, Ca, which were most probably originally present in the PCA as an impurity. In the PCA catalysts these elements were found to be strongly concentrated at the catalytic surface. Depth profiling with XPS on heavily loaded PCA squares of low dispersion produced information on the oxidation state of the various elements comprising the catalyst. SEM/EDX analysis on some PCA catalysts that exhibited poor dispersion due to the formation of large crystals (size ca. 0.5 μ), tentatively shows that Ni deposition from the oil onto the catalyst surface occurs predominantly on the Co-Mo crystal with little being deposited on the bare PCA support structure.

SIMS and ISS were also performed on a commercially manufactured CoO-MoO_3/Al_2O_3 catalyst both in a fresh state, and after it had been used to demetallate a mixture of nickel and vanadyl porphyrins dissolved in a white oil.

The XPS work with the aged model catalysts reveals that during reaction some reduction of the Co and Mo atoms has occurred, and that nickel from the cracked porphyrin molecule probably exists on the catalyst surface in the metallic state. More importantly, and not surprisingly, the entire catalyst surface is shown to be heavily coked. However, an XPS molybdenum signal is still detectable before sputtering, and this tempts us to postulate that the working surface of an oxidic Co-Mo/Al_2O_3 hydrotreating catalyst should be viewed as one principally covered with a carbonaceous overlayer, but having a small concentration of uncovered Mo surface sites, which are always present. We believe that the carbonaceous

overlayer should be viewed as an integral part of the working Co-Mo hydrotreating catalyst, and less in the role of an unwanted poison. A conceptual model of the working catalyst surface is outlined which integrates many of these experimental observations.

Before detailing our results a few words on our experimental philosophy are warranted. Surface analysis dictates the use of ultra high vacuums (10^{-8} torr) while industrial catalysis occurs at much higher pressures (1-100 atm). If the multitude of surface analytical techniques available (for list see Ref. (17)) are to be useful in breathing new life into the field of industrial catalysis, then researchers must invent techniques for transferring catalysts from the working environment into the UHV environment, such that the catalysts' surface structure is unaltered during the transfer process. Apparatuses designed by Somorjai's group (18) are particularly noteworthy.

Studies on aged Co-Mo/Al_2O_3 hydrodemetallation catalysts using this approach appear to be non-existent. This state of affairs is in part due to the difficulties which exist in preparing the catalyst in a physical form amenable to study by any of the surface sspectroscopic techniques. The most typical forms of the Co-Mo/Al_2O_3 catalyst obtained from either plant or laboratory hydrotreating studies is as a powder or an extrudate. Powders require to pelletized into a small diameter (8mm) discs, while the typical extrudate normally has a projected surface area which is too small for meaningful analysis, by, for example XPS.

It was for these reasons that we decided to conduct some HDM studies over model catalysts comprised of Co and Mo oxides supported on low surface area (ca. 1 cm^2) polycrystalline alumina squares. These catalysts are

rigid and easily handled, in contrast to the brittle pressed disks from a pelletized Co-Mo/Al_2O_3 powder. Their exposed surface area (ca. $1cm^2$) and flat slab configuration allow them to be easily analyzed, by for example, XPS, which does not have good spatial resolution.

Each of the surface experimental techniques used in this study has its strengths and weaknesses, however, we believe that by directing them all at one particular catalyst a pitfall of one technique will be cancelled by a strength of another, so that in total we will have obtained a clear picture of the real catalyst surface. For example, both ISS and SIMS are extremely surface sensitive probes (1 monolayer) but suffer from an inability to generate good quantitative information, whereas, XPS has a comparatively poor depth resolution (10-30A), but provides a good quantitative composition analysis from the sampled depth (21).

III. C. Experimental

III. C. 1. Catalysts and their preparation

In total, four different types of catalysts were employed in this study. Their properties are listed in Table 1. The majority of work has been performed with the Co and Mo impregnated polycrystalline alumina squares of different Co/Mo atomic composition ratio, at a fixed Mo loading. Two Mo loadings were used, producing what we have termed lightly loaded catalysts (catalyst code LPcA = Light polycrystalline alumina; Table 1) and heavily loaded catalysts (code HPcA). Catalysts LPcA are estimated to be loaded with enough Mo to uniformly cover the $1cm^2$ PCA square to a depth of ca. 50 monolayers, while catalysts HPcA have ca. 10^4 monolayers of Mo. Our initial objective was to generate the PCA analogue of the real HDS-16A catalyst, however, since the Mo loading on this high surface area catalyst

Table 1 Catalyst Properties

Catalyst		$CoO-MoO_3/\gamma-Al_2O_3$	$NiO-MoO_3/\gamma-Al_2O_3$ +	$CoO-MoO_3$/PCA	$CoO-MoO_3$/PCA
Code		HDS-16A	HDS-9A	LPCA	HPCA
Preparation method		Industrially made, preparation method unknown		Coimpregnation	Coimpregnation
Lot #		MTG-S-0573	MTG-S-0155	self-made	self-made
Composition (wt%)*	CoO	5.7	-	Lightly loaded model catalysts ca. 50 monolayers of Mo deposited. Mo loading held constant at 2.777×10^{16} g atoms/cm^2	Heavily loaded model catalysts ca. 10^4 monolayers of Mo deposited. Mo loading held constant at 3.07×10^{18} g atoms/cm^2
	NiO	-	3.2		
	MoO_3	12.2	17.5		
	Na_2O	0.03	0.03		
	Fe	0.04	0.03		
	SO_4	-	0.4		
	SiO_2	-	0.5		
Atomic ratio Co/Mo (nominal value)		0.90	-	0, 0.3, 0.5, 0.9, 1.0, 1.5, 2.0 and ∞(Co only)	0, 0.2, 0.4, 0.7, 0.9, 1.4, 2.0 and 25.0
Surface area		$176 m^2/g$	$170 m^2/g$	$1 cm^2$ total	$1 cm^2$ total
Physical form during HDM reaction		crushed and sized 170-200 mesh (74-88μ) from 1/16" diameter extrudates		One side of a 1cm x 1cm x 1mm PCA square, catalytically active	

*Compositions of HDS-16A and HDS-9A supplied by American Cyanamid.

+Only used as reference during XPS.

is less than one monolayer, this proved to be impractical, since the sensitivity of the surface analytical techniques AES and XPS is a few monolayers at best. Therefore, in order to strike a balance between a PCA supported catalyst that was sufficiently close to the real world catalyst in terms of MoO_3 loading, and one that was amenable to surface analysis, a compromise loading of ca. 50 monolayers was used.

Catalysts HPcA obviously bear little resemblance to the real catalyst because of their heavy Co and Mo metals loadings, however, they proved useful in XPS depth profiling.

The preparation technique for the PCA catalysts is schematically depicted in Fig. 1. The polycrystalline alumina support was supplied by Coors Porcelain Company (99.9% Al_2O_3, Grade AD-999). This substrate is completely non-porous. From the as received PCA sheets, of dimensions 2" x 3.75" x 0.04", 1cm x 1cm squares were cut, using a diamond cut off wheel on a tool makers surface grinder. The squares were also notched for identification (Fig. 1, Step 1). The squares were then cleaned by alternately soaking them in chromic acid-sulfuric acid cleaning solution (Fisher Scientific Co.) for 1 minute and rinsing them in distilled water. This process was repeated ten times (Steps 2 and 3). The PCA squares were then calcined at 600°C for one day by placing them in fused silica boats in a Lindberg tube furnace under flowing air (Matheson, Zero gas) (Step 4). The squares were cooled under an air flow, and immediately co-impregnated with the desired amount of Co and Mo by depositing 30 µl of an aqueous solution of the salts ammonium molybdate [$(NH_4)_6Mo_7O_{24}.4H_2O$, (Fisher Scientific Co.)] and cobalt nitrate [$Co(NO_3)_2.6H_2O$ (Mallinckrodt, Inc.)] dropwise onto the PCA surface from a syringe (Hamilton Co., Model 1710).

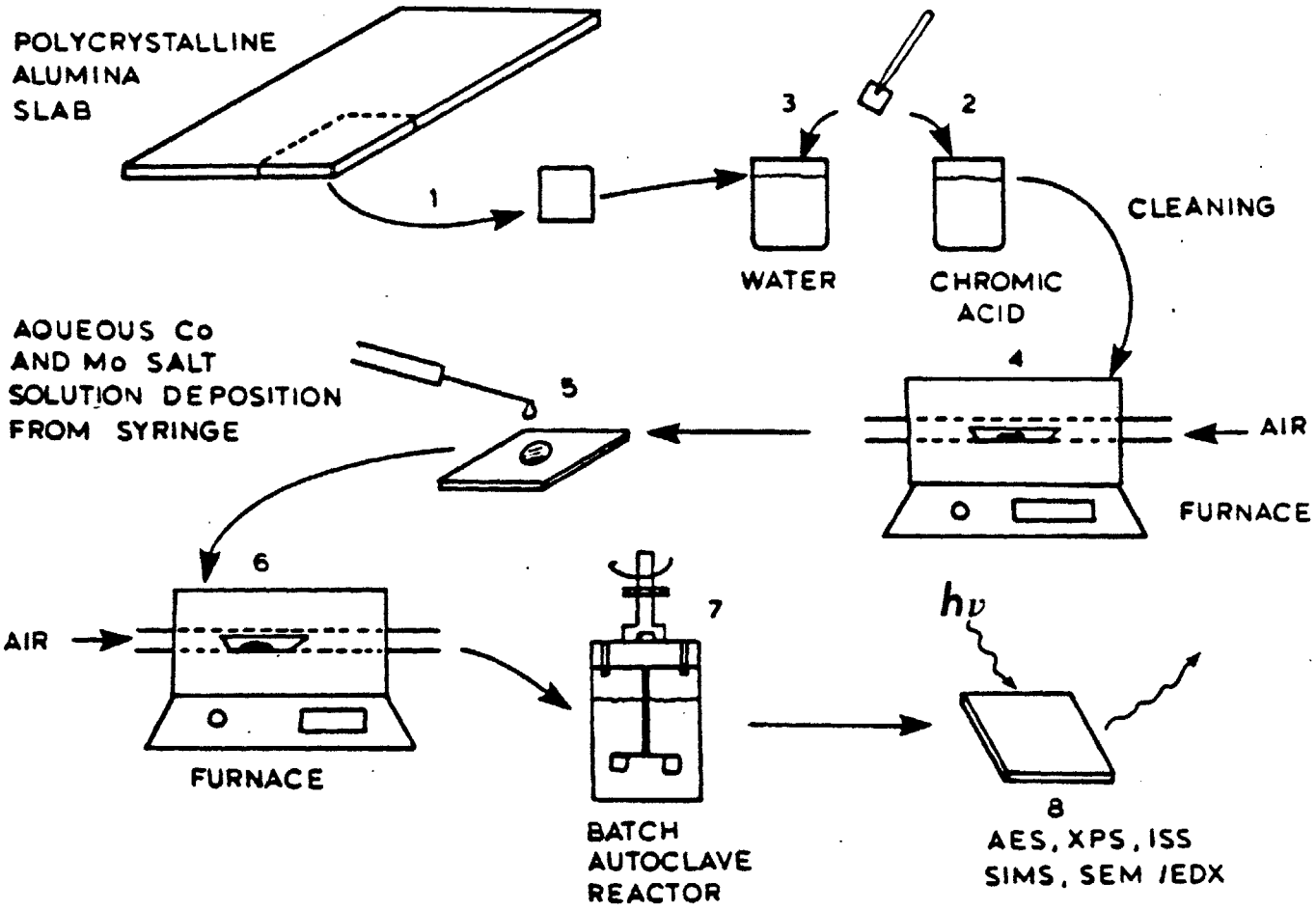

Figure 1: Schematic pathway showing LPCA and HPCA catalysts preparation procedure. See text for details. 1) ca. 1cm^2 square of polycrystalline alumina is cut from larger, as supplied, slabs; 2) Catalyst is washed alternately in chromic acid/sulfuric acid cleaning solution and 3) water. 4) PCA square is then calcined at 600°C, for one day, in a tube furnace. 5)PCA is square is co-impregnated with Co and Mo aqueous salt solution, and then dried and calcined overnight at 600°C in a tube furnace. 7) PCA squares are then reacted in oil for the hydrodemetallation reaction, by suspending spinning them in small baskets and attached to the batch autoclave's impeller shaft. Typical reaction conditions for hydrodemetallation reaction were 340°C, 1000 psig H_2 pressure, and a run time of ca. 240 hrs. 8) PCA catalysts are carefully removed from reactor system (7) under an inert Argon atmosphere and transferred to surface analytical equipment where they are characterized by the techniques of AES, XPS, ISS, SIMS, and SEM/EDX.

Great care was exercised during this process to ensure that the squares were laid perfectly flat, and that a uniform coating of impregnating solution covered the surface. This latter requirement was difficult to attain. After several trials it was found that the procedure that gave the most uniform coating of Co and Mo, was to deposit the 30µl solution as a drop in the center region of the PCA square and then swirl it at needlepoint to cover the surface. Despite these precautions great heterogeneity of the surface somtimes occurred as evidenced by scanning electron microscopy. SEM micrographs of the aged catalyst surface will be dicussed in the results section. The center of the PCA squares held Co and Mo in a highly dispersed state, realistically mimicking their real industrially used counterparts; however, higher concentrations of Co and Mo were always found on the PCA squares periphery, probably due to capillary wave effects as the impregnating solution evaporated. Calculations for how much material to deposit proceed as follows. The Schuit and Gates (22) model of the MoO_3 monolayer on γ-Al_2O_3 predicts that the surface area occupied per MoO_3 group is ca. 18Å^2. This figure has been independently experimentally verified by Sonnemans and Mars (23). Therefore, to cover a $1cm^2$ area to an average depth of 50 monolayers of MoO_3 requires that 2.777×10^{16} atoms of Mo be deposited. Deposition of 30µl of a solution of concentration 0.2714 g. ammonium molybdate/liter provides us with the LPcA series of catalysts (Table 1). As Table 1 shows the LPcA catalysts also had promoter Co atoms incorporated into them, always at the same Mo loading of 2.777×10^{16} atoms Mo/cm^2. The Co/Mo atomic ratio was varied from 0 to 2 (see Table 1). It is worth remarking that American Cyanamid's HDS-16A has a Co/Mo ratio of 0.90 based on the composition given in Table 1. The

LPcA catalyst which simulates HDS-16A therefore had 30µl of an aqueous solution of 0.2714 g ammonium molybdate/liter and 0.4023 g. cobalt nitrate/liter deposited dropwise on the PCA substrate.

With the heavily loaded series of catalysts (HPcA, Table 1) all attempts to produce a model catalyst which would simulate HDS-16A in its highly dispersed form were disregarded. Our objective with the HPcA catalysts was to lay down a thick Co-Mo layer on the PCA which would give very strong signals during UHV surface analysis, after they had been aged in the HDM of the model oil (Fig. 1, Step 7). In the HPcA catalysts the Mo loading was always ca. 3.07×10^{18} atoms Mo/cm^2, which was realized by depositing 30µl of a 300 g. ammonium molybdate/liter solution on the 1 cm^2 PCA surface. HPcA catalysts with different Co concentrations were similarly prepared by co-impregnation by dissolving the required amount of cobalt nitrate in the impregnating solution. In this way the Co/Mo ratio in the HPcA catalysts was varied over the range 0 to 2 (see Table 1).

The American Cyanamid catalyst HDS-16A, supplied as 1/16" diameter extrudates, was crushed and sieved to the size cut 74-88µ (170-200 mesh), before being used in HDM. Catalyst HDS-9A, although included in Table 1, was simply used as a reference Ni containing catalyst in our XPS work. All HDM experiments were performed with the catalysts in the oxide form.

III. C. 2. Oil

Model metals containing residua were manufactured by dissolving well characterized Ni and VO-porphyrins in a white mineral oil. Working with this synthetic crude eliminates many of the problems that would be introduced in working with a real crude, such as lack of knowledge regarding the structure of the metals bearing molecules. Also, our system

contains no sulfur or nitrogen compounds, and can thus be considered clean.

The metallo-porphyrins that were used in this study are Ni(II)-tetra(3-methylphenyl) porphyrin (Ni-T3MPP) and VO(II)-Etioporphyrin (V-EP). They were purchased in a pure crystalline state from Midcentury Chemicals (Posen, Illinois). Their structures are depicted in Fig. 2. The metallo-EP series are found in real crudes (24,25), while, metallo tetraphenyl porphyrins are not. However, they may be representative of condensed porphyrins of higher aromaticity which have been speculated as comprising asphaltenes (26).

The mineral oil was a white oil marketed under the name Nujol (Plough, Inc., TN). It consists of a mixture of napthenes, paraffins and iso-paraffins (27), is sulfur and nitrogen free, and is essentially inert at reaction conditions.

The procedure for dissolving Ni-T3MPP and V-EP in Nujol has been described elsewhere (9,10), and essentially consists of stirring a solution of the metallo-porphyrin in deaerated Nujol, under a helium atmosphere, at ca. 300°C. The resulting solution is then filtered to remove undissolved porphyrin.

III. C. 3. Reactor

A schematic of the reactor system is shown in Fig. 3. The system was designed to stand at least 5400 psig pressure and was positioned in a 1/8" steel plate-barricaded vehicle. The one-liter baffled autoclave (Autoclave Engineers, PA) was used in batch mode. The reactor temperature was controlled to ± 1°C with a PID controller (LFE Corp., MA, Model 230). Half micron stainless steel porous filters (New Met Inc., CT) were placed on the inlet gas line and outlet liquid sampling line, to respectively provide

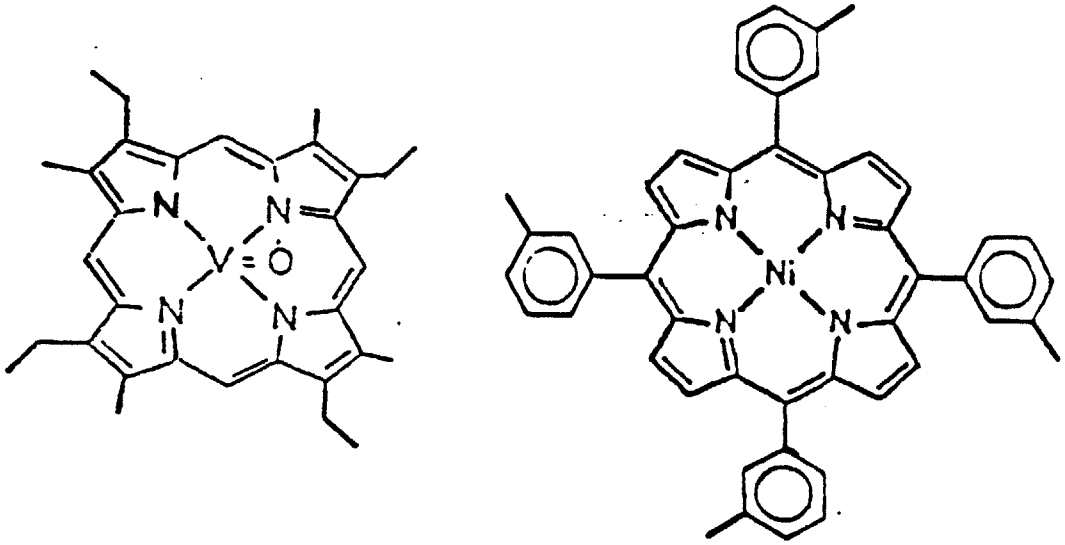

VO-Etio (I)

Ni-TETRA(3-METHYLPHENYL)PORPHYRIN
(Ni-T3MPP)

Figure 2: Structures of model metal bearing compounds

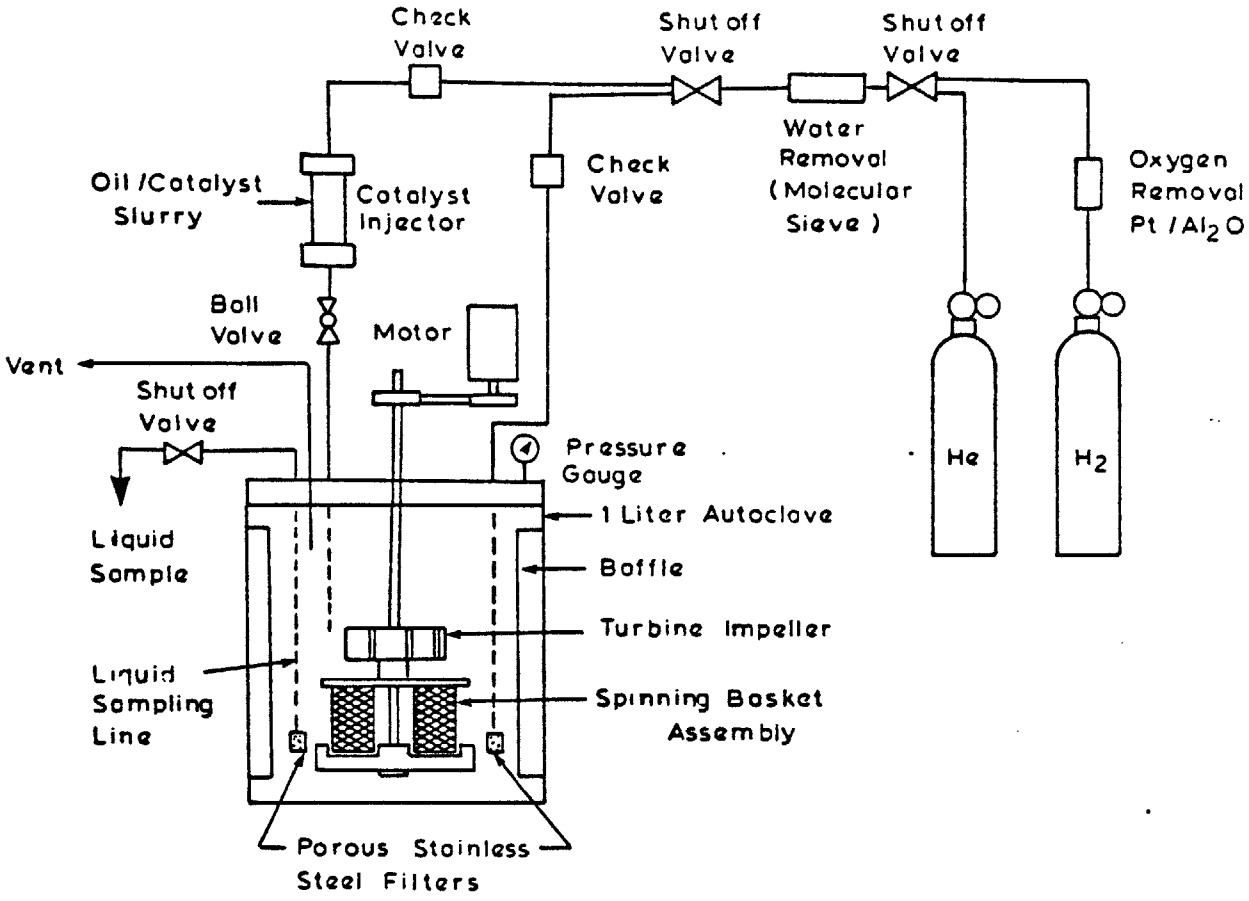

Figure 3: Schematic of high pressure autoclave for hydrodemetallation studies showing catalyst-oil injection system (for powdered catalyst), and spinning basket assembly (for PCA supported catalysts).

good gas dispersion and keep the catalyst particles (on experimentation with HDS-16A catalyst) in the reactor.

The reactor was run in two configurations. For performing HDM over the powdered form of the HDS-16A catalyst, the catalyst injector attachment (Fig. 3) was used for injecting the catalyst (slurried in a small quantity of oil) into the autoclave once the desired operating temperature had been attained. This method eliminates problems of "pre-reaction" during the long heat-up time, and permits precise definition of zero time. Once the catalyst/oil slurry is injected it is immediately well mixed into the oil mass in the autoclave by a turbine impeller spinning at 500 rpm.

The above mode of operation is unsuitable for conducting HDM over the LPCA, and HPCA catalysts. A four basket assembly was fabricated from four 440μ size strainer elements (Nupro Co., OH). This assembly could hold a total of eight PCA model catalysts simultaneously (two squares per basket; unimpregnated faces back to back), and was bolted concentrically beneath the impeller. When powdered HDS-16A catalyst was used the basket assembly was not in place.

III. C. 4. Procedure

Three separate experiments were performed to age the three different types of HDM catalysts: HDS-16A, LPCA (at various Co/Mo ratios) and HPCA (at various Co/Mo ratios). Operating conditions for each run are listed in Table 2.

For run 1 the HDS-16A catalyst was heated overnight at 400°C in a tube furnace under flowing dry helium (99.995% purity, Matheson Gas Products, MA). There was a 9.9% weight loss, probably due to water evaporation. Approximately 400g of the Ni-T3MPP and VO-Etio in Nujol oil mixture was

Table 2 Operating Conditions

Run #	1	2	3
Catalyst	Co-Mo/γ-Al_2O_3 American Cyanamid HDS-16A	Co-Mo/PCA Lightly loaded polycrystalline Al_2O_3 (LPCA)	Co-Mo/PCA Heavily loaded polycrystalline Al_2O_3 (HPCA)
Initial Catalyst state	oxide	oxide	oxide
Oil	Ni-T3MPP and VO-Etio in Nujol	Ni-T3MPP in Nujol	Ni-T3MPP in Nujol
Metal concentration* start: (ppm)	Ni-T3MPP: 55.0 VO-Etio: 30.0	61.9	61.7
finish:	complete demetallation	53.7	50.3
Mass oil (g)	5 batches of 420g	423	423
Mass catalyst (g)	0.904	N/A	N/A
Temp (°C)	353 (average)	330	355
Hydrogen Pressure (psig)	1000	1000	1000
Length of run (hr)	each batch ca. 70 hr	236	256
Catalytic surface area in reactor (cm^2)	1.59×10^6	8	8
Impeller speed (rpm)	500	500	500

*Measured by Atomic Absorption Spectrophotometry

placed in the autoclave, and the system brought to operating temperature uner a helium atmosphere. Immediately prior to a run the helium in the reactor was vented and the system was purged with hydrogen to saturate the oil. Simultaneously, the dried HDS-16A catalyst was removed from the tube furnace after it had cooled under helium flow, slurried with ca. 20g of oil mixture, and placed in the catalyst injector, which was then quickly assembled above the reactor (Fig. 3). All gas was then vented from the autoclave and the catalyst injector's pressure was brought to 1000 psig of hydrogen with the injector's ball valve shut. The run was subsequently initiated by opening the ball valve, thus rapidly forcing the catalyst/oil slurry into the reactor. This catalyst slug is expected to be immediately well mixed in the oil batch with the impeller running at 500 rpm. The total pressure during the run was adjusted by the inlet hydrogen pressure from the cylinder. The hydrogen was of ultra high purity with less than .3 ppm O_2 and at least 99.999% H_2 (Matheson Gas Products, MA).

Liquid samples were withdrawn periodically through the liquid sampling line and analyzed for both porphyrin and metals concentrations. We must emphasize that the objective of these runs was simply to generate a series of catalysts which had been aged under HDM conditions. For this reason little emphasis will be laid on interpretation of the intrinsic HDM kinetics. These results are reported elsewhere (see Chap. I).

At the end of run 1, the autoclave was dismantled, and the last oil batch containing the now nickel, vanadium and coke covered HDS-16A catalyst was quickly filtered through a 5μ filter (Millipore Corp., MA). Approximately 0.2g of the recovered catalyst was then pelletized in a 13mm diameter pellet die (NSG Precision Cells, NY) at 10,000 psi. The resulting

pellets were stored in a dessicator in a glove box under an argon atmosphere, while they awaited surface analysis. At all times the catalyst pellets were carefully handled with stainless steel tweezers, and air exposure was minimized.

In runs 2 and 3 with the LPCA and HPCA catalysts a similar procedure was followed except that eight different catalysts, with different Co/Mo ratios were simultaneously placed in the baskets for each run. The eight catalysts were located two to a basket, with their unimpregnated sides touching each other, so that the Co-Mo impregnated faces were always exposed to the oil. When the batch reactor was run with the baskets in place the catalyst injector was removed from the system. Runs 2 and 3 can be viewed as model catalyst, competitive demetallation experiments, in that eight different catalysts simultaneously complete for the metal in the oil. Our rationalism is that the most active catalyst(s) will accumulate the most metal deposits (Ni), which can then be measured by surface spectroscopy.

After preparation the eight catalyst squares were simultaneously calcined overnight at 600°C in a tube furnace, cooled, and carefully transferred with tweezers to the baskets (Fig. 1, Steps 6 and 7). Great care was exercised in handling so that the tweezers only contacted a point on the outermost edge of a PCA square. The baskets were assembled and bolted to the impeller. With the oil charge in place, the reactor was brought to run temperature, under helium pressure, and then switched to hydrogen to commence the HDM experiment. On completion of an experiment (ca. 10 days), the reactor was cooled, and the reactor header quickly removed, and placed in a glove box maintained under an Argon atmosphere

(99.995% purity, Matheson Gas Products, MA). The basket assembly was dismantled and the LPCA and the HPCA aged catalysts were stored in a dessicator in the glove box.

All catalysts aged during runs 1, 2 and 3 were transferred to the surface analytical equipment in a glove bag (Instruments for Research and Industry, PA) which was continuously purged with argon. Every precaution was exercised to minimize air contamination of the samples. Some aged catalysts were shipped to Dr. Alan Miller at the Alcoa Technical Center, PA, in argon-filled air-tight vials for analysis by ISS and SIMS.

III. C. 5. Analysis

Surface analysis of the aged HDM catalysts was performed by XPS, AES, ISS, SIMS and SEM/EDX. Oil metal and metallo-porphyrin concentrations were measured by atomic absorption and U.V.-visible spectrophotometry, respectively.

(i) X-Ray Photoelectron Spectroscopy (XPS)

XPS spectra were taken on a Perkin-Elmer Physical Electronics Model 548 spectrometer which has been digitally interfaced to a PHI Multiple-technique Analytical Computer System (MACS) supplied by the company (Perkin-Elmer, Physical Electronics Division, (PHI, MN). Non-monochromatized Mg Kα radiation was the excitation source. The digital data were processed on a Digital pdp11/04 computer using PHI Version VI software. The relative atomic sensitivity factors for each of the elements we analyzed for are listed in Table 3 (28). The spectrometer X-ray source was operated at 10kV and 40mA. The system pressure was 10^{-8} torr or lower. A cylindrical mirror analyzer (PHI model 15-255G) was used, operated at 25eV with a 4mm slit width. Ion sputter profiling was performed with a

Table 3 Relative Atomic Sensitivity Factors for XPS and AES

	XPS		AES	
Element	Line	Area atomic sensitivity factor (relative to F(1s)=1.00) (see Ref. 28)	Electron energy (ev)	Atomic sensitivity factor (primary electron energy= 3keV)
C	1s	0.25	272	0.18
O	1s	0.66	503	0.50
Al	2s	0.23	1396	0.047
Co	2p doublet	3.8	775	0.27
Ni	2p doublet	4.5	848	0.27
Mo	3d doublet	2.75	186	0.34

differentially pumped Ar ion gun (PHI model 04-303) at 5keV. The ion beam was rastered over a 3mm x 3mm area on the catalyst sample. The ion beam is aligned so that the incident ions strike the catalyst surface at ca. 30° to the surface normal. The ion gun sputtering rate was estimated to be ca. 100 Å/min, at these conditions, as found by sputtering a layer of precisely known thickness of Ta_2O_5 on Ta (sample supplied by PHI). Except where specifically mentioned all binding energies (BE) were referenced to the C(1s) line of adventitious carbon at 284.6eV. This line was always strong on the aged catalysts due to coking. Spectra were also collected on some fresh unaged catalysts, which served as references. Here the BE of Au ($4f_{7/2}$) at 83.8eV was the reference state. Small gold dots (ca. 2mm diameter) were deposited on the fresh catalysts by masking the pelletized catalyst disks with aluminum foil, exposing the area to be gold coated by piercing a hole in the foil, and then evaporating gold onto the surface (Edwards-E306A evaporator).

Sample charging due to the insulating nature of the Al_2O_3 support was always a problem which was minimized by irradiating the samples with an electron flood gun. For this reason the Au ($4f_{7/2}$) (fresh catalysts) and the C(1s) (aged catalysts) peak positions were always measured before and after data were collected on each of the other elements of interest, particularly Co, Mo and Ni. Any shift in the peak positions with time, due to charging, could then be compensated for.

(ii) Auger Electron Spectroscopy (AES)

AES spectra were taken on a Perkin-Elmer Physical Electronics Model 590 scanning Auger microprobe which was also digitally interfaced to MACS. The primary electron beam was operated at 3keV, 0.073μA, and a modulation

voltage of 6V peak-to-peak. These conditions had to be used because of sample charging with the LPCA catalysts. Sample charging was so severe with the HPCA catalysts that AES could not be performed on them. The analyzer was of the cylindrical mirror type (PHI Model 25-110). Digital data processing was performed on the same computer system as for XPS. The AES relative atomic sensitivity factors are listed in Table 3.

Ion sputter profiling combined with AES used an argon ion gun (PI model 04303) at 3keV. At this condition the sputtering rate is approximately 100 Å/min.

(iii) Ion Scattering Spectrometry (ISS)

ISS spectra were collected on a 3M Company Model 525 spectrometer which uses a cylindrical mirror analyzer to measure the energies of the backscattered ions. The spectra were obtained with a mixed primary ion beam of ^{4}He (100nA) and ^{20}Ne (50nA) at 2keV. An area of about 0.5 x0.5 mm^2 was rastered with a ca. 400μ diameter beam. The primary ion beam impact angle was normal to the catalyst surface. The base pressure of the spectrometer was ca. 10^{-8} torr before backfilling with the noble gas. The ISS spectrum E/Eo region of 0.1 to 1.0 was analyzed with a scan time of 1 min. Depth profiling was performed at a sputter rate of ca. 7Å/min, based on data collected on Al_2O_3 anodic oxide films (29).

(iv) Secondary Ion Mass Spectrometry (SIMS)

SIMS and ISS spectra were collected simultaneously in a combination spectrometer (see ISS above). The detection unit for SIMS was a UTI-100C quadrupole mass spectrometer, which was used for collecting positive ion spectra, in the 0 to 100 amu mass range. Severe charging problems were encountered which were alleviated by using a hot filament neutralizer.

(v) Scanning Electron Microscopy (SEM)/Energy Dispersive X-Ray Analysis (EDX)

An AMR (Model 1000A) scanning electron microscope equipped with a Tracor Northern model TN2000 X-ray analyzer was used at a 20keV beam energy. For X-ray analysis, the counting time for all the samples was 25 seconds. No precautions were taken to minimize the exposure of the SEM/EDX catalyst sample to air, except for storing them in an argon filled dessicator before analysis. Tweezer handled catalysts were mounted on SEM specimen mounts (E.F. Fullam, Inc. NY) with double sided tape, and gold coated to a depth of ca. 200Å in an evaporative coater (Edwards, Model E306A) immediately before being placed into the microscope.

(vi) Oil Analysis

The oil samples periodically withdrawn from the reactor during an HDM experiment, were diluted with xylene, such that their total nickel concentration was in the range 0-5 ppm. They were then analyzed for total nickel and nickel porphyrin concentrations by atomic absorption spectrophotometry (Perkin-Elmer model 360), and UV-Visible spectrophotometry (Bausch and Lomb Spectronic 2000), respectively. Details have been described elsewhere (9). During experimentation with the HDS-16A (Run 2, Table 2) and the mixed nickel and vanadium oil, vanadium concentrations were also similary determined (10).

III. D. Results

III. D. 1. AES on LPCA catalysts

The results of our AES studies are displayed in Figs. 4 and 5. AES was only used to examine our lightly loaded PCA catalysts; that is, catalysts LPCA (Table 1), which were simultaneously aged in Run 2 (Table

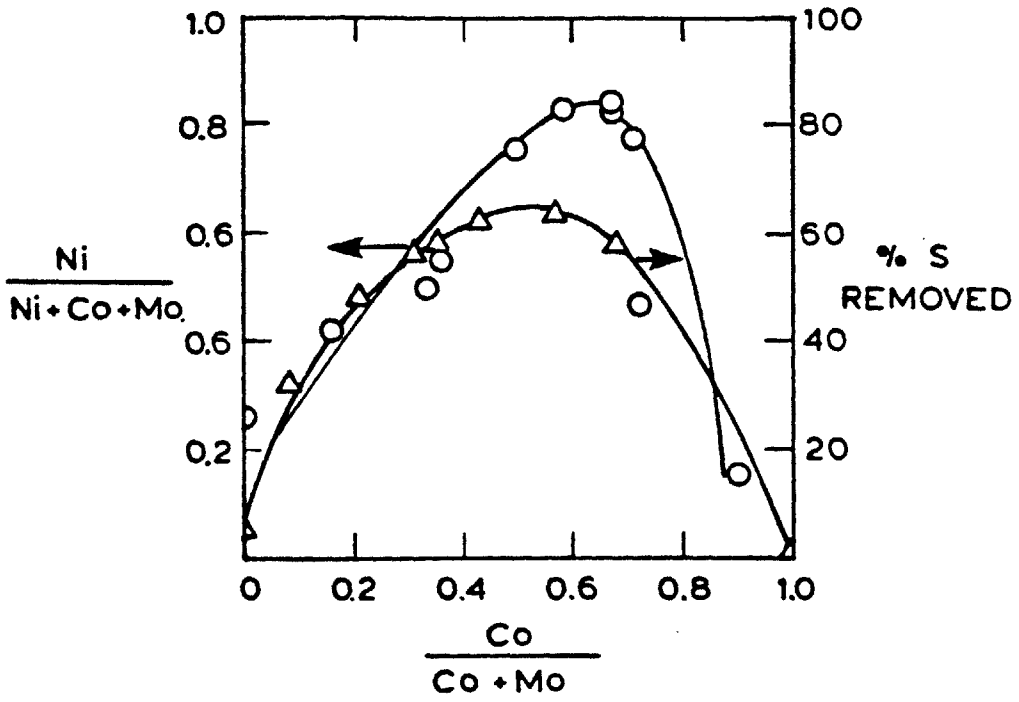

Figure 4: Effect of catalyst composition on the amount of nickel on LPCA catalyst at completion of HDM run number 2, Table 2. Catalyst compositions were measured by AES. HDM run conditions were 61.9 ppm Ni, 330°C, 1000 psig H_2. All LPCA catalysts of different composition were simultaneously mounted in baskets (Fig. 3) and competitively demetallized the oil. Also shown is thiophene hydrodesulfurization rate data, from Wivel et al (13), as a function of supported Co-Mo/Al_2O_3 catalyst composition.

2). There, the oil comprised of Ni-T3MPP in Nujol at 61.9 ppm Ni. Process conditions were 330°C and 1000 psig H_2 for 236 hours. Using the relative atomic sensitivity factors listed in Table 3, the atomic compositions of the different LPCA catalysts' surfaces were then measured. The catalysts were not sputtered, and as a result C was always present. Even though the porphyrin molecules contain 4 atoms of N per atom of Ni, no nitrogen could be detected on the LPCA catalysts by AES. A typical relative atomic composition is C, 20.3%; O, 13.7%; Al, 62%; Mo, 1.6%; Co, 0.8%; Ni, 1.6%, for a catalyst that was nominally prepared with a Co/Mo atomic ratio of 0.90. Our reason for running the LPCA catalysts simultaneously was to see which catalyst composition produced the greatest HDM rate, as measured by the amount of nickel each catalyst accumulated. The results are shown in Fig. 4 where the atomic ratio Ni/(Ni+Co+Mo), representative of the amount of nickel the particular LPCA catalyst had accumulated is plotted against the atomic ratio Co/(Co+Mo) which is a measurement of the catalysts' surface composition. Due to the surface sensitivity of AES, these relative atomic compositions are those existing in the uppermost 20Å (on average) of the model catalyst surface (21).

Eleven data points are shown in Fig. 4 since measurements were made at two different points on three of the eight LPCA catalysts which were aged. These three catalysts had nominal Co/Mo atomic composition ratios of 0.3, 1.0, and 2.0. The nominal (as prepared) catalyst composition is not always in exact agreement with the AES measured composition. This can be attributed to the heterogeneous nature of the catalyst, and the non-uniformity of the impregnated material. This point is amplified later in relation to our SEM/EDX observations.

We note from Fig. 4, that there exists a catalyst composition, r[=(Co/(Co+Mo))], between 0.6 and 0.7, where the amount of nickel deposited on the catalyst is a maximum. Also plotted for comparison is some literature data (13) on thiophene desulfurization as a function of catalyst composition. The maximum rate of desulfurization occurred when r was in the range 0.4 to 0.6. Thus the range of optimum r for desulfurization appears to be less than for HDM.

Sputter depth profiling with Ar^+, at constant beam current and ion current voltage, was also performed on a few of the aged LPCA model catalysts. A representative AES depth profile is shown in Fig. 5, for an aged LPCA catalyst from run number 2 (Table 2), that was nominally prepared with Co/Mo at 0.40. Two points are evident. The Co/Mo atomic concentration ratio actually achieved on the catalyst surface was <0.40, and could be due to a loss of the active metal's from the polycrystalline support during reaction in the oil. The model catalyst surface has a heavy carbon loading, which can be envisaged as being similar to the coke which causes the initial activity decline of real hydrotreating catalysts (36).

With sputtering all elements which were deposited on the pure PCA squares, either by impregnation (Co, Mo) or through the HDM aging reaction (C, Ni), are easily removed. The LPCA catalyst surface is essentially sputtered clean after 1 minute of Ar^+ sputtering. At this time, we have probably removed ca. 100Å of the LPCA catalyst surface at the particular operating conditions of the ion gun. Figure 5 shows that the C concentration drops from ca. 30% atomic composition (AC) to ca. 5% AC in 0.6 min. of sputtering, while Mo falls from ca. 11% AC to ca. 2% in the same time period.

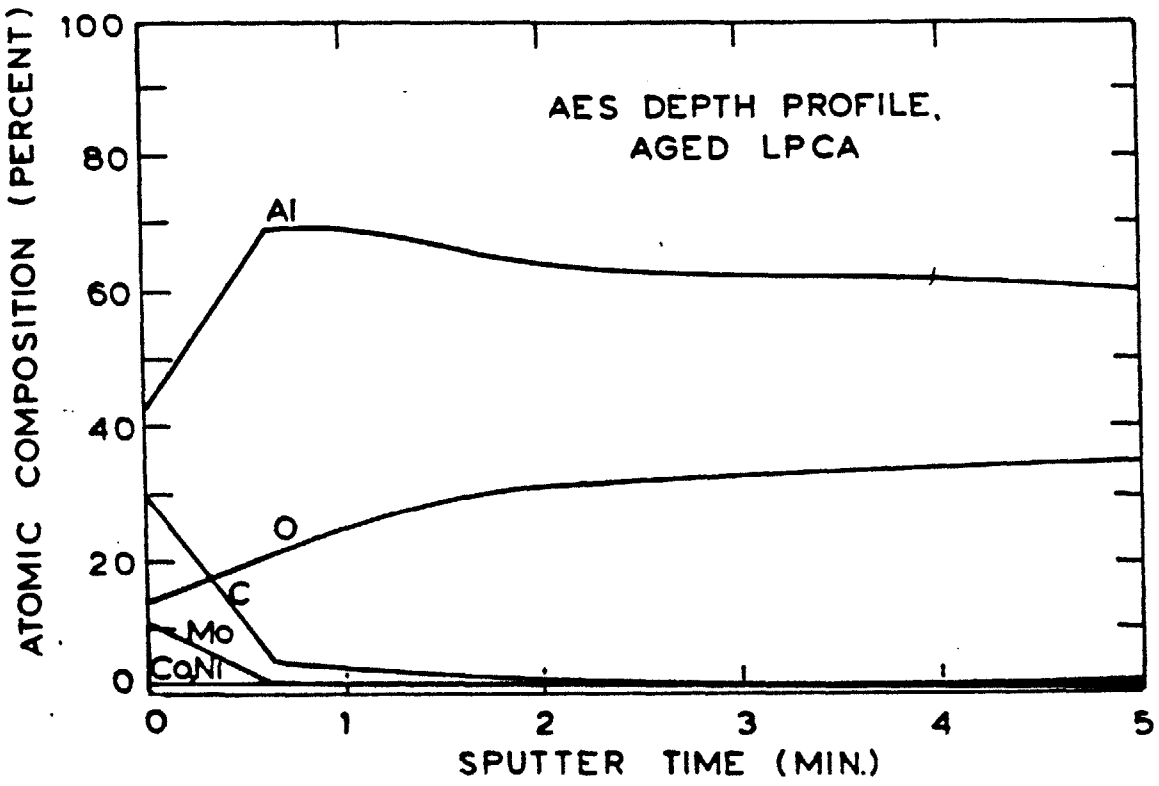

Figure 5: AES depth profile for principle elements in LPCA catalysts, namely, C, O, Al, Mo, Co and Ni. Catalyst was aged in run 2, Table 2, at 330°C, 1000 psig H_2, and 61.9 ppm Ni in the model oil. Catalyst was nominally prepared with Co/Mo atomic ratio as 0.40.

As we would expect for an oxidic alumina support, both the O and Al % AC's steadily increase, and then plateau with sputtering time, as the bulk of the PCA support is reached.

Sample charging was a continuous problem when performing AES on the LPCA catalysts, due to the insulating nature of the support, and the impregnated metal oxides. For this reason the spectrometer was run with the primary electron beam at 3keV, and 0.073μA.

III. D. 2. XPS on HPCA catalysts

We then focussed our attention on the HPCA catalysts (heavily loaded polycrystalline alumina squares; Table 2), which were aged in run 3, Table 3. The model oil was again Ni-T3MPP in Nujol, and the run conditions were at 355°C, 1000 psig H_2 for 56 hours. The HPCA catalysts of different compositions were simultaneously aged by spinning in the basket assembly, in a competitive demetallation experiment--each catalyst competes for the metal in the oil, in a well mixed environment. The total metal concentration in the oil remains effectively constant because of the low HDM catalytic surface area that is available (c.f. Table 2; 8 cm^2 for PCA catalysts, versus 1.59×10^6 cm^2 for an experiment with American Cyanamid HDS-16A). We initially attempted to analyze a few of the aged HPCA catalysts by AES, however, even with the Auger primary electron beam conditions as "mild" as 1keV and 25nA, sample charging precluded the possibility of taking meaningful data. Therefore XPS was employed, in the hope that charging would not be so severe when the HPCA catalysts were flooded with X-rays, and an electron flood gun was used. Moreover XPS could provide information on the chemical oxidation state (albeit qualitative) of the supported elements. Depth profiling on the HPCA

catalysts was also performed with an Ar^+ ion gun, for evidence of changes in composition and oxidation state with depth, from the surface of the catalyst. Like AES, XPS samples the top 20Å of the exposed catalyst surface (21).

Detailed XPS spectra of $Mo(3d_{5/2,3/2})$, $Co(2p_{3/2})$ and $Ni(2p_{3/2})$ were measured in two aged HPCA catalysts from run 3. Their nominal Co/Mo atomic composition ratios were 1.4 and 2.0. XPS spectra were collected after sputtering for zero time (the unaltered aged catalyst), 10, 20 and 30 min. We estimate sputtering occurred at a rate of ca. 100 Å/min. (see Analysis section), a value which is typical (33). Reference spectra for Mo, Co and Ni were also measured on the oxide forms of the commercially supplied hydrotreating catalysts HDS-16A and HDS-9A. Their compositions are listed in Table 1. All XPS data for aged catalysts were charge referenced to C(1s) at 284.6eV. The C(1s) peak on the aged HPCA catalysts was always strong, after reaction in the hydrocarbon oil. The fresh reference catalysts HDS-16A and HDS-9A were referenced to the $Au(4f_{7/2})$ at 83.8eV. In what follows, we will directly compare spectra referenced to C(1s) and $Au(4f_{7/2})$. However, independently we have shown that for our aged catalysts these reference lines are equivalent to within $\pm$0.1eV, which is the accuracy of our peak position measurement. Intuitively, we should also expect this to be correct since the C(1s) line from adventitous hydrocarbon on gold appears at 284.6eV (33).

Figures 6 and 7 show the $Mo(3d_{5/2,3/2})$ spectra for the aged HPCA catalysts, with Co/Mo (nominal) values of 2 and 1.4, respectively. The $Mo(3d_{5/2,3/2})$ spectra from the unaged HDS-16A and HDS-9A are also included for reference. Figure 6 also includes a specta for the unaged calcined

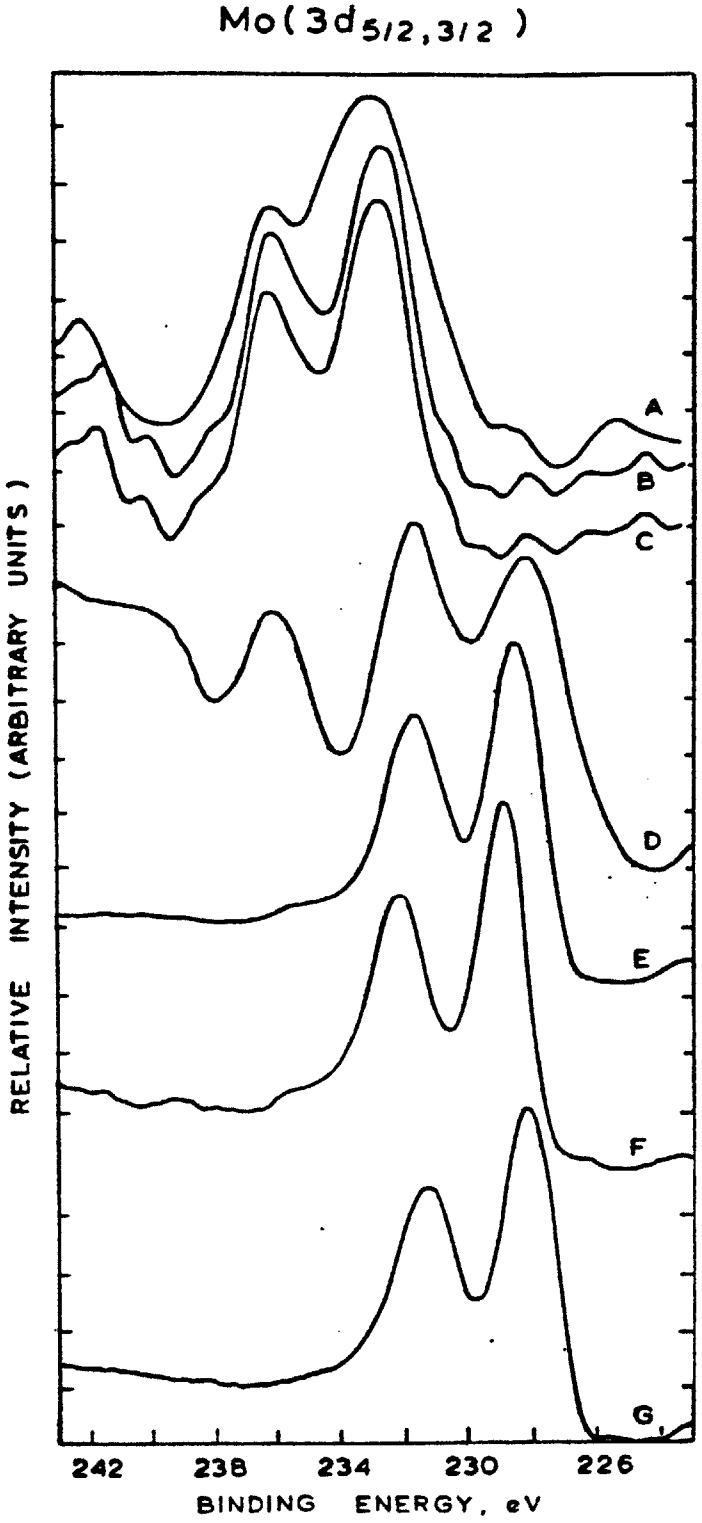

Figure 6: XPS spectra of Mo($3d_{5/2,3/2}$) levels in unaged reference catalysts HDS-16A and HDS-9A, and unaged and aged HPCA catalysts with nominal Co/Mo atomic ratio of 2. (A) Fresh HDS-9A, (B) Fresh HDS-16A, (C) unaged HPCA (Co/Mo=2), (D) aged HPCA, no sputter, (E) aged HPCA, 10 minute sputter, (F) aged HPCA, 20 minute sputter, (G) aged HPCA 30, minute sputter. Sputter rate ca. 100 A min.

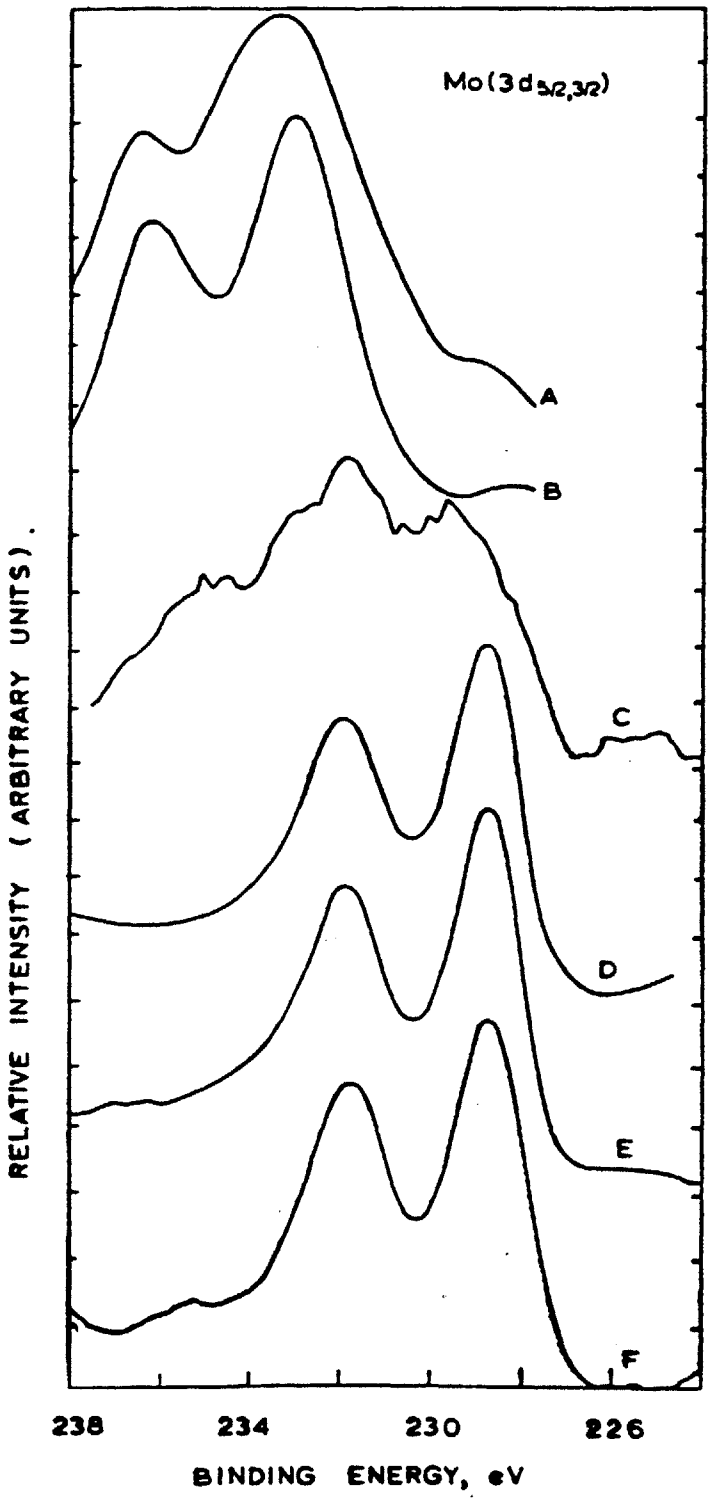

Figure 7: XPS spectra of Mo($3d_{5/2,3/2}$) levels in unaged reference catalysts HDS-16A and HDS-9A, and an aged HPCA catalyst with nominal Co/Mo atomic ratio of 1.4. (A) Fresh HDS-9A, (B) Fresh HDS-16A, (C) aged HPCA, no sputter, (D) aged HPCA, 10 minute sputter, (E) aged HPCA, 20 minute sputter, (F) aged HPCA, 30 minute sputter. Sputter rate ca. 100 A/min.

form of HPCA (Co/Mo=2).

In an XPS investigation of both the oxide and reduced states of a Co-Mo/Al_2O_3 catalyst Patterson et al (30) deconvoluted the Mo($3d_{5/2,3/2}$) spectra for various stages of catalyst reduction, and concluded that Mo^{6+} in the oxidic catalyst was gradually reduced to Mo^{5+} and Mo^{4+}. Deconvolution of their spectra gave the Mo($3d_{5/2,3/2}$) line positions in Table 4. These BE's can be used to interpret Figs. 6 and 7.

In Fig. 6, spectra A to C show that the majority of the calcined catalysts HDS-9A, HDS-16A, and HPCA (Co/Mo=2) are in the Mo^{6+} oxidation state. The Mo(VI)($3d_{5/2,3/2}$) peaks at 232.7eV and 236.1eV are strong. A small peak at ca. 228.2eV indicates that a small quantity of Mo^{4+} is present even in the calcined form of the oxide catalyst. The agreement between the Mo($3d_{5/2,3/2}$) doublet of the model HPCA catalyst (spectrum C) and the highly dispersed HDS-16A (Spectrum B) is particularly noteworthy. Spectra D to G are from the aged form of the HPCA catalyst, shown fresh in Spectrum C. It is apparent that during aging in the HDM reaction Mo^{6+} is reduced to Mo^{5+} and Mo^{4+}.

Spectrum D is from the aged catalyst before it was sputtered. The spectrum is a convolution of peaks contributed by Mo^{6+}, Mo^{5+} and Mo^{4+}. With sputtering, however, the Mo^{6+} peak disappears, leaving spectrum G, which is a convolution of Mo^{5+} and Mo^{4+}. This phenomenon has been recently observed for high surface area Co-Mo/Al_2O_3 catalysts (16,37). The presence of Mo^{6+} in spectrum D, could be due to air contamination of the aged catalyst as it was moved from the reactor to the spectrometer. We can tentatively infer that the Mo($3d_{5/2,3/2}$) spectra for the aged catalyst is actually spectrum G.

Table 4*

Average binding energies+ for Mo($3d_{5/2,3/2}$) lines in their IV-VI oxidation states.

	Line (BE)	
Oxidation State	$3d_{3/2}$	$3d_{5/2}$
Mo(VI)	236.1	233.0
Mo(V)	235.0	231.9
Mo(IV)	233.0	229.9

*Patterson et al (30)

+Charge referenced to Au($4f_{7/2}$) at 83.8eV

The spectra in Fig. 7 provide similar information and show that changes in the Co concentration of the catalyst do not affect the ability of Mo to be successively reduced. Spectra A and B are for fresh HDS-9A and HDS-16A, respectively. Spectrum C for an aged HPCA catalyst with a nominal Co/Mo atomic ratio of 1.4, before sputtering, indicates that the surface layer (ca. 20Å) contains Mo in all the oxidation states +6, +5, and +4. When this surface is sputtered the Mo^{6+} peak disappears, and Mo is found to exist as a mixture of Mo^{5+} and Mo^{4+}, with Mo^{4+} predominating.

Between Fig. 6's spectra D and E, and Fig. 7's spectra C and D approximately 1000Å of surface will have been removed by sputtering.

Figure 8 shows the XPS spectra of the $Co(2p_{3/2})$ level for the aged HPCA catalyst with an atomic Co/Mo ratio of 2.0. Spectrum A is a reference for $Co(2p_{3/2})$ present in fresh HDS-16A catalyst. Spectra B-D were collected on the aged HPCA catalyst, after sputtering for 10, 20 and 30 minutes, respectively. No cobalt signal was detectable on the unsputtered aged HPCA catalyst, presumably because of the carbonaceous overlayer built up during reaction.

The $Co(2p_{3/2})$ principle core lines for the sputtered aged catalyst (Spectra B-D) are shifted to a lower BE than the $Co(2p_{3/2})$ level in the fresh HDS-16A catalyst. Co in the model HDM-aged catalysts exists in a lower oxidation state than the Co in the fresh HDS-16A catalyst. Spectrum A also has very pronounced satellite structure at 5-6eV higher binding energy than the main $Co(2p_{3/2})$ core line. These peaks are also discernible in spectra B to D, although they are much weaker. These satellites are shake-up lines due to a monopole charge transfer process from O2p Co3d, and is due to the paramagnetic states Co^{2+} and Co^{3+} (16,31,33,38). Co_3O_4

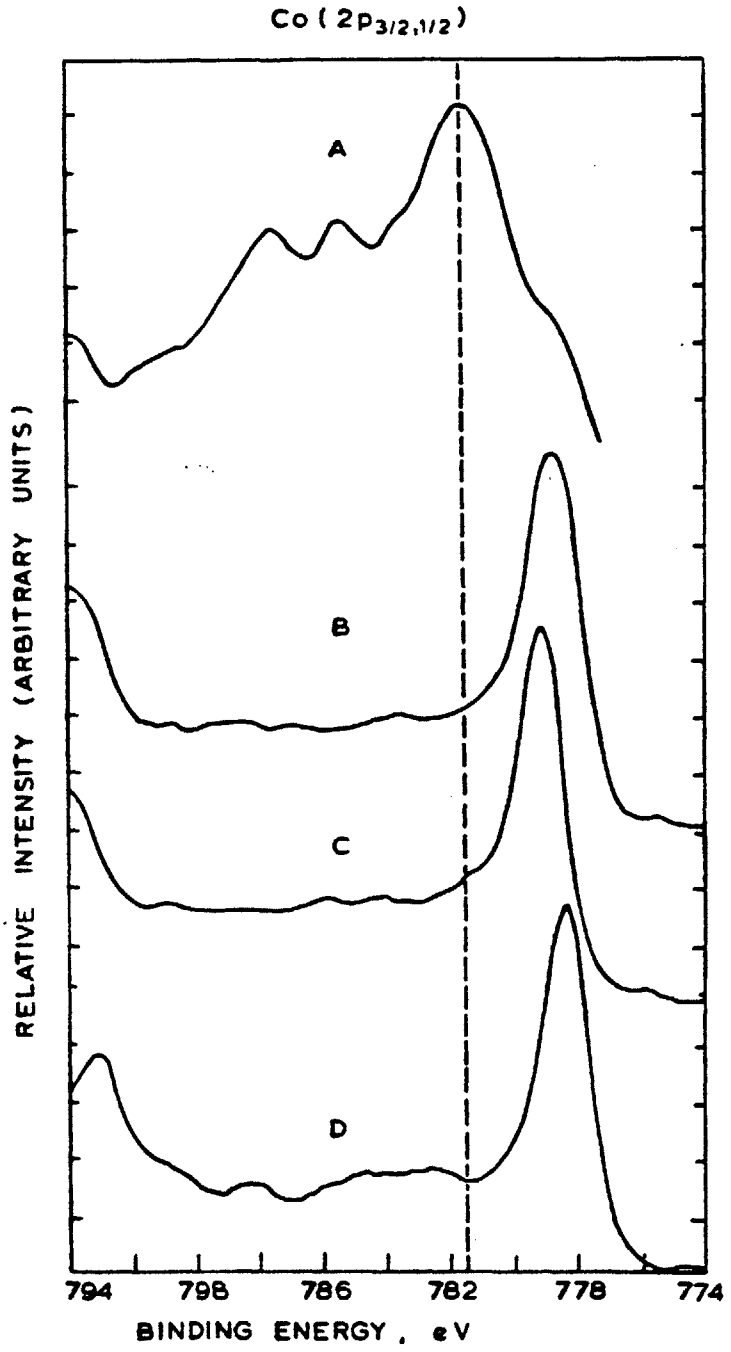

Figure 8: XPS spectra of Co($2p_{3/2}$) level in unaged reference catalyst HDS-16A, and an aged HPCA catalyst, with nominal Co/Mo atomic ratio of 2.0. (A) Fresh HDS-16A, (B) aged HPCA, 10 minute sputter, (C) aged HPCA, 20 minute sputter, (D) aged HPCA, 30 minute sputter. No Co signal is evident on unsputtered HPCA. Sputter rate ca. 100 A/min.

contains both the species Co^{2+} and Co^{3+}, and it is believed that spectrum A is a convolution of the spectra from these two species.

Furthermore, it is possible to deduce the coordination of the surface Co^{2+} ions with oxygen atoms from the energy difference between the main $Co(2p_{3/2})$ core line and the satellite peak. Oku and Hirokawa (39) have shown that this difference is 5.3eV for tetraherally coordinated Co^{2+}, and 6.2eV for octahedrally coordinated Co^{2+}. Our satellite splitting in spectrum A is ca. 5eV and averages 5.2eV for the weaker satellites of spectra B to D. These numbers suggest that when Co exists in the oxide state it is tetrahedrally coordinated to oxygen.

Little oxidic Co exists in the aged HPCA catalysts. Spectra B to D denote that metallic Co is a major constituent of these catalysts.

Similar information can be gleaned from Fig. 9's spectra A to E. Here the Co/Mo atomic ratio is nominally 1.4. For completeness the presputtered spectra B is included. No $Co(2p_{3/2})$ signal is discernable, however spectrum C, taken after a 10 minute sputter shows a strong $Co(2p_{3/2})$ signal. Spectra D and E taken after sputtering for 20 and 30 minutes respectively, show a shift of the $2p_{3/2}$ peak to higher BE (778.0→ 778.8). This indicates that at the sampled depths (2000-3000Å removed from the original catalyst surface) complete reduction of the original oxidic Co may not have occurred, during the HDM reaction. This view is further strengthened by the appearance of weak cobalt oxide shake-up line at ca. 783eV.

Figure 10, spectrum A, shows the $Ni(2p_{3/2,1/2})$ levels for fresh HDS-9A (Table 1). Figure 10B is for an aged HPCA (Co/Mo=1.4, nominally) catalyst and shows that the majority of the nickel exists as NiO. The shoulder at

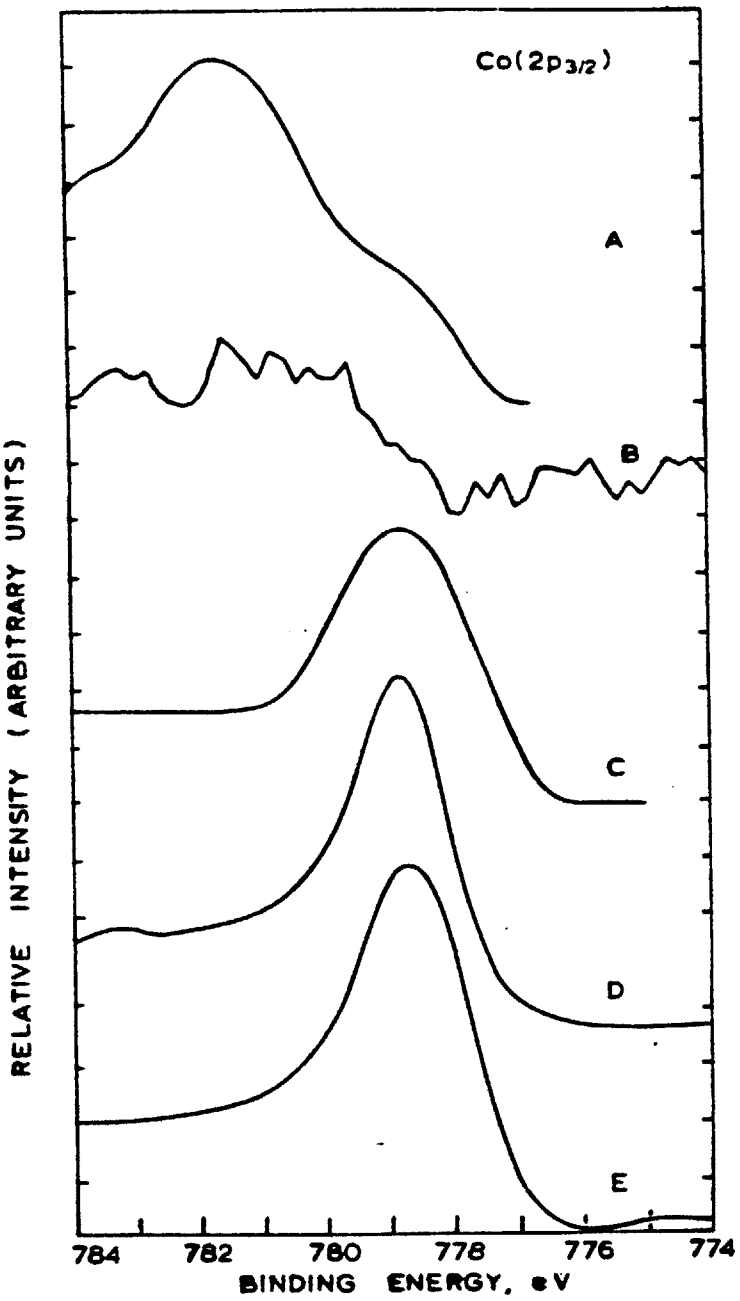

Figure 9: XPS spectra of Co($2p_{3/2}$) level in unaged reference catalyst HDS-16A, and an aged HPCA catalyst, with nominal Co/Mo atomic ratio of 1.4. (A) Fresh HDS-16A, (B) aged HPCA, pre-sputter, (C) aged HPCA, 10 minute sputter, (D) aged HPCA, 20 minute sputter, (E) aged HPCA, 30 minute sputter. Sputter rate ca. 100 A/min.

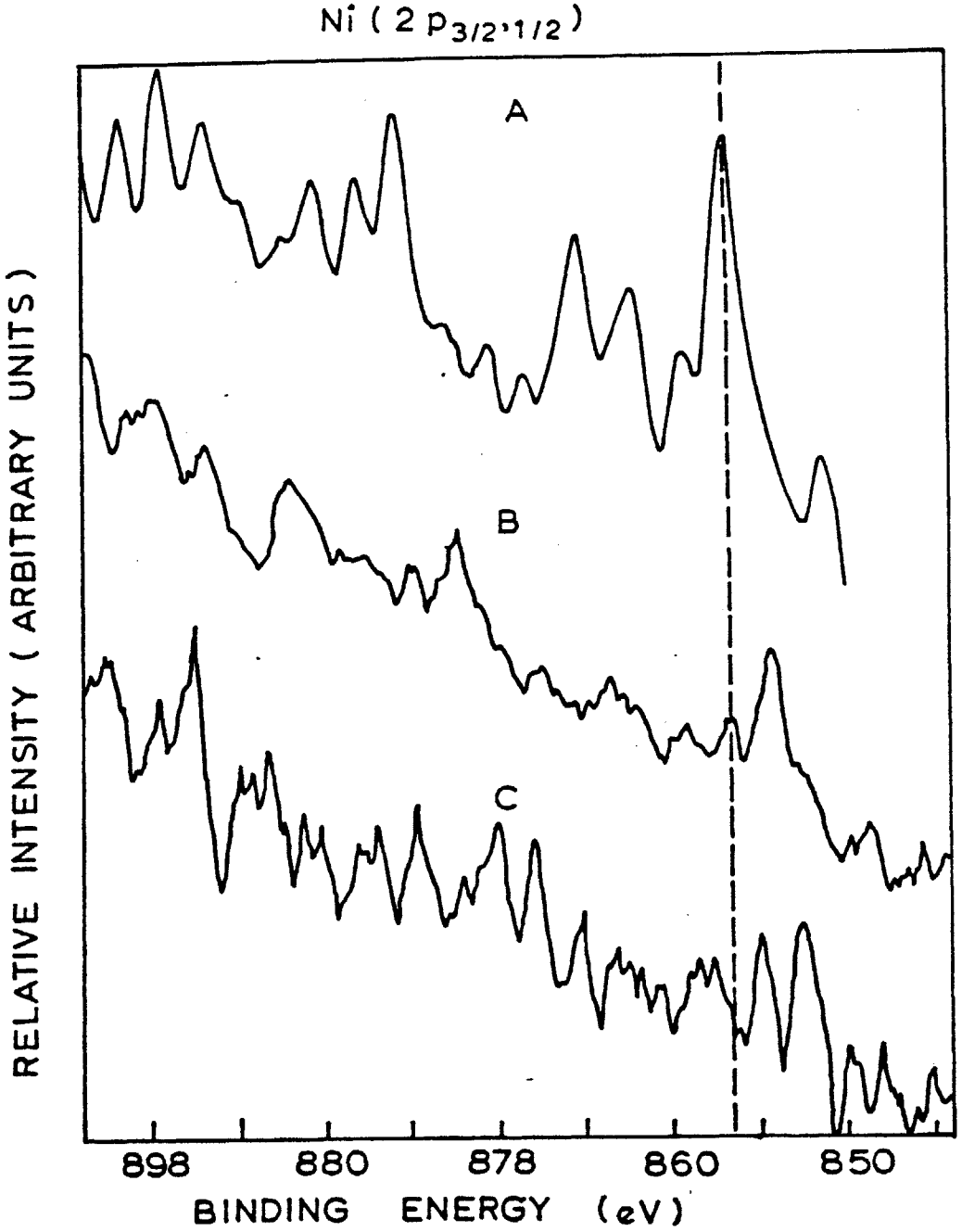

Figure 10: XPS spectra of Ni($2p_{3/2,1/2}$) core levels in unaged reference catalyst HDS-9A, and an aged HPCA catalyst, with nominal Co/Mo atomic ratio of 1.4. (A) Fresh HDS-9A (B) aged HPCA, no sputter, (C) aged HPCA, 10 minute sputter. Sputter rate ca. 100 A/min.

852.0eV on the main Ni($2p_{3/2}$) peak at 856.5eV is due metallic nickel whose $2p_{3/2}$ core line is placed at ca. 852.3eV (33). Spectrum 10B is thus due to a convolution of metallic Ni and NiO peaks (32,35). The presence of NiO is unexpected and is probably due to an oxide film which has formed on our aged HPCA catalyst surface, despite the precautions we exercised to keep the surface free from air.

This hypothesis is partially confirmed by Spectrum 10C which was taken after sputtering the spectrum 10B surface for 10 minutes. The Ni($2p_{3/2}$) line due to metallic Ni now predominates over the Ni($2p_{3/2}$) due to NiO. No change in this condition was observed with longer sputtering times; NiO and Ni always co-existed. It appears that the nickel which is removed from the porphyrinic ring on the surface of the catalyst, may initially exist as the metal. However, on an initially oxide form of the supported Co-Mo catalyst some oxidation of the Ni may occur, even in the reducing environment of the HDM reaction.

Depth profiling in combination with XPS was also conducted on an aged HPCA catalyst, which was prepared with a nominal Co/Mo atomic composition ratio of 25/1. The result is shown in Fig. 11. The sputter rate is ca. 100Å/min. The nickel loading due to the demetallation reaction is low. This is to be expected, however, because the catalyst's composition is not optimal for HDM, as was shown in Fig. 4, which was obtained by experimentation with the LPCA catalysts. In terms of their ability to perform catalytic HDM as a result of their composition, it thus appears that the lightly and heavily loaded catalysts perform similarly. The carbon content of the catalyst surface is high at 80 atom %, however it rapidly decreases with sputtering.

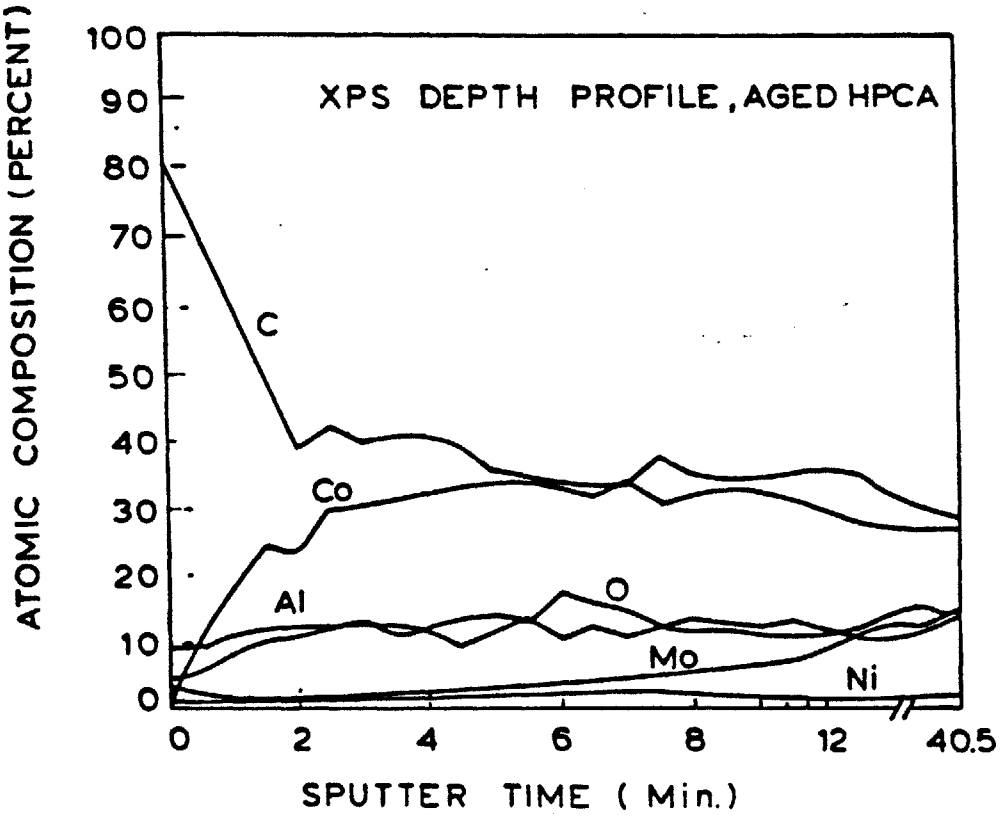

Figure 11: XPS depth profile for carbon, cobalt, aluminum, oxygen, molybdenum and nickel, in an aged HPCA catalyst. Co/Mo atomic ratio is nominally 25/1. Sputtering was conducted with 5keV Argon beam. Sputter rate is ca. 100 A/min.

After ca. 200Å (2 min.) of the catalyst surface have been removed the C content is 40 atom %. The rate of C decline now slows, and is still high at ca. 30 atom % after ca. 4000A of the surface has been sputtered off. During the initial rapid decline in C content, the Co concentration rapidly rises and appears to peak at ca. 33 atom % Co at a depth of 600A into the original catalyst. the aluminum content remains uniform with depth at ca. 10 atom %, indicating that during sputtering we never completely sputtered through the Co-Mo-C catalytic layer, supported on the PCA base.

The molybdenum atomic composition initially shows a small decrease with sputtering during the first minute. Thereafter it gradually increases to ca. 15 atom % Mo indicating segregation of the molybdenum towards the PCA support.

III. D. 3. ISS and SIMS on HDS-16A, LPCA, and HPCA catalysts

Ion scattering spectrometry (ISS) and secondary ion mass spectrometry (SIMS) were performed on fresh and aged (Table 2, Run 1) forms of American Cyanamid HDS-16A, and aged forms of LPCA (Table 2, Run 2) and HPCA (Table 2, Run 3).

The ISS and SIMS spectra were simultaneously collected. The data acquisition time for each spectrum was 1 minute. A mixed ^{4}He, ^{20}Ne beam was used (see Analysis section for details), hence scattering peaks due these two primary ions are present. Each of the spectra are labelled with a scan number which signifies the sputtering time, in minutes, which has elapsed.

The ISS and SIMS spectra for unaged HDS-16A catalyst are shown in Figs. 12 an 13, respectively. The ISS spectra expectedly show the presence of Co (plus Fe which cannot be resolved), Mo, O, Al, K and Ca. The last

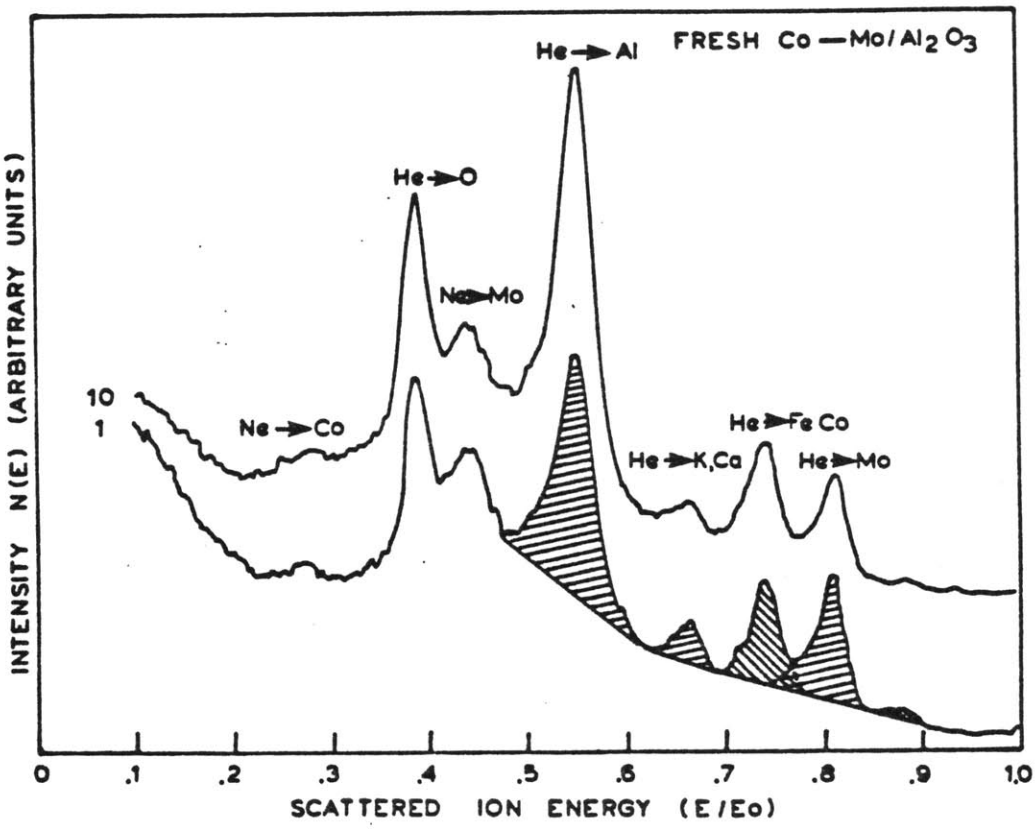

Figure 12: ISS spectra of unaged HDS-16A, Co-Mo/Al_2O_3 catalyst. The incident ion beam was ^4He and ^{20}Ne at an energy of 2keV, and 150nA total current. The beam was rastered over a 0.5 x 0.5 mm^2 area. The scan time was 1 minute. 1. Initial scan, in 0-1 min; 10. 9-10 min. Hatched areas depict areas used for ion scattering intensities. Integration was performed over a linear background.

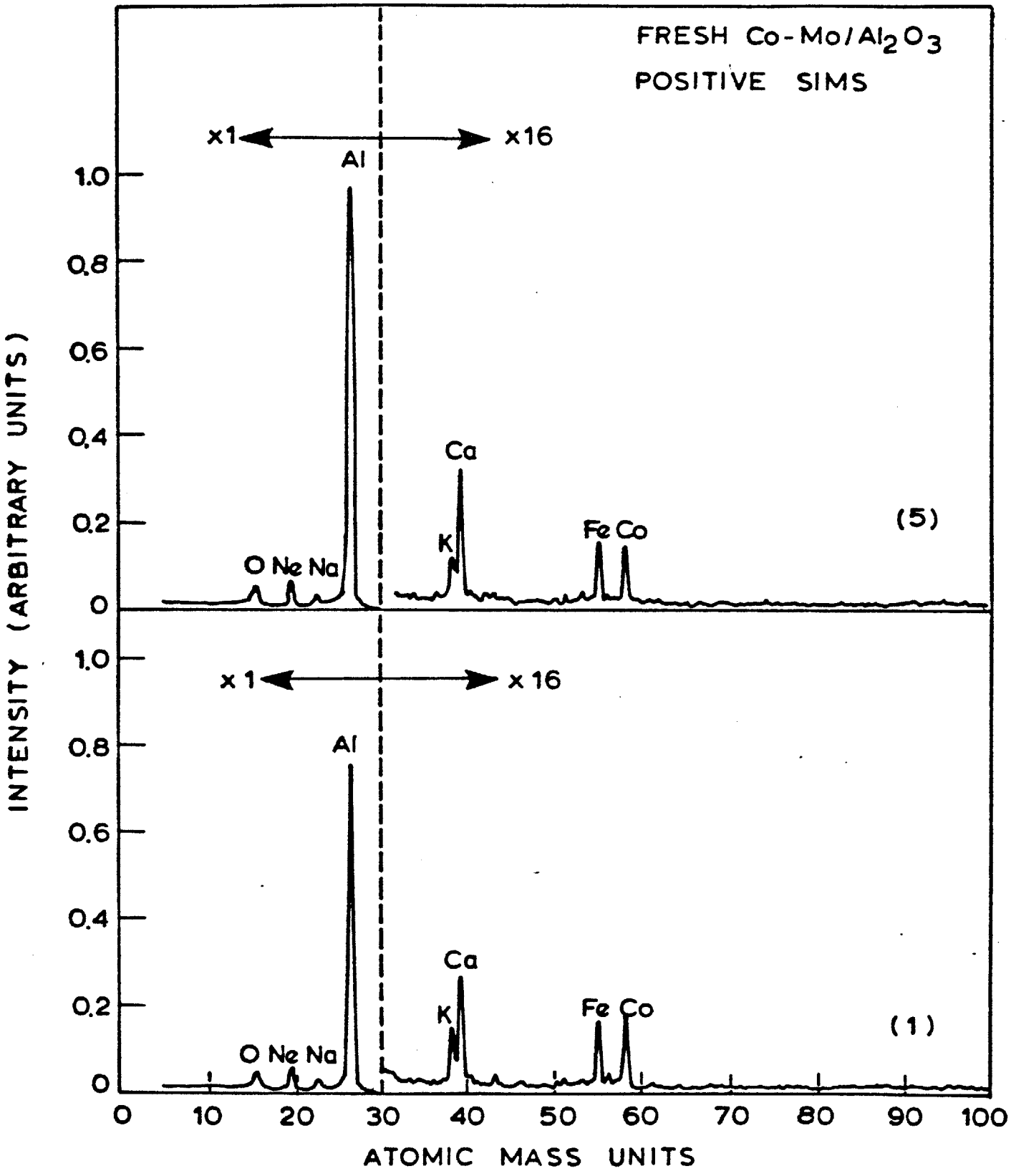

Figure 13: SIMS spectra of unaged HDS-16A catalyst. 1. Initial scan, 0-1 min; 5. 4-5 min.

two elements are not reported by the manufacturer as being present in a significant quantity (Table 1). The ISS sodium peak is swamped by the Al peak, however Na does appear in the positive ion SIMS spectra in Fig. 13, along with the rest of the elements detected by ISS.

During the collection of ISS/SIMS spectra data were accumulated over 1 minute time intervals, and the peak intensities of each of the elements was determined by an integration over each of the peaks on a background that was linear. This is explained in Fig. 12, Scan 1, where the peak intensities for Al, (K, Ca), (Fe, Co) and Mo are shown hatched. Since some peaks overlapped e.g. Co and Mo, deconvolution of their spectra was performed.

Figure 14 shows the variation in the ISS intensities of the elements Co, Mo, K, O, and Al with sputtering time for the unaged HDS-16A catalyst. The sputter rate is ca. 7Å/min. Moreover, since ISS and SIMS only sample the top-most monolayer of the catalyst sample (21), the results we present in this section are far more accurate representations of what is actually present at the catalyst surface (where the reactions do occur) than the preceding XPS/AES results. There, the sampling depth is ca. 20Å (21), and sputtering rate ca. 100Å/min.

Figure 14 shows that Mo and K are surface concentrate, while the O and Al concentrations increase as we penetrate the Al_2O_3 support. The Co concentration increases to a maximum at a depth of about 20A from the original surface and then declines to a steady state value. This indicates the presence of a cobalt rich oxide layer underlying a surface layer that is molybdenum oxide rich. Unfortunately no information on the Na distribution can be obtained due to its signal being completey dominated by

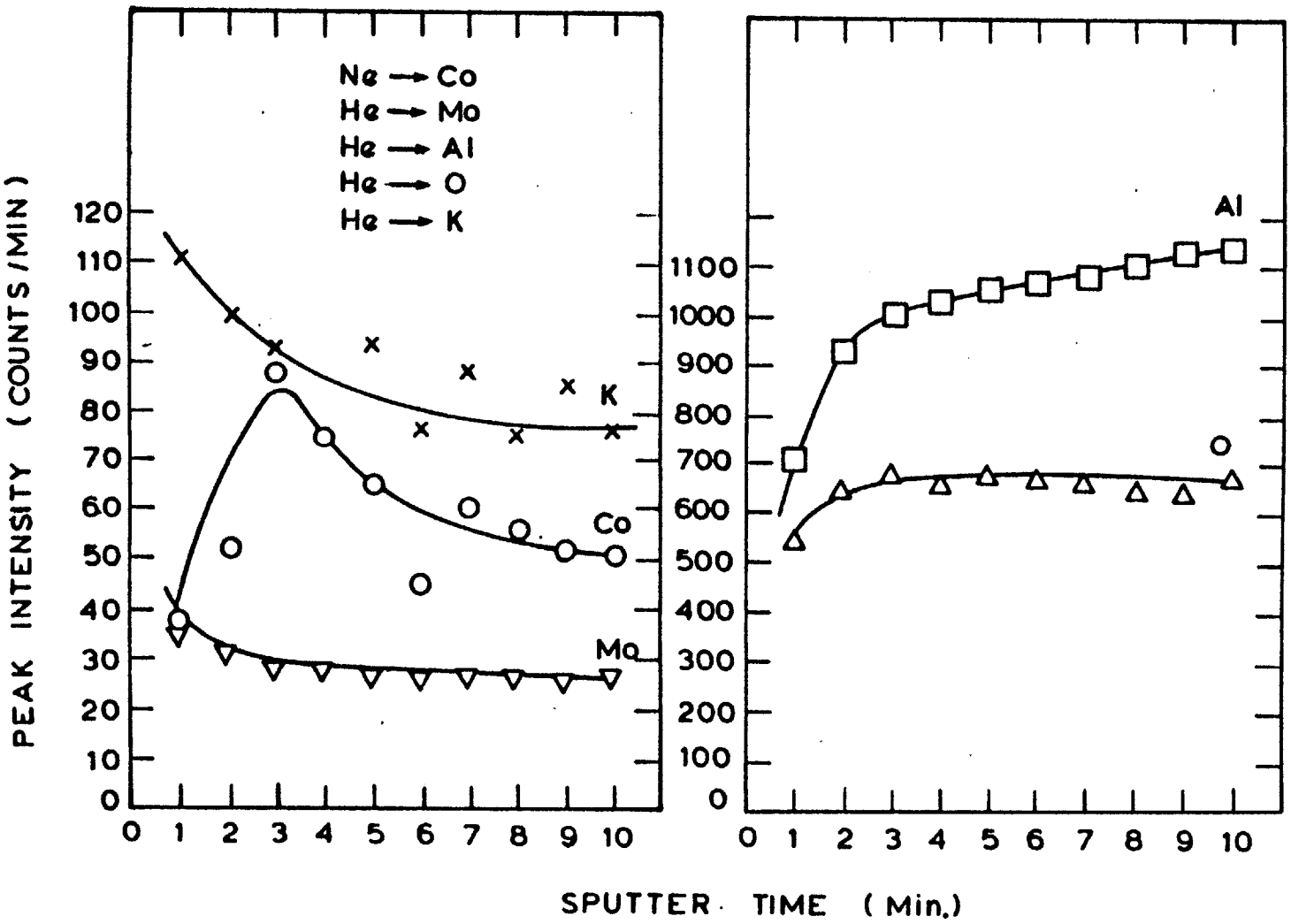

Figure 14: Time dependence of the ISS peak intensities for unaged HDS-16A catalyst. Sputtering rate is ca. 7A/min. See text for ion beam conditions.

that of Al.

Figures 15 to 17 show similar ISS/SIMS data for an aged HDS-16A catalyst. The aging was conducted in run 1 (Table 2) with a mixed nickel and vanadium containing oil. The structures of the porphyrins used are given in Fig. 2. The aging procedure has already been described.

The first ISS spectrum of Fig. 15, taken during the first minute of sputtering shows weak peaks for each of the element O, Al, V and Mo. The signals are probably weak due to heavy surface carbon contamination, however, only a weak C peak is evident in SIMS scan 2 of Fig. 16. As sputtering continues ISS peaks in Fig. 15 become more pronounced and a convoluted shoulder at E/Eo=0.76 appears, due to either Ni, Co or Fe. This convoluted shoulder could not be deconvoluted to determine which of the three elements were actually present, however, the SIMS spectra of Fig. 16, taken at 2 and 5 minutes of sputtering time, show no evidence for the presence of Co; only Fe and Ni peaks are evident. These findings are consistent with the picture of the Co-Mo catalyst derived from the spectra taken on the fresh catalyst; that is, that Co lies beneath a surface Mo layer. The basic elements Na and K were again detected in the aged catalyst (Fig. 16), even though it was presumably heavily coked, indicating their surface seeking tendancies.

The ISS depth profiles of element peak intensity versus sputtering time of the aged HDS-16A catalyst is depicted in Fig. 17. Since the aged catalyst surface is presumably heavily coked (a fact already ascertained for our model HPCA catalysts with XPS--see Figure 11), the maximum in the Mo profile at 15Å in from the original surface, is expected. The Al and O profiles also increase as we would expect as we penetrate a contaminated

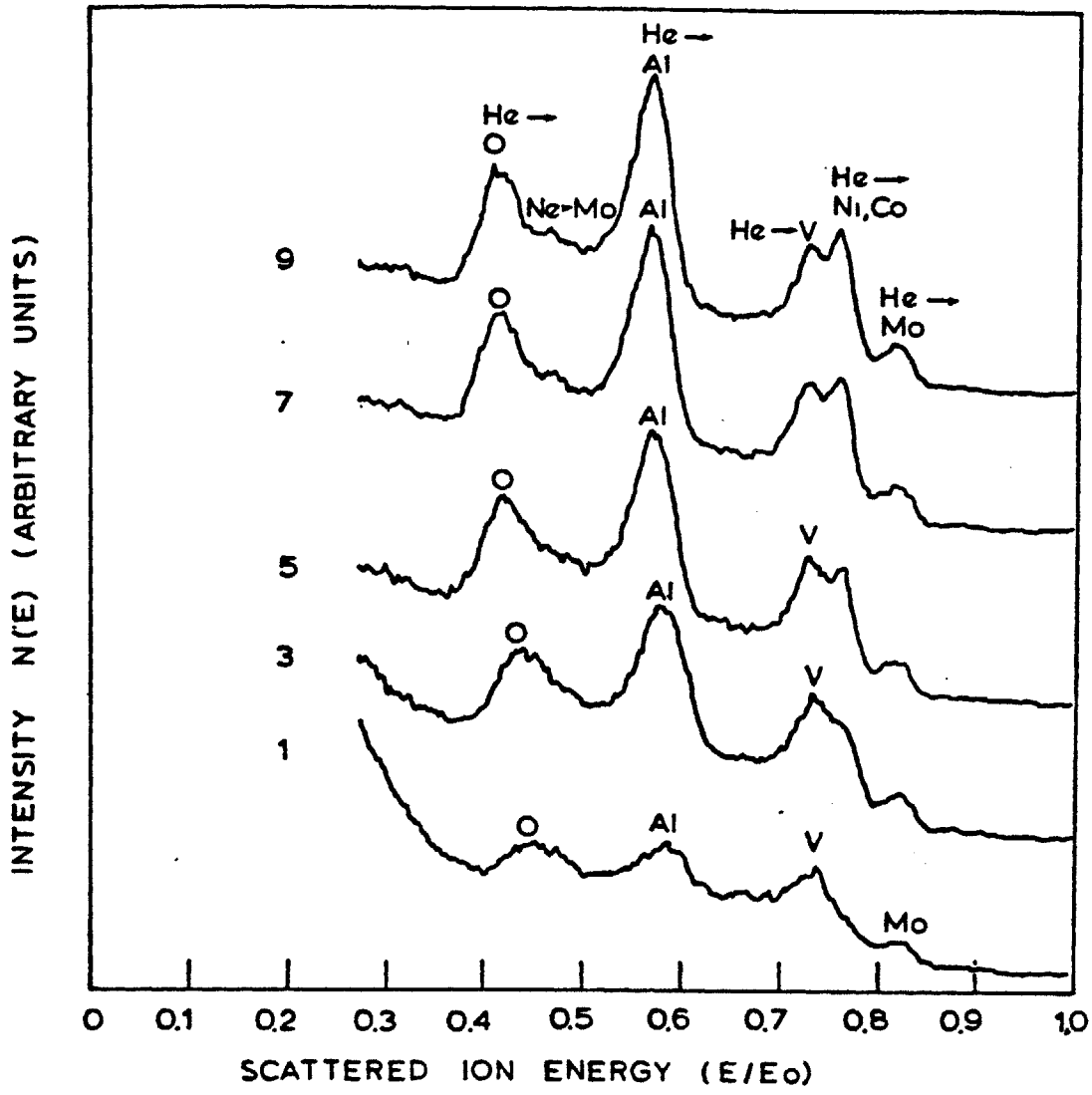

Figure 15: ISS spectra of aged HDS-16A catalyst. Aging was done in run 1, (Table 2). The incident ion beam was ^{4}He and ^{20}Ne at an energy of 2keV, and 150nA total current. The beam was rastered over a 0.5 x 0.5mm^2 area. The scan time was 1 minute.

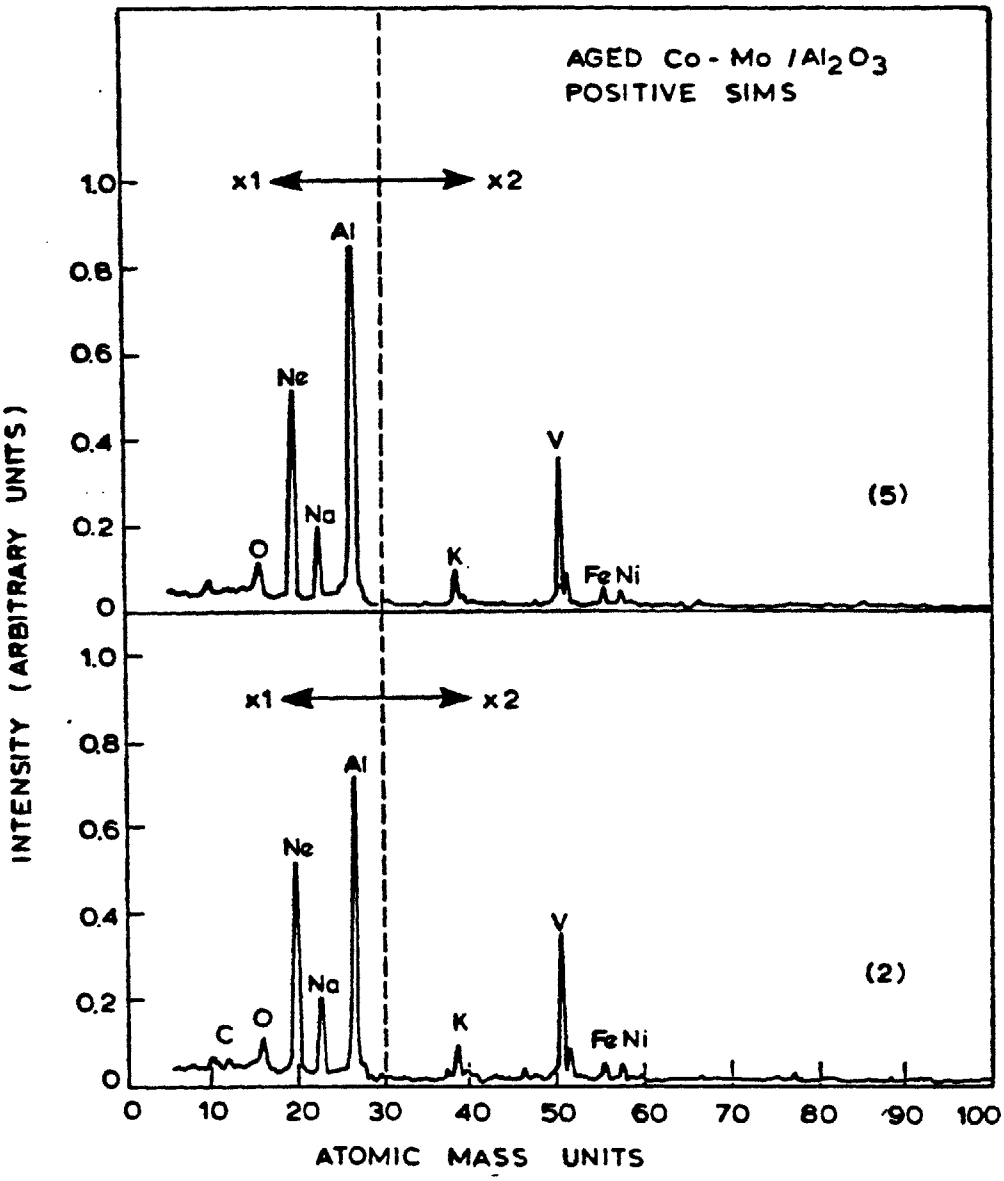

Figure 16: SIMS spectra of aged HDS-16A catalyst. Catalyst was aged in Run No. 1 of Table 2. Scan 2 in sputtering time period 1 to 2 minutes. Scan 5 in sputtering time period 4 to 5 minutes.

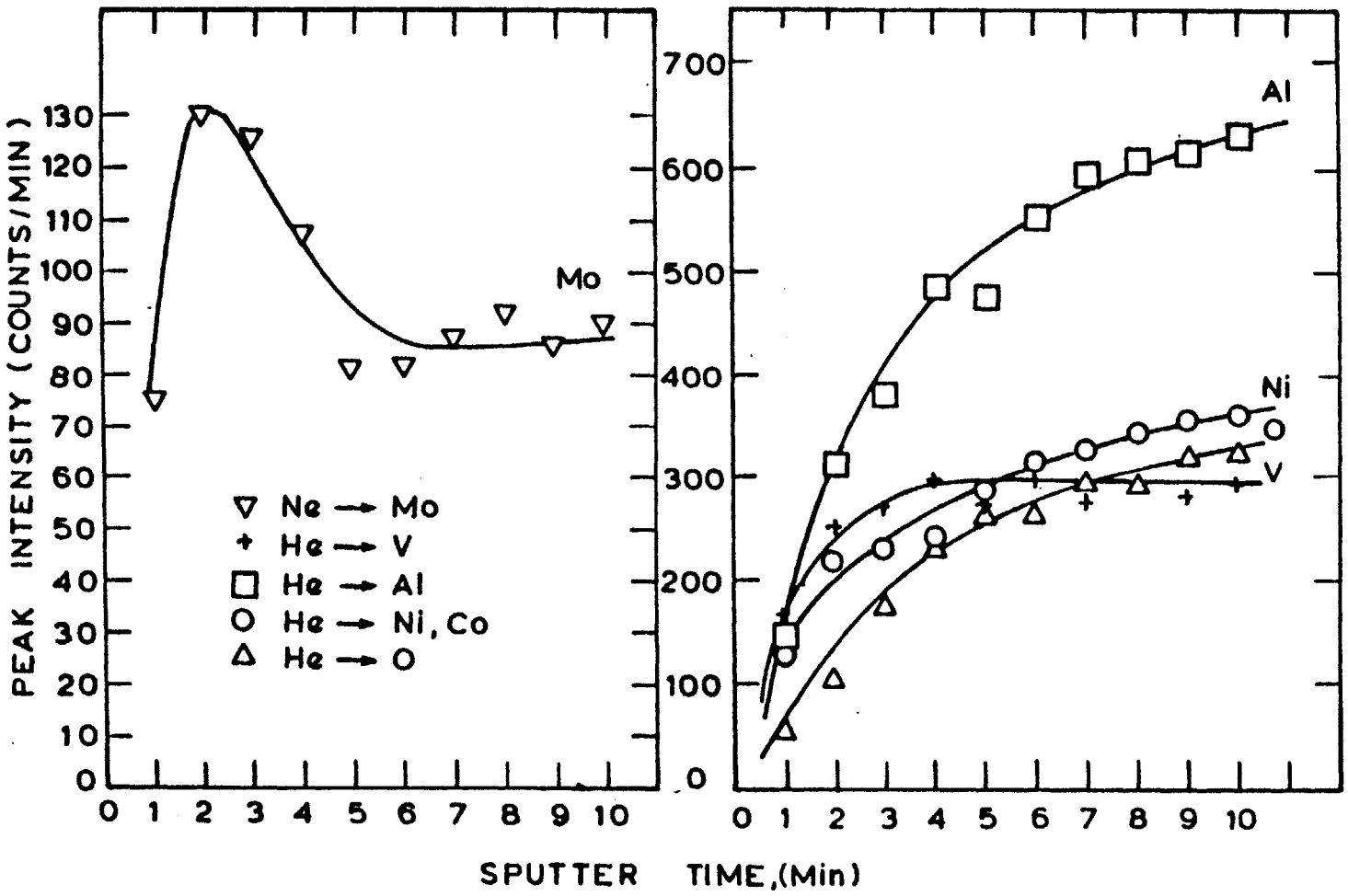

Figure 17: Time dependence of the ISS peak intensities for aged HDS-16A catalyst. Catalyst was aged in Run No. 1 of Table 2. Sputtering rate is ca. 7A/min. See text for ion beam conditions.

Al_2O_3 surface. Only the contaminant Ni and V profiles are contrary to our expectations. In an independent study we have measured the intrinsic demetallation kinetics of a mixed Ni-T3MPP and VO-Etio containing model oil (40). VO-Etio demetallates faster than Ni-T3MPP, and even suppresses the demetallation rate of the latter. This implies that V is first deposited on the catalyst surface, to be topped by a Ni layer. The ISS depth profiles of Fig. 17 disagree with these findings, suggesting that it is the V which predominates at the catalyst surface, while the Ni concentration exceeds the V concentration at depths greater than ca. 35A. The SIMS spectra of Fig. 16, taken up to 5 min. sputter time, suggest that the V concentration still exceeds the Ni concentration at that depth (ca. 35A). ISS/SIMS data on an aged LPCA catalyst (nominally, Co/Mo=0.9) are shown in Figs. 18-20. The aging run was number 2 of Table 2, and the model residua only contained Ni-T3MPP as the metal contaminant (i.e. no V). In Fig. 18, a convoluted Co, Fe and Ni ion scattering signal is evident at E/Eo=0.76. The SIMS spectra in Fig. 19 independently confirms that all three elements are indeed present. The ISS spectra also indicates a weak Mo signal at E/Eo=0.815, which remains as the surface is sputtered. Mo does not appear in the SIMS spectra, probably as a result of its relatively high atomic weight (95.9 amu). The basic elements Na, K and Ca, are detected by both ISS (Fig. 18) and SIMS. The Na and K signals are both strong in the mass spectrum; K is not significantly reduced by sputtering (compare scans 1 and 5), while Na is to a greater extent. These basic elements must originally have been present as impurities in the PCA slabs, and migrated to the surface during the catalyst calcination step.

Figure 20 shows the ISS depth profile results for the lightly loaded

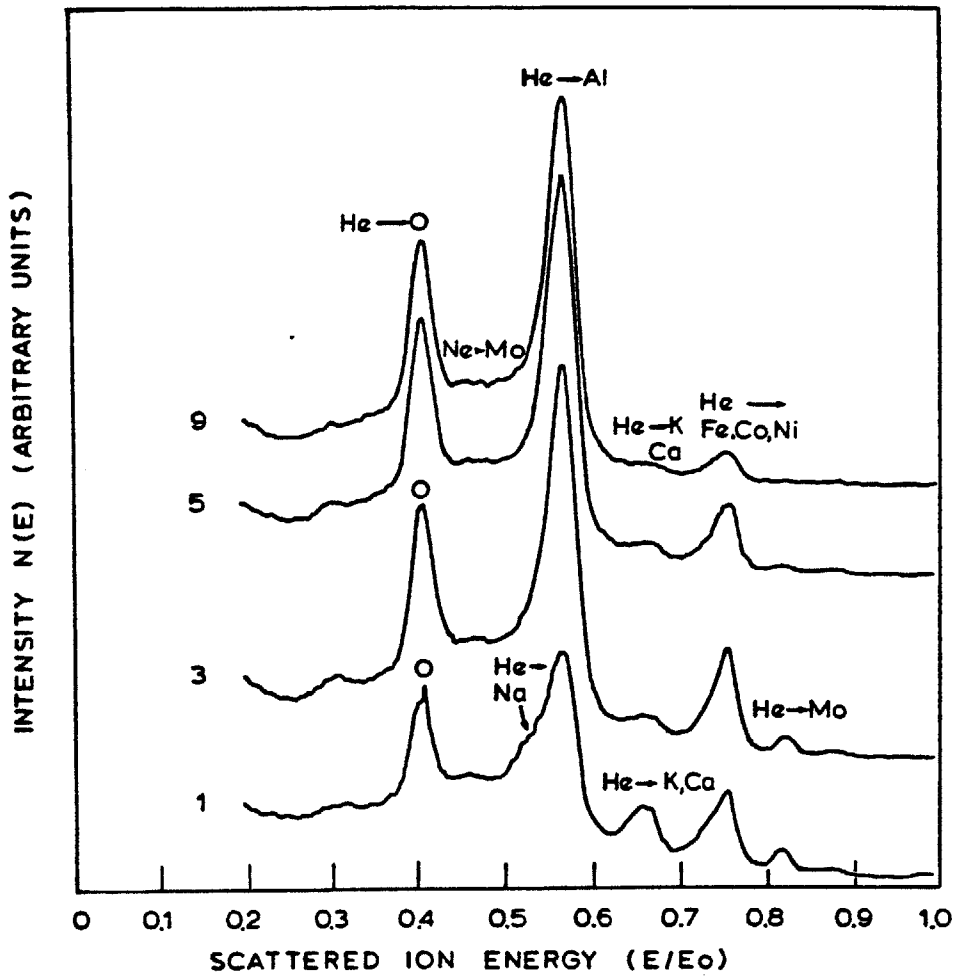

Figure 18: ISS spectra of aged LPCA catalyst. Catalyst composition has a nominal Co/Mo atomic ratio of 0.9. Aging was done in Run No. 2 of Table 2. For spectrometer operating conditions see legend of Fig. 15 and main text.

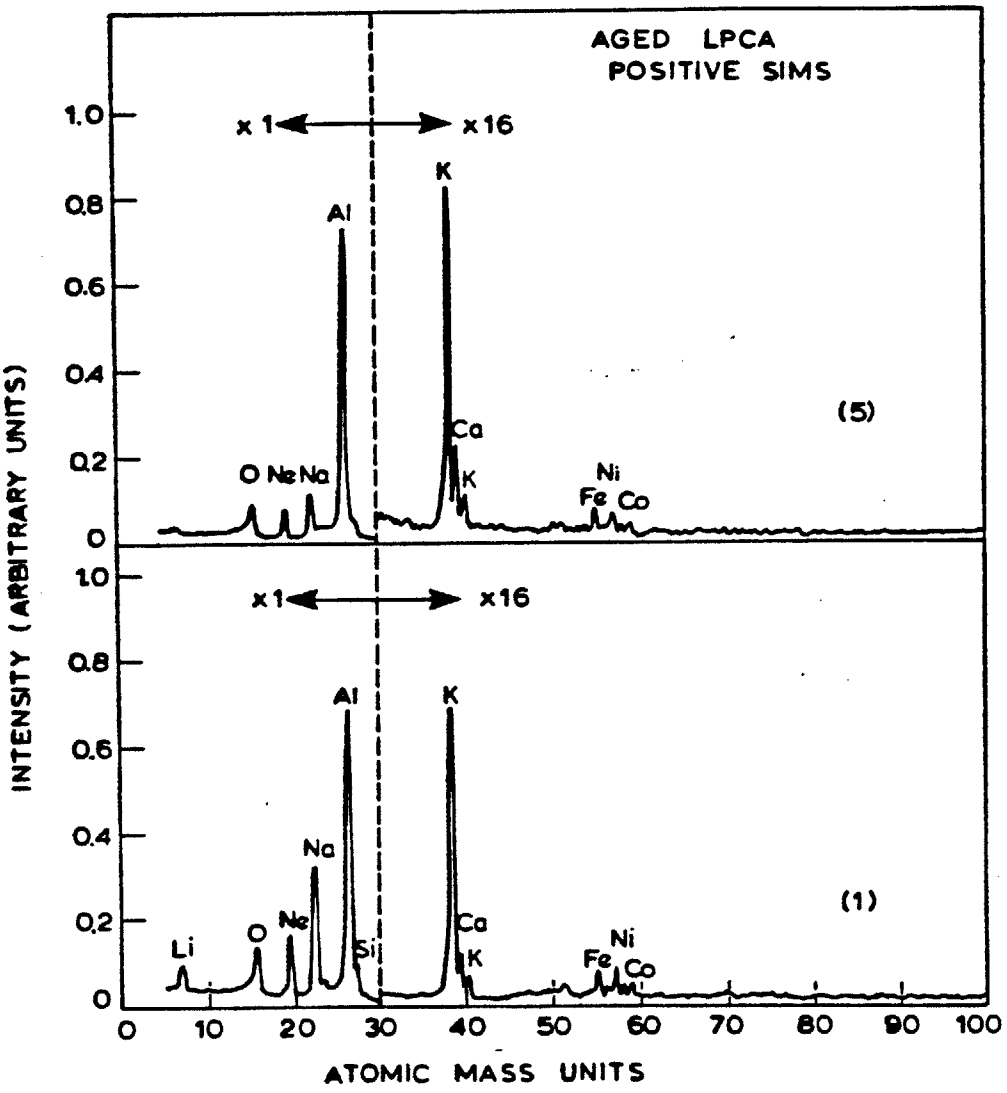

Figure 19: SIMS spectra of aged LPCA catalyst. Catalyst composition has a nominal Co/Mo atomic ratio of 0.9. Aging was done in Run No. 2 of Table 2. Scan 1 is initial scan; 0-1 min; Scan 5 in time 4 to 5 min.

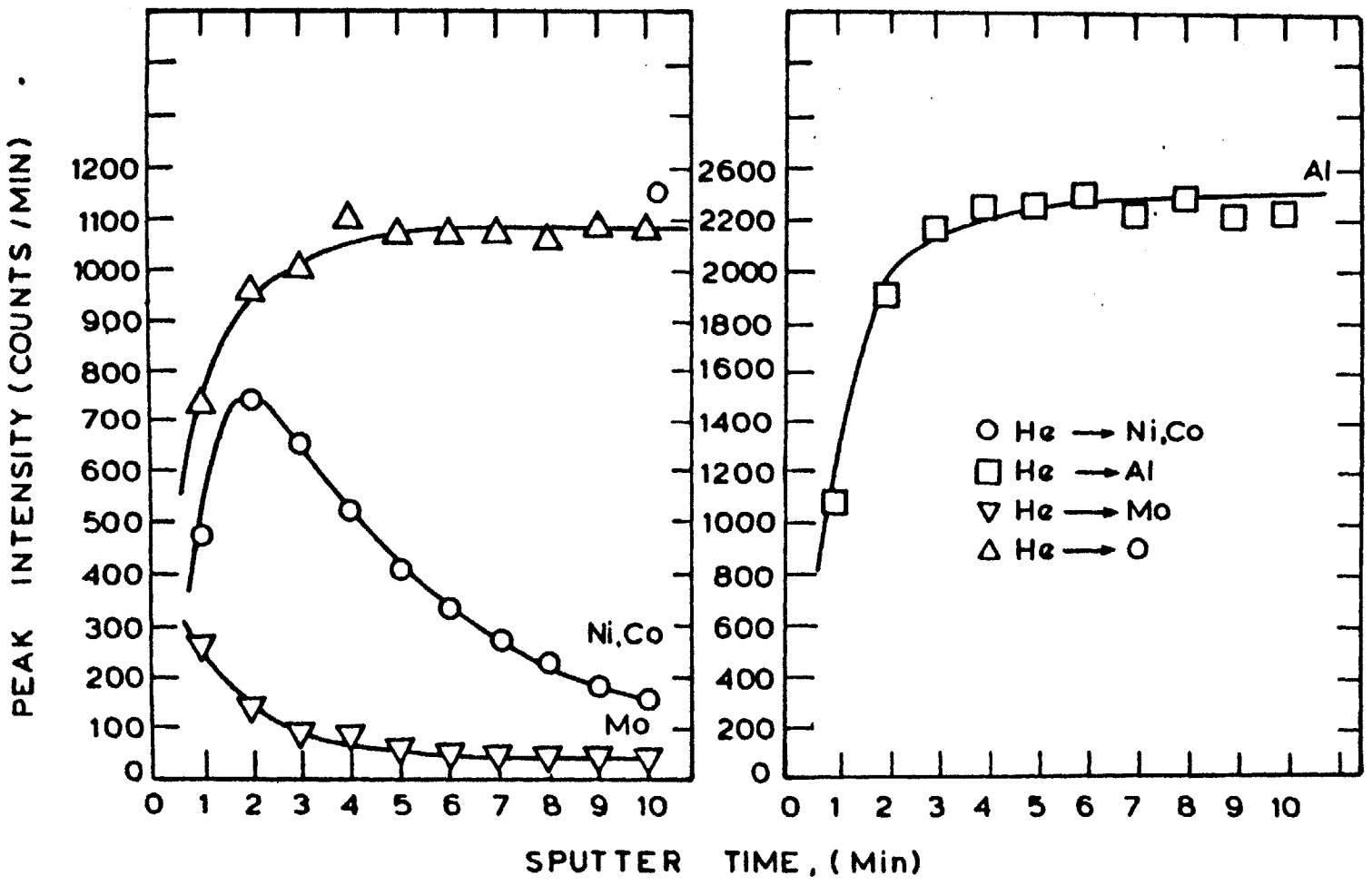

Figure 20: Time dependence of ISS peak intensities for aged LPCA catalyst (Table 2, Run 2). Sputterng rate is ca. 7A/min. See text for ion beam conditions.

aged model PCA catalyst. The Mo intensity decreases, while the O and Al intensities monotonically increase as we sputter into the PCA support. The ion scattering Fe-Co-Ni signal in Fig. 18 could not be deconvoluted, however, it is believed to be primarily due to Co. The Co intensity then shows a maximum after approximately 15Å of surface have been sputtered off. We therefore have a remarkable agreement between how the Co and Mo atoms are physically arranged on the surface of the real supported Co-Mo/Al_2O_3 catalyst, and our model Co-Mo/PCA catalyst. Both catalysts possess a Co-Mo double layer, with Mo being the surface dominant element in the fresh catalysts.

Finally, ISS/SIMS was also performed on an aged HPCA catalyst (nominally, Co/Mo=0.7), and the results are shown in Figs. 21 and 22. The catalyst was aged in run 3 of Table 2. The ion scattering spectrum of Fig. 21 definitively detects only the presence of O, Co, and Mo. Each of their signal intensities increase as the model catalyst is sputtered to remove the carbonaceous overlayer, which almost obliterates the presence of any signal during scan 1. Small, but finite, signals for Co and Mo are then present, which suggest that the carbonaceous overlayer is not complete and some uncovered Co and Mo sites do exist. No Al is detected. This is expected, since, during catalyst preparation the PCA support was loaded with approximately 10^4 monolayers of Mo. (Some Scanning Electron Micrographs of the heavily loaded PCA catalysts are presented in the next section, which indicate the thickness of the Co-Mo phase.)

Figure 22 shows the ISS depth profile. Ni cannot be detected due to the large Co signal. Both Co and Mo concentrations increase in a sigmoidal fashion as carbon is sputtered from the catalyst surface. $(CH)_n$ type

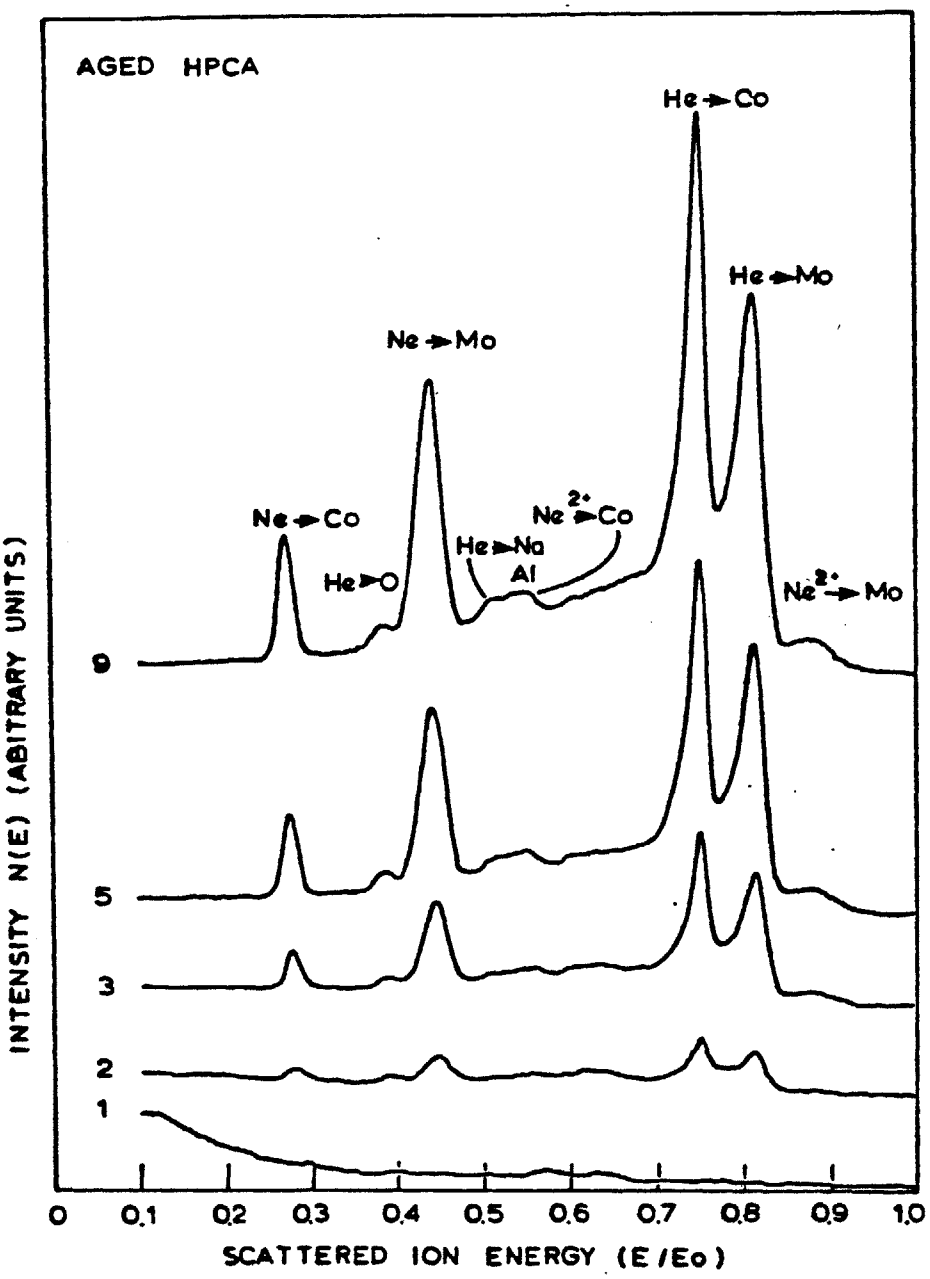

Figure 21: ISS spectra of aged HPCA catalyst. Catalyst composition has a nominal Co/Mo atomic ratio of 0.7. Aging was done in Run 3 of Table 2. For spectrometer operating conditions see main text.

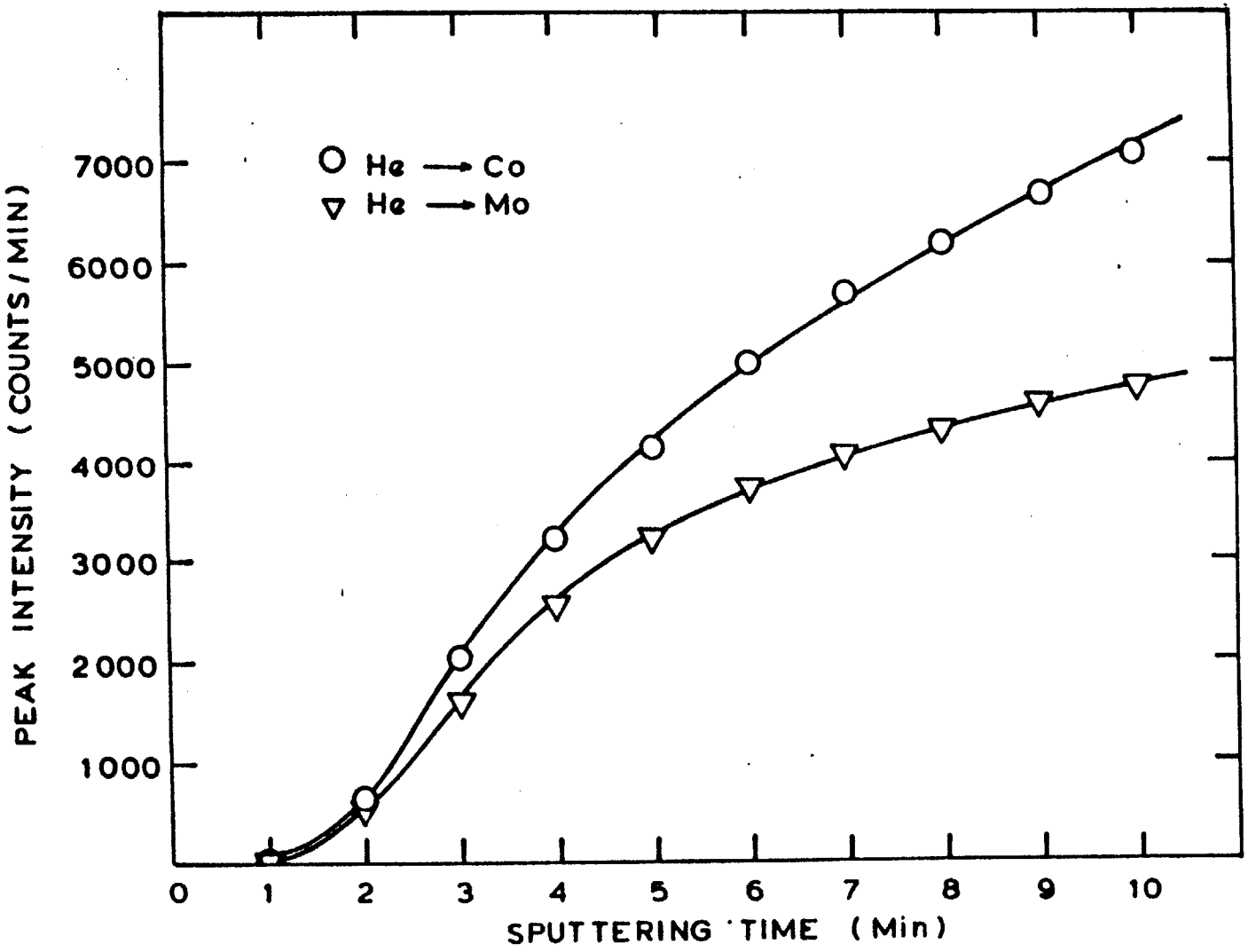

Figure 22: Time dependence of the ISS peak intensities for aged HPCA catalyst. Catalyst was aged in Run 3 of Table 2. Sputtering rate is ca. 7A/min. See text for ion beam conditions.

species were detected by SIMS during the first minute of sputtering. Even after sputtering to a depth of ca. 70Å (10 minute sputter time) no maximum in the Co profile is evident.

III. D. 4. SEM/EDX investigation of aged LPCA and HPCA model catalysts

The surface morphology of aged HPCA and LPCA catalysts was examined by scanning electron microscopy in combination with energy dispersive X-ray analysis. EDX has micron spatial resolution and is a powerful technique for quickly assessing the elemental composition of one-μm^3 volumes on the catalyst surface (41,42).

Figures 23 and 24a are scanning electron micrographs (SEMS) depicting the surface morphologies of a pressed disk of aged HDS-16A catalyst from run 1 (Table 2), and an aged HPCA catalyst from run 2, respectively. The HPCA catalyst has a nominal Co/Mo atomic ratio of 0.90. The size scale and magnification of the SEM's are given in the panel at the bottom of the micrograph. For example, in Fig. 24a the white bar denotes a length of 10 microns. Figure 24b shows a close-up view of the surface of the HPCA catalyst. Figure 24c is an X-ray spectrum, using EDX, over the area viewed in Fig. 24b. The sampling depth on EDX is ca. 1 micron making the technique more of a "bulk" sampling technique when compared to the AES, XPS, SIMS and ISS methods already discussed. In Fig. 24c the number of X-rays emitting the sampling area is plotted as a function of their energy of emission, in the range 0-10.24keV. The type and energies of the X-ray emission lines of interest to us are listed in Table 5.

As expected, in Fig. 24c, X-ray signals due to Mo (convoluted with Au), Co (both Kα and Kβ lines) and Ni (Kα) are evident. The Ni (Kα) signal appears convoluted with the Co(Kβ) signal as a shoulder at ca. 7.5keV.

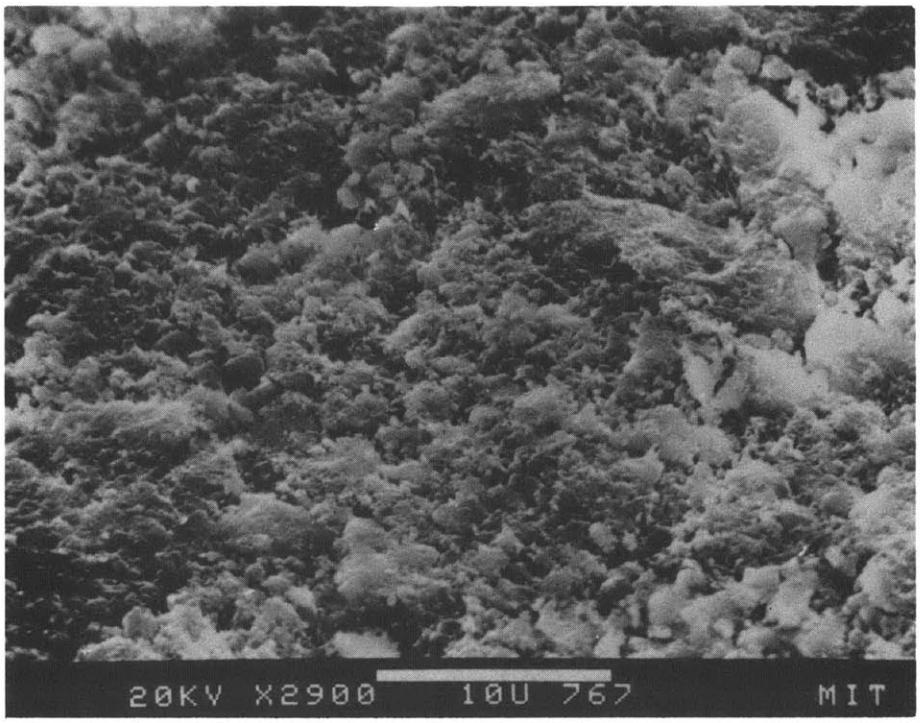

Figure 23: Scanning electron micrograph of unaged, pressed HDS-16A powder. Powder was pelletized at a pressure of 10,000 psi in an IR press. Marker bar is 10 microns.

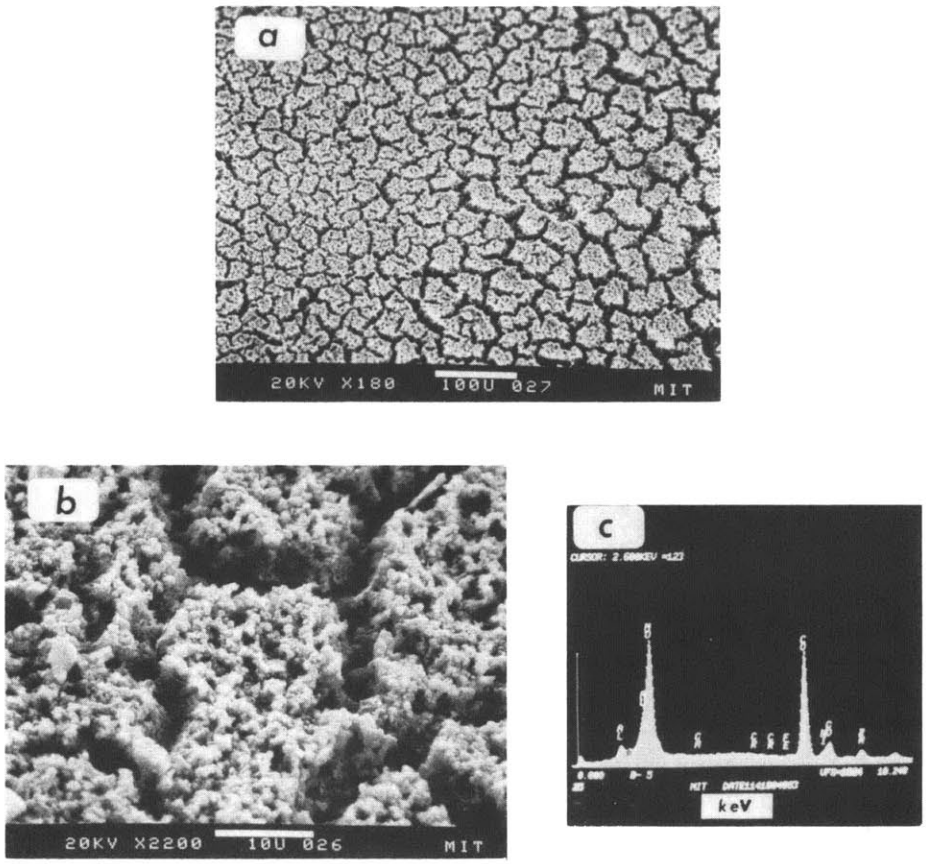

Figure 24: (a) Low magnification scanning electron micrograph of aged HPCA catalyst (Co/Mo=0.9, nominally). Marker bar is 100 microns. The cobalt-molybdate surface is cracked and little of the polycrystalline alumina support is exposed.
(b) Close up of Fig. 24a. Marker bar is 10 microns.
(c) EDX spectrum of the area depicted in Fig. 24b. Ni ($K\alpha$) line is evident as it skews the symmetry of the Co ($K\beta$) line. The strong Mo ($L\alpha$)line dominates the weaker Al ($K\alpha$) line indicating that the surface is impregnated to a depth of ca. 1 micron.

Table 5

Energies of X-ray emission lines*

Element	Type	Energy (keV)
Al	Kα	1.486
Co	Kα	6.915
	Kβ	7.649
Mo	Lα	2.289
Ni	Kα	7.461
Au+	Mα	2.123

*Bearden, J.A., "X-ray Wavelengths and X-ray atomic energy levels," NSRDS-NBS14, National Bureau of Standards, Washington, D.C., 1967.

+Evaporated onto catalyst surface for SEM analysis.

The surface morphology of the HPCA catalyst, heavily impregnated with the Co-Mo phase, is unlike the surface of the working HDS-16A catalyst (compare Figs. 23 and 24b). Figure 24b shows that the HPCA catalyst surface is a cracked surface layer. The surface cracking occurs during catalyst calcination. The underlying PCA support is visible through the cracks. The catalytic surface layer is a few microns thick.

The LPCA catalysts were made to more closely simulate the working Co-Mo/Al_2O_3 catalysts than the HPCA catalysts. In making the LPCA catalysts, our goal was to produce a highly dispersed Co-Mo phase, that was spectroscopically measurable. These are two conflicting requirements, since a highly dispersed Co-Mo phase, supported on PCA, which closely mimics the surface structure of the real porous γ-Al_2O_3 supported catalyst, may have surface concentrations that are not quantitatively detectable by XPS, or ISS. Our results have shown that the metallic phases supported on the LPCA catalysts are quantitatively measurable by surface spectroscopy. The question remaining is: how highly dispersed is the supported phase? We sought answers to this question by taking SEM's on an aged LPCA catalyst (Co/Mo=0.9, nominally).

SEM's of the LPCA catalyst are depicted in Figs. 25a to 25d. Figures 25h to 25g are EDX spectra on areas of the aforementioned figures. Figure 25a is a view of the center region on the model catalyst. The surface appears clean, however, it was in regions of this morphology that the AES, SIMS and ISS work was performed. These techniques detected the presence of the impregnated metals Co and Mo, and the poison Ni, which was deposited during the HDM reaction. The Co-Mo phase evidently exists in a highly dispersed state in this region, providing a realistic model for the HDS-16A

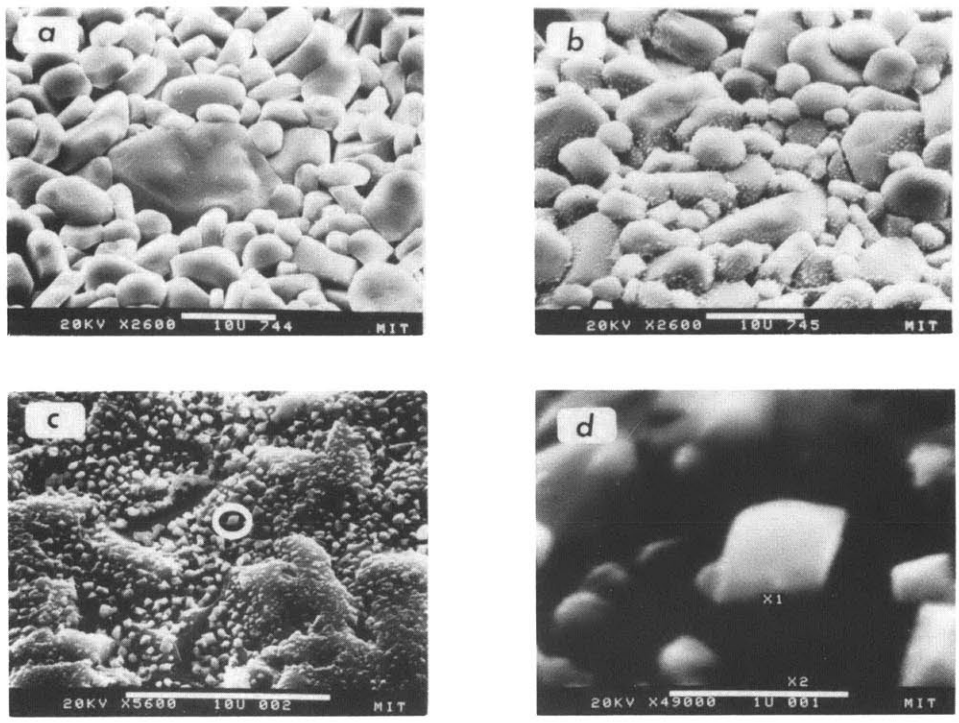

Figure 25: (a) SEM of center region of unaged LPCA catalyst. The catalyst's atomic composition is Co/Mo=0.9. It is regions such as this that the AES, XPS, ISS and SIMS measurements were performed. These techniques revealed that Co, Mo and Ni were present. The support's alumina crystals are clearly visible. Marker bar is 10 microns.

(b) SEM at edge of support area of LPCA catalyst shown in (a). Cobalt molybdate crystals are visible. Marker bar is 10 microns.

(c) SEM of edge region of LPCA catalyst depicted in (a) and (b) that has now been aged in Run 2 of Table 2. Aging conditions were 330°C, 1000 psig H_2 and 236 hours run time at a nickel porphyrin concentration of ca. 60 ppm Ni. Large cobalt-molybdate crystallites are strongly bound to the support surfac and not removed during run. One crystallite is identified and focussed on in Fig. 25d. Marker bar is 10 microns.

(d) Cobalt-molybdate crystallite identified in Fig. 25c is shown magnified. Marker bar is 1 micron. Two regions are identified. 1 is on crystal. 2 is on alumina support.

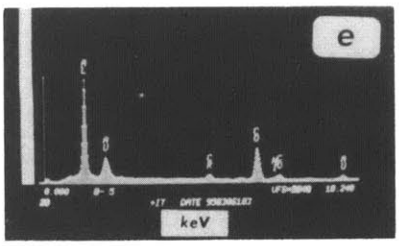

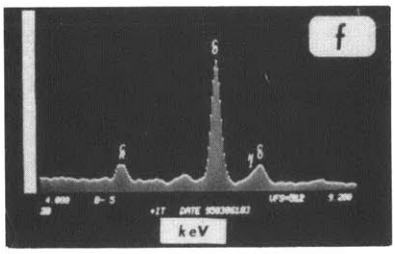

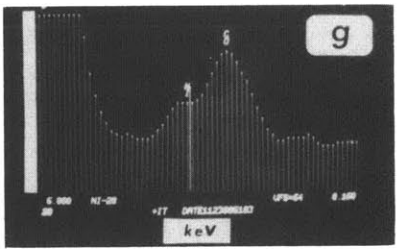

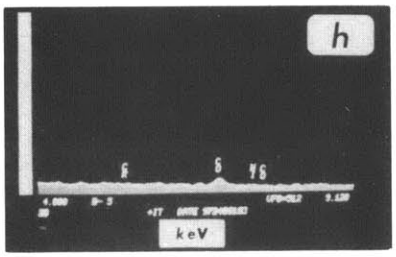

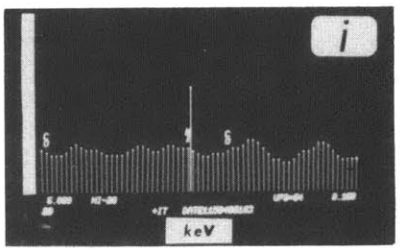

Figure 25: (e) EDX spectrum of area 1 in Fig. 25d. Sampling area was ca. 1 micron.
(f) Portion of EDX spectrum in Fig. 25e.
(g) Portion of EDX spectrum in Fig. 25e. Nickel is present on the Co-Mo crystal. The Ni ($K\alpha$) line appears as a shoulder on the Co($K\beta$) peak.
(h) EDX spectrum of area 2 in Fig. 25d. Sampling area is ca. 1 micron^2.
(j) Portion of EDX spectrum in Fig. 25h. No EDX detectable quantities of Ni or Co exist on the alumina support surface.

catalyst. The SEM's in Figures 25b and c were taken on the periphery of the LPCA catalyst square. The deposited Co-Mo phase is clearly visible as small crystallites, which are formed during the drying step following wet impregnation of the support (Fig. 1, steps 5 and 6). It is because of this mal-distribution of the impregnated phase that we have always quoted nominal (or average) LPCA catalyst compositions. It also explains why our measurements of LPCA catalyst compositions by AES sometimes differed dramatically from the nominal composition. We emphasize again, that surface spectroscopy measurements were always made in the highly dispersed central region, whose surface is shown in Fig. 25a.

Figure 25d is a close up of a Co-Mo phase crystallite originally identified in Fig. 25c. Two spots (1, and 2) are marked. Region 1 is on the Co-Mo phase, while region 2 is on the bare PCA support. With the electron beam probe size reduced to ca. 1μm, EDX spectra were taken on regions 1 and 2. They are shown in Figs. 25e to g, and Figs. 25h to j, respectively.

Figures 25e to g depict selected regions of the EDX spectra taken on the crystallite and indicate the presence of Al, Co, and Ni. The Ni signal appears as a shoulder on the Co(Kβ) line (Fig. 25g). The Mo signal has been occluded by the Au peak. When the electron beam is now moved a distance of ca. 1μm across the catalyst surface to region 2 (Fig. 25d), the EDX spectra of Figs. 25h and j result. The signal is essentially background noise with no detectable elemental concentrations.

These facts suggest that the Co-Mo crystallites which form on the periphery of the PCA squares during light impregnation, are highly active for conducting HDM, in comparison with the surrounding Al_2O_3 support.

III. E. Discussion

Considerable work has been done in the surface characterization of both nickel and cobalt promoted hydrotreating catalysts. The catalytically active metal is either molybdenum or tungsten, with the former metal being more popular. Surface characterization has been performed with a multitude of techniques (for review, see e.g. refs. 15,43). Most work has been done with the Co and Mo oxides supported on porous γ-Al_2O_3. The catalysts are generally fresh (44), that is, they have not been aged in a hydrotreating environment, although exceptions exist (19). Considerable XPS work has been done on the sulfided form of the Co-Mo/Al_2O_3 catalyst (16,30,45-47) which is generally viewed as the active form of the catalyst during HDS, HDN and HDM (15,43). Little work has been reported on the surface characterization of Co-Mo/Al_2O_3 catalysts which have been aged in an HDM reaction. The objectives of this paper were to rectify this situation and probe the surface of highly idealized model catalyst with a range of surface diagnostic techniques, thereby exploiting the strengths of each individual method, and build up a conceptual picture of the surface of the working hydrotreating catalyst. Moreover, our work has been performed on the model catalysts, which have been aged in a model hydrodemetallation reaction. The following discussion explains why we believe our model catalysts are a good representation of Co-Mo/γ-Al_2O_3 system.

The promotional effect of either Co or Ni in the heteroatom (S or N) removal activity of Mo/Al_2O_3 catalysts is well known (48-50,13,15,43). The Co-Mo/Al_2O_3 catalyst is commercially manufactured such that the atomic ratio Co/(Co+Mo) is in the range of 0.3 to 0.6 (43). At these catalyst compositions both HDS and HDN rates are maximized (13).

The reason for the enhancement in catalytic activity with the addition of promoter is a complex effect, and has thus been the subject of a number of theories (15). The three most popular models are the "synergy-by-contact" model (51,52), the "intercalation" model (53,54) and the "monolayer model" (55). The monolayer model only applies to the oxidic form of the catalyst. Other models attempt to explain the promoter effect by invoking concepts such as electron transfer (56), hydrogen spill-over (57), p-semiconductivity (58) and surface acidity (59).

In the calcined form of the working Co-Mo/Al_2O_3 catalyst the oxymolybdenum species which are formed occur as one dimensional chains, with the Mo highly dispersed and interacting strongly with the Al_2O_3 support. The presence of Co suppresses the formation of bulklike MoO_3 and helps stabilize the Mo monolayer (60,61). The cobalt exists primarily in two forms: Co_3O_4, which interacts strongly with the molybdenum layer, and as a surface spinel, $CoAl_2O_4$ (15,43). Catalyst manufacturers appear to attempt to minimize formation of the latter compound, which effectively removes Co from the catalyst surface, by controlling the order of impregnation (62), or by inhibiting the solid-state reaction between Co and Al_2O_3 (63).

In the working environment the Co-Mo/Al_2O_3 catalyst, which is initially in an oxidic form, is sulfided, with the result that the oxidation states of both Co and Mo are reduced. More will be said about these species later, however, suffice it to say that the promotional role of Co is similar in both cases. The enhancement in catalyst activity due to the mutual interaction between both ions on the surface of the carrier can be attributed to the enhancing effect of Co on the dispersion of Mo

(64), or by a stabilization effect of Co on Mo (65). Cobalt may play a similar role after catalyst sulfidation, where it is thought to lend structural stability to the MoS_2 crystallites (43). At higher Co loadings, where the ratio Co/(Co+Mo) exceeds 0.5, the hydrodesulfurization activity of the catalyst decreases (49), because Co starts segregating to form a separate phase of Co_9S_8 (51), which has low catalytic activity (43).

We have observed a similar promotional effect of Co in our model Co-Mo/PCA catalysts for the catalytic hydrodemetallation of Ni-T3MPP dissolved in Nujol. The results of a competitive demetallation experiment, with catalysts of different compositions are displayed in Fig. 4. The nickel loading on the model LPCA catalyst, measured by AES, and reported as the atomic raio Ni/(Ni+Co+Mo), is plotted against the catalysts' composition, Co/(Co+Mo). On the same figure, for comparison, thiophene HDS data (13) are also plotted as a function of catalyst composition. The catalyst compositions which give the maximum activities for both HDS and HDM are in remarkable agreement. (Co/(Co+Mo) is ca. 0.65 for HDM, while it is ca. 0.5 for HDS). We should bear in mind that the HDM activity is indirectly estimated by measuring the amount of nickel deposited on a particular catalyst during the time of the HDM experiment. The rationale is that the catalyst with the optimal Co/Mo ratio will accumulate the most Ni.

Two points should be be emphasized. Our reactions were conducted in the complete absence of sulfur, with the result that our model catalysts were unsulfided, although they were reduced as confirmed by XPS (see Figs. 6 to 9). Therefore, even with the unsulfided catalyst we have observed the promotional role of Co in the HDM reaction. This is in disagreement with

the results of Declerck-Grimee et al (47) who believe that only the sulfided Co species has a promotional effect on the active phase in HDS. Strong disagreement exists in the literature regarding what Co species are actually present in the sulfided catalyst, and because the most rational explanation appears to be that only partial catalyst sulfidation takes place, generating mixed oxysulfides (66), it is not unreasonable that we observe the promotional role of Co in HDM in our sulfur free system. Brinen and Armstrong (45) concluded that Co was reduced, but not sulfided. If the catalyst calcination temperature is high, substantial quantities of $CoAl_2O_4$ are formed which resits sulfidation (67,68,45). Schuit and Gates (55) reported that Co was inaccessible to sulfur, while, in contrast, De Beer et al (67) showed that 70% of the Co was converted to Co_9S_8.

The second point we wish to emphasize is that while many publications have shown volcano activity curves, like Fig. 4, for HDS and HDN (49,50,15), we believe this is the first time such behavior has been reported for HDM. When the similarities between the HDM and HDS and HDN reaction mechanisms are recognized the volcano effect is not unexpected. As shown by work with model compounds for HDS (69), HDN (70) and HDM (11), the reaction mechanism for the removal of the heteroatom involves a sequence of hydrogenation steps, before the heteroatom is removed in a final hydrogenolysis step. (In HDS, however, the S atom can be removed from the heterocyclic before the aromatics are saturated). All of these mechanisms are conceptually similar, and it is probable that hydrogenation and hydrogenolysis in each mechanism occur over different types of sites (22,71). Moreover, the hydrogenation sites on the catalyst will catalyze the hydrogenation reactions in each of HDS, N and M. The same will be true

for the hydrogenolysis sites. Because of these facts we should not be surprised that HDM activity over Co-Mo catalysts of different compositions is volcano shaped.

The XPS spectra for the $Mo(3d_{5/2,3/2})$ core lines in the aged HPCA catalysts, with two different Co/Mo atomic ratios, 2 and 1.4, are shown in Figs. 6 and 7, respectively. For reference, the $Mo(3d_{5/2,3/2})$ spectra of the commercially manufactured HDS-16A (Co-Mo) and HDS-9A (Ni-Mo) are included. The $Mo(3d_{5/2,3/2})$ spectra from the aged model catalysts are shown as a function of sputter time at 0, 10, 20 and 30 minutes. The spectra taken before sputtering (Fig. 6-D, and 7-C) indicate the presence of Mo^{6+}, Mo^{5+} and Mo^{4+}. With sputtering (Figs. 6E-G, 7D-F) the surface oxide layer containing high concentrations of Mo^{6+} is removed, revealing Mo primarily in the +4 state. We attribute the surface Mo^{6+} layer, which is the primary state of Mo in the unaged HPCA catalyst (Fig. 6-C), to post-run partial oxidation of the catalyst, as it was transferred from the HDM environment to the XPS equipment. The underlying Mo^{5+} and Mo^{4+} layers is the state in which the HPCA catalysts exist during and HDM experiment, even though they were initially charged to the reactor primarily as Mo^{6+}. *In situ* reduction has taken place during the course of the experiment.

These results are supported by literature observations. From XPS measurements on supported catalysts Cimino and de Angelis (72) found that after reduction at 400°C (close to our run temperature of 355°C) the lowest oxidation state that could be obtained is Mo^{4+}. The initial supported Mo, primarily present as Mo^{6+} was only partially reduced to $Mo4+$, with part of it remaining as Mo^{5+}. Patterson *et al* (30) reduced a commercial $Co\text{-}Mo/Al_2O_3$ catalyst at 500°C for up to 15 hours, and found by XPS that the

mole fraction distribution between the individual oxidation states was Mo^{6+} (25%), Mo^{5+} (35%), and Mo^{4+} (40%). They confirmed that Mo^{5+} was an intermediate in the reduction mechanism of Mo^{6+}. However, in a later series of experiments by the same group, Chin and Hercules (16) reported that reduction at similar conditions converted all Mo^{6+} to Mo^{5+} (40%) and Mo^{4+} (60%). The existence of the Mo^{5+} intermediate has also been proven by Seshadri and Petrakis (73) and Hall and LoJacono (74).

In our HPCA catalysts, due to the thickness of impregnation (see SEM's in Figs. 24a and b), it is unlikely the PCA support will exert any influence on the majority of the supported phase. This is confirmed by the sharpness of the Mo($3d_{5/2,3/2}$) spectra which evolve through sputtering. A broader spectra, such as that of Figs. 6A and B are indicative of strong interaction of the Mo with the support (45,72). The lack of Mo-support interaction also explains why our HPCA catalysts are readily reduced in the HDM environment, and also why no detectable amounts of Mo^{6+} remain after sputtering. The degree to which a supported catalyst can be reduced is far less than an unsupported one (15).

It appears that the disagreement over the exact extent of reduction of Mo in the literature (15,43), primarily arises from the different reduction procedures employed. From our afore-discussed work on model HPCA catalysts, aged in the reducing environment of an HDM reaction, we tentatively conclude that Mo in the 4^+ state will be primarily responsible for catalytic activity.

Figures 8 and 9 show XPS spectra for the Co($2p_{3/2}$) line for aged HPCA catalysts with atomic composition ratios of 2 and 1.4, respectively. The scan range in Fig. 8 is sufficiently wide that useful information can also

be gathered on the $Co(2p_{1/2})$ line. For both the catalysts no Co signal was discernible without sputtering (see Fig. 9-B). We attribute this lack of signal to the carbonaceous overlayer (coke) which resides on the surface of an aged catalyst. More will be said about the carbonaceous overlayer later in the discussion, however, suffice it to say that it can be easily sputtered away to reveal the underlying Co. In the Results section we argued that small quantities of Co^{2+} are present because of the weak satellite structure at ca. 5eV higher binding energy than the $Co(2p_{3/2})$ core line, which is located at ca. 779eV. However, because (i) the position of the $Co(2p_{3/2})$ line in the HPCA catalysts is shifted ca. 2eV to lower BE than it appears in the oxidic HDS-16A catalyst (compare Figs. 8-A an 8-D), (ii) the satellite structure at ca. 784eV is weak, and (iii) the spin orbit separation for the aged HPCA catalyst at long sputtering times is ca. 15eV (Fig. 8-D), we believe that Co is primarily present in the metallic state (Co^0).

Such a conclusion is in agreement with Brinen and Armstrong (45) who made an XPS study on supported Co-Mo/Al_2O_3 catalysts that had been reduced in a 10% H_2S, 90% H_2 mixture at 400°C for ca. 1 hour. They believed that the catalyst surface was rich in a reduced, but not sulfided, cobalt species (Co^0). However, the concensus of opinion is that about 10-30% of the Co in a reduced high surface area catalyst remains in an oxidic environment (46). This is most likely the Co fraction that is trapped as $CoAl_2O_4$ during the calcination step (15). Since, in our low surface area, heavily impregnated HPCA catalysts, the amount of Co spinel which ran form, relative to that in the high surface catalysts, must be miniscule, it is to be expected that Co^0 is the dominant cobalt species.

Figure 10 shows the XPS Ni($2p_{3/2,1/2}$) spectra, for Ni as a promoter in an unaged oxidic Ni-Mo/Al_2O_3 catalyst (American Cyanamid HDS-9A), (Fig. 10A), and as deposited on an aged model HPCA catalyst (Co/Mo=1.4) in the HDM experiment. The nickel loadings are extremely low, which makes interpretation of the XPS spectrum difficult. However, since a surface NiO layer (Fig. 10-B) is sputter removed to reveal underlying layers containing elemental Ni (Fig. 10-C), as evidenced by a shift in the Ni($2p_{3/2,1/2}$) peaks to lower binding energies, we believe Ni is initially deposited onto a hydrotreating catalyst, working in the HDM environment, in the metallic state. The NiO we observed is probably a result of air contamination of the HPCA catalyst. However, the fate of nickel deposited onto a hydrotreating catalyst has not been unequivocally determined. Its effect on the catalyst's activity will probably strongly depend on the state of the catalyst it encounters. If the catalyst is fresh then the Ni may, for a period, operate in a similar fashion as the promoter Co, and help stabilize the Mo monolayer (52), rather than immediately poison the active sites. Our XPS composition depth profiles on both the LPCA (Fig. 5) and HPCA (Fig. 11) catalysts have revealed the model catalyst surface to be heavily carbon covered (or coked) after an HDM run. However, Ni reportedly has the capability of dissolving and migrating into coke (75) and of readily forming a surface spinel with Al_2O_3 (76). Formation of such a spinel places some of the Ni in an oxidic environment, rationalizing the idea that, like Co (45), a small fraction of the deposited Ni may exist in a non-reducable form. The majority, however, will exist in the metallic state, as indicated by this study (Fig. 10), and by the work of Ng *et al* (32) and Kibby *et al* (77) who reduced Ni-Mo/Al_2O_3 catalysts at 450°C in H_2

and found only Ni^0.

The deposited Ni may also retard rapid build-up of the carbonaceous overlayer, or at least lower its equilibrium deposition level of 10 to 20 wt % carbon (78), by acting as a catalytic hydrogenation site for coke precursors. For example, in the HDS of thiophene Laine and Brito (79) found that a Ni promoted catalyst contained less carbon than an unpromoted catalyst.

The surface carbon coverage on an unaged hydrotreating catalyst is substantial, falling in the range 10-20 wt % carbon (78,80). Carbon deposition is extremely rapid. Beuther and Schmid (78) found than one half of the carbon deposited in the 16 days of operation was deposited in the first 12 hours. The XPS depth profile in Fig. 11 reveals that our model HPCA catalysts also built up a carbonaceous overlayer. Before sputtering the HPCA catalyst's surface composition was ca. 80 atom % C. The carbon content tended to stabilize at ca. 35 atom % C after ca. 200Å of surface had been removed at a sputter rate of ca. 100 Å/minute. We believe these depth profiling studies to be more meaningful when conducted on our PCA catalysts, rather than on ill-defined compressed amorphous Al_2O_3 disks.

That the hydrotreating catalyst can continue to function in the presence of such a carbonaceous overlayer is quite remarkable, and will be one of the focal points of a conceptual model we will subsequently propose for the working hydrotreating catalyst surface.

It is instructive to estimate an average depth for the carbonaceous overlayer assuming it is uniformly distributed over the catalyst surface. If the surface area available is $150 m^2/g$, and the carbon loading is 20 wt % in a graphitic structure with a lattice constant of 3.6Å (81), then the

overlayer depth would be ca. 9 monolayers. This is substantial, and is especially noteworthy, when we recall that the average Mo coverage is approximately a monolayer (22).

Carbonaceous overlayers, as they occur in hydrocarbon reactions over Pt single crystals, have been subject to extensive scrutiny by Somorjai and coworkers (82-86). We believe some this work may bear a direct relation to some of the events occurring with the working Co-Mo/Al_2O_3 hydrotreating catalyst. Somorjai was attempting to mimic the performance of the highly dispersed Pt/Al_2O_3 reforming catalyst by working with single Pt crystals, while we are attempting to probe the workings of the Co-Mo/Al_2O_3 hydrotreating catalyst with model polycrystalline Al_2O_3 supported catalysts. Some pertinent points, noted and proposed by Somorjai, are,

(i) up to a monolayer of disordered carbonaceous material is deposited on the catalyst surface during the first 10-200 seconds of reaction (82),

(ii) the carbonaceous overlayer can store hydrogen, which can be made available to reacting molecules via hydrogen transfer reactions (84). In fact, thermal desorption studies revealed that the carbonaceous deposit contained about 10 times as much desorbable hydrogen, as the clean Pt surface (83).

(iii) each surface Pt atom can be associated with 2-4 carbon atoms (84), while the H/C atomic ratio in the carbonaceous overlayer is 1.6-1.0 (84).

and

(iv) a small steady state concentration of uncovered clean Pt sites exists, which are active in catalyzing all types of hydrocarbon

converion reactions (84).

From the work of Inoguchi et al (80) on the characterization of deposits on aged HDS catalysts we can calculate that the atomic H/C ratio of the coke decreased from ca. 2.4 after 100 hours on stream to ca. 0.91 after 2000 hours. Inoguchi et al (80) believed the deposited C to be amorphous, however, because of substantial decline in H/C ratio it is probable that graphitization of the coke is occurring at long run time. Graphitic coke will tend to have less hydrogenation catalytic activity than amorphous coke because of its lower hydrogen content (84). Moreover, grahitic coke can be considered as more of an irreversible poison than amorphous coke (87).

All of the above information leads us to postulate that the carbonaceous overlayer which exists at a steady state loading of ca. 20 wt% on the working hydrotreating catalyst, must be considered as a fundamental feature of the catalyst. It must play an integral role in any model that is proposed for the working surface. A detailed explanation of this model will be delayed until after we have gleaned further information by interpreting our ISS/SIMS, and SEM/EDX results.

Compared to the widespread use of XPS and AES to supported catalyst characterization, the application of ISS and SIMS remains in its infancy. Both techniques possess extreme surface sensitivity and probe only the uppermost surface layer. This makes them ideally suited for studying catalysts, since it is at the surface monolayer of a supported catalyst that the reaction occurs.

The application of ISS to practical catalysts remains scarce (88), however, some recent work, all performed on γ-Al_2O_3 supported catalysts

suggests that the technique is gaining acceptance (89-93). Delannay et al (14) and Chin and Hercules (16) performed ion scattering from the surface of unaged Co-Mo/Al_2O_3 catalysts and convincingly confirmed the presence of a Co-Mo double layer. The molybdenum layer sits on top of the cobalt layer. Such an arrangement was earlier proposed by Gajardo et al (44) based on XPS and diffuse reflectance spectroscopy results.

By using ISS and SIMS on our model Co-Mo/PCA catalysts and comparing the results to ISS depth profile on the commercial HDS-16A, we have shown that the two catalyst systems (real v's model) have inherent similarities. Fig. 14 shows depth profiles for the HDS-16A catalyst's principle constituents. The right hand panel indicates that both O and Al increase as we penetrate the Al_2O_3 support. Mo and K decrease while Co shows a maximum, with increasing sputter depth. These results are in agreement with the ISS findings of Delannay et al (14) and Chin and Hercules (16), that Co is at a maximum concentration some distance removed from the surface of the catalyst.

Figs. 20 and 22 show similar data for an aged LPCA catalyst, and an aged HPCA catalyst, respectively. The data of Fig. 20, on the lightly loaded, highly dispersed form of the Co-Mo/PCA catalyst, exhibit similar behavior to that in Fig. 14 for the real catalyst. Most significant, is the indication that the double layer, Mo overlying Co, is present in the model LPCA catalyst. The double layer is not present in the HPCA catalyst (Fig. 22). The existence of the double layer is intimately linked to the catalyst's dispersion, and the ability of $CoAl_2O_4$ to form (44). If Co cannot interact with the support then the bilayer will not form. This is the situation in the HPCA catalyst of low dispersion. With the LPCA

catalyst, the dispersion is sufficiently high on the PCA support, that the model system apparently mimics the real catalyst and develops a bi-layer. The bi-layer is also sustained through the HDM experiments.

The SIMS spectra in Figs. 13, 16 and 19 show that considerable quantities of Na, Ca, and K tend to segregate at the catalyst surface. While it is known that Na is purposely added to the HDS-16A catalyst (Table 1), both Ca and K are most probably present as impurities. These elements, though, because of their basic character could moderate the catalytic activity at the strong acid sites present in the fresh molybdenum catalyst (79). These acid sites are active in hydrocracking reactions which produce coke (94). Furthermore, Ca has been shown to associate with bulk MoO_3 when it forms (95).

In contrast to Fig. 14 for the fresh HDS-16A, the Mo ISS profile in Fig. 17 for the Ni and V aged HDS-16A catalyst also has an internal maximum. This is probably due to coke deposition on the catalyst surface, which moves the apparent surface of the catalyst outwards.

Fig. 21 shows ISS spectra taken over an HPCA catalyst, that had been aged in run 3 (Table 2). The XPS depth profile in Fig. 11 indicates that these catalysts were heavily coked and had accumulated ca. 80 atom % C in the surface layers. Bearing in mind the extreme surface sensitivity of ISS (only the top most monolayer is sampled) it is notable that we do see small signals for Co an Mo in scan 1 of Fig. 21. After approximately 7Å have been sputter removed, the Co and Mo signals are much stronger as evidenced in scan 2. With continued sputtering both Co and Mo signals increase (scans 3, 5, and 9). We can rationalize these observations by suggesting that not all the catalyst surface is covered by the carbonaceous overlayer,

and when covered, the coke deposit depth is not uniform.

We suggest that the working surface of the Co-Mo/Al_2O_3 catalyst is heavily coked (to ca. 20 wt % C) during steady state operation, but there exists a small steady state concentration of uncovered high turnover number sites which remain carbon free. The role that these carbon covered sites play in a functioning hydrotreating catalyst will be more fully explained in the next section, where we propose a conceptual model for the working Co-Mo/Al_2O_3 hydrotreating catalyst.

Our SEM/EDX work is presented in Figs. 23 to 25. Fig. 23 shows a micrograph of the surface of the unaged HDS-16A catalyst. Figs. 24a and b are micrographs of the aged HPCA catalyst with a nominal Co/Mo atomic ratio of 0.9. Figs. 25a to c are micrographs of the aged LPCA catalyst (again Co/Mo atomic ratio = 0.9, nominally), which being more highly dispersed more closely mimics the real amorphous Al_2O_3 supported catalyst. Fig. 25a focusses on the center region of the PCA square where the Co-Mo phase is highly dispersed, and not physically visible in the micrograph. Figs. 25b and 25c are micrographs of the periphery of the impregnated surface. They show that a separate Co-Mo crystal phase has formed because of uneven distribution of this phase on the PCA support surface. All our surface spectroscopic work on the aged LPCA catalysts was performed in centrally located regions of high dispersion. The surface morphology of the γ-Al_2O_3 supported real catalyst (Fig. 23) differs considerably from that of the more bulk-like HPCA catalyst (Figs. 24a and b), and the highly dispersed LPCA catalyst (Figs. 25a to c) which was used to simulate, for spectrocopy studies, the real catalyst.

Because individual crystals of a Co-Mo phase formed on the periphery

of the LPCA catalyst (Figs. 25b and c), it was possible to focus on one of these crystals, sized at about 1 micron, and determine its nickel loading relative to that of the surrounding PCA support. The crytal we focussed on is identified in Fig. 25c and shown in close-up in Fig. 25d.

The EDX spectrum in Fig. 25g indicates that Ni-T3MPP has undergone demetallation on the Co-Mo crystal surface at a rate far greater than on the PCA support. Fig. 25g is the EDX spectrum from point 1 of Fig. 25d and shows the presence of nickel. In contrast, Fig. 25j shows the spectrum collected on point 2 of Fig. 25d. No nickel is present, indicating that the PCA support has little activity for HDM.

We can extrapolate this concept to the real catalyst, where by using ISS Jeziorowski et al (93) concluded that the molybdate phase on the Al_2O_3 support forms three dimensional islands while uncovered support surface remains, even though the loading corresponds to a theoretical monolayer capacity. Therefore with the γ-Al_2O_3 supported catalyst we can expect that the catalytically deposited metals, Ni and V, will be non-uniformly deposited over the catalyst surface, and possess maximum concentrations on the Co-Mo islands.

III. F. A conceptual model for the working Co-Mo/Al_2O_3 hydrotreating catalyst

Many models exist which attempt to explain the surface structure of the Co-Mo/γ-Al_2O_3 hydrotreating catalyst (15). As already mentioned the three most popular models are the synergy-by-contact model (51,52), the intercalation model (53,54), and the monolayer model (55). All these models deal with the fresh, unaged catalyst and are chemical in nature, in that they attempt to explain the chemical state of each of the catalyst's

components when placed in intimate contact, in a highly dispersed state on the Al_2O_3 support.

The fact remains, however, that the working form of the Co-Mo/Al_2O_3 hydrotreating catalyst which functions efficiently for many months in the hydrotreater, is at a condition far removed from the oxidic catalyst which is initially charged to the reactor. The catalyst has become sulfided, and accumulates great quantities of carbon (10-20 wt %) (80) and metals; primarily Ni and V at similar loadings as the carbon (80,96). These deposits must be viewed as an integral feature of the working catalyst and included in any model that is proposed for the working surface.

In this section we propose such a model for the catalyst, which, however, is more conceptual than chemical. The model explains the roles played by the carbonaceous overlayer, and deposited metals (especially Ni) in catalytic oil upgrading. Our objective is to make the reader consider the functioning form of the catalyst, not just as Co-Mo/Al_2O_3, but as Co-Mo-C-(deposited metals)/Al_2O_3. Our model is constructed from our own findings, plus information taken from the literature.

The model will be explained with continued reference to Fig. 25, which presents schematic views of the catalyst surface. The fresh catalyst is shown in Fig. 26a. Molybdenum lies in a monolayer, in a highly dispersed state, on the Al_2O_3 support (43,55,97). Since the molybdenum loadings on commercial catalysts are sufficiently low that the molybdenum phase cannot completely cover the Al_2O_3 support, we have included a bare patch in Fig. 26a (97). Jeziorowski et al (93) have reported that the distribution state of the molybdate phase depends on the catalyst calcination temperature. When calcined at temperatures < 500°C the molybdate phase forms three

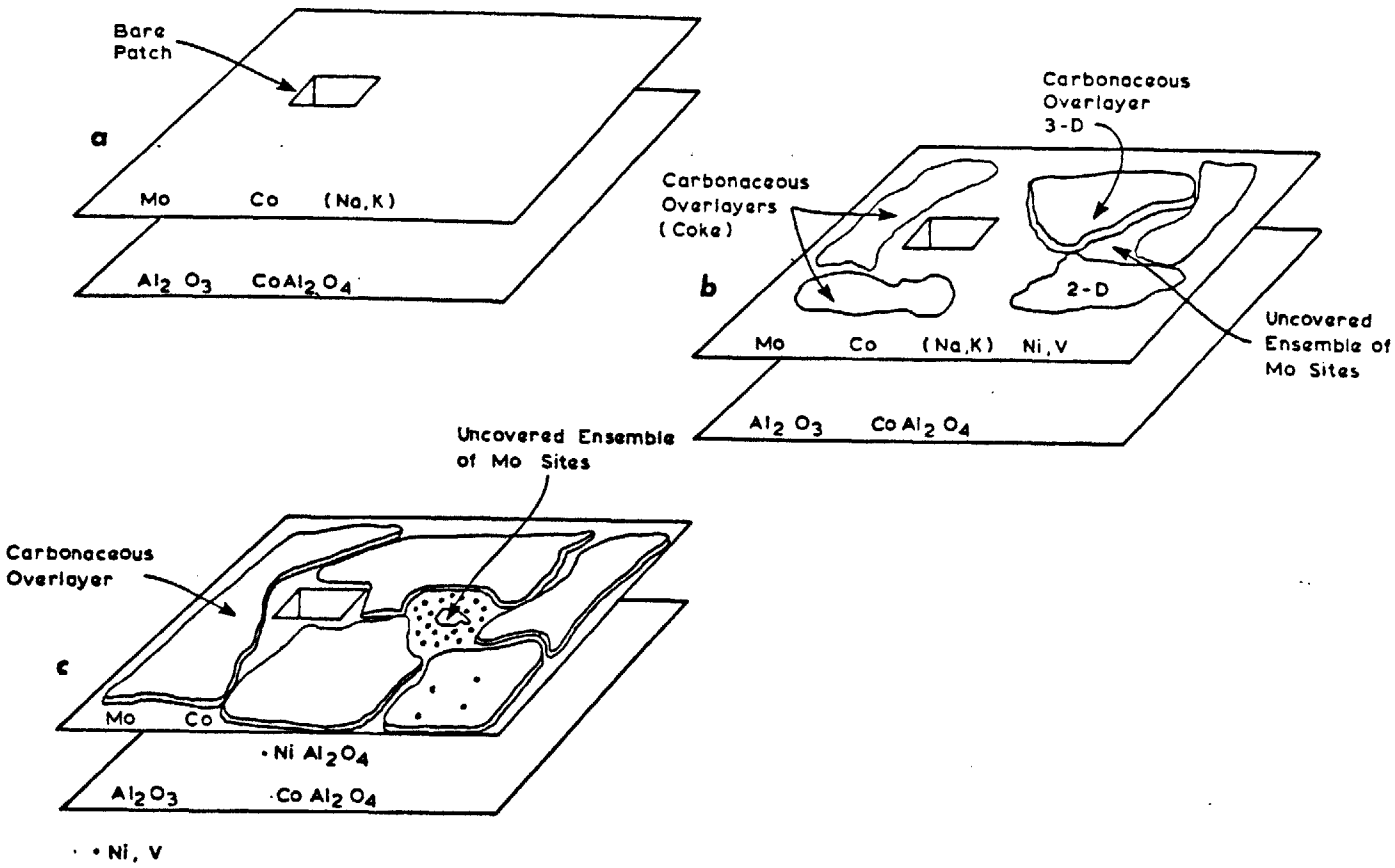

Figure 26: (a) Conceptualization of the surface of the unaged Co-Mo/γ-Al_2O_3 catalyst. Holes can exist in the Mo monolayer. Part of the cobalt is associated with the Mo monolayer and part with the Al_2O_3 phase in the form of a $CoAl_2O_4$ spinel. This catalyst exists when freshly charged to the reactor and is representative of the catalyst's state at a reduced time of zero in Fig. 27.

(b) State of the catalyst surface which is rapidly established during stage 1 of Fig. 27, and persists into stage 2, when the deposited metals content is still relatively low. The catalyst surface possesses a carbonaceous overlayer which can be either 2-dimensional or 3-dimensional. The carbonaceous overlayer can store hydrogen for use in hydrogen exchange reactions and can thus be viewed as an hydrogenation site. It also facilitates the desorption of product molecules. The bare Mo sites which exist are active for hydrogenation and hydrogenolysis.

(c) State of the catalyst surface during stages 2 and 3 of Fig. 27. The carbonaceous overlayer is now primarily 3-dimensional and performs the same functions as in Fig. 26b. The Ni and V atoms deposited by the HDM reaction are shown surrounding a bare Mo patch (still actively conducting hydrogenation and hydrogenolysis) and hindering the encroachment of the carbonaceous overlayer. The deposits can act as hydrogenation sites for coke precursors and thereby maintain the carbonaceous overlayer coverage at a steady value. Nickel aluminate ($NiAl_2O_4$) is also shown to exist.

dimensional islands while uncovered support remains, even though the loading corresponds to a theorectical monolayer capacty. However, if the catalyst is calcined at 600°C, the molybdate phase spreads uniformly over the support giving a closed monolayer. Kibby et al (77) found by XPS and ISS that Mo dispersions were lowered after catalyst reduction, again suggesting the creation of areas of uncovered Al_2O_3. Our own ISS results for the fresh HDS-16A catalyst reported in Fig. 12 also substantiate the concept of bare batches. ISS only samples the uppermost monolayer, and in scan 1 of Fig. 12, where the catalyst surface will have been little damaged by the ion scattering sputtering process, a strong Al signal prevails.

Fig. 26a also indicates that the promoter Co is distributed between the molybdate phase and alumina substrate. It has been estimated that between 10 to 30% of the Co occurs associated with the alumina (45,46) as the Co spinel, $CoAl_2O_4$ (15). In fact, during catalyst preparation every attempt is made to minimize the wasteful trapping of Co by Al_2O_3, by impregnating the support first with the molybdate phase (15). The Co that resides in the surface monolayer with Mo (Fig. 26a) is responsible for the promotional effect that Co has on the catalytic activity of Mo for HDS, N and M. Co stabilizes the molybdate layer (22). The ion scattering work of Chin and Hercules (16), and Delannay et al (14,88) have confirmed the bilayer model of Gajardo et al (44) where the catalyst surface is primarily Mo, with little Co exposed. Our ISS work reported in Figs. 14 and 20, for real and model catalysts are also consistent with this model.

Commercial catalysts also contain small quantities of the basic elements, Na, and K (see Table 1, for composition of HDS-16A). Our ISS and SIMS results suggest that these elements are strongly surface

segregated (see Fig. 14), and that is why they are included in the molybdate monolayer in Fig. 26a. Here these basic atoms can interact strongly with the molybdenum sites and perhaps temper the strongly acidic character of the fresh molybdate catalyst (79). These strong, active, acid sites are detrimental in that they catalyze hydrocracking reactions which lead to rapid coking of the catalyst surface, and deactivation (98). Sodium has also been reported to increase the bulk Co_3O_4 content, at the expense of Co trapped as the $CoAl_2O_4$ spinel (15).

Residuum hydroprocessing catalysts deactivate in a very characteristic fashion (96,99). In practice the catalyst temperature is gradually raised to compensate for the deactivation, and thereby maintain a constant product specification. A typical "S"-shaped deactivation curve taken from the work of Tamm et al (96) is shown in Fig. 27. Deactivation has three stages, each of which have been identified in Fig. 27. The initial rapid deactivation in stage 1 is thought to be due to rapid coke build-up on the catalyst, while deactivation during stage 3 is blamed on pore mouth plugging by the deposited metals (100).

The catalyst described by Fig. 26a only exists at a reduced time of zero in Fig. 27. During subsequent operation the catalyst is rapidly coked to an equilibrium carbon loading of ca. 20 wt % C during stage 1 (80). The metals loading at this stage will still be relatively small. The important consideration is that after the virgin catalyst surface of Fig. 20a is contacted with oil, the carbonaceous deposit is a fundamental feature of the surface of the catalyst. The catalyst surface model must therefore be modified. The coked catalyst model, applicable during stages 1 and 2, with light metal poison loadings, is shown in Fig. 26b.

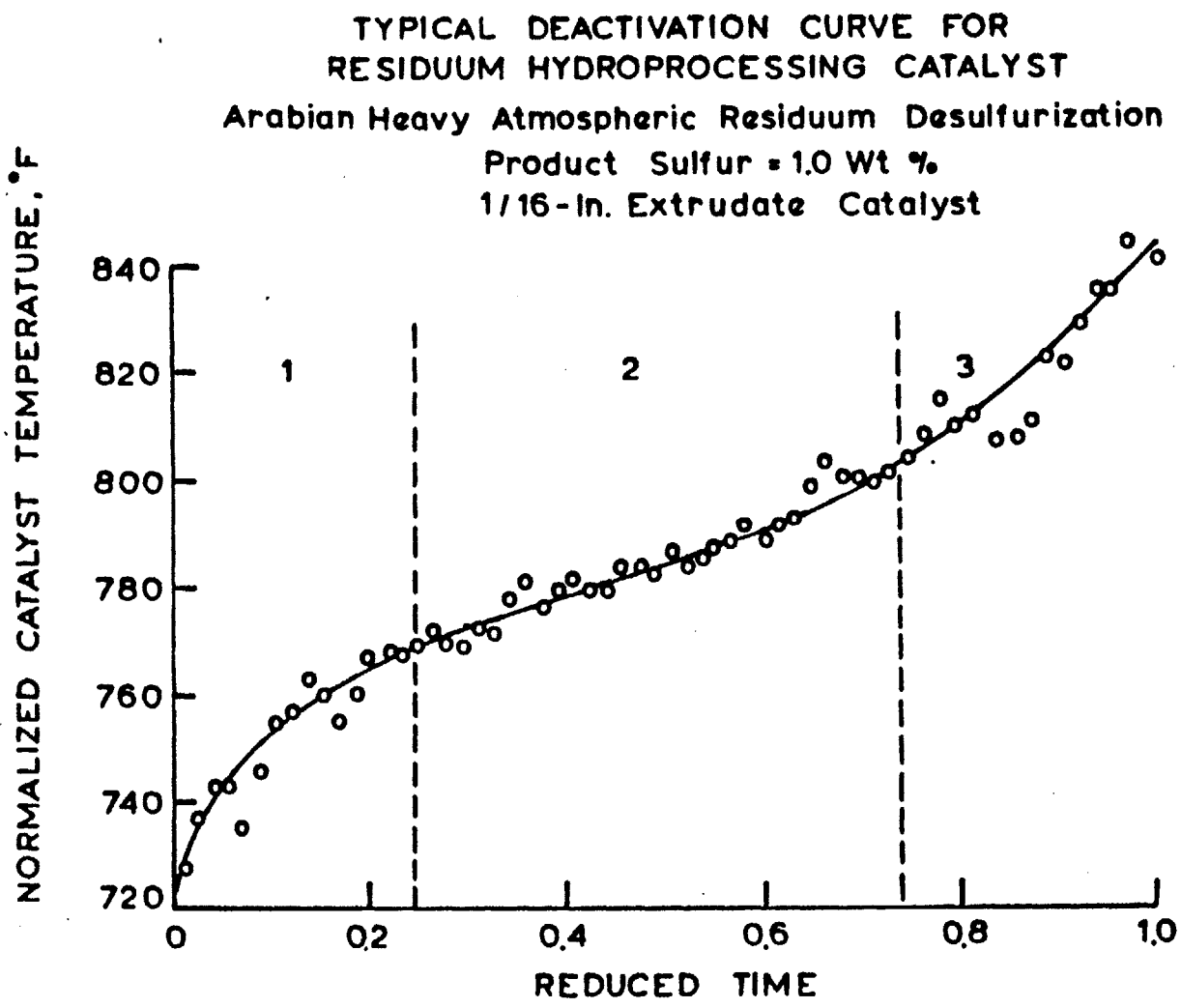

Figure 27: A typical deactivation curve for a residuum hydroprocessing catalyst, from Tamm et al (96). Three distinct stages of deactivation exit.

The carbonaceous overlayer (coke) is shown as existing in patches; two dimensional or three dimensional. In the Discussion section we noted that if a real catalyst has to accommodate a carbon loading of ca. 20 wt %, then its surface depth must be uniform at about 9 monolayers. Depth profiling work by XPS on our model HPCA catalysts (Fig. 11) showed the surface composition to be as high as 80 atom-% carbon. The presence of uncovered Mo sites is justified by our ISS results from the same catalysts. Fig. 21 shows ISS spectra for an HPCA catalyst. Scan 1 taken in the time period 0 to 1 minute indicates weak but finite signals for both Co and Mo. Scan 2 taken in the time period 1 to 2 minutes, shows strong Co and Mo signals.

Further evidence that the carbonaceous overlayer exists in patches comes from the work of Somorjai and co-workers (82-86) who investigated various hydrocarbon reactions over Pt single crystals, in an attempt to simulate the Pt/Al_2O_3 reforming catalyst. On an industrial scale these catalysts continue to function with carbon loadings as high as those reported on hydrotreating catalysts (94). The Somorjai group believes that at medium temperatures (200-500°C) catalysis occurs on bare Pt islands surrounded by coke. The integrity of these islands is maintained during reaction, as the coke builds up to an equilibrium level.

We contend that a similar situation exists on the working hydrotreating catalyst. Rapid coke build-up occurs to an equilibrium level of ca. 20 wt % carbon, during stage 1 of Fig. 27. Thereafter the catalyst surface is in a state of dynamic equilibrium. Coke is continually being hydrogenated from the catalyst surface, at the same rate it is being replenished. A small steady state concentration of uncovered Mo sites always exists during reaction, which are crucial to the catalytic activity

of the catalyst. The carbonaceous overlayer is also an important feature of the working catalyst.

On a hydrotreating catalyst the carbonaceous overlayer rapidly builds up to a steady state condition (in a time span of a few hours) because of the strong acidity of the virgin catalyst which promotes coke formation. This is common with any metal catalyzed hydrocarbon transformation. For example, Davis and Somorjai (82) found that ca. 1 monolayer of carbonaceous material was deposited during the first 200 seconds of cyclohexene hydrogenation and dehydrogenation reactions over Pt single crystals.

While the build-up of the carbonaceous overlayer decreases the overall activity of the catalyst, especially during stage 1 of Fig. 27, it also changes the selectivity of hydrogenation reactions relative to hydrogenolysis reactions. Satterfield and Cocchetto (101) when investigating the reaction network and kinetics of quinoline HDN observed a 60% decline in hydrogenolysis activity, while the hydrogenation activity only fell 20%. This can be rationalized with the conceptual model of Fig. 26b, when the following information is also brought to bear.

(i) The carbonaceous overlayer can store hydrogen, which can later be used in hydrogenation reactions. Davis et al (83,84) found that the amount of hydrogen which was stored by the carbonaceous deposit on a Pt single crystal catalyst, represented at least ten times more hydrogen than could be chemisorbed on a clean Pt surface.

(ii) The carbonaceous overlayer can conduct hydrogen transfer reactions, by using the aforementioned stored hydrogen. Most of this hydrogen will exist in a more weakly bound state than if it had chemisorbed directly on the clean catalyst surface (82). Weinberg et al (102)

believed that the carbonaceous overlayer is the catalytic site for the hydrogenation of ethylene on the Pt (111) surface. Gardner and Hansen (103) propose a similar scenario for the same reaction over tungsten. (It is noteworthy that tungsten is often used in place of molybdenum in hydrotreating catalysts (49)).

We propose that the uncovered Mo atoms in Fig. 26b are active sites for both hydrogenation and hydrogenolysis reactions. Carbon covered sites are only active for hydrogenation reactions. The clean catalyst of Fig. 26a has strong acid strength, and cokes rapidly reducing the number of hydrogenolysis sites. The number of hydrogenation sites is less severely affected by the coking process, however, because the carbon covered sites can still perform hydrogenation, although probably at a lower rate. This explains why hydrogenolysis rates decline more rapidly than hydrogenation rates during stage 1 of Fig. 27. This also agrees with the work of Pookote et al (104), who in working with a Co-Mo/SiO_2-Al_2O_3 cracking catalyst found that coke formation was primarily associated with deactivation of the acidic function, and that hydrogenation sites could still operate when covered with a carbonaceous overlayer.

We should note that our model also implies that some fraction of the hydrogen which is catalytically incorporated into the hydrotreated oil, has resided on the catalyst surface, in the carbonaceous overlayer for a relatively long period. The atomic ratio of hydrogen to carbon in the carbonaceous overlayer decreases with increasing reaction temperature (or time on stream, Fig. 27). Inoguchi et al (80) analyzed carbon deposits on used resid hydrotreating catalysts and found that the atomic H/C ratio decreased from 2.38 to 0.91 at run times of 100 and 3000 hours,

respectively. Davis et al (84) observed that the composition of their carbonaceous overlayers on Pt decreased from about 1.6 to 1.0 as the temperature was raised from 300°C to 400°C. Thus, the hydrogen storage capacity of the carbonaceous overlayer decreases with increasing reaction temperature, and could explain the drop in H/C ratio observed by Inoguchi. The Chevron data (96) in Fig. 27 indicate that the catalyst's temperature is raised by ca. 70°C in industrial operation to maintain product specifications. This action will cause a decline in the hydrogen storage capabilities of the coke, with a concomitant decrease in catalyst hydrogenation activity.

We believe that the hydrogenation activity of the coke is dependent on the coke's hydrogen content. When it is high (ca. 2) a fraction of the hydrogen is weakly bound (82) and easily incorporated into a reactant molecule chemisorbed on the carbonaceous overlayer. At lower hydrogen contents, caused by increased temperatures, the coke's hydrogen exchange abilities are reduced. In the limit it appears that the coke may graphitize, completely losing its hydrogen storage and exchange functionalities, and ultimately cause accelerated catalyst poisoning. This process may be taking place in the latter parts of stage 2 and into stage 3 in Fig. 27. Inoguchi et al (80) believed that the decrease in H/C ratio of the coke was due to its increasing crystallinity. Myers et al (94) showed that the atomic H/C ratio of the coke can be increased by hydrogen treatment, however, complete dehydrogenation of the overlayer appears to be largely irreversible (84).

It is this condition of excess hydrogen depletion of the carbonaceous overlayer which must be avoided, for then the overlayer does not contribute

any hydrogenation activity to the catalyst, but simply acts as a site-blockage poison. Increasing the reactor's temperature to maintain product specifications is necessary (Fig. 27), but should probably be done in parallel with raising the hydrogen pressure to keep the coke hydrogen saturated.

It is now apparent that coke formation on the catalyst surface should not be viewed totally as deletrious, as long as it does not graphitize. Also since the binding energies of hydrocarbons will be lowered on the carbon covered patches (84), relative to the bare Mo patches, it is possible that the overlayer is a site for the desorption of the cracked fragments of the heteroatom containing molecules. Hydrogenolysis will occur on the bare patches in Fig. 26b, and the resulting fragments can then surface diffuse onto the carbonaceous overlayer and desorb.

How the deposited metals Ni and V affect the catalyst surface remains uncertain. During region 3 of Fig. 27 the deposited metals content will exceed the carbon loading, which reaches an equilibrium loading. Deactivation during region 3 is normally assigned to catalyst pore mouth plugging, primarily by metals (96). Our conceptualization of the heavily metal contaminated catalyst surface is shown in Fig. 26c. Nickel and vanadium have been removed from the porphyrinic molecules and deposited in close proximity to the uncovered acidic Mo sites. As the deposited metal loading builds up it encroaches on, and reduces the surface area of, the uncovered Mo sites. Ni is known as a good hydrogenation and hydrocracking catalyst, at least in the absence of sulfur, and may substitute for Mo sites once they are covered. The nickel's hydrogenation role will also help suppress coke formation, and the situation depicted in Fig. 26c may

develop where the deposited nickel keeps patches on the catalyst surface carbon free, in the vicinity of Mo sites. This idea is substantiated by Brito et al (105) who found that in a reducing atmosphere, Ni-Mo/Al_2O_3 catalysts had less carbon deposition than Co-Mo/Al_2O_3; they assigned this observation to the good hydrogenation activity of Ni.

A similar theory was advanced by Beuther and Larson (107) to explain the deactivation of bifunctional metal site-acid site hydrocracking catalysts. They presented evidence to show that one of the principle roles of the metal in hydrocracking is to keep acidic sites "clean" and active through the hydrogenation of coke precursors. The only useful acidic sites were those in close proximity to the metal crystallites. Therefore in the working hydrotreating catalyst it is reasonable to assume that the only hydrogenolysis sites which perform efficiently, and maintain activity in the presence of large quantities of coke, are those that are protected by an adjacent hydrogenation site (101). This phenomenon could ultimately dictate the catalyst's activity.

We have shown little nickel associated with the coke in Fig. 26c, because (i) the overlayer is not the site of hydrogenolysis reactions, (ii) nickel is known to migrate into coke (75,105) and (iii) readily forms a surface spinel with alumina. In fact spinel formation is easier with nickel than cobalt (106) which suggests that the deposited nickel could be capable of displacing some cobalt from the $CoAl_2O_4$ phase, to the catalyst's surface.

In the presence of sulfur the hydrogenation activity and thus its protective role will be diminished since nickel sulfides have no hydrogenation activity (107). However, Ni_3S_2 may exhibit an apparent

hydrogenation activity as sulfur atoms are continuously removed from the surface as H_2S, thereby forming transitory metallic regions.

Our conceptual model of the working hydrotreating catalyst, shown in Fig. 26 has been assembled from a wide range of reported facts on the real catalyst. Some of the ideas were experimentally substantiated by our surface spectroscopic investigations on both real and model catalysts, presented earlier in the paper. It is clear that both the carbonaceous overlayer and the deposited metals (we focussed primarily on Ni) are an important feature of the working catalyst, and should not be viewed solely as unwanted poisons. For example, the carbonaceous overlayer appears to store hydrogen on the catalyst surface which can be used in hydrogenation reactions. It also provides facile desorption sites for product molecules. The deposited nickel can help maintain the carbonaceous overlayer at a steady state loading by hydrogenating coke precursors.

III. G. Conclusions

We have examined the catalytic hydrodemetallation (HDM) of a model nickel containing residua (Ni (II)-tetra(3-methylphenyl) porphyrin dissolved in Nujol) over a series of well characterized model Co-Mo catalysts. Polycrystalline alumina (PCA) was used as the catalyst support. HDM was carried out over a range of catalyst compositions. The Co/Mo atomic ratio of the catalysts were varied primarily in the range of 0 to 2. The amount of nickel deposited on each of these catalysts as a function of its composition was determined by XPS and AES. Like other hydrotreating operations such as desulfurization and denitrogenation we found that an optimum Co/(Co+Mo) atomic ratio for HDM was in the range 0.5 to 0.7 (Fig. 4). By XPS we also ascertained that the aged catalyst was heavily coked

(Fig. 11).

The chemical shifts in the XPS spectra of Co, Mo and Ni on both fresh and aged model PCA supported catalysts were measured. Even though the model catalysts were placed in the reactor in an oxide form they were partially reduced in situ. When depth profiling the model catalyst surface we found increasing quantities of Mo (IV) (Fig. 6). This appears to be the catalytically active form of molybdenum in the hydrotreating environment. Cobalt is reduced to the metal (Fig. 8). We found both Ni and NiO on the aged PCA surface (Fig. 10), however, the presence of NiO was attributed to air-contamination of the catalyst as it was tranferred from the reaction environment to the UHV chamber.

We probed the suppermost monolayer of fresh and aged PCA catalysts by ISS and SIMS (Figs. 12-22). The surface of both the real and model catalysts was shown to be enriched in Mo relative to Co, verifying the recent findings of other research groups (14,16,104). Moreover, by this observation we convincingly proved that our model PCA catalysts are good structural simulations of the real γ-Al_2O_3 supported catalysts. Their handling ease, rigidity and zero porosity make them ideally suited for aging in HDM and subsequent surface characterization by ultra-high vacuum techniques. By depth profiling with ISS (Figs. 14, 17 and 20) we showed that the Co concentration is at a maximum some distance removed from the outermost surface of the catalyst, while the basic elements Na and K concentrate at the surface. By SEM and EDX the metal deposition sites in HDM were found to be primarily in the cobalt-molybdate phase, rather than on the bare Al_2O_3 surface (Fig. 25).

By assimilating all our own experimental findings and some from the

literature we have proposed a conceptual model for the working hydrotreating catalyst (Fig. 26). It incorporates a carbonaceous overlayer and deposited metals and suggests the catalytic roles these entities play in the aging catalyst. We believe that both these deposits should not be solely viewed as poisons, since they both play an integral role in HDM, HDN and HDS catalysis.

III. H. References

1. Houalla, M., Nag, N.K., Sapre, A.V., Broderick, D.H., and Gates, B.C. AIChE J. 24, 1015 (1978).

2. Shih, S.S., Katzer, J.R., Kwart, H., and Stiles, A.B., Amer. Chem. Soc., Div. Pet. Chem. Preprints, 22, 919 (1977).

3. Ebel, R.H., Amer. Chem. Soc., Div. Pet. Chem. Preprints 17 (3), C46 (1972).

4. Ohtsuka, T. Catal. Rev.-Sci. Eng. 16, 291 (1977).

5. Frayer, J.A., Montagna, A.A., and Yanik, S.J., Japan Petroleum Institute Fuel Oil Desulfurization Symposium, Tokyo, May 8, 1975.

6. Brunn, L.W., Montagna, A.A., and Paraskos, J.A., Amer. Chem. Soc., Div. Pet. Chem. Preprints 21, (1), 173 (1976).

7. Speight, J.G., "The Desulfurization of Heavy Oils and Residua," Marcel Dekker, Inc., New York (1981).

8. Yen, T.F., Boucher, L.J., Dickie, J.P., Tynan, E.C., and Vaughan, G.B., Amer. Chem. Soc., Div. Pet. Chem. Preprints 13 (1), 59 (1968).

9. Hung, C-W., and Wei, J., Ind. Eng. Chem. Proc. Des. Dev. 19, 250 (1980).

10. Hung, C-W., and Wei, J., Ind. Eng. Chem. Proc. Des. Dev. 19, 257 (1980).

11. Agrawal, R., "Kinetics and Diffusion in Hydrodemetallation of Nickel and Vanadium Porphyrins," Sc.D. Thesis, M.I.T., August, 1980.

12. Ware, R.A., and Wei, J., Paper presented at AIChE, Annual Meeting, Los Angeles, California, Nov. 14-19, 1982.

13. Wivel, C., Candia, R., Clausen, B.S., Mørup, S., and Topsøe, H., J. Catal. 68, 453 (1981).

14. Delannay, F., Haeussler, E.N., and Delmon, B. J. Catal, 66, 469 (1980).

15. Grange, P., Catal. Rev.-Sci. Eng. 21, 135 (1980).

16. Chin, R.L., and Hercules, D.M., J. Phys. Chem. 86, 3079 (1982).

17. Somorjai, G.A. "Chemistry in Two Dimensions: Surfaces," Cornell University Press, Ithaca, New York, 1981, Chap. 2.

18. Blakely, D.W., Kozak, E.I., Sexton, B.A., and Somorjai, G.A., J. Vac. Sci. Technol. 13, 1091 (1976).

19. Bouwman, R., and Toneman, L.H., J. Catal. 61, 146 (1980).

20. Brinen, J.S., Graham, S.W., Hammond, J.S., and Paul, D.F., Paper presented at Joint New York-New England Catalysis Societies Spring Symposium, Yale University, New Haven, Connecticut, March 16, 1983.

21. Swingle, R.S., and Riggs, W.M., Critical Reviews in Analytical Chemistry, 5, (3), 267 (1975).

22. Schuit, G.C.A., and Gates, B.C., AIChE J. 19, 417 (1973).

23. Sonnemans, J. and Mars, P., J. Catal. 31, 209 (1973).

24. Baker, E.W., and Palmer, S.E. in "The Porphyrins" (D. Dolphin, E.) Vol 1, Chap. 11, Academic, New York, 1978.

25. Yen, T.F. in "The Role of Trace Metals in Petroleum" (T.F. Yen, Ed.) Chap. 1, Ann Arbor Science, Michigan, 1975.

26. Vaughan, G.B., Tynan, E.C. and Yen, T.F., Chem. Geol. 6, 203 (1970).

27. Fiero, G.W., Annals Of Allergy, 23, 226 (1965).

28. Wagner, C.D., Davis, L.E., Zeller, M.V., Taylor, J.A., Raymond, R.H, and Gale, L.H., Surf Int. Anal. 3, 211 (1981).

29. Miller, A., ALCOA Technical Center, Pennsylvania, personal communication, March, 1983.

30. Patterson, T.A., Carver, J.C., Leyden, D.E., and Hercules, D.M., J. Phys. Chem. 80, 1700 (1976).

31. Kim, K.S., Phys. Rev. B11, 2177 (1975).

32. Ng, K.T., and Hercules, D.M. J. Phys. Chem. 80, 2094 (1976).

33. Wagner, C.D., Riggs, W.M., Davis, L.E., Moulder, J.F., and Muilenberg, G.E. (Ed.) "Handbook of X-ray Photoelectron Spectrocopy," Perkin-Elmer Corp., Physical Electronics Division, Minnesota (1979).

34. McGuire, G.E., Schweitzer, G.K., and Carlson, T.A. Inorg. Chem. 12, 2450 (1973).

35. McIntyre, N.S. and Cook, M.G., Anal. Chem. 47, 2208 (1975).

36. Tamm, P.W., Harnsberger, H.F., and Bridge, A.G., Ind. Eng. Chem., Proc. Des. Dev., 20, 262 (1981).

37. Zingg, D.S., Makovsky, L., Brown, F.R., and Hercules, D.M., J. Phys. Chem., 89, 2898 (1980).

38. Chuang, T.J., Brundle, C.R., and Rice, D.W., Surf. Sci. 59, 413

(1976).

39. Oku, M., and Hirokawa, K., J. Electron Spectroscopy 8, 475 (1976).

40. Webster, I.A., and Wei, J., in preparation (1984).

41. Dexpert, H., Freund, E., and Lynch, J. in "Quantitative Microanalysis with High Spatial Resolution," The Metals Society, London, 1981, p. 101.

42. Goldstein, J.I., Newbury, D.E., Echlin, P., Joy, D.C., Fiori, C., and Lifshin, E., Scanning Electron Microscopy and X-Ray Microanalysis, Plenum, New York, 1981.

43. Ratnasamy, P., and Sivasanker, S., Catal. Rev.-Sci. Eng. 22, 401 (1980).

44. Gajardo, P., Grange, P. and Delmon, B., J. Catal. 63, 201 (1980).

45. Brinen, J.S. and Armstrong, W.D., J. Catal 54, 57 (1978).

46. Declerck-Grimee, R.I., Canesson, P., Friedman, R.M., and Fripiat, J.J., J. Phys. Chem. 82, 885 (1978).

47. Declerck-Grimee, R.I., Canesson, P., Friedman, R.M., and Fripiat, J.J., J. Phys. Chem. 82, 889 (1978).

48. Ochoa, O., Galiasso, R. and Andreu, P. in "Preparation of Catalysts II," (B. Delmon, P. Grange, P. Jacobs, and G. Poncelet, Eds.) p.493, Elsevier, New York, 1979.

49. Ahuja, S.P., Derrien, M.L. and Le Page, J.F., Ind. Eng. Chem. Prod. Res. Dev. 9, 272 (1970).

50. Pratt, K.C., Sanders, J.V. and Tamp, N. J. Catal. 66, 82 (1980).

51. Delmon, B., Preprints Div. Pet. Chem., ACS., 22 503 (1977).

52. Hagenbach, G., Courty, P., and Delmon, B., J. Catal. 31, 264 (1973).

53. Farragher, A.L., and Cossee, P. in "Proceedings of the 5th International Congress on Catalysis," (J.W. Hightower, Ed.) p.1301, North Holland, Amsterdam, 1972.

54. Voorhoeve, R.J.H., J. Catal. 23, 236, 243 (1971).

55. Schuit, G.C.A. and Gates, B.C., AIChE J. 19, 417 (1973).

56. Ueda, H., and Todo, N., Bull. Chem. Soc. Japan 43, 3698 (1970).

57. de Beer, V.H.J. and Schuit, G.C.A. in "Preparation of Catalysts," (B. Delmon, P.A. Jacobs, and G. Poncelet, Eds.) p.343, Elsevier,

Amsterdam, 1976.

58. Wentrek, P.R., and Wise, H., J. Catal. 51, 80 (1978).

59. Laine, J., Brito, J., and Yunes, S., Preprints Div. Pet. Chem. ACS, 25, 438 (1980).

60. Martinez, N.P., Mitchell, P.C.H., and Chiplunkar, P., in "Proceedings of the 2nd International Conference on the Chemistry and Uses of Molybdenum," p.164, Climax Molybdenum Co., London, 1976.

61. Knozinger, H., and Jeziorowski, R., J. Phys. Chem. 82, 2002 (1978); ibid, 83, 1166 (1979).

62. Ramaswamy, A.V., Sivasanker, S., and Ratnasamy, P., J. Catal. 19, 85 (1970).

63. Lafiteau, H., Neel, E., and Clement, J.C. in "Preparation of Catalysts," (B. Delmon, P.A. Jacobs, and G. Poncelet, Eds.) p. 393, Elsevier, Amsterdam, 1976.

64. Martinez, N.P., Mitchell, P.C.H., and Chiplunker, P. J. Less-Common Met. 54, 333 (1977).

65. Okamoto, Y., Nakano, H., Shimakawa, T., Imanaka, T., and Teranishi, S., J. Catal. 50, 447 (1977).

66. Ripperger, W., and Sawm, W., J. Less-Common Met. 54, 353 (1977).

67. De Beer, V.H.J., Bevelander, C., Van Sint Fiet, M., Werter, P.G.A.J., and Amberg, C.H., J. Catal. 43, 68 (1976).

68. Apecetche, M.A., and Delmon, B., React. Kinet. Catal. Lett. 12, 385 (1979).

69. Broderick, D.H., and Gates, B.C., AIChE J. 27 663 (1981).

70. Satterfield, C.N., and Yang, S.H., Ind. Eng. Chem. Proc. Des. Dev., in press.

71. Stevens, G.C. and Edmonds, T., J. Less-Common Met. 54, 321 (1977).

72. Cimino, A., and de Angelis, B.A., J. Catal. 36, 11 (1975).

73. Seshadri, K.S., and Petrakis, L. J. Catal. 30, 195 (1973).

74. Hall, W.K., and Lo Jacono, M. in "Proceedings of the 6th International Congress on Catalysis," (G.C. Bond, P.B. Wells, and F.C. Tompkins, Eds.) p.246, Chemical Society, London, 1977.

75. Trimm, D.L., Catal. Rev.-Sci. Eng. 16, 155 (1977).

76. Lo Jacono, M., Cimino, A., and Schuit, G.C.A., Gazz. Chim. Ital. 103, 1281 (1973).

77. Kibby, C.L., Eddy, E.L., Petrakis, L., Houalla, M. and Hercules, D.M., Preprints, Div. Pet. Chem., ACS. 28, 504 (1983).

78. Beuther, H. and Schmid, B.K. in "Proceedings 6th World Petroleum Congress" Sec III, Paper 20, p. 297 (1963).

79. Laine, J., and Brito, J., Preprints, Div. Pet. Chem. ACS 26, 706 (1981).

80. Inoguchi, M., Kagaya, H., Daigo, K., Sakurada, S., Satomi, Y., Inaba, K., Tate, K., Nishiyama, R., Onishi, S., and Nagui, T., Bull. Jap. Pet. Inst. 13, 153 (1971).

81. Barrett, C.S., Structure of Metals, 2nd ed., McGraw-Hill, New York (1953).

82. Davis, S.M. and Somorjai, G.A., J. Catal. 65, 78 (1980).

83. Davis, S.M. and Somorjai, G.A., Surf. Sci. 91, 73 (1980).

84. Davis, S.M., Zaera, F., and Somorjai, G.A., J. Catal. 77, 439 (1982).

85. Blakely, D.W. and Somorjai, G.A., J. Catal. 42, 181 (1976).

86. Somorjai, G.A. and Blakely, D.W., Nature. 258, 580 (1975).

87. Trimm, D.L. in "Progress in Catalyst Deactivation" p.3, NATO Advanced Study Institute Series, Series E, Vol 54, 1982.

88. Delannay, F. and Defosse, C., Preprints, Div. Pet. Chem. ACS., 26, 385 (1981).

89. Zingg, D.S., Makovsky, L.E., Tischer, R.E., Brown, F.R., and Hercules, D.M., J. Phys. Chem. 84, 2898 (1980).

90. Chin, R.L. and Hercules, D.M. J. Phys. Chem. 86, 360 (1982).

91. Chin, R.L. and Hercules, D.M. J. Catal. 74, 121 (1982).

92. Wu, M. and Hercules, D.M. J. Phys. Chem. 83, 2003 (1979).

93. Jeziorowski, H., Knozinger, H., Taglauer, E., and Vogdt, C. J. Catal. 80, 286 (1983).

94. Myers, C.G., Lang, W.H., and Weisz, P.B. Ind. Eng. Chem. 53, 299 (1961).

95. Delannay, F., Gajardo, P., and Grange, P., J. Micros, Spectr. Electr. 3, 411 (1978).

96. Tamm, P.W., Harnsberger, H.F., and Bridge, A.G., Ind. Eng. Chem. Proc. Des. Dev. 20, 262 (1981).

97. Lipsch, J.M.J.G. and Schuit, G.C.A., J. Catal. 15, 174 (1969).

98. Holloway, P.H. and Kramer, D.K., Report SAND-77-1389 (1977).

99. Henke, A.M., Oil Gas J. 68, (14), 97 (1970).

100. Rajagopolan, K. and Luss, D., Ind. Eng. Chem. Proc. Des. Dev. 18, 459 (1979).

101. Satterfield, C.N. and Cocchetto, J.F., Ind. Eng Chem. Proc. Des. Dev. 20, 53 (1981).

102. Weinberg, W.H., Deans, H.A., and Merrill, R.P., Surf. Sci. 41, 312 (1974).

103. Gardner, N.C. and Hansen, R.S., J. Phys. Chem. 74, 3298 (1970).

104. Pookote, S.R., Dranoff, J.S., and Butt, J.B. in "Chemical Reaction Engineering-Boston" p.283, American Chemical Society Symp. Ser., No. 196, 1982.

105. Brito, J., Golding, R., Severino, F., and Laine, J. Preprints, Div. Pet. Chem. ACS, 27, 762 (1982).

106. Lo Jacono, M., Cimino, A., and Schuit, G.C.A., Gazz. Chim. Ital. 103, 1281 (1973).

107. Beuther, H., and Larson, O.A., Ind. Eng. Chem. Proc. Des. Dev. 4, 177 (1965).

CHAPTER IV

Intrapellet Nickel Profiles Obtained in the Hydrodemetallation (HDM) of Nickel-tetra (3-methylphenyl) porphyrin (Ni-T3MPP) over Co-Mo/Al_2O_3. The presence of Pd/Al_2O_3 and its effect in eliminating pore mouth plugging.

IV. A. Summary of Chapter

During the hydroprocessing of heavy oils the hydrodemetallation (HDM) of metalloporphyrins causes the metals (Ni,V) to deposit within the Co-Mo catalyst extrudates. The HDM reaction is diffusion limited and steep metal profiles exist. The ultimate lifetime of the catalyst is dictated by pore plugging by deposited metals. We report on the HDM mechanism of nickel tetra (3-methylphenyl) porphyrin (Ni-T3MPP) when dissolved in a clean white oil, and show how it is possible to achieve a more uniform intrapellet nickel profile when the porphyrin is prehydrogenated to a species not originally present in the oil (Ni-X). The Ni-T3MPP hydrogenation was carried out over Pd/Al_2O_3 catalyst. The ultimate fate of the nickel is in the Co-Mo/Al_2O_3 extrudates. It is speculated that demetallation from the Ni-X pool (possibly containing species such as Ni-dipyrromethene) generates uniform intrapellet Ni gradients, because the effective diffusivity of Ni-X is higher than that of Ni-T3MPP.

IV. B. Introduction

During the hydroprocessing of heavy oils to remove such elements as

sulfur and nitrogen, metals such as nickel and vanadium are deposited on the catalyst (1). These metals appear to primarily exist as metalloporphyrins (2,3) which are oil soluble. The main objective of the oil refiner when operating a hydroprocessing unit is to maximize the catalyst lifetime. The catalysts, which are typically 1/16" diameter extrudes of alumina impregnated with either Co-Mo or Ni-Mo, deactivate in a very characteristic fashion (1,4), with their ultimate lifetime being dictated by pore mouth plugging. The metals which are catalytically deposited in a diffusion limited reaction, exhibit pellet edge maxima in concentration (1,5) which dictate how accessible the interior of the catalyst pellet is to reactant molecules.

A well designed catalyst, therefore, is one which can store high concentrations of metal deposits and produce uniform intrapellet metal profiles. In the past, this objective has been tackled by replacing the older unimodal pore size distribution catalysts (100A diameter) with bimodal supports (pore sizes 100A and 10,000A). The large pores provide avenues by which the large (20A) metalloporphyrin molecules can rapidly penetrate the support, before they react and deposit their metal in the micropores. These catalysts, however, suffer from the disadvantage that they have a lower catalytic surface area than their unimodal counterparts.

Methods by which the metal deposits can be forced deeper into the catalyst extrude, thereby generating uniform intrapellet metal profiles, therefore merit further investigation. We have been conducting model crude hydrodemetallation (HDM) studies at a fundamental level (6-10). We have separately demetallized metalloporphyrins over alumina supported Co-Mo (7) and Group VIII (10) metal catalysts. Reaction mechanisms have been

evaluated. In this chapter we demonstrate how it is possible to achieve practically uniform intra-pellet metal deposition profiles when our model crude is pretreated with a Pd/Al_2O_3 catalyst before it subsequently deposits its metal on the $Co\text{-}Mo/Al_2O_3$ extrudates. This effect is a direct result of the metalloporphyrin HDM mechanism, wherein the porphyrin undergoes hydrogenation through successively less stable intermediates before it is finally cracked and deposits its metal on the catalyst. To date, the use of supported Group VIII metals in hydroprocessing, has received only cursory attention (11-14).

IV. C. Experimental

The exact details of all experimental apparatus and procedures are documented elsewhere (6,8-10). The model heavy oil is made by dissolving nickel tetra (3-methylphenyl) porphyrin (Ni-T3MPP) at 65 ppm Ni in a clean white oil (Nujol). The structure of Ni-T3MPP is given in Fig. 1. The catalysts used in the experiments were Pd (5%)/Al_2O_3 (Strem Chemicals) and $Co\text{-}Mo/Al_2O_3$ (American Cyanamid, HDS-16A) of conventional composition (5.7 wt % CoO, 12.2% MoO_3). The Pd catalyst was crushed and sieved into the size range 75-90 microns and prereduced overnight at 400°C under flowing hydrogen. Contact with air was minimized prior to its injection into the autoclave reactor. The Co-Mo catalyst is unimodal with an average pore diameter of 80A, and was used in the form of 1.6mm diameter by 7mm length extrudates. Before use the catalyst was heated overnight under flowing helium, at 400°C.

The stirred batch autoclave reactor with its catalyst injection system is described in Ref. 6. The injector was used for introducing the Pd/Al_2O_3 catalyst (ca. 0.05 g.) into the oil once it had achieved reaction

temperature. The Pd catalyst was used in Experiments I and III. The latter experiment also had Co-Mo present. The Co-Mo extrudates (ca. 0.90 g.) were used in Experiments II and III where they were held and spun in a special basket assembly which has been detailed before (8). Both HDM experiments were run at 336°C and 1000 psig H_2, which are conditions representative of industrial practice.

Nickel concentrations in the oil were measured by atomic absorption spectrophotometry and nickel porphyrins by visible spectrophotometry. Intrapellet nickel profiles were measured by energy dispersive X-ray analysis (EDX), on xylene washed extrudates which had been ground down to expose their mid-section (9). The presence of nickel on the spent Pd/Al_2O_3 catalysts was also checked for by EDX.

IV. D. Results and Discussion

We have reported elsewhere the hydrodemetallation (HDM) mechanism for Ni-T3MPP (7,10). The reaction sequence is shown in Fig. 1. The porphyrin is rapidly hydrogenated through two intermediates, namely Ni-chlorin ($Ni\text{-}T3MPPH_2$) and Ni-isobacteriochlorin ($Ni\text{-}T3MPPH_4$). From the $Ni\text{-}PH_4$ species there are two routes to metal deposition on the catalyst: nickel can be deposited directly from $Ni\text{-}PH_4$, or through a contracted ring structure (similar to a hydrogenated nickel-corrin) we have called Ni-X. In Ni-T3MPP HDM we have always observed the terminal hydrogenolysis steps to be rate limiting with $k_6<k_7$ (10). Subsequently, a large pool of relatively unreactive Ni-X always builds up during Ni-T3MPP HDM.

While Ware (15) has attempted to unequivocally determine the structure of Ni-X using mass-spec and infrared analysis, and has assigned it the structure in Fig. 1 it is likely that the "Ni-X pool" is comprised of other

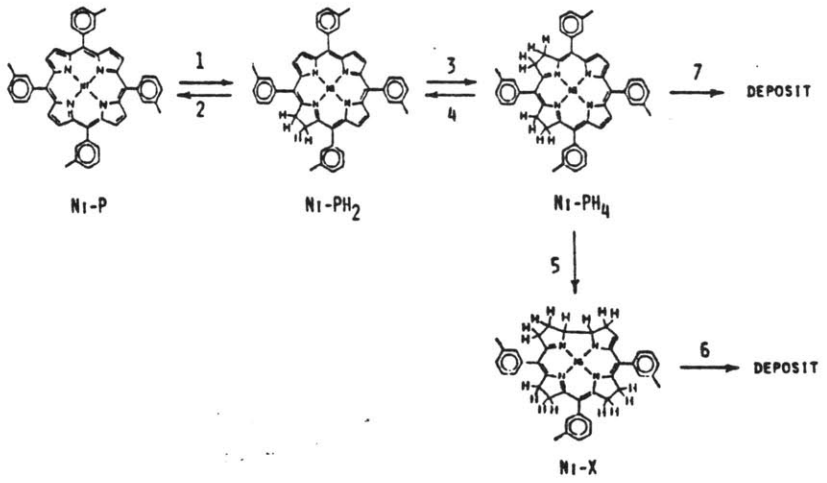

Figure 1: Reaction sequence for Ni-tetra (3-methylphenyl) porphyrin. For further details see Refs. 7 and 10.

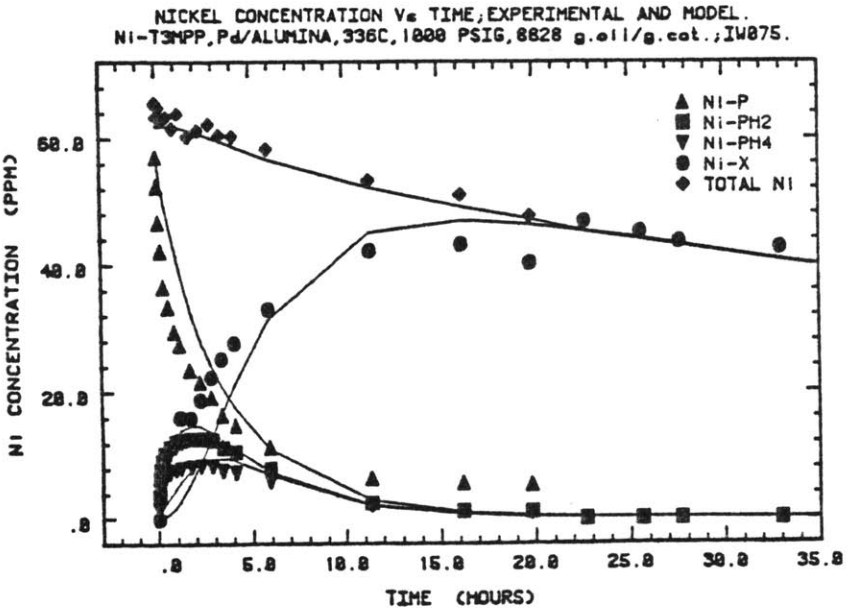

Figure 2: Experiment I: Concentration versus time results from the batch autoclave demetallation of Ni-T3MPP over Pd/Al_2O_3 at 336°C, 1000 psig H_2 and 8828 g. oil/g. cat. Solid lines are model calculations from Ref.10.

types of equally unreactive molecules. They will probably be formed by fragmentation of the Ni-PH_4 macrocyclic ring. One such species may be Ni-dipyrromethene (16). Dipyrromethenes are structures formed by two pyrrole rings bridged by a methylene carbon, and are essentially half of a porphyrin ring. Indeed, there is evidence from UV-Visible spectra collected on our reacted oil that such species do exist (7). The existence of such species is advantageous from the point of view of utilizing the interior of the catalyst pellet for metal storage, since a cracked metal bearing porphyrin fragment will have a higher intra-pellet effective diffusivity. The deposited nickel will therefore be more uniformly distributed within an extrudate.

In separate experiments we have shown (10) that the Group VIII metal catalysts Pd and Pt have good porphyrin hydrogenation activity and generate a large pool of Ni-X. They are, however, relatively inactive for removing nickel from the oil via reaction steps 6 and 7 (Figure 1). The following shows how we have used Pd/Al_2O_3 to rapidly catalyze the Ni-T3MPP hydrogenation reactions, and then demetallized the resulting intermediates over Co-Mo extrudates. The intrapellet nickel profiles obtained with this operation are more uniform than if the Ni-T3MPP HDM reaction is carried out exclusively over the Co-Mo extrudates.

The results of Experiment I where Pd/Al_2O_3 was used to demetallize Ni-T3MPP (0.0478 g. Pd (5%)/Al_2O_3, 422 g. oil at 65 ppm Ni, 336°C, 1000 psig H_2) are shown in Fig. 2. All porphyrinic species are destroyed leaving a large pool of oil soluble nickel present as Ni-X. The Pd catalyst is ineffective at removing Ni from the oil, because it possesses low hydrogenolysis activity (10). It basically can only efficiently

catalyze the forward reactions 1, 3 and 5 (Fig. 1) and transform all the Ni-T3MPP into Ni-X.

In Experiment II, Co-Mo extrudates were used to demetallize a 65 ppm Ni batch of Ni-T3MPP. A sectioned extrudate from the experiment is shown in the SEM in Fig. 3(a). An X-ray line scan for Ni(Kα) is superimposed on the micrograph. Steep intrapellet nickel profiles exist with the majority of nickel concentrated at the periphery of the pellet. There is an indication that the Ni profile exhibits intrapellet maxima. Potential reasons for this effect have been given elsewhere (1,7,17).

Experiment III is a combination of Experiments I and II. The Pd catalyst is injected through the catalyst injection system, while extrudates are held in the baskets and spun in the oil. The masses of catalysts and oil, and the process conditions are the same as for the first two experiments. Our objective is to see what effect prehydrogenation of Ni-T3MPP to Ni-X, and the subsequent demetallation of Ni-X by Co-Mo, has on the resulting intrapellet nickel profile.

An intrapellet Ni profile from Experiment III is shown in Fig. 3(b). Compared to Fig. 3(a)'s profile, the nickel is more uniformly distributed within the pellet. The sharp profiles in the edge maxima, which would ultimately lead to pore mouth plugging, have been removed. We believe this result is a direct consequence of the fact that in Experiment III the Co-Mo extrudates are demetallizing the Ni-X pool. The Ni-X species, because of their physically smaller size (cracked porphyrin fragments), have a higher effective diffusivity than Ni-T3MPP, and are thereby able to penetrate the extrudate more deeply before depositing their nickel. EDX measurements were performed on the spent Pd catalyst from Experiment III. Only trace

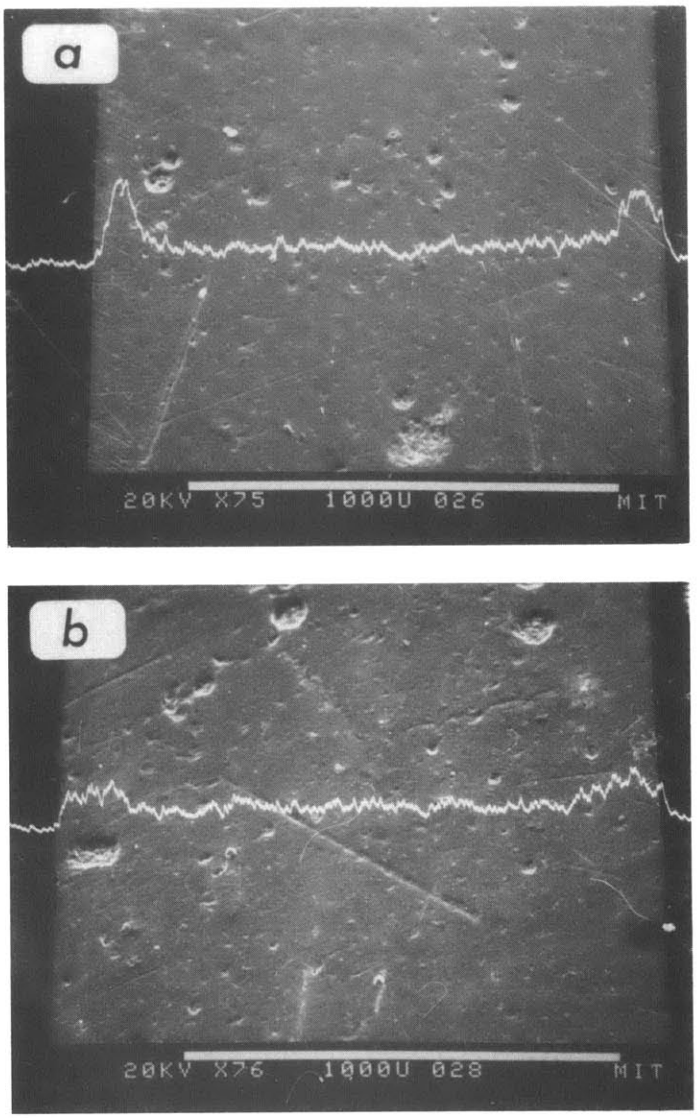

Figure 3: (a) Experiment II: Intra-Co-Mo/Al_2O_3 extrudate Ni profile measured by SEM/EDX. Conditions are 336°C, 1000 psig H_2 and 454.8 g. oil/g. cat. Initial nickel concentration was 65 ppm Ni in oil.

(b) Experiment II: Intra-Co-Mo/Al_2O_3 extrudate Ni-profile measured by SEM/EDX when the Ni-T3MPP is prehydrogenated with Pd/Al_2O_3. Autoclave contained 422 g. Ni-T3MPP at 65 ppm Ni; 0.91 g. Co-Mo/Al_2O_3 in baskets; 0.05 g Pd/Al_2O_3 injected into oil. Conditions are 336°C, 1000 psig H_2. Marker bar is 1000 microns.

quantities of Ni were found, lending further support to our belief that all the Pd catalyst effectively does is catalyze the hydrogenation reactions. The ultimate fate of the Ni is in the Co-Mo extrudates.

In summary, we have shown how we can achieve uniformity of the intrapellet nickel profile in a model HDM reaction by catalytically hydrogenating the metalloporphyrin to an oil soluble nickel species, not originally present in the oil, which has a higher diffusivity than the porphyrin. Our findings are significant since the lifetime of an industrially operating HDM catalyst is usually limited by pore mouth plugging due to deposited metals (4,18). We can visualize a two stage process. The oils' metalloporphyrins are hydrogenated in the first stage, however, no nickel is removed from the oil, thereby protecting the expensive, highly selective hydrogenation catalyst. The second stage contains a cheaper catalyst, possessing more cracking activity. Nickel is deposited on this catalyst, and because of the prehydrogenation stage, deep metal penetration can be achieved.

IV. References

1. Tamm, P.W. Harnsberger, H.F. and Bridge, A.G., Ind. Eng. Chem. Proc. Des. Dev. 20, 262 (1981).

2. Corwin, A.H. and Baker, E.W., ACS. Div. Pet. Chem. Preprints. 9(1), 19 (1964).

3. Rankel, L.A. and Rollmann, L.D., Fuel 62, 44 (1983) and references 1 to 12, therein.

4. Galiasso, R., Blanco, R., Gonzalez, C. and Quinteros, N., Fuel 62, 817 (1983).

5. Sie, S.T. in "Catalyst Deactivation," (B. Delmon and G.F. Froment, Eds.) p.545, Elsevier, Amsterdam, 1980.

6. Hung, C.-W. and Wei, J., Ind. Eng. Chem. Proc. Des. Dev. 19, 250, 257 (1980).

7. Ware, R.A. and Wei, J., Paper No. 61a, presented at AIChE Annual Meeting, Los Angeles, California, Nov. 14-19, 1982.

8. Webster, I.A. and Wei, J., this thesis, Chap III.

9. Webster, I.A. and Wei, J., this thesis, Chap II.

10. Webster, I.A. and Wei, J., this thesis, Chap I.

11. Pecoraro, T.A. and Chianelli, R.R., J. Catal. 67, 430 (1981).

12. Northcott, R.P. and Housam, E.C., U.S. Patent 2, 793, 984.

13. Tate, R.W. and Hemminger, C.E., U.S. Patent 2, 773, 804; British Patent 973, 817.

14. Adams, C.E. and Kimberlin, C.N., U.S. Patent 2, 880, 165.

15. Ware, R.A., Sc.D. Thesis, MIT, September, 1983.

16. Murakami, Y., Matsuda, Y., and Sakata, K., Inorg. Chem. 10, 1728 (1971).

17. Wei, J. and Wei, R.G., Chem. Eng. Commun. 13, 251 (1982).

18. Newson, E., Ind. Eng. Chem. Proc. Des. Dev. 14, 27 (1975).